Chiral amine synthesis by oxidoreductases

Jongkind, E.P.J.

DOI
10.4233/uuid:0c8a0757-08e0-4db1-92b5-78c8a40e3172

Publication date
2024

Document Version
Final published version

Citation (APA)
Jongkind, E. P. J. (2024). *Chiral amine synthesis by oxidoreductases*. [Dissertation (TU Delft), Delft University of Technology]. https://doi.org/10.4233/uuid:0c8a0757-08e0-4db1-92b5-78c8a40e3172

Chiral amine synthesis by oxidoreductases

Proefschrift

ter verkrijging van de graad van doctor

aan de Technische Universiteit Delft,

Op gezag van de Rector Magnificus Prof.dr.ir. T.H.J.J. van der Hagen,

voorzitter van het College voor Promoties,

in het openbaar te verdedigen op
maandag 3 februari 2025 om 15:00 uur

door

Ewald Piet Jürgen JONGKIND

Master of Science in Life Science & Technology, Technische Universiteit Delft, Nederland

Geboren te Alphen aan den Rijn, Nederland

Dit proefschrift is goedgekeurd door de promotoren.

Samenstelling promotiecommissie bestaat uit:

Rector Magnificus	voorzitter
Dr. C.E. Paul	Technische Universiteit Delft, promotor
Prof. dr. U. Hanefeld	Technische Universiteit Delft, promotor

Onafhankelijke leden:

Em. prof. dr. W.J.H. van Berkel	Wageningen University & Research
Prof. dr. ir. J.G. Daran	Technische Universiteit Delft
Dr. R. Eelkema	Technische Universiteit Delft
Dr. F. Mutti	University of Amsterdam
Dr. J. Schrittwieser	University of Graz, Austria

Reserve lid:

Prof. dr. F. Hollmann	Technische Universiteit Delft

Sleutelwoorden: chiral amines, reductive amination, oxidoreductase

Geprint door: Proefschriftspecialist

Boekomslag: Ewald Jongkind

ISBN: 978-94-6384-715-5

Table of Contents

Samenvatting **5**
Summary **7**
Chapter 1: Introduction **9**
Chapter 2: Synthesis of chiral amines via a multi-enzymatic cascade using an ene-reductase and amine dehydrogenase: **31**
Chapter 3: Native amine dehydrogenases can catalyze the direct reduction of carbonyl compounds to alcohols in the absence of ammonia **71**
Chapter 4: Mechanistic insights in *Lactobacillus brevis* alcohol dehydrogenase: stability and active site role of Ser143 and Tyr156 ..... **99**
Chapter 5: Discovery and synthetic applications of a NAD(P)H-dependent reductive aminase from *Rhodococcus erythropolis* **133**
Chapter 6: Discovery and synthetic applications of thermostable NAD(P)H-dependent reductive aminases **179**
Chapter 7: Outlook **219**
Curriculum vitae **227**
Acknowledgements **229**

Samenvatting

Chirale amines zijn waardevolle componenten in de farmaceutische industrie. Het is mogelijk om deze chirale amines te maken met behulp van organokatalyse, metallokatalyse en sinds kort ook via biokatalyse. Enzymen zijn zeer selectieve biokatalysatoren, wat ze bij uitstek interessant maakt voor chirale aminesynthese. Het doel van het onderzoek in dit proefschrift was om verschillende biokatalytische routes toe te passen met oxidoreductasen om chirale amines te synthetiseren.

In **Hoofdstuk 1** laten wij een overzicht zien van enzymen en reacties die zijn gebruikt voor aminesynthese, met een nadruk op oxidoreductasen. Wij houden ons bezig met het onduidelijke onderscheid tussen twee recentelijk ontdekte enzymen: imine redutases (IREDs) en reductive aminases (RedAms). In de daaropvolgende hoofdstukken beschrijven wij de verschillende manieren om oxidoreductasen toe te passen voor aminesynthese.

Als eerste onderzochten wij in **Hoofdstuk 2** een multi-enzymatische cascade, bestaande uit een Old Yellow Enzyme (OYE) en een natieve amine dehydrogenase (AmDH). Door te starten met een onverzadigd keton of aldehyde, konden twee chirale centra worden verkregen in de amine producten. Wij verkregen een breed scala aan amine producten door de reactiecondities aan te passen en we konden de selectiviteit aanpassen door het type OYE te veranderen.

Naast het vormen van amine, observeerden wij ook alcoholvorming als bijproduct in de cascade. Daarom onderzochten wij in **Hoofdstuk 3** de promiscuïteit van deze AmDHs door de reacties uit te voeren zonder ammonia. Onder deze omstandigheden tonen AmDHs activiteit die vergelijkbaar is met alcohol dehydrogenases (ADHs). Wij stelden een voorkeur vast voor vrijwel-neutrale pH, dus het gehalte aan alcohol bijproduct kon worden verminderd door de pH te verhogen.

Omdat we bij deze AmDHs ADH-activiteit observeerden, en deze enzymen neigen om een matige stabiliteit en een klein substraat bereik te vertonen, kozen we er voor om een standaard ADH te modificeren om AmDH activiteit te verkrijgen. In **Hoofdstuk 4**, richtten wij ons op de *Lactobacillus brevis* ADH (*Lb*ADH) met een combinatie van rationeel ontwerpen, en het energie-minimaliseringsalgoritme genaamd FuncLib. Helaas waren wij niet in staat om AmDH activiteit van de ontworpen mutanten te detecteren, slechts een lichte reductie van een specifiek imine in het amine product, dus matige IRED-promiscuïteit was bereikt. Desondanks hebben we kennis opgedaan over de activiteit, stabiliteit en opslagomstandigheden van de *Lb*ADH, en daarmee bijgedragen aan de huidige kennis over dit enzym.

In **Hoofdstuk 5** richten we ons de RedAms, en omdat er bij de start van het onderzoek alleen RedAms uit schimmels gekarakteriseerd waren in de literatuur, zochten wij naar bacteriële RedAms om de enzymfamilie te vergroten en aan te vullen. Onze aanpak was gebaseerd op het zoeken naar genen met een hoge aminozuur sequentie identiteit, actief centrum residu identiteit/overeenkomstigheid en Hidden Markov Modelling (HMM). Beide methoden waren gebaseerd op de nauwkeurig gekarakteriseerde RedAm van de schimmel *Aspergillus oryzae* (*Asp*RedAm). Gebaseerd op alleen sequentie identiteit, leverden de door ons geselecteerde hits drie RedAms op met katalytische activiteit. Door HMM-modellering toe te passen op onze in-huis *Rhodococcus* database, ontdekten wij een paar hits, voornamelijk een veelbelovende hit oorspronkelijk uit *Rhodococcus erythropolis* (*Ryt*RedAm). De complete karakterisering en kristalstructuur leveren inzichten op over de cofactor specificiteit voor zowel NADH als NADPH, een unieke eigenschap voor RedAms, net als de zeldzame *S*-selectiviteit voor chirale amines.

Na deze succesvolle HMM-benadering, zochten wij naar potentiële RedAm hits in de SINTEF-database, zoals beschreven in **Hoofdstuk 6**. Van de vijf geselecteerde kandidaten, toonden drie RedAms potentie, en deze RedAms werden gekarakteriseerd. Opmerkelijk genoeg behielden de RedAms activiteit bij 30 en 40 °C na twee dagen, en zijn ze dus ongewoon stabiel voor dit type enzymen. Wij konden deze RedAms toepassen in cascades met verschillende OYEs, en verkregen complexe amines met twee chirale centra in hoge zuiverheid.

Kortom, dit proefschrift draagt bij aan de momenteel bekende chemische routes om chirale amines te synthetiseren. De beschreven methodes bewijzen hun potentieel als methodes om amines te maken via biokatalyse. Deze kennis biedt inzicht om deze enzymen in de toekomst te gebruiken op een grotere, industriële schaal.

Summary

Chiral amines are valuable compounds in the pharmaceutical industry. These valuable compounds have been made via organocatalysis, metallocatalysis but in the last two decades also via biocatalysis. Enzymes are highly selective, making them attractive catalysts to target chiral amine synthesis. The aim of this dissertation was to apply different biocatalytic pathways with oxidoreductases to synthesize chiral amines.

In **Chapter 1**, we give an overview of the enzymes and their chemical reactions that have been applied for this synthesis, with an emphasis on oxidoreductases. We engage in the challenging distinction between the two recently discovered enzyme families: imine reductases (IREDs) and reductive aminases (RedAms). We then proceed to describe the different approaches employed to apply oxidoreductases for chiral amine synthesis in this dissertation.

For instance, in **Chapter 2** we explored a multi-enzymatic cascade, consisting of an ene reductase from the Old Yellow Enzyme (OYE) family and a native amine dehydrogenase (AmDH). By starting from the unsaturated ketone or aldehyde substrate, up to two stereocenters could be achieved in the amine products. We obtained a wide range of amine products by altering the reaction conditions and could alter the selectivity by changing the type of OYE.

Besides amine formation, we also observed alcohol formation as a by-product in this cascade. Therefore, in **Chapter 3**, we investigated the promiscuous activity of these AmDHs by performing the reactions in absence of ammonia. Under these conditions, AmDHs showed activity similar to that of alcohol dehydrogenases (ADHs). We established AmDH preferred near-neutral pH, therefore alcohol by-product formation could be diminished by increasing the pH.

As ADH activity was observed with AmDHs, and these enzymes tend to display poor stability and substrate scope, we envisioned to engineer an industrial workhorse ADH to gain AmDH activity. In **Chapter 4**, we targeted the *Lactobacillus brevis* ADH (*Lb*ADH) with a combination of rational design, and the energy minimization algorithm called FuncLib. Unfortunately, we were unable to detect AmDH activity of our mutants, only obtaining the reduction of a specific imine into the amine product, thus poor IRED promiscuity was achieved. Nevertheless, we gained knowledge on the activity, stability, and storage of the *Lb*ADH, which could contribute to the current knowledge of this enzyme.

Focusing on RedAms, at the time when only fungal RedAms were characterized, we searched for bacterial RedAms to expand and complement this family of enzymes, which we describe in **Chapter 5**. Our approach was via sequence identity, active site residues identity/similarity, and Hidden Markov Modelling (HMM). Both methods were based on the well-characterized fungal

RedAm from *Aspergillus oryzae* (*Asp*RedAm). Based on sequence identity alone, our selected hits provided three RedAms with catalytic activity. Applying HMM modelling on our in-house *Rhodococcus* database, we discovered a few hits, especially a promising one originating from *Rhodococcus erythropolis* (*Ryt*RedAm). The full characterization and crystal structure provide insights on its cofactors specificity for both NADH and NADPH, a unique property for RedAms, as well as the rare *S*-selectivity to chiral amines.

Following this successful HMM approach, we mined potential RedAm hits in the SINTEF database, as shown in **Chapter 6**. From five selected candidates, three RedAms showed potential and were characterized. Remarkably, these discovered bacterial RedAms retained activity at 30 and 40 °C over two days, thus are uncommonly thermostable for RedAms. We could apply these RedAms in cascades with different OYEs, and obtain complex amines with two chiral centers in high purity.

Overall, this dissertation contributes to the currently known pathways to synthesize chiral amines. The described approaches prove their potential as methods to synthesize amines with biocatalysis. This knowledge provides insight to use these enzymes for future applications on a larger industrial scale.

Chapter 1: Introduction

Chiral amine synthesis

In the 1870s, Jacobus Henricus van 't Hoff graduated from the Delft University of Technology as a physical chemist. Besides being the first Nobel Prize winner in Chemistry in 1901, he is well known for his groundbreaking discoveries in stereochemistry. According to his findings from 150 years ago, molecules with carbons binding to four diverse groups form a tetrahedron with the carbon atom at its center. Because of this structure, these types of molecules are enantiomers of each other and polarize light in opposite directions, making their differences observable, hence the synonym 'optically active compounds'.[1]

Optically active compounds such as chiral amines, amino acids and amino alcohols are highly targeted in the pharmaceutical, agrochemical and chemical industries.[2] The demand for optical purity started due to incidents where drugs contained racemic mixtures in which the 'wrong' enantiomer caused harm. Therefore, in 1992, the United States Food and Drug Association (FDA) installed strict regulations to characterize the effects of relative enantiomers.[2] Since this milestone, other industries as the agrochemical industry focused on the synthesis of chiral compounds as well. By only synthesizing the active enantiomers, processes are more efficient which could decrease costs and environmental impact.[3]

Chiral amines are valuable in the pharmaceutical industry as building blocks to synthesize drugs,[4-7] with approximately 40% of all small drug molecules containing this moiety.[2] In 2020, the global demand was such that the chiral amine market was valued at 14 billion USD.[8] Previously, crystallization of carboxylic acids with chiral amines was and is still used as a method to obtain chiral amines from a racemic mixture.[3] The main challenge of this approach is the maximal yield of 50%, therefore, synthetic routes were designed to overcome this threshold. One approach is hydrogenation of the corresponding imine, which needs the activation of hydrogen by metal catalysts, such as rhodium and ruthenium, to accelerate imine hydrogenation for many applications.[2, 9] Most metal catalysts are precious and non-renewable, and are difficult to remove from the product due to metal leaching.[10] Besides metal catalysts, organocatalysts are small molecules acting as a catalysts, with proline as its best-known example.[11, 12] The challenge of organocatalysts is the need for high catalyst loading.[10]

Over the last decades, enzymes, biocatalysts, have emerged as new potential catalysts to overcome the challenges in amine synthesis by organocatalysis and metal catalysts. Enzymes display high potential and are of high interest due to their high enantioselectivity and efficiency and require milder conditions to implement in comparison with other catalysts, such as neutral pH,

room temperature and atmospheric pressure. Using catalysts under milder conditions are from an economic but also environmental point of view valuable properties in academia and industry.[13] However, large-scale applications are challenging because of the low stability of enzymes.[2] Some enzymes also rely on expensive cofactors and could decrease in activity over time due to product inhibition. Furthermore, despite the advantage of mild reaction conditions, the pH and temperature scale in which enzymes are active is narrow.[13] Besides these general challenges, specific types of enzymes from different types of classes have their own challenges, which need to be tackled individually.

Out of the seven enzyme classes, chiral amine synthesis is achieved by enzymes from three classes: oxidoreductases, transferases and hydrolases. Oxidoreductases catalyze redox reactions combined with either an electron donor or acceptor, here employed for asymmetric reductive amination. Transferases catalyze the transfer of a specific group from one molecule to the other, in this case transferring an amine. Hydrolases inherently catalyze reactions using water to break bonds or releasing water to form bonds, and can also catalyze the enantioselective acylation of a racemic amine using an ester as the acyl donor in an anhydrous solvent. Five different enzymatic approaches are currently available: (dynamic) kinetic resolution, C-H amination, hydroamination, transamination and asymmetric reduction/reductive amination (**Figure 1**).

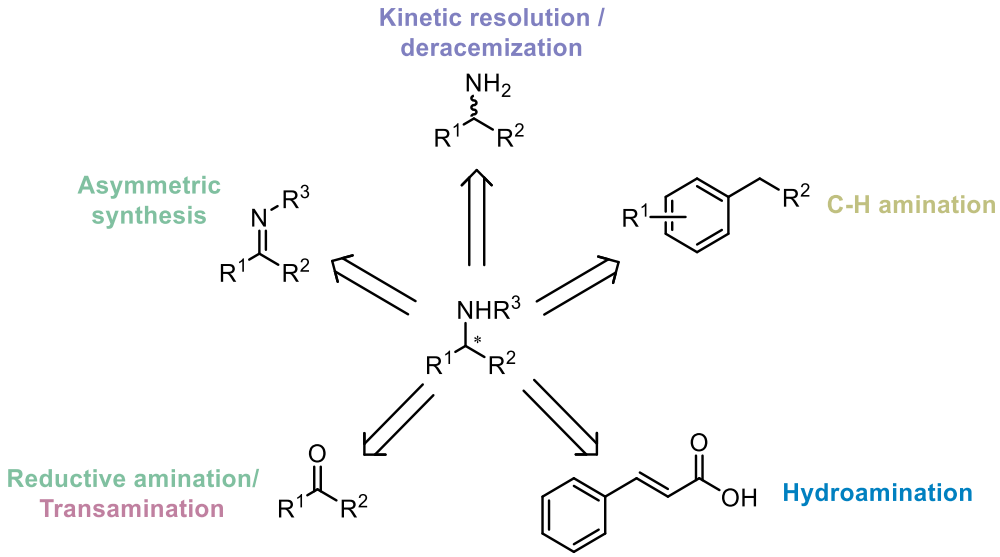

Figure 1. Retrosynthetic biocatalytic approaches for chiral amine synthesis.

(Dynamic) kinetic resolution/deracemization

To overcome the threshold of 50% conversion from racemic mixtures due to kinetic resolution (KR), strategies of racemizing the unaccepted enantiomer

have been applied, also known as dynamic kinetic resolution (DKR). This approach is used in chiral amine synthesis with lipases, which catalyze the acylation of alcohols or amines into the corresponding ester or amide, respectively.[2] Lipases display high enantioselectivity, so in a racemic mixture of amines, only one of the enantiomers is acylated. [14] By racemizing the substrate, conversion of over 50% is possible. An example of amines formation by DKR is by adding a Pd/C-catalyst, racemizing the non-acylated amine enantiomer (**Figure 2**). Thus, the chiral acylated product accumulates, while the amine is racemized until all is converted by the lipase.[15]

Another approach starts from a racemic mixture in which an enzyme converts one of the enantiomer into an achiral product. This approach, deracemization, is used for instance with monoamine oxidases (MAOs). MAOs catalyze the oxidation of amines into the corresponding imines with high selectivity, using a flavin cofactor and reducing oxygen in hydrogen peroxide.[16] Subsequently, the imine is reduced by a chemical reductant such as ammonia borane (NH_3:BH_3), yielding the desired chiral amine (**Figure 2**).[17]

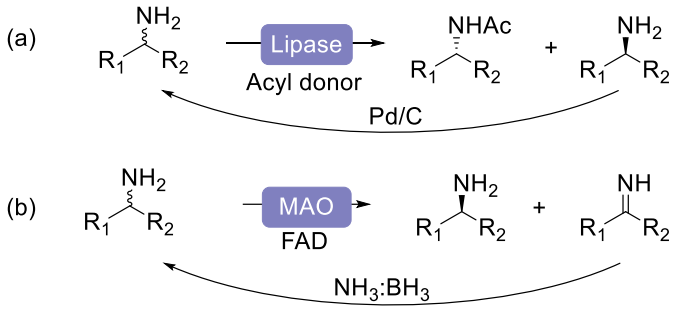

Figure 2. Overview of different biocatalytic reactions using dynamic kinetic resolution, either by a lipases (a)[15] or MAOs (b).[17]

Hydroamination

Hydroamination enables an amino group addition to an unsaturated carbon. This reaction is usually catalyzed by phenylalanine ammonia lyases (PALs).[18] The native reaction of PAL is the deamination of phenylalanine to *trans*-cinnamate and ammonia, from which the reverse reaction is hydroamination (**Figure 3**). PALs have been discovered amongst many different organisms, and many applications rose to form a variety of chiral building blocks.[19-21]

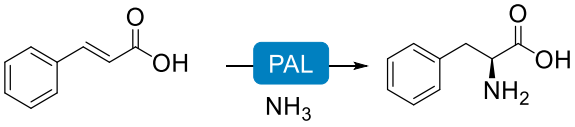

Figure 3. Example of PAL-catalyzed hydroamination. Adapted from Weise *et al*.[21]

C-H amination

C-H bond activation requires cleaving the C-H bond and replacing it with another bond, such as with an oxygen or nitrogen atom. Among iron heme-, non-heme iron-dependent and artificial metallo-enzymes that can yield chiral amines by C-H amination, here we highlight P450 monooxygenases (P450s). These enzymes contain an iron heme cofactor and catalyze a variety of reactions, such as hydroxylation, epoxidation and oxidation.[22, 23] After the iron heme binds with the carbon monoxide, the maximum absorbance is shown at 450 nm, hence the name P450.[23] These enzymes have been engineered to catalyze C-H amination to obtain chiral amines. A serine ligated P450 called P411, allowed the amine transfer towards hydrocarbons (**Figure 4**), which was further improved by protein engineering.[24] In this way, C-H amination was possible with tosyl azide (TsN_3) as the amine source.[25, 26]

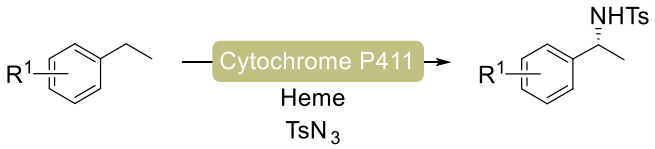

Figure 4. Example of amine synthesis using a serine ligated P450, also known as P411. Adapted from Deane *et al*.[26]

Transamination

Transaminases (TAs) catalyze the transfer of an amine group towards carbonyl substrates to form the corresponding amines, mediated by cofactor pyridoxal phosphate (PLP).[27] TAs can be classified into two groups depending on the substrates.[28] α-TAs convert alpha amino and keto acids, (α -TAs). ω-TAs do not rely on the carboxylic acid group on the substrate, and, besides keto-acids are capable of aminating aldehydes and ketones.[29] TAs catalyze a reversible reaction in which PLP is required as a cofactor and mostly alanine as amine donor, although the corresponding product, pyruvate, is inhibitory for TAs.[30] To overcome this challenge, various efforts have been made to remove pyruvate from the reaction mixture (**Figure 5**).[31] Although these approaches are the most commonly used, a few examples also apply DKR[30, 32] or and deracemization.[33]

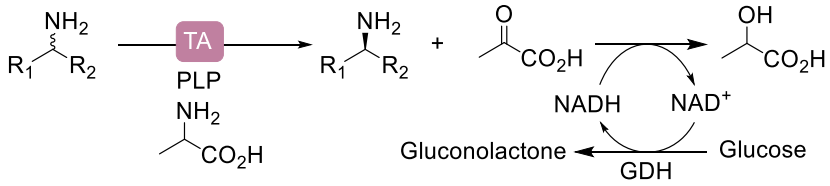

Figure 5. Example of transamination reaction where the equilibrium is forced by reducing the pyruvate byproduct. From Gomm *et al*.[27]

Asymmetric synthesis/reductive amination

Most enzymes used for chiral amine synthesis belong to the oxidoreductase class and rely on a redox cofactor, such as the ubiquitous nicotinamide amine dinucleotide (phosphate) NAD(P)H. The substrate is reduced via hydride transfer from NAD(P)H resulting into a chiral product when starting from a prochiral substrate, hence the term 'asymmetric reduction'. In the case of chiral amine synthesis, the reaction starting from a carbonyl and amine substrate combination to yield an amine is called reductive amination. This thesis focuses on enzymes catalyzing asymmetric reduction reactions, therefore below these enzymes are described in more detail.

Amino acid dehydrogenases (AADHs) catalyze the reductive amination of carboxylic acids into the corresponding amino acids with NAD(P)H (**Figure 6**). The carboxylic acid group is coordinated by charged, polar amino acid residues. Bommarius and co-workers engineered AADHs to accept carbonyl substrates without the carboxylic acid group, as the first known amine dehydrogenases (AmDHs).[34, 35] These AmDHs catalyze the reductive amination of carbonyl substrates with ammonia as external amine donor to obtain primary, chiral amines using NAD(P)H.[36]

Opine dehydrogenases (OpDHs) catalyze the reductive amination of α-ketoacids, similar to AADHs,[37] with an amino acid as the amine donor instead of ammonia (**Figure 6**). In general, OpDHs use NADH as cofactor,[38] except for one that is flavin-containing.[39] Because OpDHs yield chiral amino acids, engineering these enzymes is required to synthesize chiral amines.[37, 40, 41] Only one example is described in a patent from Codexis® where engineering resulted into the synthesis of complex tertiary amines.

The discovery of AADHs and OpDHs was unique since no enzymes were capable of reductive amination of carbonyl substrates without engineering. In 2016, the Génomique Métabolique group from Génoscope discovered a wide panel of native amine dehydrogenases (nat-AmDHs, **Figure 6**).[42-44] The continued exploration of metagenomic data had led to the discovery of more families of nat-AmDHs.[45] Besides this work, after engineering, nat-AmDHs accepted larger alkyl aldehydes- and ketones.[46]

AmDHs have a homodimer structure, and the mechanism of the reductive amination by nat-AmDHs is proposed to be similar to some AADHs (**Figures 7-8**).[47] Upon binding the nicotinamide cofactor, the AmDH folds into its *holo* structure, and ammonia is accepted as amine donor by binding to the negatively charged glutamate residue (Glu108). The substrate carbonyl group binds to the tyrosine (Tyr168) hydroxyl through hydrogen bonding, while the ammonium gets deprotonated by Glu108, so it can act as a nucleophile, eventually leading to releasing water and the formation of the iminium ion intermediate, which is

reduced by the nicotinamide cofactor. In this way, the chiral primary amine is formed. Nat-AmDHs have been shown to catalyze asymmetric reduction with ammonia, and in some cases methylamine as amine donor, therefore for larger, more complex secondary and tertiary amines, other enzymes are of interest, such as imine reductases.

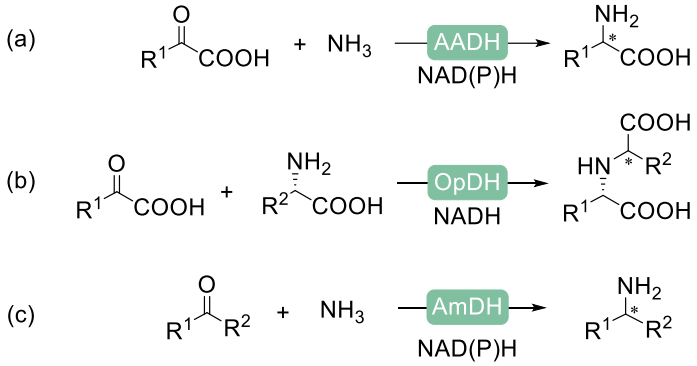

Figure 6. Overview of different native biocatalytic reactions by asymmetric reduction. Via engineering, AADH (a)[34] and OpDHs (b)[40] can catalyze these reactions without acid groups in the substrate, whereas nat-AmDHs (c)[42] already accepted ketone substrates.

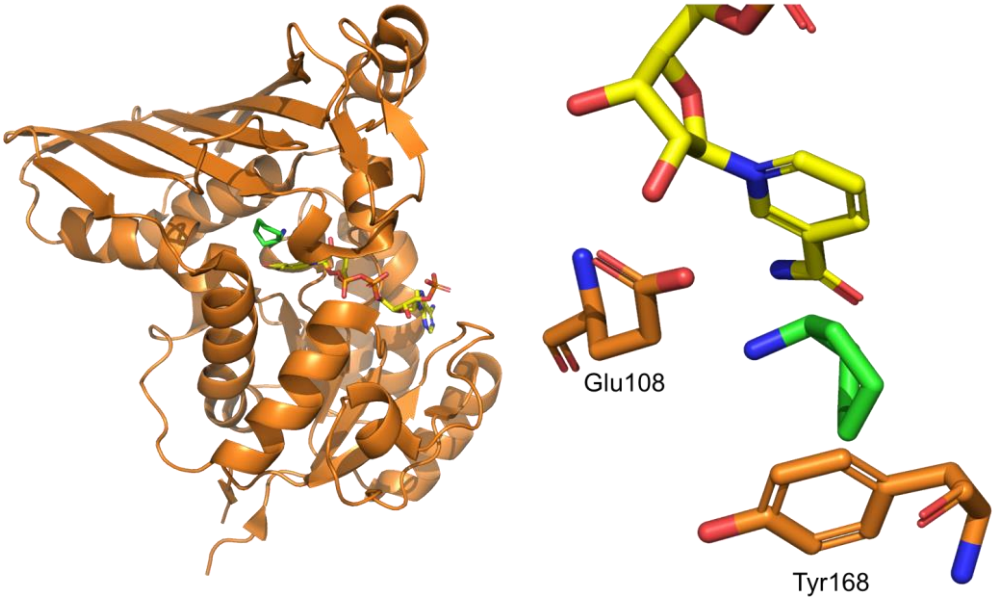

Figure 7. Crystal structure of the AmDH from *Cystobacter fuscus* (*Cfus*AmDH) monomer (left) and the close-up of the active site (right), containing the nicotinamide cofactor $NADP^+$ (yellow), the product cyclohexylamine (green) and the catalytic amino acid residues (orange). PDB 6IAU.[43]

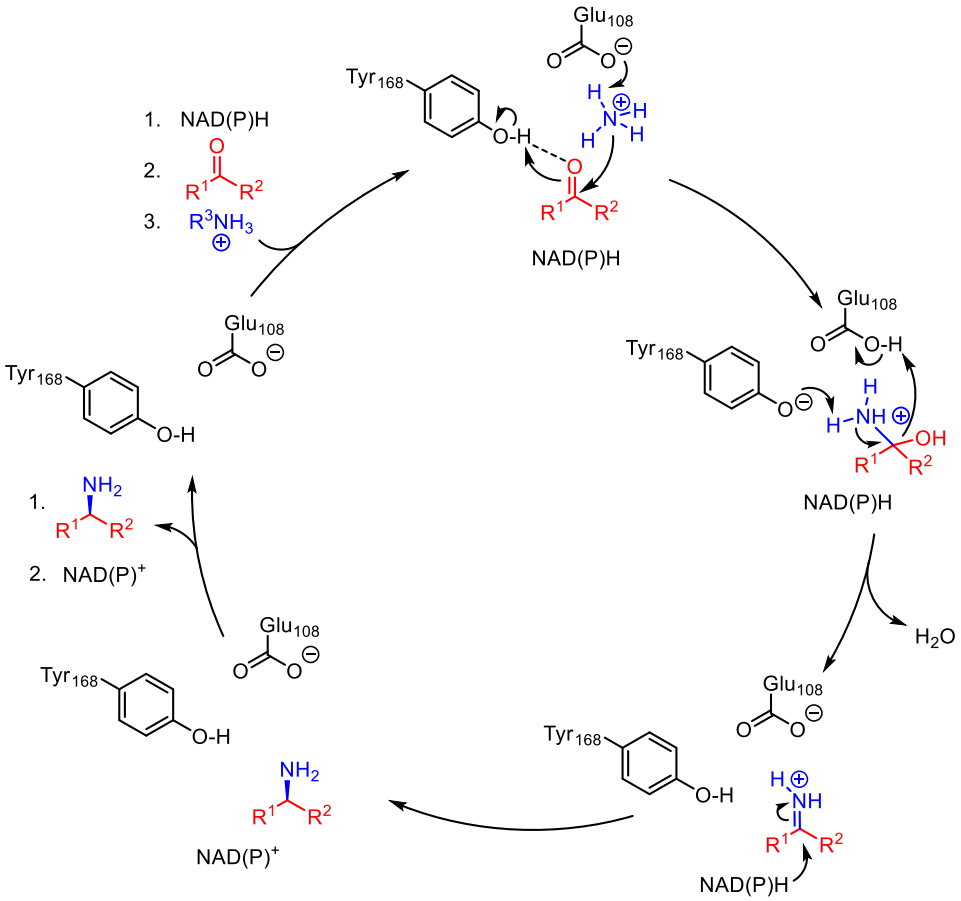

Figure 8. Proposed mechanism of *Cfus*AmDH. Adapted from Mayol *et al*.[43]

IREDs and RedAms

Imine reductases (IREDs) catalyze the asymmetric reduction of imines to amines (**Figure 9**).[48] These enzymes have been used in many characterizations and applications since their discovery in 2010.[49-51] IREDs have also been investigated for amine synthesis starting with a carbonyl substrate and amine donor (**Figure 9**).[52] Because IREDs rely on the presence of imines in solution, which easily hydrolyze, the reaction equilibrium needs to be forced towards imine formation. Imine formation is for instance facilitated by adding higher mole equivalents of amine donor and increasing the pH. Due to the required high excess (up to 500 mM) of amine donor, the efficiency of IREDs is far from optimal.

In 2017, a fungal enzyme was discovered to be a reductive aminase (RedAm), catalyzing both reductive amination of a carbonyl substrate with an amine donor as well as asymmetric reduction of the corresponding imine (**Figure 9**).[53] This enzyme showed promising conversions in presence of a wide range of

ketones with one mole equivalent of amine donor, or more depending on the carbonyl substrate. The authors defined a RedAm with the condition that the reaction: i) gives quantitative conversions at a 1:1 mixture of carbonyl and amine; ii) is equally efficient at neutral pH compared to pH 9.0; iii) exhibits ter-bi kinetics for the carbonyl:amine reagents. The latter is rarely performed for all reactions suggested to be reductive aminations but where an enzyme reaction fulfils the first two criteria, the enzyme would justifiably be acting as a RedAm. Since this discovery, several RedAms have been characterized in fungi[54] and bacteria.[55, 56] Because of the versatility and efficiency of RedAms, these enzymes are interesting catalysts to apply in new methods to synthesize valuable building blocks. However, it can be challenging to distinguish RedAms from IREDs in literature.

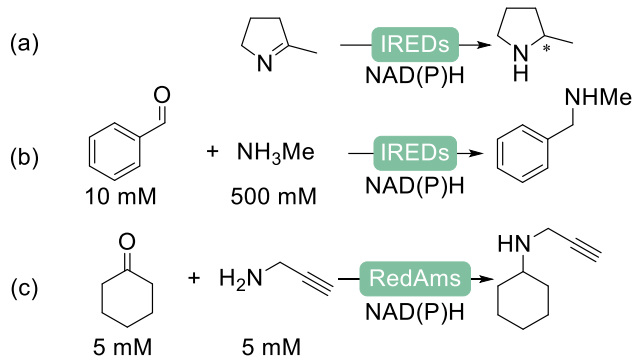

Figure 9. Overview of different biocatalytic reactions via asymmetric reduction. IREDs reduce the imine (a), either as a substrate or as an intermediate pre-formed in solution (b), whereas RedAms catalyze reductive amination and asymmetric reduction in low molar equivalents (c).

Host organism and metabolic role

Whereas the first characterized IREDs originated from bacteria,[57, 58] the first enzyme classified as a RedAm was discovered from fungi. As mentioned before, multiple enzymes have been characterized from fungi since this discovery. However, in the last few years, a few examples have emerged from bacterial organisms.[55, 56] Based on these developments, classifications based on host organism is no longer suitable.

Because of the instable nature of imines, imines need to be pre-formed in solution. Nevertheless, imine-reducing enzymes have been confirmed to have important roles in biosynthesis. For instance, dihydrofolate reductase (DHFR) is involved in folate biosynthesis, also known as vitamin B9.[59] Pyr2C-reductase is involved in L-proline biosynthesis.[60]

IREDs and RedAms are often annotated in databases as 3-hydroxyisobutyrate dehydrogenase or 6-phosphogluconate dehydrogenases,

from the superfamily of β-hydroxyacid dehydrogenases (β-HADs). β-HADs are a different family of enzymes which oxidize ß-hydroxyacid substrates.[61] Within this family, a tartronate semialdehyde reductase is involved in the synthesis of glycerate, possibly to store energy in bacteria.[61, 62] The native reaction of these enzymes is the reduction of 3-hydroxyisobutyrate in methylmalonate semialdehyde with NADH as cofactor in *Arabidopsis thaliana*.[63] In this plant, the 3-hydroxyisobutyrate dehydrogenase is involved in the degradation of valine and isoleucine catabolism.[64] D-Phenylserine dehydrogenases are involved in the metabolism of branched chain amino acids.[65] Potentially, β-HADs also play a role in the succinic semialdehyde catabolism, involved in different metabolisms depending on the organism and kingdom.[66] Increased levels of hydroxyisobutyrates are reported in diseases, possibly correlated with a lack of activity of hydroxyacid dehydrogenases.[67] Both IREDs and RedAms are often annotated as β-HADs, tartronate semialdehyde reductases, 3-hydroxyisobutyrate dehydrogenases or any other protein falling within the class of β-HADs, although they can be distinguished based on their active-site residues. Based on these observations, although the physiological function is unknown for many IRED types, IREDs and RedAms probably have essential roles in the metabolism among all types of organisms.

Structure

Both IREDs and RedAms consist of a homodimeric structure with a Rossmann fold. Both contain the cofactor binding motif GxGxxG. Most IREDs contain the more specific motif GLGxMG. Both contain the residue arginine in the cofactor binding motif, which indicates the preference for NADPH over NADH.[68] This motif is a target for engineering cofactor preference, albeit with high K_M.[69] Based on the structure, it is difficult to distinguish RedAms from IREDs. Although both IREDs and RedAms are often annotated as β-HADs in public databases, IREDs and RedAms bind their substrate by domain swapping, whereas β-HADs bind the substrate with only one monomer.[68, 70] IREDs and RedAms contain hydrophobic residue side chains in the active site, whereas β-HADs contain nucleophilic and electrophilic active site residues. Besides, β-HADs contain a lysine residue for stabilizing the carbonyl substrate,[68] whereas RedAms and IREDs do not have this residue. It is also difficult to make a distinction between IREDs and RedAms based solely on their structure.

Active site residues

Three residues are involved in the reaction mechanism of the reductive aminase from *Aspergillus oryzae* (*Asp*RedAm, **Figure 10**). The proposed reaction mechanism is similar to that of AmDHs (**Figure 11**), but the RedAm active site pocket is larger than of AmDHs, causing a preference for larger primary and

secondary amines instead of ammonia. The asparagine residue at position 93 contributes to stabilizing the amine donor in the active site. The glutamic acid residue at position 169 is negatively charged and stabilizes the positively charged iminium intermediate. The tyrosine residue at position 177 acts as a proton donor. Besides these three catalytic residues, the substrate pocket consists of tryptophan (209), methionine (239) and glutamine (240). Turner and co-workers stated that, although these residues suggest reductive aminase activity, the pool of potential RedAms is not necessarily limited to these exact residues in the active site. The same group described the screening of a wide range of IREDs with varying active site residues.[52] Remarkably, some IREDs catalyzed reductive amination with a serine substituted for the asparagine. One example even contained a tyrosine residue instead of a negatively charged aspartic acid. However, these enzymes were not classified as RedAms, because the researchers could not confirm enzymatic imine formation, since reactions in this work were run at pH 9 and an unknown concentration of IRED was added as a lysate.

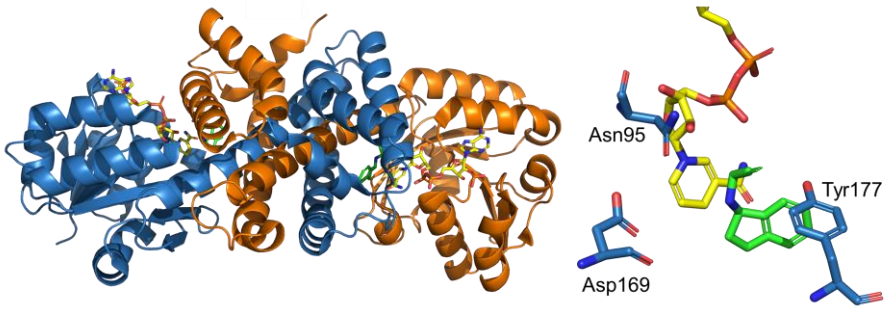

Figure 10. Crystal structure of *Asp*RedAm (left, PDB 5G6S) and a close-up of its active site (right) containing NADP (yellow), amine product rasagiline (green) and the catalytic residues (Asn95, Asp169 and Tyr177, blue).[53]

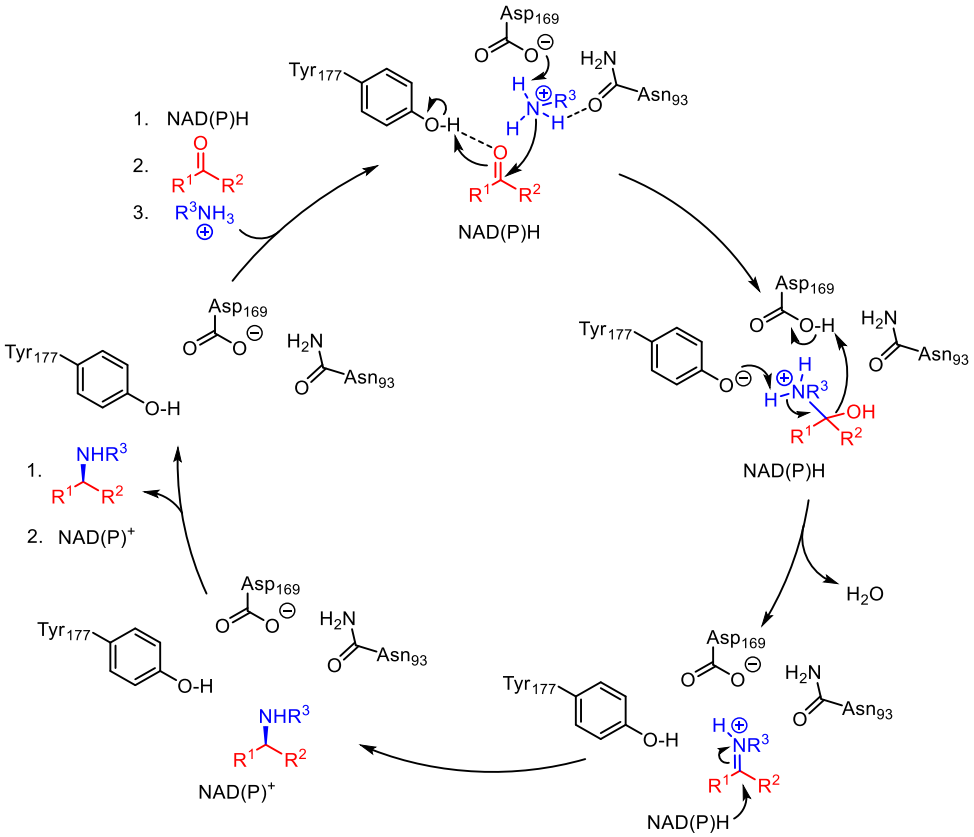

Figure 11. Proposed mechanism of *Asp*RedAm. Adapted from Sharma *et al*.[54]

Reductive amination activity

Imine formation between an aldehyde and an amine donor is favored under basic conditions, as is shown with benzaldehyde and methylamine.[71] Because IREDs require the imine substrate to be present in solution, a basic pH is preferred in combination of a carbonyl substrate and amine donor. Whereas IRED catalyzed amine formation was possible at pH 9, no amine product was present when the reaction pH equaled 7.

Turner and co-workers measured the reductive aminase specific activity towards hexanal and allylamine. The IREDs used in this work are over 100-fold more active at pH 9 than at pH 7.[53] This specific activity ratio (relative activity in pH 9 over pH 7) is only 1.3 for the *Asp*RedAm, which proves this enzyme does not rely on pH to catalyze reductive amination. *Asp*RedAm acts both as an IREDs and a RedAm because there is an increase in activity at pH 9. The ratio would result in a RedAm 'spectrum,' where a low ratio corresponds to a RedAm, and a higher corresponds to an IRED. This factor was only described in the work from

the Turner group, but previous work has shown several activity-based classifications.

For instance, work from Cárdenas-Fernández *et al.* describes the discovery of a panel of new IREDs.[72] 29 different IREDs displayed activity toward 2-methyl-1-pyrroline. In pH 7 and 9, with either NADH or NADPH, the authors determined activity amongst all conditions. They also found activity in the presence of 20 mM cyclohexanone and 160 mM methylamine. Instead of naming these enzymes RedAms, the authors describe these enzymes as IREDs with RedAm activity.

In collaboration with Pfizer (New York City, US), work from Grogan and co-workers describes the engineering of a so-called reductive aminase from the Pfizer in-house library.[73] The library contains IREDs, from which some were screened for their desired carbonyl substrate-amine donor combination. Initial screening contained 20 mM substrate and 40 mM amine donor in a Tris-HCl buffer pH 8. No reactions are done at pH 7 or pH 9, so we cannot determine the aforementioned activity ratio to classify the enzymes as IREDs or RedAms. After screening and site-selected mutagenesis, the authors obtained 43% conversion (enantiomeric excess (*ee*): 98.4%) from an upscale reaction with 50 g/L substrate loading. After establishing this impressive scale-up performance, the enzyme was described as a RedAm.

Other work om Pfizer describes how a RedAm from *Streptomyces purpureus* (*Sp*RedAm) catalyzes the synthesis of abrocitinib, a drug used for atopic dermatitis treatment.[74] After different rounds of enzyme engineering, the researchers isolated a total of 311 kg of product with high purity in 60 h. Because this *Sp*RedAm catalyzed reductive amination with methylamine to provide the secondary amine, we can state this is a RedAm. However, this enzyme also came from the Pfizer IRED database. The work also reports an initial performance of the *Sp*RedAm wild-type (wt) conversion towards the desired reaction, which was only 0.75% from 100 g/L substrate and 1.5 g/L enzyme after 24 h. Besides, the *Sp*RedAm sequence is retrieved from work from Li *et al.*, where the enzyme is annotated as an IRED.[75] Apparently, the distinction between IRED and RedAm is made here based on product yield.

Gilio *et al.* interestingly reported that RedAms can switch to being only imine reducing depending on the substrate.[76] This classification is based on comparing the reductive amination of different potential RedAms with sodium cyanoborohydride ($NaBH_3CN$) as a catalyst. In case $NaBH_3CN$ catalyzes this reaction at a higher rate than the enzyme, it can be classified as an imine reducing enzyme, but if the enzyme shows more conversion, it would be classified as a reductive aminase. Although this comparison with stoichiometric reducing reagent shows a change in reaction rate dependent on the substrate, it is difficult to classify an enzyme with unspecified concentrations.

Chen *et al.* shows an imine reductase from the fungus *Penicillium camemberti* capable of reductive amination of sterically hindered amines.[77] With the wildtype enzyme, good conversions were obtained with aldehyde substrates, low amine equivalents and neutral pH. However, this enzyme is named an "IRED with unusual reductive amination reactivity". Why the enzyme was called an IRED instead of a RedAm is unclear, a common pattern in literature.

EneIRED activity

Besides IRED/RedAm catalyzed asymmetric reduction and reductive amination, Turner and co-workers described the discovery of an EneIRED from *Pseudomonas* sp., capable of catalyzing the asymmetric reduction of an activated alkene as well as reductive amination.[78] Remarkably, this enzyme is solely active in presence of an amine donor. The active site contains an additional tyrosine residue, unlike most known IREDs and RedAms, with a few exceptions.[78] In the reported phylogenetic tree, there is no clear subgroup of EneIREDs present. Thorpe *et al.* showed by crystal structure how the EneIRED active site contains multiple tyrosine residues. Tyr177 aligned with other known IREDs, but Tyr181 replaced the leucine normally located in IREDs. Through single point mutations Y177A and Y181A, Thorpe *et al.* concluded both tyrosine residues contributed to the catalytic activity, but Y177A affected only the C=C reduction step.[78] Although this explains how the enzyme catalyzes both C=C reduction and reductive amination, no conclusions were made whether these tyrosine residues are essential to determine EneIRED activity.

In addition, Turner and co-workers screened a range of EneIREDs with either selectivity to form the (*R*)- or (*S*)-product.[79] Instead of enones as substrate, this work tested the reduction of ene imines. Both the C=C and N=C bonds are reduced by the enzymes, hence the name EneIRED. It is not described whether these enzymes could catalyze reductive amination.

Amino acid sequence – activity relationship

Because of the variety in activity and inconsistency in annotations, we compared the (mostly) characterized IRED, RedAm and EneIRED sequences and focused on the active site residues (**Table 1**) and phylogeny (**Figure 12**). The NDY-WMQ active site motif in *Asp*RedAm is present in all currently characterized fungal RedAms, except for *Pc*IRED. RedAms from bacteria such as IR-77 contain only one out of the six residues. However, both a negative charge for amine donor stabilization and a hydrogen(bond) donor for imine reduction are required. A few exceptions include *Sk*IRED, *Ao*IRED, *Bc*IRED and *Sa*IRED, all solely IREDs dependent on high amine donor concentrations and basic pH. In all these cases, the preformed imine is likely to be uncharged, and therefore, no charged residues may be necessary in the active site. However, we found two exceptions. IR007

was engineered to produce a precursor of a CDK 2/4/6-inhibitor. Although the enzyme was only ready for industrial use after several rounds of engineering, it still displayed reductive amination activity at pH 8. Interestingly, the improved activity was independent of adding a negatively charged residue to the active site. The EneIRED discovered by the Turner group also contains no negative charge in the active site, but reactions are performed at pH 9, possibly causing deprotonation of the amine donor. The hypothesized mechanism is uncommon, where the enone substrate is coordinated in a different orientation in the active site than the imine intermediate.[78] Therefore, it is hard to argue why this enzyme does not rely on negatively charged residues in the active site.

In the majority of the enzymes listed in the table, amino acids potentially functioning as hydrogen(bond) donor are present within the six active site residues. Either Y or W acts as a hydrogen bond donor, but also S, T or W are present on the 177 position. Normally, the catalytically active site residues N, D and Y are at positions 93, 169 and 177, but a few examples, such as the *Ryt*RedAm (discussed in Chapter 5) contains a tyrosine located on position 240. Only *Pc*IRED contains a serine instead, but overall, this type of residue is conserved.

Phylogenetic tree

When analyzing the relation of these enzymes, we prepared a phylogenetic tree (**Figure 12**). We tried to cluster enzymes groups based on the branches in which these are separated and their reported activity. A bacterial IRED (I) and fungal RedAm branch (II) are clearly separated into two groups in the tree. However, most of the enzymes are not easily distinguishable based on the phylogenetic tree or activity. We only observe a group of bacterial enzymes more related to the fungal RedAms (III), all with RedAm activity and a sequence identity of 40%. All enzymes in these group could be classified as RedAms. This branch seems distinctive from the largest group which contains IREDs, RedAms and EneIREDs (IV), without a clear basis to classify these enzymes. Although a small group of fungal RedAms and bacterial IREDs form a cluster, there is no clear bacterial RedAm, IRED or EneIRED subfamily.

Table 1. Multiple sequence alignment of different IRED/RedAm/EneIRED active site residues mentioned in this work. Numbering and sequence identity (Seq. id.) is compared to *Asp*RedAm as query sequence. Negatively charged residues are highlighted in green, potential hydrogen donors are in pink, putative hydrogen-bond donors in purple.

Enzyme	93	169	177	210	239	240	Seq. id. (%)	Reported activity
*Asp*RedAm[53]	N	D	Y	W	M	Q	100	RedAm
*Ac*RedAm[55]	N	D	Y	W	M	Q	65	RedAm
*At*RedAm[54]	N	D	Y	W	M	Q	60	RedAm
*Nfis*RedAm[80]	N	D	Y	W	M	Q	60	RedAm
*Nf*RedAm[80]	N	D	Y	W	M	Q	59	RedAm
*Ba*RedAm[55]	N	D	Y	W	M	Q	51	RedAm
*Shy*RedAm[a]	N	D	Y	W	M	Q	50	RedAm
IR-G36wt[81]	N	D	Y	W	M	Q	45	RedAm
*Stro*RedAm[a]	N	D	Y	W	M	Q	43	RedAm
*Strep*RedAm[a]	N	D	Y	W	V	N	43	RedAm
pQR2600[72]	T	D	T	W	M	M	42	RedAm
*Pih*RedAm[a]	N	D	Y	Y	M	Q	41	RedAm
*Bac*RedAm[a]	N	D	Y	Y	M	Q	40	RedAm
*Pau*RedAm[a]	N	D	Y	W	M	Q	40	RedAm
*Sk*IRED[82]	S	Y	W	T	M	G	40	IRED
*Ao*IRED[83]	S	N	Y	W	M	N	38	IRED
*Sp*RedAm-wt[74]	T	D	W	W	V	Q	38	RedAm
EneIRED-07[79]	T	D	W	M	V	H	37	EneIRED
GSK-IR10[84]	T	D	W	M	V	H	37	RedAm
*Pc*IRED[77]	N	D	S	L	V	Q	36	RedAm
pQR2595[72]	S	D	W	I	T	D	36	RedAm
pQR2601[72]	S	D	W	L	T	E	36	RedAm
*Sr*IRED[70]	S	D	W	W	T	H	36	IRED
EneIRED[78]	T	Y	Y	S	V	H	35	EneIRED
pQR2612[72]	A	D	W	V	S	V	34	RedAm
GSK-IR13[84]	S	D	W	A	T	H	33	RedAm
*Ms*IRED[85]	S	D	W	E	A	H	33	IRED
*Bc*IRED[86]	S	Y	W	M	M	G	32	IRED
GSK-IR22[84]	A	D	W	S	S	V	32	RedAm
*Sk*IRED(2) [87]	S	D	W	G	T	H	32	IRED
IR-77wt[76]	S	D	W	A	P	H	31	RedAm
*Ryt*RedAm[a]	T	D	F	T	V	Y	31	RedAm
IR007[73]	S	Y	L	F	M	M	30	RedAm
*Sa*IRED[82]	S	Y	W	F	M	G	30	IRED
GSK-IR49[84]	T	D	F	S	T	C	28	RedAm
*Nh*IRED[86]	S	Y	W	N	M	D	28	IRED

[a]RedAms later discussed in this dissertation.

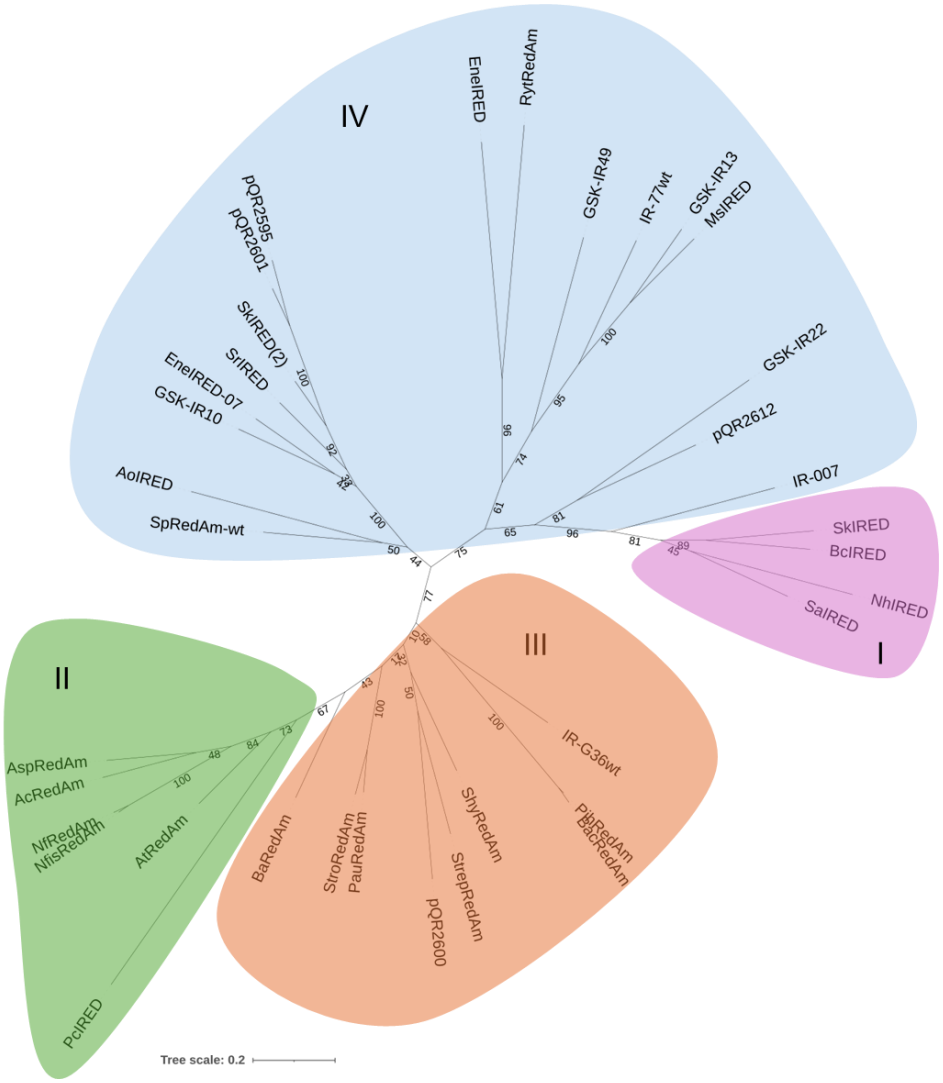

Figure 12. Phylogenetic tree of different IREDs, RedAms and EneIREDs from literature. The corresponding alignment was produced via ClustalW alignment. The maximum likelihood distance tree was computed by MegaX with replications of 500 bootstraps. Corresponding values are shown as nodes at all branches. Layout was further adapted with iTOL.[88-90]

Final remarks

Most enzymes from the phylogenetic tree either catalyze the reduction of (pre-formed) imines or reductive amination. The phylogenetic tree splits the enzymes into two branches. The bottom two groups, the fungal RedAms (II) and bacterial RedAms (III) are similar in sequence identity and activity. Enzymes in this group have been shown to be active as RedAms. Because of the similarity with the fungal RedAms (40% identity with *Asp*RedAm or higher), the substrate

scope is also likely to be similar. However, the enzymes from the upper groups (I and IV) are enzymes with reported imine reducing, reductive amination or 'EneIRED' activity. Enzymes from this class are not guaranteed to function as RedAms, but enzymes displaying reductive amination activity also contain rare properties in comparison with fungal RedAms. Therefore, subfamilies II and III are more likely to contain RedAms than subfamily IV, whereas subfamily I contains imine reducing enzymes only, which can be ascribed to the presence of a tyrosine residue instead of an aspartate at position 169.

The activity assay from Aleku *et al.* shows a potential measurable approach to distinguish RedAms from IREDs.[53] Uniting the three conditions previously mentioned, i) quantitative conversions with 1:1 mixture of carbonyl and amine, ii) catalytic efficiency at neutral pH, iii) exhibiting ter-bi kinetics for the carbonyl:amine reagents, enables to experimentally classify these enzymes. Until a better approach is discovered, these criteria remain the best method to distinguish a reductive aminase from an imine reducing enzyme.

Challenges

Although oxidoreductases display high atom efficiency and enantioselectivity, each type of enzyme comes with its own challenges. Enzymes such as RedAms so far remain uncommon, so little is known about these enzymes. AmDHs are known for their poor stability, and current IREDs and RedAms rely on engineering for applicability for larger scale reactions. Therefore, biocatalytic chiral amine synthesis via asymmetric reduction requires further research to implement efficient reaction processes yielding a wider variety of complex amines.

Goal

The goal of this thesis was to apply biocatalytic pathways using oxidoreductases to synthesize chiral amines. In Chapter 2, we describe a multi-enzymatic cascade, using an Old Yellow Enzyme ene reductase (OYE) and a native AmDH. Since both enzymes catalyze asymmetric reduction, their combination resulted into amine products with two chiral centers. We further investigated the AmDHs for their observed alcohol by-product formation in Chapter 3. Based on this outcome, we explored whether an alcohol dehydrogenases could be engineered to obtain amine dehydrogenase activity in Chapter 4, in which active site mutants of the alcohol dehydrogenase from *Lactobacillus brevis* (*Lb*ADH) were investigated. In Chapters 5 and 6, we searched for reductive aminases from genomic databases via different approaches. In Chapter 5, a NAD(P)H-dependent reductive aminase from *Rhodococcus erythropolis* (*Ryt*RedAm) was discovered and characterized. In Chapter 6, three other RedAms were characterized from actinobacteria.

References

[1] J. H. Van 't Hoff, *Voorstel tot uitbreiding der tegenwoordig in de scheikunde gebruikte Structuur-Formules in de ruimte*, Utrecht, **1874**.

[2] D. Ghislieri, N. J. Turner, *Top. Catal.* **2014**, *57*, 284-300.

[3] M. Breuer, K. Ditrich, T. Habicher, B. Hauer, M. Kesseler, R. Sturmer, T. Zelinski, *Angew. Chem. Int. Ed.* **2004**, *43*, 788-824.

[4] M. Höhne, U. T. Bornscheuer, *ChemCatChem* **2009**, *1*, 42-51.

[5] N. J. Turner, *Nat. Chem. Biol.* **2009**, *5*, 567-573.

[6] C. E. Paul, M. Rodríguez-Mata, E. Busto, I. Lavandera, V. Gotor-Fernández, V. Gotor, S. García-Cerrada, J. Mendiola, Ó. de Frutos, I. Collado, *Org. Process Res. Dev.* **2014**, *18*, 788-792.

[7] T. C. Nugent, M. El-Shazly, *Adv. Synth. Catal.* **2010**, *352*, 753-819.

[8] G. de Gonzalo, I. Lavandera, *Biocatalysis for Practitioners: Techniques, Reactions and Applications*, John Wiley & Sons, Hoboken, New Jersey, US, **2021**.

[9] Z. H. Guan, K. Huang, S. Yu, X. Zhang, *Org. Lett.* **2009**, *11*, 481-483.

[10] I. R. Shaikh, *J. Catal.* **2014**, 35.

[11] J. L. Li, T. Y. Liu, Y. C. Chen, *Acc. Chem. Res.* **2011**, *45*, 1491-1500.

[12] K. L. Jensen, G. Dickmeiss, J. H., L. Albrecht, K. A. Jorgensen, *Acc. Chem. Res.* **2011**, *45*, 248-264.

[13] K. Faber, *Biotransformations in Organic Chemistry*, Springer, Cham, Switzerland, **2018**.

[14] O. Verho, J. E. Bäckvall, *J. Am. Chem. Soc.* **2015**, *137*, 14.

[15] M. T. Reetz, K. Schimossek, *Chimia* **1996**, *50*, 668-669.

[16] A. Sugawara, D. Matsui, M. Yamada, Y. Asano, K. Isobe, *J. Biosci. Bioeng.* **2015**, *119*, 629-635.

[17] S. Herter, F. Medina, S. Wagschal, C. Benhaïm, F. Leipold, N. J. Turner, *Biorg. Med. Chem.* **2018**, *26*, 1338-1346.

[18] A. Kawatra, R. Dhankhar, A. Mohanty, P. Gulati, *Biochim.* **2020**, *177*, 142-152.

[19] N. J. Weise, S. T. Ahmed, F. Parmeggiani, J. L. Galman, M. S. Dunstan, S. J. Charnock, D. Leys, N. J. Turner, *Sci. Rep.* **2017**, *7*, 13691.

[20] S. T. Ahmed, F. Parmeggiani, N. J. Weise, S. L. Flitsch, N. J. Turner, *ACS Catal.* **2018**, *8*, 3129-3132.

[21] N. J. Weise, S. T. Ahmed, F. Parmeggiani, E. Siirola, A. Pushpanath, U. Schell, N. J. Turner, *Catal. Sci. Technol.* **2016**, *6*, 4086-4089.

[22] M. D. Patil, G. Grogan, A. Bommarius, H. Yun, *ACS Catal.* **2018**, *8*, 10985-11015.

[23] K. Yasuda, H. Sugimoto, K. Hayashi, T. Takita, K. Yasukawa, M. Ohta, M. Kamakura, S. Ikushiro, Y. Shiro, T. Sakaki, *Biochim. Biophys. Acta, Proteins Proteom.* **2018**, *1866*, 23-31.

[24] J. A. McIntosh, P. S. Coelho, C. C. Farwell, Z. J. Wang, J. C. Lewis, T. R. Brown, F. H. Arnold, *Angew. Chem. Int. Ed.* **2013**, *52*, 9309-9312.

[25] C. K. Prier, T. K. Hyster, C. C. Farwell, A. Huang, F. H. Arnold, *Angew. Chem. Int. Ed.* **2016**, *55*, 4711-4715.

[26] C. Deane, *Nat. Chem. Biol.* **2017**, *13*, 817-817.

[27] A. Gomm, E. O'Reilly, *Curr. Opin. Chem. Biol.* **2018**, *43*, 106-112.

[28] F. Steffen-Munsberg, C. Vickers, H. Kohls, H. Land, H. Mallin, A. Nobili, L. Skalden, T. van den Bergh, H. J. Joosten, P. Berglund, M. Höhne, U. T. Bornscheuer, *Biotechnol. Adv.* **2015**, *33*, 566-604.

[29] S. Mathew, H. Yun, *ACS Catal.* **2012**, *2*, 993-1001.

[30] D. Koszelewski, K. Tauber, K. Faber, W. Kroutil, *Trends Biotechnol.* **2010**, *28*, 324-332.

[31] I. Slabu, J. L. Galman, R. C. Lloyd, N. J. Turner, *ACS Catal.* **2017**, *7*, 8263-8284.

[32] D. Koszelewski, D. Pressnitz, D. Clay, W. Kroutil, *Org. Lett.* **2009**, *11*, 4810-4812.

[33] E. O'Reilly, C. Iglesias, D. Ghislieri, J. Hopwood, J. L. Galman, R. C. Lloyd, N. J. Turner, *Angew. Chem. Int. Ed.* **2014**, *53*, 2447-2450.
[34] M. J. Abrahamson, E. Vazquez-Figueroa, N. B. Woodall, J. C. Moore, A. S. Bommarius, *Angew. Chem. Int. Ed.* **2012**, *51*, 3969-3972.
[35] M. J. Abrahamson, J. W. Wong, A. Bommarius, *Adv. Synth. Catal* **2013**, *355*, 1780-1786.
[36] A. Pushpanath, E. Siirola, A. Bornadel, D. Woodlock, U. Schell, *ACS Catal.* **2017**, *7*, 3204-3209.
[37] L. Ducrot, M. Bennett, G. Grogan, C. Vergne-Vaxelaire, *Adv. Synth. Catal.* **2021**, *362*, 328-351.
[38] Y. Asano, K. Yamaguchi, K. Kondo, *J. Bacteriol.* **1989**, *171*, 4466-4471.
[39] S. Watanabe, R. Sueda, F. Fukumori, Y. Watanabe, *Plos One* **2015**, *10*.
[40] A. Telek, Z. Molnár, B. G. Vértessy, G. Tasnádi, *Biotechnol. Bioeng.* **2023**, *120*, 2793-2808.
[41] H. Chen, S. J. Collier, J. Nazor, J. Sukurumaran, D. Smith, J. K. Moore, G. Hughes, J. Janey, G. W. Huisman, S. Novick, N. Agard, O. Alvizio, G. Cope, W. L. Yeo, S. NG, (Ed.: Codexis), US20130302859A1, United States, **2013**.
[42] O. Mayol, S. David, E. Darii, A. Debard, A. Mariage, V. Pellouin, J. L. Petit, M. Salanoubat, V. de Berardinis, A. Zaparucha, C. Vergne-Vaxelaire, *Catal. Sci. Technol.* **2016**, *6*, 7421-7428.
[43] O. Mayol, K. Bastard, L. Beloti, A. Frese, J. P. Turkenburg, J.-L. Petit, A. Mariage, A. Debard, V. Pellouin, A. Perret, V. de Berardinis, A. Zaparucha, G. Grogan, C. Vergne-Vaxelaire, *Nat. Catal.* **2019**, *2*, 324-333.
[44] C.-I. Brändén, J. Tooze, *Introduction to protein structure*, 2nd ed., Garland Pub., New York, **1999**.
[45] A. A. Caparco, E. Pelletier, J. L. Petit, A. Jouenne, B. R. Bommarius, V. de Berardinis, A. Zaparucha, J. A. Champion, A. S. Bommarius, C. Vergne-Vaxelaire, *Adv. Synth. Catal.* **2020**, *362*, 2427-2436.
[46] L. Ducrot, M. Bennett, G. André-Leroux, E. Elisée, S. Marynberg, A. Fossey-Jouenne, A. Zaparucha, G. Grogan, C. Vergne-Vaxelaire, *ChemCatChem* **2022**, *14*, e202200880.
[47] O. Mayol, K. Bastard, L. Beloti, A. Frese, J. P. Turkenburg, J.-L. Petit, A. Mariage, A. Debard, V. Pellouin, A. Perret, V. de Berardinis, A. Zaparucha, G. Grogan, C. Vergne-Vaxelaire, *Nat. Catal.* **2019**, *2*, 324-333.
[48] J. Mangas-Sánchez, S. P. France, S. L. Montgomery, G. A. Aleku, H. Man, M. Sharma, J. I. Ramsden, G. Grogan, N. J. Turner, *Curr. Opin. Chem. Biol.* **2017**, *37*, 19-25.
[49] G. Grogan, N. J. Turner, *Chem. Eur. J.* **2016**, *22*, 1900-1907.
[50] M. Gand, C. Thole, H. Muller, H. Brundiek, G. Bashiri, M. Hohne, *J. Biotechnol.* **2016**, *230*, 11-18.
[51] S. Hussain, F. Leipold, H. Man, E. Wells, S. P. France, K. R. Mulholland, G. Grogan, N. J. Turner, *ChemCatChem* **2015**, *7*, 579-583.
[52] S. P. France, R. M. Howard, J. Steflik, N. J. Weise, J. Mangas-Sánchez, S. L. Montgomery, R. Crook, R. Kumar, N. J. Turner, *ChemCatChem* **2018**, *10*, 510-514.
[53] G. A. Aleku, S. P. France, H. Man, J. Mangas-Sánchez, S. L. Montgomery, M. Sharma, F. Leipold, S. Hussain, G. Grogan, N. J. Turner, *Nat. Catal.* **2017**, *9*, 961-969.
[54] M. Sharma, J. Mangas-Sánchez, S. P. France, G. A. Aleku, S. L. Montgomery, J. I. Ramsden, N. J. Turner, G. Grogan, *ACS Catal.* **2018**, *8*, 11543-11541.
[55] K. Zhang, Y. He, J. Zhu, Q. Zhang, L. Tang, L. Cui, Y. Feng, *Front. Bioeng. Biotechnol.* **2021**, *9*, 798147.
[56] G. A. Aleku, G. R. Titchiner, G. W. Roberts, S. R. Derrington, J. R. Marshall, F. Hollfelder, N. J. Turner, D. Leys, *ACS Sustain. Chem. Eng.* **2022**, *10*, 6794-6806.

[57] K. Mitsukura, M. Suzuki, K. Tada, T. Yoshida, T. Nagasawa, *Org, Biomol. Chem,* **2010**, *8*, 4533-4535.
[58] K. Mitsukura, M. Suzuki, S. Shinoda, T. Kuramoto, T. Yoshida, T. Nagasawa, *Biosci. Biotechnol. Biochem.* **2011**, *75*, 1778-1782.
[59] D. P. Baccanari, R. L. Tansik, S. S. Joyner, M. E. Fling, P. L. Smith, J. H. Freisheim, *J. Biol. Chem.* **1989**, *264*, 1100-1107.
[60] M. Goto, H. Muramatsu, H. Mihara, T. Kurihara, N. Esaki, R. Omi, I. Miyahara, K. Hirotsu, *J.Biol. Chem.* **2005**, *280*, 40875-40884.
[61] R. K. Njau, C. A. Herndon, J. W. Hawes, *Chem. Biol. Interact.* **2001**, *130-132*, 785-791.
[62] J. Osipiuk, M. Zhou, S. Moy, F. Collart, A. Joachimiak, *J. Struct. Funct. Genomics* **2009**, *10*, 249-253.
[63] P. Schertl, L. Danne, H. P. Braun, *Plant Physiol.* **2017**, *175*, 51-61.
[64] T. M. Hildebrandt, N. A. Nesi, W. L. Araújo, H. P. Braun, *Mol. Plant.* **2015**, *8*, 1563-1579.
[65] S. Ueshima, H. Muramatsu, T. Nakajima, H. Yamamoto, S.-i. Kato, H. Misono, S. Nagata, *Enzyme Res.* **2010**, *2010*, 597010.
[66] Y. Zhang, Y. Zheng, L. Qin, S. Wang, G. W. Buchko, R. M. Garavito, *Biochim.* **2014**, *104*, 61-69.
[67] A. Tchigvintsev, A. Singer, G. Brown, R. Flick, E. Evdokimova, K. Tan, C. F. Gonzalez, A. Savchenko, A. Yakunin, *J. Biol. Chem.* **2012**, *287*, 1874-1883.
[68] S. Fademrecht, P. N. Schell, B. M. Nestl, B. Hauer, J. Pleiss, *Proteins* **2016**, 600-610.
[69] N. Borlinghaus, B. M. Nestl, *ChemCatChem* **2018**, *10*, 183-187.
[70] M. Lenz, S. Fademrecht, M. Sharma, J. Pleiss, G. Grogan, B. M. Nestl, *Protein Eng. Des. Sel.* **2018**, *31*, 109-120.
[71] P. N. Scheller, M. Lenz, S. C. Hammer, B. Hauer, B. M. Nestl, *ChemCatChem* **2015**, *7*, 3239-3242.
[72] M. Cárdenas-Fernandez, R. Roddan, E. M. Carter, H. C. Hailes, J. M. Ward, *ChemCatChem* **2023**, *15*, e202201126.
[73] J. Steflik, A. Gilio, M. Burns, G. Grogan, R. Kumar, R. Lewis, C. Martinez, *ACS Catal.* **2023**, *13*, 10065-10075.
[74] R. Kumar, M. J. Karmilowicz, D. Burke, M. P. Burns, L. A. Clark, C. G. Connor, E. Cordi, N. M. Do, K. M. Doyle, S. Hoagland, C. A. Lewis, D. Mangan, C. A. Martinez, E. L. McInturff, K. Meldrum, R. Pearson, J. Steflik, A. Rane, J. Weaver, *Nat. Catal.* **2021**, *4*, 775-782.
[75] H. Li, Z. J. Luan, G. W. Zheng, J. H. Xu, *Adv. Synth. Catal.* **2015**, *357*, 1692-1696.
[76] A. K. Gilio, T. W. Thorpe, A. Heyam, M. R. Petchey, B. Pogrányi, S. P. France, R. M. Howard, M. J. Karmilowicz, R. Lewis, N. J. Turner, G. Grogan, *ACS Catal.* **2023**, *13*, 1669-1776.
[77] F.-F. Chen, X.-F. He, X.-X. Zhu, Z. Zhang, X.-Y. Shen, Q. Chen, J.-H. Xu, N. J. Turner, G.-W. Zheng, *J. Am. Chem. Soc.* **2023**, *145*, 4015-4025.
[78] T. W. Thorpe, J. R. Marshall, V. Harawa, R. E. Ruscoe, A. Cuetos, J. D. Finnigan, A. Angelastro, R. S. Heath, F. Parmeggiani, S. J. Charnock, R. M. Howard, R. Kumar, D. S. B. Daniels, G. Grogan, N. J. Turner, *Nature* **2022**, *604*, 86-91.
[79] V. Harawa, T. W. Thorpe, J. R. Marshall, J. J. Sangster, A. K. Gilio, L. Pirvu, R. S. Heath, A. Angelastro, J. D. Finnigan, S. J. Charnock, J. W. Nafie, G. Grogan, R. C. Whitehead, N. J. Turner, *J. Am. Chem. Soc.* **2022**, *144*, 21088-21095.
[80] J. Mangas-Sánchez, M. Sharma, S. C. Cosgrove, J. I. Ramsden, J. R. Marshall, T. W. Thorpe, R. B. Palmer, G. Grogan, N. J. Turner, *Chem. Sci.* **2020**, *11*, 5052-5057.
[81] J. Zhang, D. Liao, R. Chen, F. Zhu, Y. Ma, L. Gao, G. Qu, C. Cui, Z. Sun, X. Lei, S. S. Gao, *Angew. Chem. Int. Ed.* **2022**, *61*, e202201908.

[82] T. Huber, L. Schneider, A. Präg, S. Gerhardt, O. Einsle, M. Müller, *ChemCatChem* **2014**, *6*, 2248-2252.
[83] G. A. Aleku, PhD Thesis, University of Manchester, **2016**.
[84] G. D. Roiban, M. Kern, Z. Liu, J. Hyslop, P. L. Tey, M. S. Levine, L. S. Jordan, K. K. Brown, T. Hadi, A. F. Ihnken, M. J. B. Brown, *ChemCatChem* **2017**, *9*, 4475-4479.
[85] P. Stockinger, N. Borlinghaus, M. Sharma, B. Aberle, G. Grogan, J. Pleiss, B. M. Nestl, *ChemCatChem* **2021**, *13*, 5210-5215.
[86] H. Man, E. Wells, S. Hussain, F. Leipold, S. Hart, J. P. Turkenburg, N. J. Turner, G. Grogan, *ChemBioChem* **2015**, *16*, 1052-1059.
[87] M. Rodríguez-Mata, A. Frank, E. Wells, F. Leipold, N. J. Turner, S. Hart, J. P. Turkenburg, G. Grogan, *ChemBioChem* **2013**, *14*, 1372-1379.
[88] E. Zuckerkandl, L. Pauling, in *Evolving Genes and Proteins* (Eds.: V. Bryson, H. J. Vogel), Academic Press, **1965**, pp. 97-166.
[89] K. Tamura, G. Stecher, S. Kumar, *Mol. Biol. Evol.* **2021**, *38*, 3022-3027.
[90] I. Letunic, P. Bork, *Nucleic Acids Res.* **2021**, *49*, W293-W296.

Chapter 2: Synthesis of chiral amines via a multi-enzymatic cascade using an ene-reductase and amine dehydrogenase

E.P.J. Jongkind,[1] A. Fossey,[2] O. Mayol,[2] A. Zaparucha,[2] C. Vergne-Vaxelaire,[2]* C.E. Paul[1]*

[1]Biocatalysis, Department of Biotechnology, Delft University of Technology, Van der Maasweg 9, 2629 HZ Delft, The Netherlands
[2]Génomique Métabolique, Génoscope, Institut François Jacob, CEA, CNRS, Univ Evry, Université Paris-Saclay, 91057 Evry, France

Based on *ChemCatChem*, **2022**,*14*, e202101576. doi: 10.1002/cctc.202101576

Summary

Access to chiral amines with more than one stereocenter remains challenging, although an increasing number of methods are emerging. Here we developed a proof-of-concept multi-enzymatic cascade, consisting of an ene reductase and amine dehydrogenase (AmDH), to afford chiral diastereomerically enriched amines in one pot. The asymmetric reduction of unsaturated ketones and aldehydes by ene reductases from the Old Yellow Enzyme family (OYE) was adapted to reaction conditions for the reductive amination by amine dehydrogenases. By studying the substrate profiles of both reported biocatalysts, thirteen unsaturated carbonyl substrates were assayed against the best duo OYE/AmDH. Low (5%) to high (97%) conversion rates were obtained with enantiomeric and diastereomeric excess of up to 99%. We expect our established multi-enzymatic cascade to allow access to chiral amines with both high enantiomeric and diastereomeric excess from varying alkene substrates depending on the combination of enzymes.

Introduction

Chiral amines are encountered in a myriad of building blocks and are valuable chemicals used in pharmaceutical and fine chemical industries. Besides their synthesis by metal-assisted catalysis or by more sustainable organocatalytic alternatives,[1, 2] biocatalytic methods have been increasingly developed over the last decade.[3, 4] Among the panel of enzymes reported to date for this transformation, amine dehydrogenases (AmDHs; EC 1.4.1) are described to catalyze the reductive aminations of carbonyl-containing compounds to corresponding primary amine products with ammonia as amine source and the 1,4-dihydronicotinamide adenine dinucleotide (NAD(P)H) cofactor. Particularly, native AmDHs have been reported to be active toward various aliphatic aldehydes and ketones to access a variety of amine products with *S*-configuration in case of chiral amines.[5, 6] Their implementation in biocatalytic cascade reactions could allow access to various substituted (chiral) products.

Biocatalytic cascades, *i.e.* the combination of at least two reaction steps in a single reaction vessel without isolation of the intermediates, have been reported for the synthesis of many compounds,[7] allowing to save reagents, time and operational workup steps, with easier access or more appropriate initial substrates. Particularly, the use of two catalysts in *in vitro* linear sequences have been applied for the synthesis of amines. Ramsden *et al.* have described the one-pot combination of reductive aminase (RedAm) from *Aspergillus oryzae* with choline oxidase or carboxylic acid reductase to perform biocatalytic *N*-alkylation of amines through *in situ* generation of aldehydes.[8] Hydrogen-borrowing asymmetric amination was carried out by coupling alcohol dehydrogenase (ADH) and AmDH/RedAm to prepare various (*R*)-amines,[9] including with co-immobilized biocatalysts.[10] By adding another step catalyzed by P450 monooxygenase, unfunctionalized alkanes can be employed to access amines with isolated enzymes[11] or *E. coli* whole cells.[12]

Ene reductases (EREDs) of the Old Yellow Enzyme family (OYEs; EC 1.6.99.1) catalyze the asymmetric reduction of unsaturated ketones and aldehydes in high conversion and enantiomeric excess, and are promising biocatalysts for industrial applications.[5] OYEs have already been applied in cascade reactions, especially for the synthesis of carboxylic acids also in a hydrogen-borrowing concept,[13] or in combination with ADH to access α-substituted alcohols.[14-16] The transformation of enones to amines was accomplished with OYEs and transaminases (TAs) chosen unreactive toward the starting enones. Moderate to high diastereomeric excess of (1*R*,3*S*)-, (1*S*,3*S*)-, (1*R*,3*R*)-1-amino-3-methylcyclohexane and substituted aryl amines were obtained depending of TA from Codexis and wild-type or engineered OYE used.[17, 18]

Here we envisioned a multi-enzymatic cascade combining OYE and native AmDH to obtain a panel of amine compounds, several with various methyl substitutions leading to chiral products (Scheme 1). With the extending substrate scope of AmDHs and the growing number of characterized OYEs, it appeared interesting to prove the viability of such a cascade and to apply it on a large number of substrates. This one-pot biocascade circumvents the need for isolation and purification of intermediates while retaining the enantioselectivity of each enzyme. A NAD(P)H cofactor recycling system with the well-established glucose dehydrogenase (GDH) provides the necessary electrons for the system *via* inexpensive glucose. After an extended substrate scope study of both OYEs and AmDHs, we describe here the results obtained with the best duo OYE/AmDH for the biocatalytic conversion of nine common substrates. Several key cascade reactions were conducted at a 10 mM concentration to demonstrate the viability of this setting.

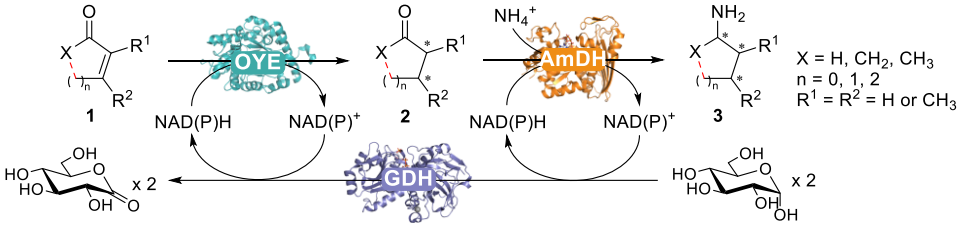

Scheme 1. Overview of the one-pot multi-enzymatic cascade to obtain chiral amines, from asymmetric reduction catalyzed by an OYE to reductive amination with ammonia and AmDH.

Results and Discussion

OYE specific activity towards substrate scope

In this study, we focused our effort on the following characterized AmDHs: *Cfus*AmDH from *Cystobacter fuscus*, *Apau*AmDH from *Aminomonas paucivorans, Msme*AmDH from *Mycobacterium smegmatis, Micro*AmDH from *Microbacterium* sp. MA1, *Chat*AmDH from *Hungatella hathewayi*, and IGCAmDH5 and MATOUAmDH2 from metagenomic data. Their reported substrate scope are mainly aliphatic aldehydes and ketones, linear or cyclized.[19] No or very low activity were described for carbonyl compounds bearing an aromatic group. Therefore, we selected unsaturated enones structurally identical or similar to this preliminary list, despite the scarce activity data of OYEs for this type of substrate. We extended this list to methyl-substituted unsaturated aldehydes to take advantage of the stereoselectivity of OYEs toward substituted enones and access diastereoisomers *via* the cascade process, resulting in the selection of differently substituted cycloalkenones **1a**-**1f**, aliphatic enones **1g**-**1i**,

methyl-substituted unsaturated aldehydes **1j**-**1l** and unsaturated aldehyde **1m** (**Figure 1**).

We started screening the activity toward substrates **1a**-**1m** with available OYEs from *Thermus scotoductus* (*Ts*OYE),[20] *Saccharomyces cerevisiae* (OYE2),[21] *Bacillus subtilis* (YqjM),[22] *Gluconobacter oxydans* (GluER)[23] and *Geobacillus kaustophilus* (*Gk*OYE).[24] *Ts*OYE was already described to catalyze the reduction of maleimides and cycloalkenones,[25] and was expected to accept substrates such as aliphatic, unsaturated aldehydes and ketones not yet explored but known as OYE substrates.[26] Compared with other OYEs, we initially chose *Ts*OYE as a model enzyme due to its high solvent and thermal stability. The specific activity for the reduction of substrates **1a**-**1m** with *Ts*OYE was measured by spectrophotometry under standard conditions (**Figure 1**).

The highest specific activity was obtained with 3-buten-2-one **1g** (18.8 U/mg) and decreased with increasing alkyl chain length, with 2-penten-3-one **1h** (16.8 U/mg) and 3-penten-2-one **1i** (1 U/mg), as well as with α-methyl substituents, from *trans*-pentenal **1m** (10.3 U/mg) to *trans*-2-methyl-pentenal **1l** (8.7 U/mg). The activity was lower for cyclic substrates cyclopentenone **1a** and cyclohexenone **1d** compared with linear ones, and the same activity decrease was observed with α- and β-methylated substrates (**1b**, **1c**, **1e** and **1f**). In particular, β-methyl substituted substrates 3-methylcyclopentenone **1c** and 3-methylcyclohexenone **1f** afforded no observable activity with *Ts*OYE. Therefore, we also probed the double mutant *Ts*OYE-C25D/I67T[27] (0.30 U/mg) and OYE2 (0.06 U/mg) with 3-methylcyclohexenone **1f** (**Figure 1**). For cyclohexenone **1d**, the highest activities were obtained with *Ts*OYE followed by OYE2, then YqjM (**Table 1**).[28] In case of enals **1k** and **1l**, there specific activities were also tested toward *Gk*OYE and GluER but *Ts*OYE remained the most active one in the tested conditions (**Figure S4**). Thus, we established that the selected OYEs had a substrate scope highly compatible with the preliminary data reported for the studied AmDHs, with high activity toward aliphatic unsaturated aldehydes and cyclohexenone, and some notable activity toward the other tested ketones/substituted cycloalkenones.

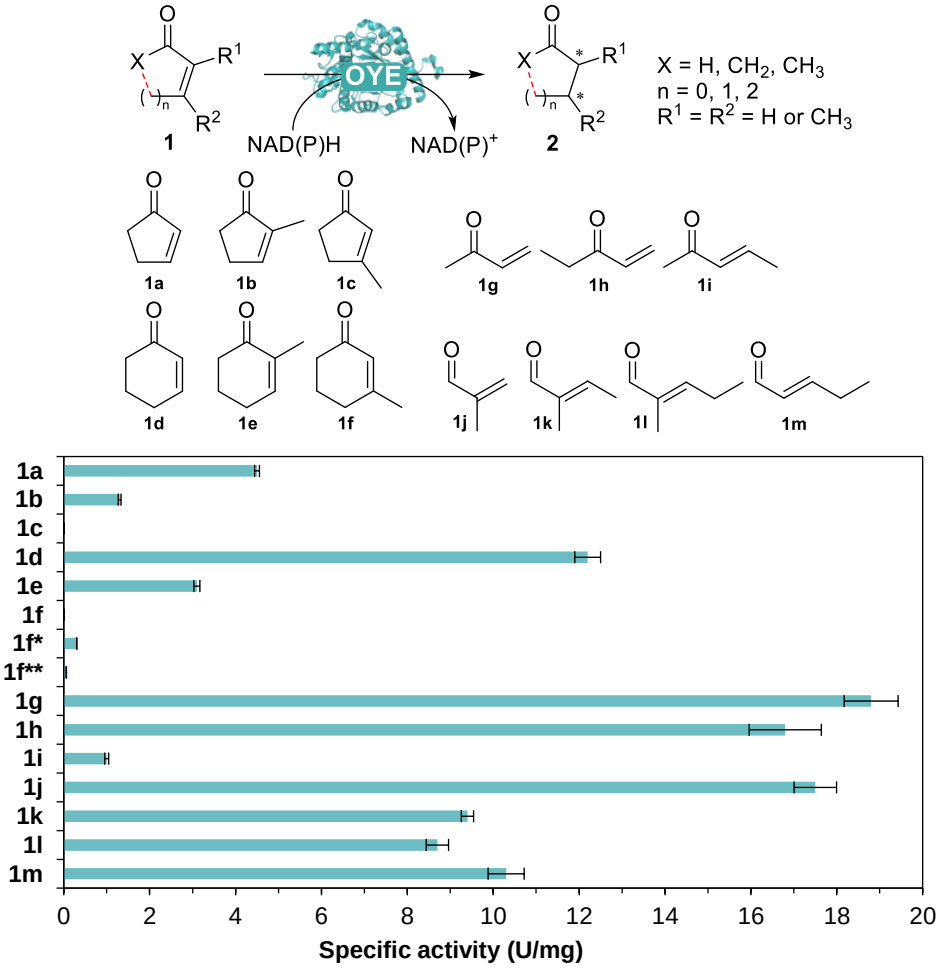

Figure 1. Specific activities of *Ts*OYE for unsaturated ketone and aldehyde substrates 1a-1m. Conditions: 10 mM substrate 50 mM Tris-HCl buffer pH 8.0, *Ts*OYE. 10.0 U/mL glucose oxidase (GOx), 20 mM glucose, 0.2 mM NADPH. 3-methylcyclohexenone **1f*** was tested with *Ts*OYE-C25D/I67T and **1f**** with OYE2 and 0.2 mM NADH. Average of duplicates.

Impact of reaction conditions on OYE activity

Next, we chose cyclohexenone **1d** as a model to determine reaction conditions for OYEs that would be compatible with AmDH activity, this substrate giving good activity and being one of the least volatile. To design one-pot cascade reactions, reaction conditions must fit to all the enzymes involved in the steps. In case of enzymes working with specific conditions, the other enzymes must tolerate these conditions sufficiently to ensure the success of the cascade without this being to the detriment of the use of too large quantity of catalysts. In our case, a high ammonia concentration is essential for AmDH activity, mainly due to the

very high K_M of ammonia. Thus, the main parameter to be studied was the tolerance of OYEs to high ammonia concentrations.

In addition to commonly used buffers, 0.25–1.00 M ammonium formate buffers were tested. At 50 mM, *Ts*OYE gave the highest activity with MOPS-NaOH at pH 7.0 and Tris-HCl at pH 8.0, decreasing from 12.0 to 6.5 - 7.3 U/mg when increasing the pH to 9.0 (**Table 1**). This significant activity decrease at pH 9.0 can be ascribed to deprotonation of tyrosine 177,[29] known to play an important role as proton donor in the OYE active site.[20, 30] Notably, the specific activity of *Ts*OYE with and without glucose oxidase (GOx) to remove molecular oxygen *in situ* showed no significant difference (see **Figure S3**). The use of ammonium formate as buffer at 0.25–1.00 M concentration resulted in a significant decrease in activity, all the more important as the concentration increased (**Table 1**).

Table 1. Specific activity of OYEs for substrate cyclohexenone **1d**.[a]

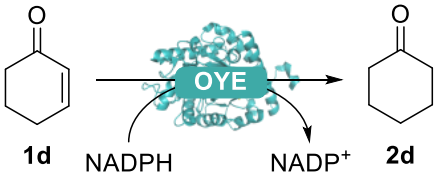

OYE	Buffer	[Buffer] (M)	pH	Spec. act. (U/mg)
OYE2	Tris-HCl	0.05	8.0	3.3 ± 0.1
YqjM	Tris-HCl	0.05	8.0	2.1 ± 0.0
*Ts*OYE	MOPS-NaOH	0.05	7.0	12.0 ± 0.0
*Ts*OYE	Tris-HCl	0.05	8.0	12.2 ± 0.3
*Ts*OYE	Tris-HCl	0.05	8.5	10.9 ± 0.1
*Ts*OYE	Tris-HCl	0.05	9.0	6.5 ± 0.0
*Ts*OYE	Na_2CO_3	0.05	9.0	7.3 ± 0.3
*Ts*OYE	NH_4HCO_2	0.25	8.0	1.4
*Ts*OYE	NH_4HCO_2	0.5	8.0	0.3
*Ts*OYE	NH_4HCO_2	1.0	8.0	0.1

[a] Conditions: specified buffer, [OYE] (0.05 M buffer: 0.05, 0.73 and 0.65 µM of *Ts*OYE, OYE2 and YqjM respectively; 0.56, 1.38 and 3.96 µM of *Ts*OYE at 0.25, 0.50 and 1.00 M NH_4HCO_2 buffer respectively), 10 U/mL glucose oxidase (GOx), 20 mM glucose, 0.2 mM NADPH, 10 mM cyclohexenone. Average of duplicates.

We carried out biocatalytic reactions monitoring conversion after one hour to determine whether these low specific activities observed at 0.25-1.00 M ammonium formate still allowed for conversion while maintaining appropriate amounts of catalysts (<0.1 mg/mL), with the substrate scope (**1a**, **1c**, **1d**, **1e**, **1f**, **1h**, **1l**, **1m**). For better understanding, these reactions were tested in four different buffers (**Figure 2**). The synthetic cofactor 1-benzyl-1,4-dihydronicotinamide

(BNAH) was used as an inexpensive alternative to NADPH to simplify screening, as using BNAH avoids a cofactor recycling system and is stable under basic conditions (**Figure S6**).[31] Overall, the conversion rates were similar for the buffers used (Tris-HCl or NH_4HCO_2), even if a concentration of at least 50 mM of Tris-HCl is preferred to sufficiently buffer the medium. Nearly complete conversions were obtained for substrates **1a**, **1d**, **1e** and **1h**, moderate (<70%) conversions for substrates **1l** and **1m**, and low to no conversions for 3-methyl-2-cyclopenten-1-one **1c** and 3-methylcyclohexenone **1f** (**Figure 3A, Table S4**).

Substrate 3-methylcyclohexenone **1f** was better reduced with the double mutant *Ts*OYE-C25D/I67T (92% *ee R*) and OYE2 (99% *ee S*), giving access to both product enantiomers, despite low conversion rates (10-20%) (see **Table S4**).[27] 25 mM and 1 M ammonium formate buffer were not tested for **1f** because of the already low conversions with Tris-HCl buffer pH 8.0. Interestingly, when we studied this same buffer effect but with NADPH/GDH recycling system planned for the whole cascade, the conversions were drastically affected by the presence of high concentrations of ammonium formate buffer (B), which was not the case with BNAH (A/B). We hypothesize the GDH may be the limiting factor in these high ionic strength conditions,[29] despite its use in many reduction processes with such buffer. Based on this buffer study, 1 M ammonium formate buffer was beneficial for the reductive amination step, benign to the OYE conversions but detrimental to the GDH regeneration system. Nevertheless, we decided to proceed with this important prerequisite for the AmDH activity, taking care of reaction times and optimized amount of OYE/GDH to counter this negative effect.

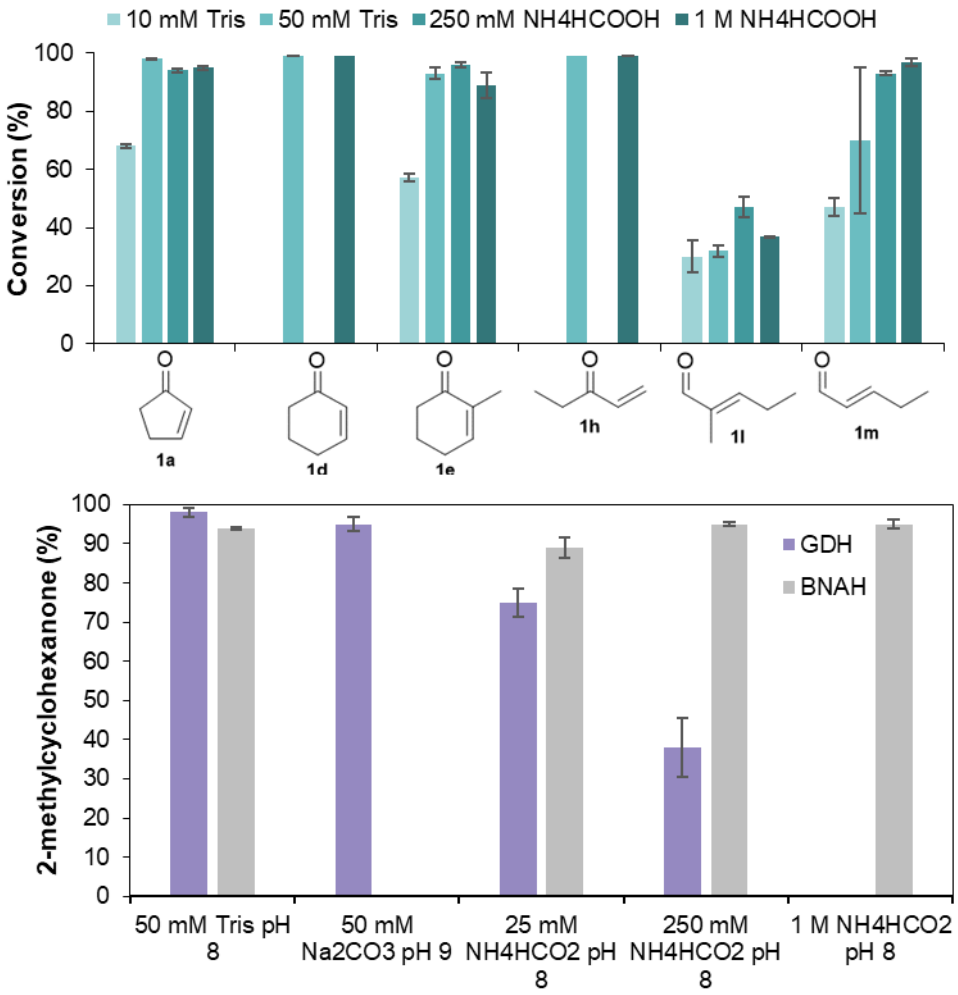

Figure 2. (**A**) *Ts*OYE-catalyzed reduction of unsaturated ketones and aldehyde substrates **1** after 1 h with BNAH. Conditions: 2 µM *Ts*OYE, 10 mM alkene **1**, 15 mM BNAH, 10% v/v DMSO, 1 mL volume. **1d** and **1h** were tested in 50 mM Tris-HCl and 1 M NH_4HCO_2 only. Average of duplicates. (**B**) *Ts*OYE-catalyzed reduction of 2-methylcyclohexenone **1e** after 1 h using GDH-recycled NADPH (in purple) or BNAH (in grey). Conditions: 1% v/v DMSO, 2 µM *Ts*OYE, 10 mM 2-methylcyclohexenone in different buffer conditions, 1 mL volume. Average of duplicates. purple: with GDH cofactor recycling system: 175 U/mL GDH-105, 0.1 mM NADPH, 12 mM glucose. grey: with 11 mM BNAH cofactor.

Substrates 2-methylbutenal **1k** and 2-methylpentenal **1l** were further screened with three OYEs for conversion and *ee*. As **1l** was a mixture of both *cis* and *trans* isomers, the conversion was limited to 50% conversion as *Ts*OYE prefers the *trans* over the *cis* isomer. Thus, we screened the *trans*-**1k** and *trans*-**1l** with *Ts*OYE, *Gk*OYE and GluER. With *Gk*OYE and GluER we obtained a

significantly higher *ee* of products 2-methylbutanal **2k** and 2-methylpentanal **2l** (**Figure 3**).

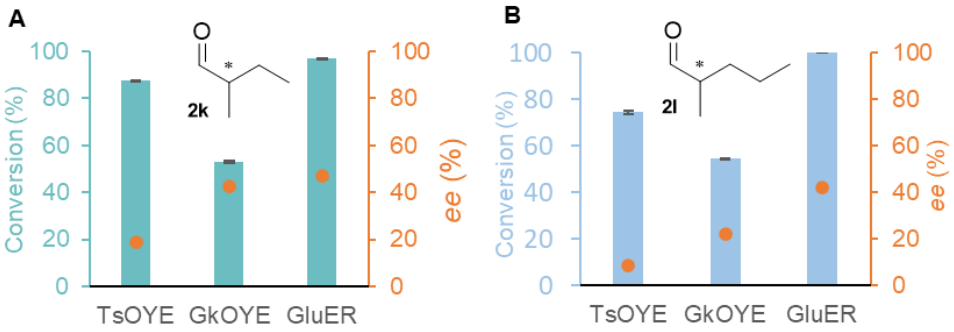

Figure 3. Conversion of unsaturated aldehydes **1k** and **1l** by *Ts*OYE, *Gk*OYE and *Glu*ER after 1 h with BNAH. Brown circles show *ee*. Conditions: 1 µM *Ts*OYE or *Gk*OYE or *Glu*ER, 10 mM substrate **1**, 15 mM BNAH, 10% v/v DMSO, 1mL volume in 50 mM Tris-HCl buffer pH 8.0. **(A)** *trans*-2-methylbutenal **1k**; **(B)** *trans*-2-methylpentenal **1l**.

In terms of nicotinamide cofactor, the selected AmDHs displayed high preference either for the phosphorylated form NADPH (*Cfus*AmDH, MATOUAmDH2, *Msme*AmDH and *Micro*AmDH) or NADH (*Chat*AmDH, IGCAmDH5 and *Apau*AmDH). The OYEs used in this study are reported to prefer NADPH over NADH, seen for **1b**, **1j-1m** (**Figure S5**), but the use of recycled NADH still provides good conversions.[31] Therefore, the preferred cofactor for AmDH enzymes were chosen in priority.

We proceeded with investigating the impact of DMSO for both types of enzymes to have a preliminary state of potential OYEs-AmDHs cascade reactions at high substrate loadings, which usually required addition of co-solvent for solubilization. For OYEs, 1 to 20% v/v DMSO were tested with *Ts*OYE toward **1d**. These amounts of DMSO have a low impact on the conversions, as the conversion at 20% v/v was 85% compared to 97% at 1% v/v DMSO (**Figure 4A**). For AmDHs, their tolerance to DMSO was studied by measuring specific activity for substrate **2j** (**Figure 4B**). All the studied AmDHs maintained at least 50% of their maximum activity at 5% v/v DMSO, except for *Chat*AmDH, for which a higher decrease was observed (37% of maximum specific activity at 5% v/v DMSO). AmDHs *Msme*AmDH, *Cfus*AmDH and *Micro*AmDH gave the highest resistance to DMSO at 5% v/v DMSO with more than 70% activity retained. Above 10% v/v DMSO, *Msme*AmDH, IGCAmDH5 and *Micro*AmDH were the more tolerant enzymes with even higher activity in the presence of DMSO for *Micro*AmDH. Based on these results, 1% v/v DMSO could be used to test each substrate in the cascade at 10 mM without high negative impact on conversions. Higher percentages than 1% v/v of this co-solvent could surely be used for further scaled up reactions at higher substrate concentrations, especially with *Micro*AmDH for

AmDH and *Ts*OYE for OYEs, subject to prior stability tests under 5-20% v/v DMSO.

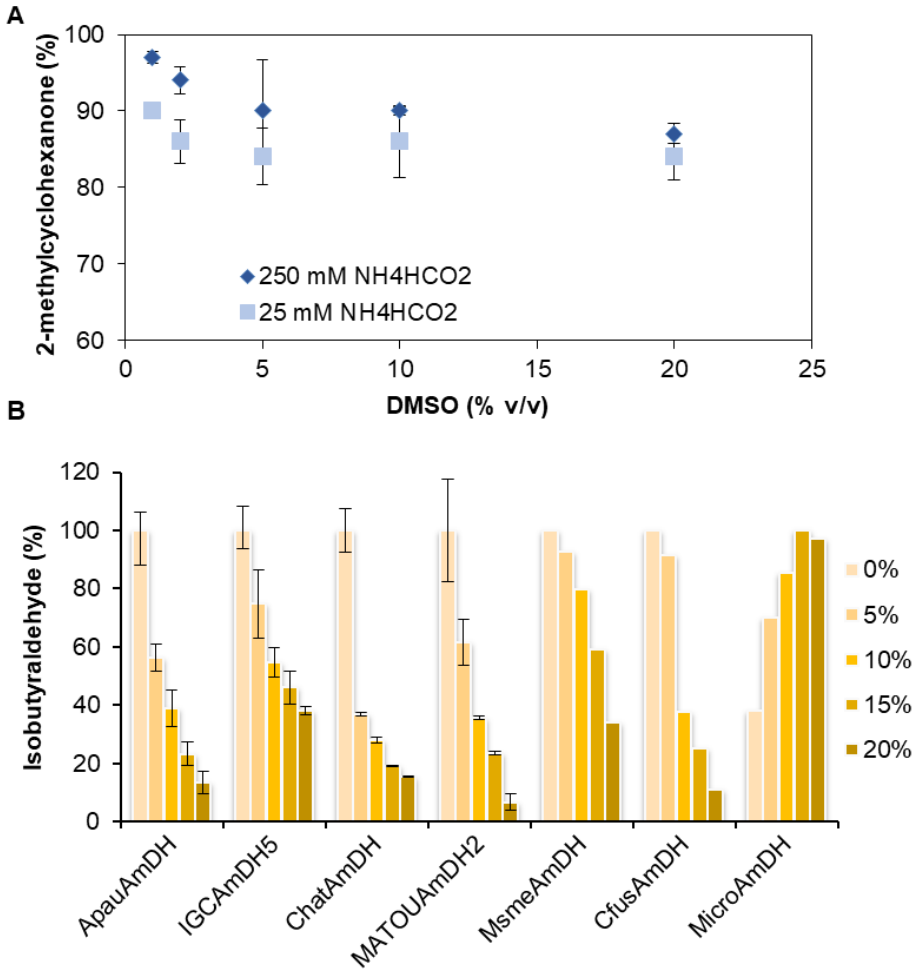

Figure 4. (A) *Ts*OYE-catalyzed reduction of 2-methylcyclohexenone **1e** to 2-methylcyclohexanone **2e** with 0-20% v/v DMSO after 1 h. Conditions: 2 µM *Ts*OYE, 10 mM**1e**, 11 mM BNAH cofactor. Average of duplicates. (**B**) Specific activities of AmDHs for isobutyraldehyde **2j** in the presence of 0, 5, 10, 15 and 20% v/v DMSO. For each AmDHs, their maximum specific activity was set up at 100%, which corresponds to specific activity without co-solvent for *Apau*AmDH, IGCAmDH5, *Chat*AmDH, MATOUAmDH2, *Msme*AmDH and *Cfus*AmDH, and to specific activity with 15% DMSO for MicroAmDH. Conditions: 5 mM substrate (**2j** for *Apau*AmDH, IGCAmDH5, *Chat*AmDH and **2d** for MATOUAmDH2, *Msme*AmDH, *Cfus*AmDH and *Micro*AmDH), 0.04-0.10 mg/mL purified AmDH, 0.4 mM NADH (NADPH for MATOUAmDH2) in 1 M ammonium formate buffer pH 9.0 at room temperature (20 °C) (*Apau*AmDH, *Msme*AmDH, *Cfus*AmDH, *Micro*AmDH) or 50 °C (IGCAmDH5, MATOUAmDH2, *Chat*AmDH). Specific activities were calculated based on spectrophotometric assay (see SI for details). Average of duplicates.

AmDH activity towards ketone and aldehyde intermediates

All AmDHs used in this study were previously characterized in term of substrate profile, however these data were in majority specific activities, not conversions rates, and did not cover all the set of substrates defined for this work. AmDHs *Cfus*AmDH, *Chat*AmDH, IGCAmDH5, *Apau*AmDH, MATOUAmDH2, *Msme*AmDH and *Micro*AmDH were therefore tested toward aldehydes and ketones **2a**-**2m** in addition to the corresponding unsaturated compounds **1a**-**1m** for reductive amination in the conditions defined for OYEs in cascade reaction.

Each series of substrate was tested with the enzyme(s) showing the highest specific activities in previous reported results toward exactly or the more structurally similar substrate. From this screening, selected enzymes for each series of compounds were the enzymes showing the higher amount of amines toward the carbonyl form while exhibiting no or very low activity toward the unsaturated carbonyl to avoid any side product of unsaturated amine **4a**-**4m** (see **Figure S8-S10** for details). This screening was carried out in 96-well plate in 100 µL total final volume at 0.5 mg/mL of purified enzyme and amine amounts were estimated using calibration curves and ultra-high performance liquid chromatography coupled to mass spectrometry (UHPLC-MS) assay (see SI). Despite some inconsistencies due to screening in 96-well plate with uncontrolled evaporation of some aldehydes, results were viable to compare the enzymes for one substrate and so to select the more appropriate enzyme(s) for the cascade reaction. These selected enzymes are highlighted in yellow for each substrate **a**-**m** in **Table 2**.

Multi-enzymatic cascade analysis

We proceeded to perform the full cascade reactions with both selected OYEs and AmDHs based on their initial individual screening for each substrates considered (**Table 3**). Each combination OYE-AmDHs-unsaturated substrate 1 was chosen to obtain the highest enantioselectivity and conversion (see SI). The reactions were carried out with the preliminary conditions defined for the cascade *i.e.* ammonium formate 1 M pH 8.0 with 1% v/v DMSO, nicotinamide cofactor preferred by the AmDH and glucose/GDH cofactor recycling system. The concentration of amine products **3a**-**3m** were quantified with GC calibration curves using standards when commercially available (**Table 3**, see SI), enantiomeric (*ee*) and diastereomeric excess (*de*) were determined by derivatization (see SI).

Table 2. AmDH screening for the reductive amination of saturated carbonyl substrates **2**.[a]

	[corresponding amines 3 a-m] (mM)												
AmDH	2a	2b	2c	2d	2e	2f	2g	2h	2i	2j[d]	2k	2l[e]	2m[e]
*Cfus*AmDH[b]	3.4		1.6							nd	7.1	1.8	0.5
*Chat*AmDH[c]										nd	8.2	0.4	0.1
IGCAmDH5[c]										nd	7.8	0.6	0.1
*Apau*AmDH[c]										nd	10.0	0.6	1.9
MATOUAmDH2[b]	4.1	0.5	0.7	3.5	1.2	1.9	2.3	0.1	0.9	nd	5.2	2.2	0.1
*Msme*AmDH[b]		0.8			2.2	3.4	2.3	1.2	1.2				
*Micro*AmDH[b]	2.9	0.5	2.4	4.3	3.7	4.5		1.5		nd			0.9

[a] Amounts of amine (mM) obtained with each enzyme toward tested ketones/aldehydes are reported. Colors indicate the favorite enzyme (**yellow**), good candidate (**orange**) and other potential candidates (**grey**) for the cascade. Conditions: 0.5 mg/mL AmDH, 10 mM substrate, [b] 0.2 mM NADP or [c] 0.2 mM NAD, 3 U/mL GDH105, 24 mM glucose, 5 mM $CaCl_2$, 1 M NH_4HCO_2 pH 8.0, 24 h at 30 °C, volume = 100 µL in 96-well plate. The amounts of amine **3** were deduced from calibrations curves after derivatization of reaction mixtures with benzoyl chloride and UHPLC-MS analysis. Reported results are average of duplicates. See SI and Figures S8 for results with enones **1**. [d] isobutylamine **3j** was not detected probably due to evaporation of this volatile compound; previously reported results allowed us to select the preferred AmDH for this substrate (data not shown); [e] these conversions are underestimated due to evaporation of the compounds; blank boxes = not tested; *nd* = not detected.

Starting from 10 mM substrate, the cascades with the cyclic pentenones (**1a**-**1c**) showed low to moderate amine concentrations (0.49 to 3.20 mM), which is in concordance with the low to moderate activity of *Ts*OYE and AmDHs toward these substrates. In the case of **3b**, very low selectivity was measured, probably due to racemization of **2b** in the reaction mixture. With OYE2 instead of *Ts*OYE we still obtained **3c** in low quantity (0.49 mM, (1*S*) = 99% *de* and (3*S*) = 99% *de*). The cyclic hexenones (**1d**-**1f**) gave reasonable conversions (3.4 to 4.9 mM), in concordance with the conversions rates of 30–83% for both *Ts*OYE toward **1e**-**1f** and *Msme*AmDH/*Micro*AmDH toward **2e**/**2f**,[5] respectively. Although these conversions remain low, the high diastereoisomeric excess obtained for (1*S*,2*R*)-**3e** ((1*S*) = 99% *de* (2*R*) = 93% *de*) and (1*S*,3*R*)-**3f** ((1*S*) = 99% *de* and (3*R*) = 99% *de*) are remarkable and demonstrate the asset of this cascade. Without the first step, amines **3e** and **3f** were previously reported to be obtained with much worse diastereoisomeric excess, respectively (2*R*) = 36% *de* and (3*S*) = 4% *de* with **2e**/*Msme*AmDH and **3e**/*Micro*AmDH.[5] Thus, the imperfect stereopreference of AmDHs toward α/β-substituted ketones can be compensated by the high stereoselectivity of *Ts*OYE C25D/I67T, and the subsequent stereochemical control of the amine center is brought by the AmDH. Starting from substituted enones and performing this cascade is so a good strategy to access α/β

substituted primary chiral amines with high controlled chirality. We also produced the opposite enantiomer **3f** by using OYE2 instead of *Ts*OYE C25D/I67T (2.4 mM, >99% *de* for (1*S*,3*S*)-**3f**) The precedent results reported for the synthesis of **3f** by coupling OYE1 and TAs gave a diastereomeric excess *de* of 98% to 99% for (1*S*,3*S*)-**3f** at 78% and 62% conversion with ATA-113 and ATA-237, respectively. In this former study, higher amounts of enzyme were used for the second step (2 mg/mL) and longer reaction time (36 h vs 24 h), but lower amount of OYE were required (60 µg/mL) as OYE2 was active toward **1f** in contrast with *Ts*OYE.

The linear aliphatic unsaturated ketones (**1g**-**1i**) were good to excellent substrates for *Ts*OYE, but poor to moderate for the AmDH chosen, namely *Msme*AmDH and *Micro*AmDH. Nevertheless, 2-aminobutane **3g** was observed with high conversion (75%) and *ee* (92%). The pentylamine **3i** was quantified to 1.5 mM, this low amine amount being certainly due to the already poor conversion obtained with *Msme*AmDH for this substrate at more appropriate pH 9.5 (27%).[5] We observed an excellent *ee* of 99% for linear aliphatic amines such as 2-aminopentane **3i**, in accordance with the high *ee* reported with the tested AmDH.[5] Even if the 3-aminopentane **3h** was obtained in only 35%, this result is highly of interest. Indeed, native enzymes performing the intrinsic or apparent reductive amination (RedAms, AmDHs, TA) are not, or very poorly, active toward substrates harboring larger substituent than methyl for the smaller substituted group. *Micro*AmDH is so a promising enzyme for reductive amination of ethyl-substituted ketones, the same for its use coupled with OYEs on corresponding enones.

Concerning aldehydes, since GluER displayed a higher selectivity for 2-methylbutanal **1k** compared with *Ts*OYE (**Figure 3**), we performed the cascade with GluER for this substrate, affording full conversion with 99% *ee* (**Table 3**). We ascribe the excellent *ee* obtained here compared with **Figure 2** to the *in situ* conversion of the reduced enal to the corresponding amine, avoiding racemization. Both *Apau*AmDH and GluER led to full conversion on isolated steps. The larger unsaturated aldehydes 2-methylpentenal **1l** and pentenal **1m** were good substrates for GluER and *Ts*OYE, but poor for the AmDHs chosen, thus explaining the lower calculated conversions (42% and 7%, respectively). Furthermore, the selectivity obtained for 2-methylpentylamine **3l** was low, also probably because of racemization of intermediate **2l** in the reaction mixture.

No formation of the unsaturated amines **4** was observed in these cascade reactions, which confirms the high chemoselectivity of the AmDHs toward saturated carbonyl substrates **2** versus unsaturated carbonyl substrates **1**, while benefiting from the much higher activity of OYEs compared with AmDHs toward enones and enones/enals **1**. Thus, the EREDs/AmDHs combination can be run in one pot cascade reactions without requiring a sequential procedure. Interestingly, presence of small amount of alcohol in reactions with substrates **1d**,

1e, **1i** and **1k**, was observed (data not shown). Formation of alcohol **5d** was quantified by GC-MS to facilitate peak attribution due to partial co-elution. The effective amount of **5d** due to MATOUAmDH2 was less than 0.14 mM in NH_4HCO_2 buffer pH 8.0. At pH 10.0, this amount was similar in reaction mixture containing the enzyme compared to the one without any AmDH (0.17-0.21 mM) (see SI). To minimize the direct reduction of ketone to alcohol while maintaining sufficient activity of OYEs, pH 9.0 was preferred over pH 8.0 for the reaction scale-up and increased the concentration of *Ts*OYE from 2 to 10 µM to compensate for its lower activity at this pH (*vide infra*). The presence or absence of alcohol was also dependent on the substrate, certainly due to varying distances and orientations between the carbon atom of the ketone/aldehyde in case of direct reduction or of the iminium intermediate in case of reductive amination. This point was not further studied in this work but was recently described by Mutti and co-workers,[32, 33] and investigated in another research article.[34]

Table 3. Overview of proposed multi-enzymatic cascade OYE-AmDH combinations per substrate.[a]

1	ER	2	AmDH	3	Cofactor	Conf.	[Amine] (mM)	*ee* (%)	*de* (%)
1a 	*Ts*OYE	2a 	MATOU-AmDH2	3a 	NADPH	-	3.2	-	-
1b 	*Ts*OYE	2b 	*Msme*-AmDH	3b 	NADPH	(*S*,*R*)	2.7	31	31
1c 	OYE2	2c 	*Micro*-AmDH	3c 	NADPH	(*S*,*S*)	0.5	99	99
1d 	*Ts*OYE	2d 	MATOU-AmDH2	3d 	NADPH	-	4.6	-	-
1e 	*Ts*OYE	2e 	*Msme*-AmDH	3e 	NADPH	(*S*,*R*)	3.4	99	93
1f 	*Ts*OYE -C25D/ I67T	2f 	*Micro*-AmDH	3f 	NADPH	(*S*,*R*)	4.9	99	99
1g 	*Ts*OYE	2g 	*Msme*-AmDH	3g 	NADPH	(*S*)	7.5	92	-
1h 	TsOYE	2h 	*Micro*-AmDH	3h 	NADPH	-	3.5	-	-
1i 	*Ts*OYE	2i 	*Msme*-AmDH	3i 	NADPH	(*S*)	1.5	99	-
1j 	TsOYE	2j 	*Micro*-AmDH	3j 	NADPH	-	2.4	-	-
1k 	GluER	2k 	*Apau*-AmDH	3k 	NADH	(*R*)	10.0	99	-
1l 	TsOYE	2l 	MATOU-AmDH2	3l 	NADPH	(*R*)	4.2	48	-
1m 	*Ts*OYE	2m 	MATOU-AmDH2	3m 	NADPH	-	0.7	-	-

[a] Conditions: 1 M NH_4HCO_2 buffer pH 8.0, 10 mM substrate, 24 mM glucose, 0.2 mM NAD(P)H, 3 U/mL GDH-105, 10 µM *Ts*OYE or 20 µM OYE2, 0.5 mg/mL AmDH, 1 mL volume. Amine products obtained after 24-h one-pot multi-enzymatic cascade reaction. Conditions: 1 mL volume containing 1 M NH_4HCO_2 buffer pH 8.0, 3 U/mL GDH-105, 24 mM glucose, 0.2 mM $NAD(P)^+$, 0.5 mg/mL AmDH indicated in Table 3, 10 µM *Ts*OYE or *Ts*OYE-C25D/I67T for **3f**, or 3 µM GluER for **3k**), or 20 µM OYE2 for **3c**, and 10 mM alkene **1**, 1% v/v DMSO. See SI for more results.

Finally, for a small scale-up synthesis we selected the best substrate 2-methylbutanal **1k** in combination with *Apau*AmDH and GluER. The multi-enzymatic cascade was carried out with 50 mM substrate **1k** in a total volume of 20 mL and afforded 21% conversion (10% isolated yield), after 24 hours, to 2-methylbutylamine **3k** with 99% *ee*. We ascribe the low conversion to non-optimized conditions with the increased substrate concentration. The pure chiral amine was isolated as a hydrochloride salt as previously described, demonstrating the applicability of this multi-enzymatic cascade (see SI).[5]

Conclusion

In this study, we established a multi-enzymatic cascade with OYE and AmDH enzymes to produce various substituted chiral amines. We explored the capacity of the cascade by determining the reaction conditions of each step, and the enantiopurity, the diastereomeric excess and conversion from substrate to amine. We designed an efficient multi-enzymatic cascade capable of producing chiral amines with high enantioselectivity and diastereomeric excess (both 99%). The lack of or very low activity of AmDHs toward enones is of great advantage to perform an easy protocol of one pot cascade in simultaneous mode. Before considering chiral amine production on a larger scale, there is still room for improvement, as most cascades resulted in amine concentrations of 5 mM from 10 mM substrate. Nevertheless, the combination of these types of enzymes shows potential to produce chiral amines efficiently.

Despite reduced performance of OYEs in reaction medium rich in ammonia required for the AmDH step, high optical purity of amine can be isolated, as exemplified with the synthesis of (2*R*)-2-methylbutanamine obtained with 99% *ee*. These results can give rise to extended amine products by using other members of OYEs and AmDHs families, still in expansion. This cascade is even more interesting as the substrates enones are substituted to access to diastereomerically enriched amines. Nevertheless, this can be also beneficial in the case of non-substituted ones. Indeed, enones can be more easily accessible than their reduced form ketones, depending on commercial resources or synthetic schemes. Enones are indeed products of key chemical reactions extensively used in synthetic strategies such as dehydration of aldol or Wittig-Horner reactions.

The portfolio of AmDHs is growing,[19] thus enabling the access of both amine chirality by using either (*S*)-selective AmDHs such as the ones used in this study, or (*R*)-selective AmDHs such as engineered-AADHs and ε-deaminating L-lysine dehydrogenase.[19] This cascade is therefore a real alternative to the already described EREDs/TA cascade and can be extended to structurally

diverse amines, again thanks to the wide substrate scope of both OYEs and NAD(P)H-dependent enzymes performing reductive amination.

Materials and Methods

General information

All chemicals were obtained from commercial suppliers Sigma-Aldrich, Acros Organics, Alfa Aesar, TCI Europe and abcr GmbH with the highest purity available and used as received. Glucose dehydrogenase GDH-105 was generously donated by Codexis®. UV-vis absorbance was measured with a Cary 60 spectrophotometer. Compound analyses were carried out on Shimadzu GC-2010 gas chromatographs (Shimadzu, Japan) with an AOC-20i Auto injector and equipped with a flame ionization detector (FID), using nitrogen or helium as the carrier gas. GC-MS analyses were performed on a GC (ThermoFisher Focus GC) coupled to a single-quadrupole mass spectrometer (ThermoFisher DSQ II). The instrument was equipped with a non-polar 30 m × 0.25 mm × 0.25 um DB-5MS column (Agilent) and split/splitless injector. Carrier gas was helium at a constant flow rate of 1 mL/min. Injection and transfer line temperature were set up at 200°C and 250 °C, respectively. MS detection was performed in electronic impact ionization, positive mode, ion source 220 °C, detector voltage 70 eV, full scan mode. Glucose dehydrogenase GDH-105 was generously donated by Codexis®. UHPLC-MS analyses were performed on a UHPLC U3000 RS 1034 bar system (Thermo Fisher Scientific, Waltham, USA) equipped with a DAD3000 diode array detector and a MSQ Plus™ Single Quadrupole Mass Spectrometer with electrospray SI in positive mode (cone voltage = 75 V, probe temperature set up at 450 °C). The UHPLC column was a Kinetex® F5 (Phenomenex) column (100 × 2.1 mm; 1.7 µm)

Example of asymmetric reduction reactions with *Ts*OYE

The reactions were performed in 50 mM Tris-HCl buffer, pH 8.0 in a final volume of 1.0 mL: 10 mM substrate **1**, with either: 0.1 mM NADPH, 11 mM glucose, 5 mg/ml GDH or 11 mM BNAH; 2 µM *Ts*OYE, 1% v/v DMSO; in a thermomixer at 900 rpm and 30 °C for 1 h on a Thermomixer (Eppendorf). Extraction was carried out with 0.5 mL EtOAc, dried over $MgSO_4$ and analyzed by GC-FID.

Example of reductive amination reactions with AmDHs

The selected AmDHs (*Cfus*AmDH, *Chat*AmDH, IGCAmDH5, *Apau*AmDH, MATOUAMDH2, *Msme*AmDH, *Micro*AmDH) were tested toward ketones **2a**-**m** and enones **1a**-**m** in 96-well plate with cofactor regeneration system using UHPLC-MS monitoring. To a reaction mixture (total volume 100 µL)

containing 10 mM substrate (10 mM of ketone **2** + 10 mM of enone **1** in case of mixture of substrate), 0.2 mM NAD(P)$^+$, 24 mM glucose, 5 mM $CaCl_2$, 3 U/mL glucose dehydrogenase (GDH-105) in 1 M NH_4HCO_2 buffer pH 8.0, was added 0.5 mg/mL of purified AmDH. The 96-well plate was covered with a lid and left for reaction 24 h at 30 °C in a thermocontrolled oven. Reaction mixtures were analyzed by UHPLC-MS after derivatization with benzoyl chloride. Background reactions were performed in the same manner but with mixtures lacking the substrate or the purified AmDH.

Example of multi-enzymatic cascade reaction

Cascade reactions were performed in 1 M NH_4HCO_2 buffer (pH 8.0, 2 M NH_4OH to adjust the pH) in a total volume of 1mL: 10 mM substrate **1**, 0.2 mM NAD(P)H, 3 U/mL GDH-105, 24 mM glucose, 0.5 mg/mL AmDH, 3-25 µM OYE, 1% v/v DMSO; in a thermomixer at 400 rpm and 30 °C. After 24 h 1 mL of 10 M NaOH was added and the mixture vortexed, followed by extraction with two times 0.5 mL EtOAc, dried over $MgSO_4$ and analyzed by GC-FID. Derivatization with Ac_2O was carried out when necessary for *ee* determination on a chiral column.[35]

The complete supporting information, including supplementary Figures S12-S25, and S29-S72 can be found at: doi.org/10.1002/cctc.202101576

Supporting information

OYE accession numbers and sequences

Thermus scotoductus Old Yellow Enzyme (*Ts*OYE) accession number B0JDW3
MALLFTPLELGGLRLKNRLAMSPMCQYSATLEGEVTDWHLLHYPTRALGGVGLILVEAT
AVEPLGRISPYDLGIWSEDHLPGLKELARRIREAGAVPGIQLAHAGRKAGTARPWEGGK
PLGWRVVGPSPIPFDEGYPVPEPLDEAGMERILQAFVEGARRALRAGFQVIELHMAHG
YLLSSFLSPLSNQRTDAYGGSLENRMRFPLQVAQAVREVVPRELPLFVRVSATDWGEG
GWSLEDTLAFARRLKELGVDLLDCSSGGVVLRVRIPLAPGFQVPFADAVRKRVGLRTGA
VGLITTPEQAETLLQAGSADLVLLGRVLLRDPYFPLRAAKALGVAPEVPPQYQRGF

Saccharomyces cerevisiae Old Yellow Enzyme 2 (OYE2) accession number Q03558
MPFVKDFKPQALGDTNLFKPIKIGNNELLHRAVIPPLTRMRAQHPGNIPNRDWAVEYYAQ
RAQRPGTLIITEGTFPSPQSGGYDNAPGIWSEEQIKEWTKIFKAIHENKSFAWVQLWVLG
WAAFPDTLARDGLRYDSASDNVYMNAEQEEKAKKANNPQHSITKDEIKQYVKEYVQAA
KNSIAAGADGVEIHSANGYLLNQFLDPHSNNRTDEYGGSIENRARFTLEVVDAVVDAIGP
EKVGLRLSPYGVFNSMSGGAETGIVAQYAYVLGELERRAKAGKRLAFVHLVEPRVTNPF
LTEGEGEYNGGSNKFAYSIWKGPIIRAGNFALHPEVVREEVKDPRTLIGYGRFFISNPDL
VDRLEKGLPLNKYDRDTFYKMSAEGYIDYPTYEEALKLGWDKN

Bacillus subtilis Old Yellow Enzyme (YqjM) accession number P54550
MARKLFTPITIKDMTLKNRIVMSPMCMYSSHEKDGKLTPFHMAHYISRAIGQVGLIIVEAS
AVNPQGRITDQDLGIWSDEHIEGFAKLTEQVKEQGSKIGIQLAHAGRKAELEGDIFAPSAI

AFDEQSATPVEMSAEKVKETVQEFKQAAARAKEAGFDVIEIHAAHGYLIHEFLSPLSNHR
TDEYGGSPENRYRFLREIIDEVKQVWDGPLFVRVSASDYTDKGLDIADHIGFAKWMKEQ
GVDLIDCSSGALVHADINVFPGYQVSFAEKIREQADMATGAVGMITDGSMAEEILQNGR
ADLIFIGRELLRDPFFARTAAKQLNTEIPAPVQYERGW

Gluconobacter oxydans Old Yellow Enzyme (*Glu*ER) accession number A1E8I9
MPTLFDPIDFGPIHAKNRIVMSPLTRGRADKEAVPTPIMAEYYAQRASAGLIITEATGISRE
GLGWPFAPGIWSDAQVEAWKPIVAGVHAKGGKIVCQLWHMGRMVHSSVTGTQPVSSS
ATTAPGEVHTYEGKKPFEQARAIDAADISRILNDYENAARNAIRAGFDGVQIHAANGYLID
EFLRNGTNHRTDEYGGVPENRIRFLKEVTERVIAAIGADRTGVRLSPNGDTQGCIDSAP
ETVFVPAAKLLQDLGVAWLELREPGPNGTFGKTDQPKLSPQIRKVFLRPLVLNQDYTFE
AAQTALAEGKADAIAFGRKFISNPDLPERFARGIALQPDDMKTWYSQGPEGYTDYPSAT
SGPN

Geobacillus kaustophilus (strain HTA426) Old Yellow Enzyme (*Gk*OYE) accession number Q5KXG9
MNTMLFSPYTIRGLTLKNRIVMSPMCMYSCDTKDGAVRTWHKIHYPARAVGQVGLIIVEA
TGVTPQGRISERDLGIWSDDHIAGLRELVGLVKEHGAAIGIQLAHAGRKSQVPGEIIAPSA
VPFDDSSPTPKEMTKADIEETVQAFQNGARRAKEAGFDVIEIHAAHGYLINEFLSPLSNR
RQDEYGGSPENRYRFLGEVIDAVREVWDGPLFVRISASDYHPDGLTAKDYVPYAKRMK
EQGVDLVDVSSGAIVPARMNVYPGYQVPFAELIRREADIPTGAVGLITSGWQAEEILQNG
RADLVFLGRELLRNPYWPYAAARELGAKISAPVQYERGWRF

OYE production and purification

The OYEs were produced as previously described *via* recombinant heterologous expression of the genes in *E. coli*. For *Glu*ER, OYE2, YqjM, and *Gk*OYE, the genes were cloned in pET-28a(+) plasmids with an *N*-terminal His-tag, with restriction enzymes NdeI and XhoI (Baseclear, Leiden, The Netherlands). *Ts*OYE wild-type and *Ts*OYE-C25D/I67T double mutant were in a pET-22b(+) plasmid without His-tag. Briefly, the plasmids were transformed into *E. coli* BL21(DE3) (BL21 Gold(DE3) for OYE2) competent cells using the supplier protocol (Novagen, Merck). 10 mL of LB overnight pre-cultures were diluted 1:100 in LB medium (0.5 L in 2-L glass Erlenmeyer flasks, or 1 L in 5-L glass Erlenmeyer flasks) shaken at 37 °C at 180 rpm until the OD_{600} reached 0.6. IPTG was added to a final concentration of 0.1 mM, and the cultures were shaken at 25 °C at 180 rpm for 18 h. The broth was centrifuged at 4 °C and 10,000 rpm for 10 min. The supernatant was removed, and the cell pellets were resuspended in 50 mM MOPS-NaOH buffer pH 7.0, then centrifuged at 4,000 rpm and 4 °C for 15 min. The supernatant was removed, and the cell pellets were stored overnight at -80 °C. The pellets were then thawed, resuspended in 50 mM MOPS-NaOH buffer pH 7.0 (1:4), and supplemented with a small spatula tip of DNase I and $MgCl_2$, and one pill of EDTA-free cOmplete™ protease inhibitor cocktail. This mixture was passed through a cell disrupter Multi Shot Cell Disruption System (one cycle)

and centrifuged at 10,000 rpm and 4 °C for 30 min. The supernatant containing the OYE enzyme was then further used for purification.

The *Ts*OYE wild-type, *Ts*OYE-C25D/I67T double mutant and *Gk*OYE were heat purified by incubation in a water bath at 70 °C for 1.5 h. The resulting mixture was centrifuged at 8,000 rpm and 4 °C for 30 min. OYE2, GluER and YqjM were purified by affinity column chromatography as previously described.[36, 37]

FMN was added (amounts determined according to protein content) to the thawed enzyme solution. The solution was then concentrated with an ultrafiltration centrifugal filter (30 kDa cut-off, Amicon® Ultra-15 Centrifugal Filter Devices). The excess of FMN was removed with a PD-10 Desalting column (GE Healthcare) with 50 mM MOPS-NaOH pH 7.0 buffer. Purified enzymes were frozen as droplets in liquid nitrogen and stored at -80 °C.

Sodium dodecyl sulphate polyacrylamide gel electrophoresis (SDS-PAGE) was run to determine enzyme purity (**Figure S1**). Samples were prepared by mixing samples with Laemmli buffer and 5% v/v dithiothreitol (DTT). Enzyme concentration was determined by UV-Vis spectrophotometry and by the bicinchoninic acid (BC) assay (Uptima BC Assay).

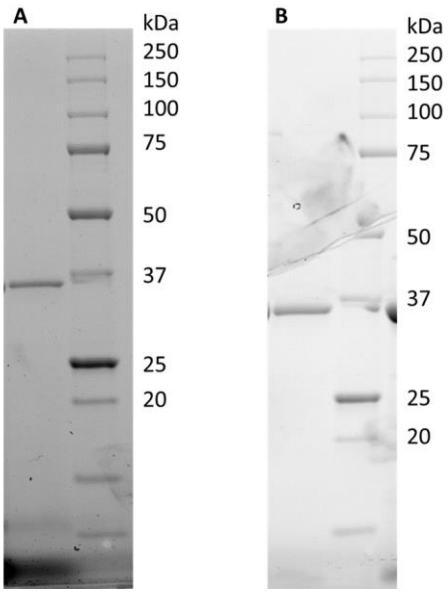

Figure S1. SDS-PAGE gels of *Ts*OYE and *Ts*OYE-C25D/I67T. **A**: *Ts*OYE after purification on the left lane, protein-ladder on the right lane. **B**: *Ts*OYE-C25D/I67T after purification on the left lane, protein-ladder on the right lane. Each sample was prepared by adding an equivalent volume of Laemmli buffer. From this mixture, 15 µL was loaded onto the gel.

AmDH production and purification

AmDHs used in this study were produced and purified as previously described. *Cfus*AmDH, *Msme*AmDH, *Apau*AmDH and *Micro*AmDH were produced and purified according to Mayol *et al*..[5] *Chat*AmDH, IGCAmDH5 and MATOUAmDH2 were produced and purified according to Caparco *et al*.[6]

Substrates, intermediates and product names

Table S1. List of alkene substrates, carbonyl intermediates and amine products with assigned numbers.

	Alkene substrates		Carbonyl intermediates		Amine products
1a	2-cyclopenten-1-one	2a	cyclopentanone	3a	cyclopentylamine
1b	2-methyl-cyclopentenone	2b	2-methylcyclopentanone	3b	2-methylcyclopentylamine
1c	3-methyl-2-cyclopentenone	2c	3-methylcyclopentanone	3c	3-methylcyclopentylamine
1d	2-cyclohexenone	2d	cyclohexanone	3d	cyclopentylamine
1e	2-methyl-2-cyclohexenone	2e	2-methylcyclohexanone	3e	2-methylcyclohexylamine
1f	3-methyl-2-cyclohexenone	2f	3-methylcyclohexanone	3f	3-methylcyclohexylamine
1g	3-buten-2-one	2g	2-butanone	3g	2-aminobutane
1h	penten-3-one	2h	diethylketone	3h	3-aminopentane
1i	penten-2-one	2i	2-pentanone	3i	2-aminopentane
1j	methacrolein	2j	isobutyraldehyde	3j	isobutylamine
1k	*trans*-2-methyl-2-butenal	2k	2-methylbutanal	3k	2-methylbutylamine
1l	*trans*-2-methyl-2-pentenal	2l	2-methylvaleraldehyde	3l	2-methylpentylamine
1m	*trans*-2-pentenal	2m	valeraldehyde	3m	amylamine

Table S2. List of enamine and alcohol by-products, with assigned numbers

	Enamine products		Alcohol products
4a	cyclopent-2-en-1-amine	5a	cyclopentanol
4b	2-methylcyclopent-2-en-1-amine	5b	2-methylcyclopentanol
4c	3-methylcyclopent-2-en-1-amine	5c	3-methylcyclopentanol
4d	cyclohex-2-en-1-amine	5d	cyclohexanol
4e	2-methylcyclohex-2-en-1-amine	5e	2-methylcyclohexanol
4f	3-methylcyclohex-2-en-1-amine	5f	3-methylcyclohexanol
4g	but-3-en-2-amine	5g	2-butanol
4h	pent-1-en-3-amine	5h	3-pentanol
4i	pent-3-en-2-amine	5i	2-pentanol
4j	2-methylprop-2-en-1-amine	5j	isobutanol
4k	*trans*-2-methylbut-2-en-1-amine	5k	2-methylbutanol
4l	*trans*-2-methylpent-2-en-1-amine	5l	2-methylpentanol
4m	*trans*-2-pent-2-en-1-amine	5m	pentanol

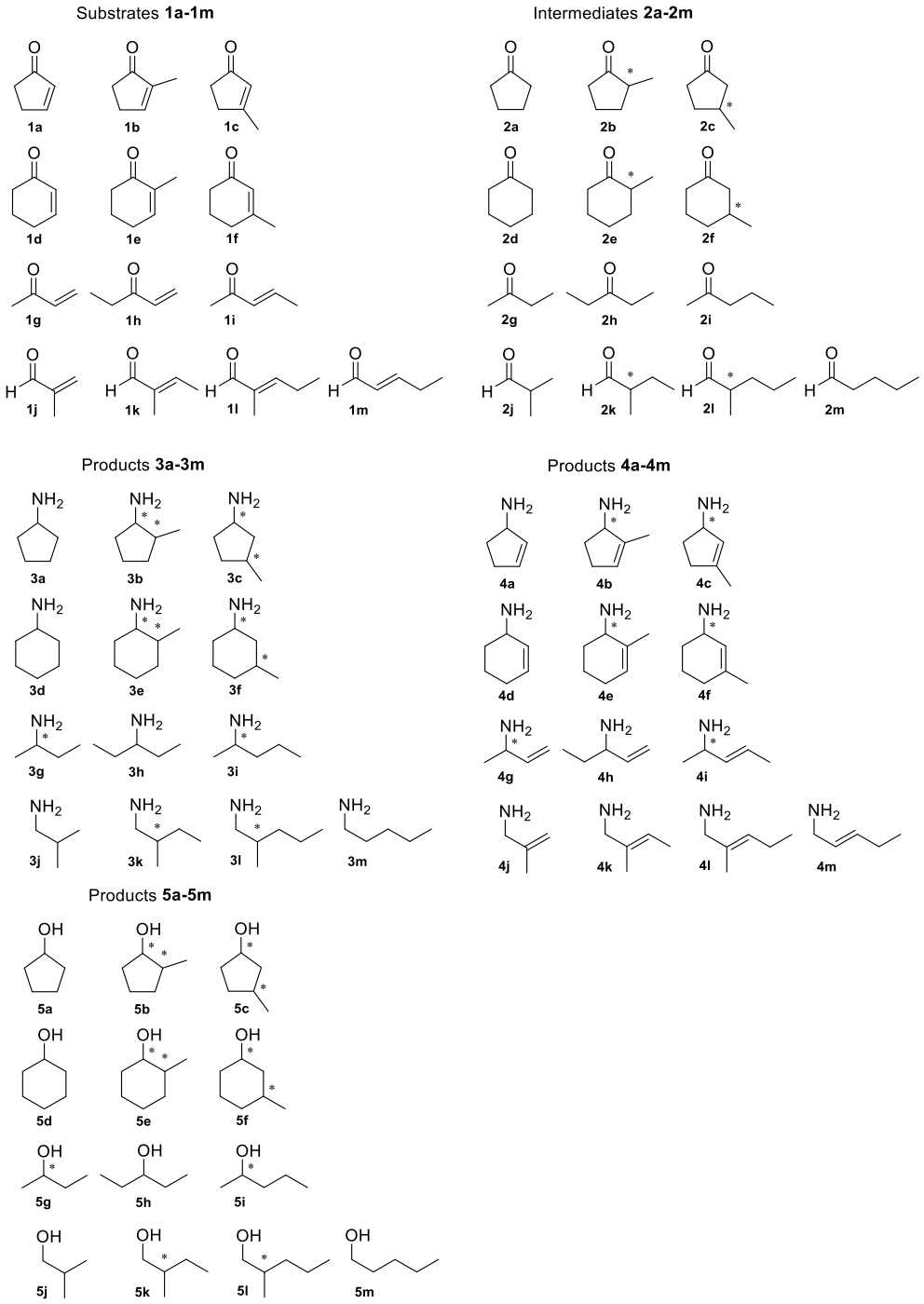

Figure S2. Structures of alkene substrates, carbonyl intermediates, amine products and alcohol by-products, with assigned numbers.

OYE specific activity measurements

For specific activity measurements, a 2 mL UV cuvette was used to monitor the decrease of NADPH at a wavelength of 340 nm on a Cary 60 UV-Vis spectrophotometer. The extinction coefficient of NAD(P)H was assumed to be 6220 $M^{-1}cm^{-1}$.[38] Once the cofactor is oxidized, it loses its absorbance at 340 nm. The addition of 20 mM of glucose and 10 U/mL glucose oxidase was tested to remove molecular oxygen.

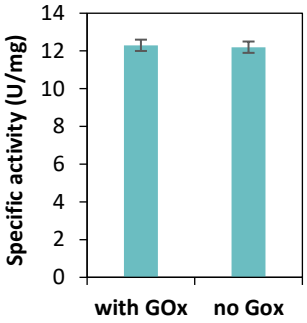

Figure S3. Activity measurements for TsOYE, with and without glucose oxidase (GOx) control. Reaction conditions: 50 mM Tris-HCl buffer pH 8.0, 0.05 µM TsOYE. 10 U/mL glucose oxidase (GOx), 20 mM glucose, 0.2 mM NADPH, 10 mM cyclohexenone. Average of duplicates.

Table S3. Concentration of *Ts*OYE, OYE2 or *Ts*OYE-C25D/I67T in the activity measurements for asymmetric reduction of our substrate scope as described in Figure 2. Conditions: 50 mM Tris-HCl buffer pH 8.0, *Ts*OYE. 10 U/mL glucose oxidase (GOx), 20 mM glucose, 0.2 mM NADPH. 3-methylcyclohexenone **1f*** was tested with *Ts*OYE-C25D/I67T and **1f**** with OYE2 and 0.2 mM NADH.

Substrate	[OYE]	(µM)
1a	*Ts*OYE	0.10
1b	*Ts*OYE	0.19
1c	*Ts*OYE	0.05
1d	*Ts*OYE	0.05
1e	*Ts*OYE	0.19
1f	*Ts*OYE	0.05
1f*	*Ts*OYE-C25D/I67T	0.94
1f**	OYE2	5.15
1g	*Ts*OYE	0.03
1h	*Ts*OYE	0.05
1i	*Ts*OYE	0.33
1j	*Ts*OYE	0.05
1k	*Ts*OYE	0.05
1l	*Ts*OYE	0.10
1m	*Ts*OYE	0.05

Activity of OYEs towards trans-2-methylbutenal **1k** and trans-2-methylpentenal **1l**

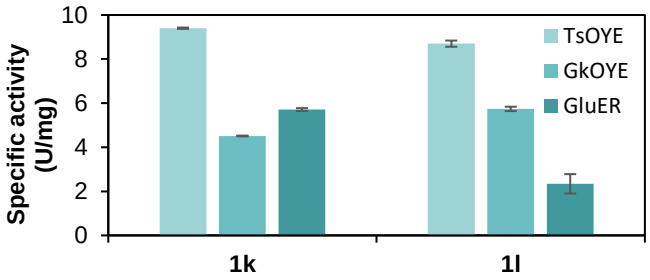

Figure S4. Specific activity of OYE for unsaturated aldehydes **1k** and **1l**. Conditions: 50 mM Tris-HCl buffer pH 8.0, 20 mM glucose, 10 U/mL glucose oxidase, 0.2 mM NADPH, 10 mM substrate. [*Gk*OYE] = 0.15 µM; [GluER] = 0.14 µM; *Ts*OYE concentrations as shown in Table S6.

Activity of OYEs with NADPH or NADH

In some cascade combinations, the native AmDHs showed a cofactor preference towards the non-phosphorylated nicotinamide cofactor NADH. We added the cofactor based on this preference, despite the preference for phosphorylated nicotinamide cofactor by *Ts*OYE and GluER. Therefore, we screened OYE for specific activity with NADH (**Figure S5**).

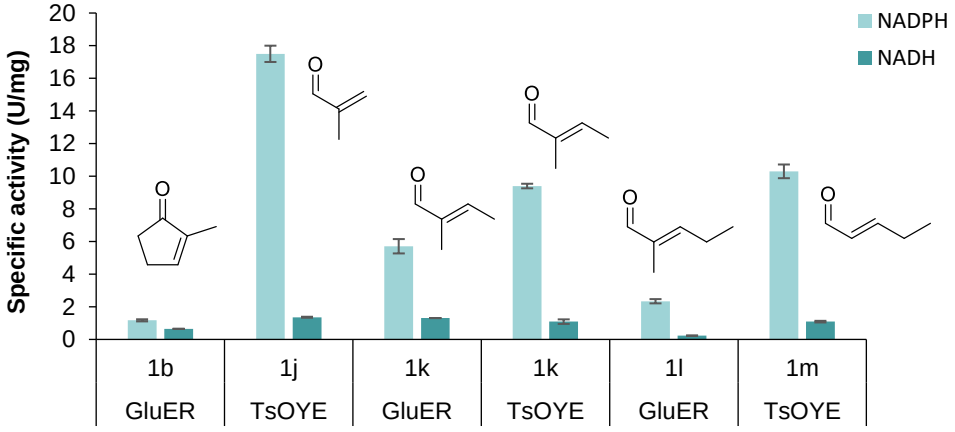

Figure S5. Specific activity of OYEs towards substrates with NADPH or NADH. Conditions: 50 mM Tris-HCl buffer pH 8.0, 20 mM glucose, 10 U/mL glucose oxidase, 0.2 mM NAD(P)H, 10 mM substrate. OYE concentrations from left to right in µM with NADPH: 0.19, 0.05, 0.14, 0.05, 0.14, 0.05 µM. With NADH: 0.61, 0.24, 0.23, 0.24, 1.2, 0.48 µM.

AmDH specific activities in presence of DMSO

All the reactions were conducted from duplicates in a spectrophotometric cell (10 mm light path) in a final reaction volume of 100 µL. To a reaction mixture of isobutyraldehyde **2j** or cyclohexanone **2d** (5 mM) in ammonium formate buffer

(1 M, pH 9.0) was added 0.4 mM of NADH (NADPH for MATOUAmDH2) and the appropriate volume of DMSO. The mixture (pre-incubated at 50 °C for 2 min in the case of reactions with IGCAmDH5, MATOUAmDH2, *Chat*AmDH) was transferred in a spectrophotometric cell (thermostated at 50 °C for reactions run at 50 °C), and an appropriate amount of enzyme (0.04 - 0.10 mg/mL) was added to initiate the reaction. The initial slope measured at 340 nm (in a temperature-controlled UV-spectrophotometer set at 50 °C for the reactions run at 50 °C) determined the specific activity of the enzyme according to Beer-Lambert's law and the molar absorptivity of β-NAD(P)H (Ɛ = 6,220 M^{-1} cm^{-1}), after subtraction of the slope obtained under the same conditions except without enzyme.

Screening of OYEs

Three buffers were initially prepared to perform the reactions: 50 mM Tris-HCl buffer pH 8.0, 50 mM Na_2CO_3 pH 9.0 and 250 mM NH_4HCO_2 pH 8.0. 25 mM NH_4HCO_2 buffer was made by diluting the 250 mM buffer 10 times (pH was measured at 7.86). The substrates were dissolved in dimethyl sulfoxide (DMSO), to make a 1 M stock. NADPH was dissolved in a 50 mM Tris-H_2SO_4 pH 7.0 buffer.

The enzymatic reactions were performed in a total volume of 1 mL in Eppendorf microcentrifuge plastic tubes. The reactions contained 2 µM *Ts*OYE and 10 mM of substrate (in the model case 2-methylcyclohexenone). NADPH or BNAH were added to the reaction. For the recycling system, 0.1 mM NADPH, 11 mM glucose and 5 mg/ml GDH (Evozymes, lyophilized powder, 35 U/mg) were added to the enzyme. Without the recycling system, 11 mM BNAH was added.

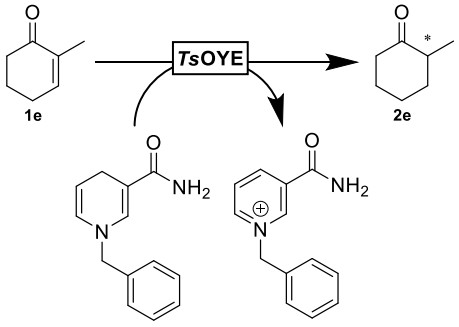

Figure S6. Reaction scheme of asymmetric reduction by *Ts*OYE with synthetic cofactor BNAH.

The reaction tubes were covered in parafilm and placed in an Eppendorf thermoshaker (900 rpm, 30 °C). The reactions were stopped after 1 h by placing the reaction plastic tubes on ice and adding 500 µL of EtOAc. This mixture was vortexed and centrifuged for 1 min at 13,000 rpm. The EtOAc was then separated and dried with $MgSO_4$ for analysis by GC.

ß-methylated enone reduction by OYE2 and *Ts*OYE-C25D/I67T

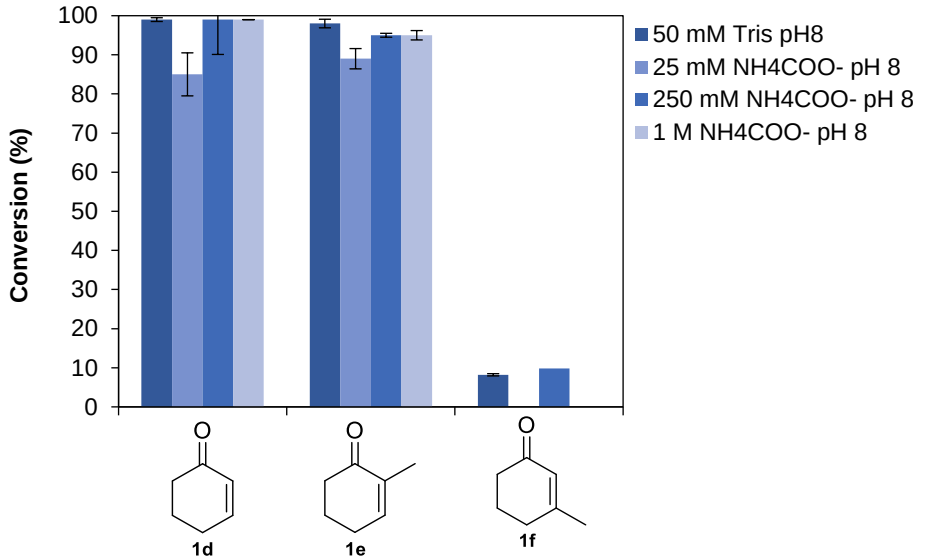

Figure S7. Conversions of substrates **1d** and **1e** by *Ts*OYE, and **1f** by *Ts*OYE-C25D/I67T after 1 h. Conditions: 50 mM Tris-HCl or varying concentrations NH_4HCOOH buffer, pH 8. 11 mM BNAH, 2 µM *Ts*OYE or *Ts*OYE-C25D/I67T. Average of duplicates.

Table S7. Asymmetric reduction of ß-methylated cycloalkenones by OYE2 and *Ts*OYE-C25D/I67T for 1 h.

Substrate	OYE	[OYE] (µM)	Conv. (%)	St. dev (%)[a]	*ee* (%)[b]
1c	OYE2	2	1.1	0.1	99 (*S*)
1c	OYE2	4	3.2	0.2	99 (*S*)
1c	*Ts*OYE-C25D/I67T	2	0	0	n.a.
1c	*Ts*OYE-C25D/I67T	4	0	0	n.a.
1f	OYE2	2	10	0.2	99 (*S*)
1f	OYE2	4	20	0.5	99 (*S*)
1f	*Ts*OYE-C25D/I67T	2	20	0.1	92 (*R*)
1f	*Ts*OYE-C25D/I67T	4	20	2.6	92 (*R*)

[a] Reactions were performed in duplicate. [b] *ee* = enantiomeric excess.

Reductive aminations catalyzed by AmDHs

The selected AmDHs (*Cfus*AmDH, *Chat*AmDH, IGCAmDH5, *Apau*AmDH, MATOUAMDH2, *Msme*AmDH, *Micro*AmDH) were tested toward ketones **2a-m** and enones **1a-m** in 96-well plate with cofactor regeneration system using UHPLC-MS monitoring. According to retention times and MS spectra, combination of substrates were done as followed to minimize the number of tests: ketones **2f**, **2i**, **2j**, **2m** and enones **1i** were tested in separate wells; ketones **2d**, **2g**, **2k**, and **2l** were tested with their corresponding enones **1d**, **1g**, **1k** and **1l**; **2a** with **2c**, **2b** with **2e**, **2h** with **2f**, **1a** with **1c**, **1b** with **1e**, **1f** with **1h** and **1j** with **1m.** To a reaction mixture (total volume = 100 µL) containing 10 mM

of substrate (10 mM of ketone + 10 mM of enone in case of mixture of substrate), 0.2 mM $NADP^+$ or 0.2 mM NAD^+, 24 mM glucose, 5 mM $CaCl_2$, 3 U/mL glucose dehydrogenase (GDH-105) in 1 M NH_4HCO_2 buffer pH 8.0, was added 0.5 mg/mL of purified AmDH. The 96-well plate was covered with a lid and left for reaction 24 h at 30°C in a thermocontrolled oven. All the reaction mixtures were analyzed by UHPLC-MS after derivatization with benzoyl chloride (BzCl). Background reactions were performed in the same manner but with mixtures lacking the substrate or with mixtures lacking the purified AmDH. In case of reactions with ketones **2a** – **2j** and **2m**, amounts of amines in reaction mixtures were deduced from calibrations curves obtained with the corresponding amines **3a**–**3j** and **3m** in mixtures containing 1 M NH_4HCO_2 buffer pH 8.0 and 10 µL of the buffer used for enzyme purification**.** In case of ketones **2l** and **2k**, the amounts of amine **3l** and **3k** were estimated from calibrations curves obtained with amines **3i** and **3g** respectively, in mixtures containing 1 M NH_4HCO_2 buffer pH 8.0 and 10 µL of the buffer used for enzyme purification. For enamines **4**, not available and not targeted, their presence in the reaction mixture were hypothesized from extraction of the corresponding m/z $[M+H]^+$ from the ESI trace (**Figure S9-S10**) but were not quantified.

BzCl derivatization

This derivatization was carried out in 96-well plate. 20 µL of reaction mixture were transferred from the enzymatic reaction plate to a second plate containing in each well 10 µL of a 1 M Na_2CO_3/$NaHCO_3$ aqueous solution pH 9.5, 40 µL of H_2O, and 30 µL of a 50 mM BzCl solution in acetonitrile. This derivatization plate was left for reaction for 40 min and then quenched by the addition in each well of 20 µL of a 1 M HCl aqueous solution and 30 µL of a 1/1 solution of H_2O/acetonitrile. After centrifugation (10,000 rpm, 10 min, room temperature) on a filtration 96-well plate (0.22 µm), the filtrate were analyzed by UHPLC-MS (eluent MeCN/H_2O + 0.1% formic acid with a linear gradient 20/80 during 1 min, then 20/80 to 70/30 in 3 min, then 70/30 during 2 min followed by re-equilibration time; flow 0.5 mL/min; temperature 25 °C; injection volume 3 µL; MS detection parameter: electrospray ionization in the positive mode, probe 450 °C, 50 V).

	Cfus	***Chat***	**IGC**	***Apau***	**MATOU**	***Msme***	***Micro***
1a	*nd*				*nd*		*nd*
2a	3.4				4.1		2.9
1b					*nd*	*nd*	*nd*
2b					0.5	0.8	0.5
1c	*nd*				*nd*		*nd*
2c	1.6				0.7		2.4
1d					*nd*		
2d					3.5		4.3
1e							
2e					1.2	2.2	3.7
1f					*nd*		
2f					1.9	3.4	4.5
1g					*nd*		
2g					2.3	2.3	
1h							
2h					0.1	1.2	1.5
1i						nd	
2i					0.9	1.2	
1j							
2j*	*nd*	*nd*	*nd*	*nd*			*nd*
1k							
2k	7.1	8.2	7.8	10.0	5.2		
1l							
2l	1.8	0.4	0.6	0.6	2.2		
1m			*nd*				
2m	0.5	0.1	0.1	1.9	0.1		0.9

Figure S8. Amounts of amines **3a**-**m** for reaction of each AmDHs toward tested ketones/aldehydes and presence or absence of enamines **4a**-**m** for reactions of AmDHs toward tested enones. Reaction conditions: 0.5 mg/mL AmDH, 10 mM substrate, 0.2 mM NADP (for *Cfus*AmDH (*Cfus*), MATOUAmDH2 (MATOU), *Msme*AmDH (*Msme*) and *Micro*AmDH (*Micro*)) or NAD (for *Chat*AmDH (*Chat*), IGCAmDH5 (*IGC*) and *Apau*AmDH (*Apau*)), 3U/mL GDH-105, 24 mM glucose, 5 mM $CaCl_2$, 1 M NH_4HCO_2 pH 8.0, 24 h at 30 °C, volume = 100 µL in 96-well plate. For amines **3a** –**3m**, the amount deduced from calibrations curves is reported in mM. Colors indicate the favorite enzyme for the cascade (green), good candidate (blue) and other potential candidates (grey). For enones **1a**-**1m**, the presence of the corresponding enamines **4a**-**4m** were hypothesized from extraction of the corresponding m/z $[M+H]^+$ from the ESI trace, quantification could not be performed due to absence of standards. Colors indicate the area measured from the integration of the correspond peak (pink: area >1500, yellow: area = 1500-10000; orange: area = 10000-30000, red: area >30000). Reported values are average of duplicates. [a] isobutylamine **3j** was not detected during this screening probably due to evaporation troubles, but already reported results allows us to select some favorite enzymes for this substrate; [b] these conversions are certainly underestimated due to evaporation troubles; blank boxes = not tested; *nd* = not detected.

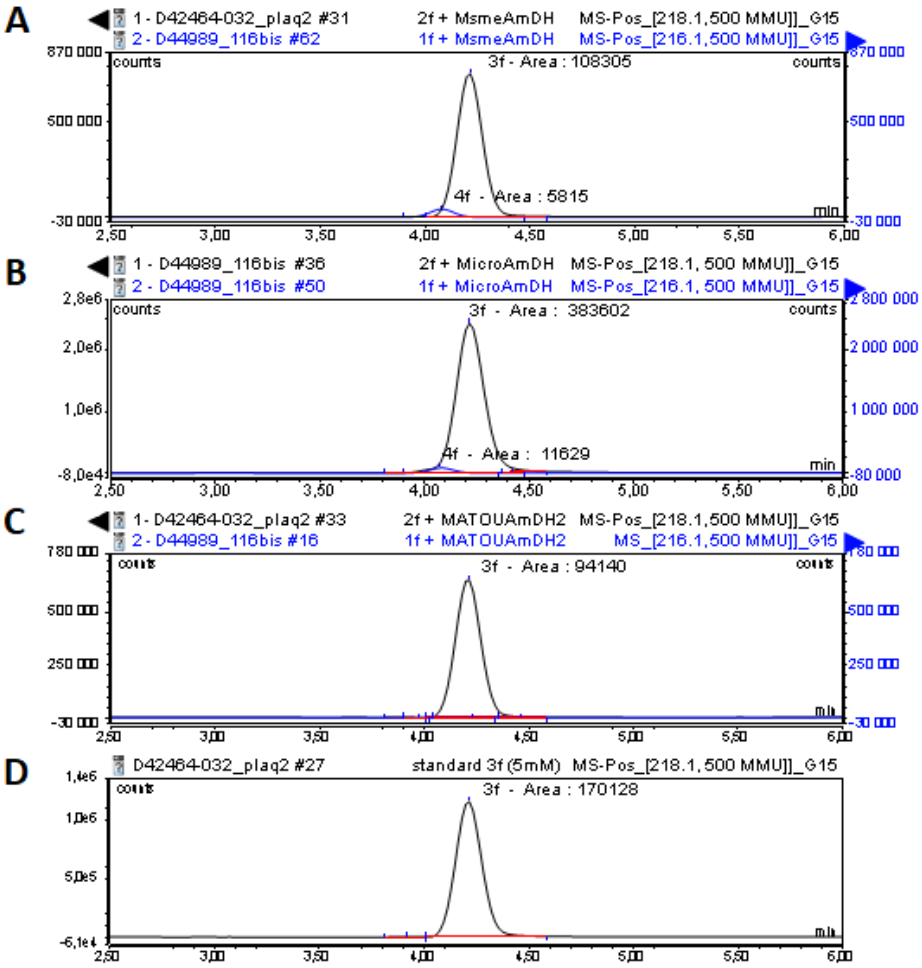

Figure S9. Examples of chromatogram obtained for reaction with **2f** and **1f**. Chromatogram of the derivatized reaction mixture with **A**) *Msme*AmDH, **B**) *Micro*AmDH, **C**) MATOUAmDH2 after extraction of m/z $[M+H]^+$ = 218.1 and m/z $[M+H]^+$ = 216.1 corresponding to derivatized 3-methylcyclohexylamine and 3-methylcyclohex-2-enamine respectively; **D**) Chromatogram of the derivatized standard 3-methylcyclohexylamine (5 mM) after extraction of m/z $[M+H]^+$ = 218.1.

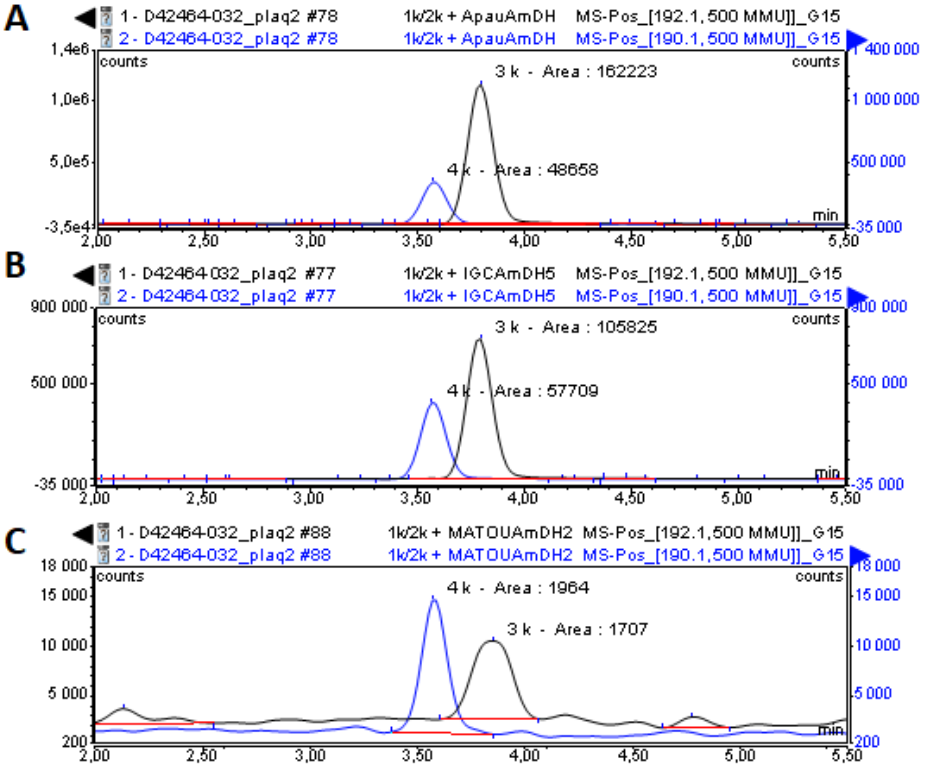

Figure S10. Examples of chromatogram obtained for reaction with **2k**/**1k**. Chromatogram of the derivatized reaction mixture with **A**) *Apau*AmDH, **B**) IGCAmDH5, **C**) MATOUAmDH2 after extraction of m/z $[M+H]^+$ = 192.1 and m/z $[M+H]^+$ = 190.1 corresponding to derivatized 2-methylbutanamine **3k** and *trans*-2-methylbuten-2-amine **4k** respectively.

Bi-enzymatic cascade reactions

Different purified amine dehydrogenases that showed activity towards the reduced substrates (**2a-m**) were used. These were the following enzymes:

- *Micro*AmDH, 2.78 mg/mL
- MATOUAmDH2, 4.18 mg/mL
- *Msme*AmDH, 6.76 mg/mL
- *Apau*AmDH, 2.07 mg/mL
- GDH-105 (Codexis), 123 mg, 50 U/mg
  For every cascade, 0.5 mg/mL of AmDH and 3 U/mL GDH-105 was used.

A 1 M glucose and a 10 mM $NADP^+$ stock were prepared in Milli-Q. Reactions were performed in a 1 M NH_4HCO_2 buffer (pH 8.0, 2 M NH_4OH to adjust the pH) at 30 °C, in a thermomixer at 400 rpm and 30 °C in a total volume of 1mL.

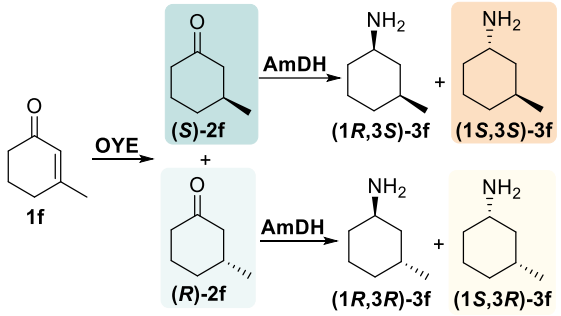

Figure S11. Selectivity for substrate 3-methylcyclohexenone **1f**.

Amine extraction and derivatization

To extract the amine from the reaction mixture, 1 mL 10 M NaOH was first added, vortexed, followed by the addition of 0.5 mL EtOAc, and vortexed. After centrifugation, the top layer was extracted. A second extraction was performed with 0.5 mL EtOAc. The combined organic layers were dried with anhydrous $MgSO_4$ for analysis on GC. Amines **3e**, **3g**, **3i** and **3k** were derivatized to determine the enantiomeric excess and diastereomeric ratio. A small spatula tip of potassium carbonate and a four drops of acetic anhydride were added to the extracted amine (in EtOAc), and shaken at 400 rpm at 30 °C for 1 h.[35] Then, 0.5 mL of Milli-Q water was added and shaken at 400 rpm at 30 °C for 30 min. After centrifugation, the EtOAc layer was separated and dried with $MgSO_4$ for analysis on GC.

Scale-up synthesis of 2-methylbutylamine preparations

The reaction volume for our upscaling was increased to 20 mL. The reaction mixture contained 50 mM pure *trans*-2-methylbutenal, 120 mM glucose, 3 U/mL GDH-105 (From Codexis, 50 U/mg), 0.2 mM NAD^+, 0.5 mg/mL *Apau*AmDH, 3 µM GluER in 1 M NH_4HCOOH-NH_4OH, pH 9.0. After 24 h reaction time, the conversion was calculated to be 21%, according to the same protocol described for 1-mL reaction. We ascribe the low conversion to the increased substrate concentration and only leaving the reaction 24 h. Reaction was stopped with 10 M NaOH until the pH was increased to over 12 (2.5 mL). To the falcon tube, 40 mL diethyl ether (Et_2O) was added. This was shaken thoroughly, and the water layer was removed with a separation funnel. This step was repeated twice with 20 mL Et_2O. The combined organic layers were dried and concentrated under reduced pressure to approximately 10 mL before addition of a solution of 2 M HCl in Et_2O . The solid was filtered, washed with cold Et_2O (3 × 5 mL) and dried over vacuum to obtain (*S*)-**3k** as a hydrochloride salt (12 mg, 10% overall isolated yield).

GC analyses

Compound analyses were carried out on Shimadzu GC-2010 gas chromatographs (Shimadzu, Japan) with an AOC-20i Auto injector equipped with a flame ionization detector (FID), using nitrogen or helium as the carrier gas. Products were confirmed by reference standards. Product concentrations were obtained with a calibration curve equations using 5 mM dodecane as an internal standard. All samples were injected with GC quality EtOAc, except where specified with Et_2O or methyl *tert*-butyl ether (MTBE).

The following chiral columns were used to determine enantiomeric excess of chiral products; details on the injection temperature, linear velocity, column flow, oven temperature program and retention times can be found for each compound below. See ESI of Jongkind *et al.* for GC chromatograms for all substrates from our scope.[39]

A. **Hydrodex ß-TBDAc** (Macherey-Nagel), 50 m × 0.25 mm × 0.25 µm (length, internal diameter, film thickness), injection at 250 °C, flow 3 mL/min, split ratio 50, linear velocity 37 cm/sec, column flow 4 mL/min, nitrogen as carrier gas.
B. **CP-Sil 8 CB** (25 m × 0.25 mm × 1.20 µm), injection at 340 °C, split ratio 100, linear velocity 30 cm/sec, column flow 4 mL/min, nitrogen as carrier gas.
C. **CP-Sil 8 CB** (50 m × 0.53 mm × 1 µm), **splitless**, injection at 340 °C, flow 20 mL/min, nitrogen as carrier gas.
D. **CP-Wax 52 CB** (50 m × 0.53 mm × 2.0 µm), **splitless**, injection at 250 °C, flow 20 mL/min, nitrogen as carrier gas.
E. **Hydrodex β-TBDM** (Macherey-Nagel), 50 m × 0.25 mm × 0.15 µm, heptakis-(2,3-di-O-methyl-6-O-t-butyldimethyl-silyl)-β-cyclodextrin, injection at 250 °C split ratio 50, linear velocity 38 cm/s, column flow 2.23 mL/min, helium as carrier gas.
F. **CP-Wax 52 CB** (25 m × 0.53 mm × 2.0 µm), injection at 250 °C, split ratio 100, flow 4 mL/min, nitrogen as carrier gas.
G. **Lipodex E** (Macherey-Nagel), 50 m × 0.25 mm × 0.25 µm, octakis-(2,6-di-O-pentyl-3-O-butyryl)-γ-cyclodextrin, split ratio 100, injection at 200 °C, linear velocity 38 cm/s, column flow 2.16 mL/min, helium as carrier gas.
H. **CP-Chirasil Dex CB** (Agilent J&W), 25 m × 0.32 mm × 0.25 µm, heptakis (2,3,6-tri-O-methyl)-β-cyclodextrin, injection at 250 °C, split ratio 150, linear velocity 30 cm/s, column flow 1.55 mL/min, helium as carrier gas.

In the case of **a**, **d**, **e**, **g** and **m**, two methods were developed: one for the separation of compound **1** and **2**, and another method to separate **1**, **2** and **3**, both methods and the corresponding GC columns are shown for each substrate.

Table S5. List of all compounds and applied internal standards (IS) with their corresponding GC columns and methods.

Cmpd	Column	GC oven program	Retention time (min)
a	C	Method 1 80 °C hold 6.83 min 30 °C/min to 325 °C hold 1 min	**1a cyclopentenone 4.0** **2a cyclopentanone 3.2**
a	B	Method 2 80 °C hold 3 min 5 °C/min to 90 °C hold 5 min 20 °C/min to 325 °C hold 1 min	**1a cyclopentenone 7.8** **2a cyclopentanone 6.7** **3a cyclopentylamine 5.8** **dodecane (IS) 16.6**
b	E	80 °C hold 5 min 5 °C/min to 100 °C hold 10 min 5 °C/min to 120 °C hold 5 min 20 °C/min to 240 °C hold 1 min	**1b 2-methylcyclopentenone 13.4** **2b 2-methylcyclopentanone 10.7, 11.0** **3b 2-methylcyclopentylamine 9.8, 9.9, 11.0** **dodecane (IS) 25.6**
c	E	80 °C hold 5 min 5 °C/min to 100 °C hold 10 min 5 °C/min to 120 °C hold 5 min 20 °C/min to 240 °C hold 1 min	**1c 3-methylcyclopentenone 21.7** **2c 3-methylcyclopentanone 12.2, 12.4** **Dodecane (IS) 25.6**
d	B	Method 1 80 °C hold 3 min 345 °C/min to 345 °C hold 1 min	**1d cyclohexenone 7.3** **2d cyclohexanone 6.9** **dodecane (IS) 9.7**
d	B	Method 2 80 °C hold 3 min 5 °C/min to 100 °C hold 4 min 25 °C/min to 345 °C hold 1 min	**1d cyclohexenone 11.6** **2d cyclohexanone 9.8** **3d cyclohexylamine 8.4** **dodecane (IS) 16.1**
e	C	Method 1 100 °C hold 3 min 25 °C/min to 140 °C hold 1 min 10 °C/min to 150 °C hold 1 min 25 °C/min to 345 °C hold 1 min	**1e 2-methylcyclohexenone 7.8** **2e 2-methylcyclohexanone 6.9**
e	C	Method 2 100 °C hold 3 min 25 °C/min to 145 °C hold 6 min 25 °C/min to 345 °C hold 1	**1e 2-methylcyclohexenone 7.8** **2e 2-methylcyclohexanone 6.9** **3e 2-methylcyclohexylamine 6.0, 6.3** **dodecane (IS) 12.2**
f	E	80 °C hold 5 min 5 °C/min to 100 °C hold 10 min 5 °C/min to 120 °C hold 5 min 20 °C/min to 240 °C hold 1 min	**1f 3-methylcyclohexenone 28.8** **2f 3-methylcyclohexanone 19.5, 20.0** **3f 3-methylcyclohexylamine 14.4, 14.7, 16.5, 16.7** **dodecane (IS) 25.6**
g	D	Method 1 50 °C hold 6 min 25 °C/min to 230 °C hold 1	**1g 3-buten-2-one 1.9** **2g 2-butanone 2.4**
g	B	Method 2 65 °C hold 6 min 230 °C/min to 345 °C hold 1 min	**1g 3-buten-2-one 4.1** **2g 2-butanone 4.3** **3g 2-aminobutane 4.0** **dodecane (IS) 14.9**
h	F	65 °C hold 6 min 20 °C/min to 345 °C hold 1 min	**1h penten-3-one 5.1** **2h 3-pentanone 4.3** **3h 3-aminopentane** **dodecane (IS) 16.6**
i	C	65 °C hold 6 min 5 °C/min to 70 °C hold 3 min 20 °C/min to 340 °C hold 1 min	**1i penten-2-one 7.3** **2i 2-pentanone 5.4** **3i 2-aminopentane 5.2** **dodecane (IS) 17.8**
j	B	65 °C hold 6 min 230 °C/min to 345 °C hold 1 min	**1j methacrolein 3.7** **2j isobutyraldehyde 3.5** **3j isobutylamine 4.4** **dodecane (IS) 14.9**

k	A	Method 1 80 °C hold 4 min 5 °C/min to 100 hold 5 min 5 °C/min to 110 hold 5 min 20 °C/min to 220 hold 1 min	**1k *trans*-2-methylbutenal 16.3** **2k 2-methylbutanal 8.9, 9.0** **dodecane (IS) 16.8**
k	C	Method 2 60 °C hold 3 min 10 °C/min to 70 °C hold 5 min 10 °C/min to 140 °C hold 3 min 20 °C/min to 340 °C hold 1 min	**1k *trans*-2-methylbutenal 7.5** **2k 2-methylbutanal 4.9** **3k 2-methylbutylamine 6.2** **dodecane (IS) 21.9**
l	A	100 °C hold 7.5 min 5 °C/min to 140 °C hold 2.5 min 25 °C/min to 240 °C hold 1 min	**1l *trans*-2-methylpentenal 10.7** **2l 2-methylvaleraldehyde 6.0, 6.2** **tridecane (IS) 13.2**
m	D	Method 1 60 °C hold 3 min 5 °C/min to 70 °C hold 2 min 25 °C/min to 245 °C hold 1 min	**1m *trans*-2-pentenal 6.3** **2m valeraldehyde 3.1** **dodecane (IS) 12.6**
m	C	Method 2 50 °C hold 4 min 5 °C/min to 60 °C hold 2 min 5 °C/min to 65 °C hold 4 min 20 °C/min to 345 °C hold 1 min	**1m *trans*-2-pentenal 10.4** **2m valeraldehyde 7.5** **3m amylamine 9.5** **dodecane (IS) 21.2**

Table S6. List of all compounds and applied internal standards (IS) with their corresponding GC columns and methods.

Cmpd	Column	GC oven program	Retention time (min)
e	G	100 °C hold 2 min 5 °C/min to 130 °C hold 15 min 25 °C/min to 225 °C hold 1 min	acetylated 2-methylcyclohexylamine **3e** 16.7, 17.0, 18.0, 18.6
g	H	100 °C hold 2 min 5 °C/min to 140 °C hold 10 min 25 °C/min to 220 °C hold 1 min	acetylated 2-aminobutane **3g**, 9.8, 10.5
i	H	100 °C hold 2 min 5 °C/min to 140 °C hold 10 min 25 °C/min to 220 °C hold 1 min	acetylated 2-pentylamine **3i**, 10.5, 11.0
k	H	100 °C hold 2 min 5 °C/min to 125 °C hold 10 min 25 °C/min to 220 °C hold 1 min	acetylated 2-methylbutylamine **3k**, 14.4, 14.5
l	H	100 °C hold 2 min 5 °C/min to 125 °C hold 10 min 25 °C/min to 220 °C hold 1 min	acetylated 2-methylpentylamine 3l, expected at 17.5 and 18.5

pH-effect on reaction composition with cyclohexanone, *Ts*OYE and MATOU-AmDH2

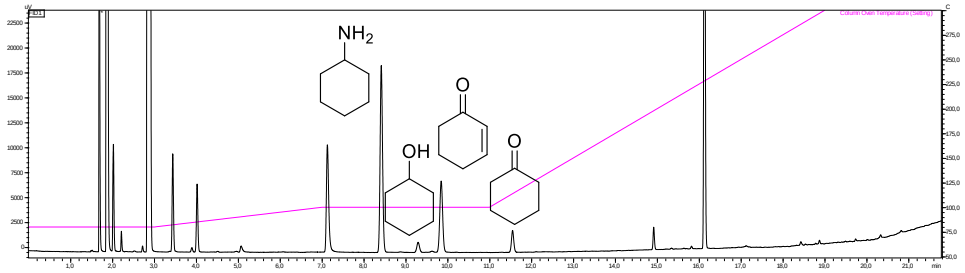

Figure S26. Gas chromatogram of cascade reaction mixture with substrate **1d** at pH 8.0. Cyclohexanol **5d** at 9.3 min. Dodecane at 16.1 min.

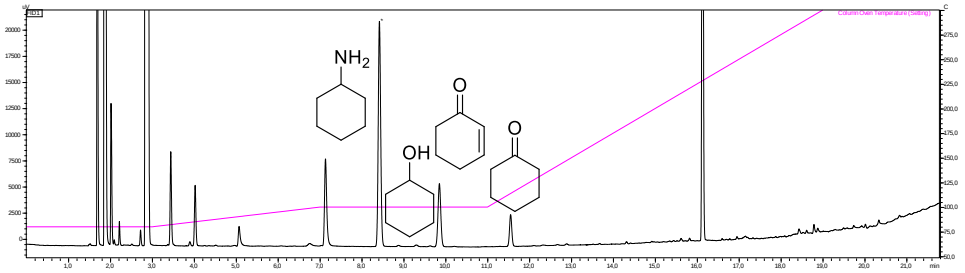

Figure S27. Gas chromatogram of cascade reaction mixture with substrate **1d** at pH 8.5. Cyclohexanol **5d** at 9.3 min. Dodecane at 16.1 min.

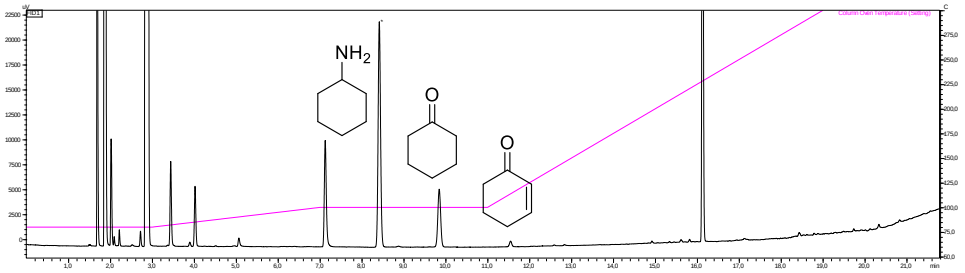

Figure S28. Gas chromatogram of cascade reaction mixture with substrate **1d** at pH 9.0. Cyclohexanol **5d** at 9.3 min. Dodecane at 16.1 min.

Alcohol formation

To a reaction mixture (total volume = 100 µL) containing 10 mM of cyclohexanone **2d**, 0.2 mM $NADP^+$, 12 mM glucose, 3 U/mL glucose dehydrogenase (GDH-105) in 1 M of specified buffer at the specified pH, was added 0.3 mg/mL of purified MATOUAmDH2 or water in case of blank reaction without AmDH. The reaction mixtures were stirred in closed 500 µL Eppendorf tubes for 21h at 30 °C and 400 rpm in an Eppendorf ThermoMixer® equipped with an Eppendorf ThermoTop®. All the reaction mixtures were analyzed by GC-MS after organic extraction: to 80 µL of reaction mixture was added 40 µL of 10 M NaOH and 100 µL of EtOAc (GC-MS quality). After rapid vortex and centrifugation, 70 µL of the organic phase were taken (× 2) dried over $MgSO_4$ and injected on GC-MS after dilution 1/10 in EtOAc. Amounts of amine **3d**, alcohol **5d** and remaining ketone **2d** were deduced from calibrations curves obtained with commercially available standards (0, 0.1, 0.3, 0.5, 1, 5 mM for **5d**; 0, 2, 4, 6, 8, 10 for **3d** and **3c**) in mixtures containing the identical buffer studied at pH 8.0 and 5 µL of the buffer used for enzyme purification. Peak areas of extracted mass 82, 99 and 98 from the full mass scan (30 – 500) were used to quantify amine **3d**, alcohol **5d** and ketone **2d** respectively (**Table S7** and **Figure S73-S74**).

Table S7. Amounts of amine **3d** and alcohol **5d** from reaction of *Chat*AmDH and MATOUAmDH2 with **2d**.

		Observed concentration (mM)		
AmDH	buffer	5d	3d	2d
MATOUAmDH2	NH_4HCO_2 pH 8.0	0.27	6.93	0.45
	NH_4HCO_2 pH 10.0	0.17	8.59	0.21
	NH_4Cl/NH_4OH pH 8.0	0.16	6.96	0.13
	NH_4Cl/NH_4OH pH 10.0	0.10	1.47	6.20
without AmDH	NH_4HCO_2 pH 8.0	0.13	nd	8.06
	NH_4HCO_2 pH 10.0	0.21	nd	9.11
	NH_4Cl/NH_4OH pH 8.0	0.11	nd	10.19
	NH_4Cl/NH_4OH pH 10.0	0.05	nd	9.84

nd: not detected

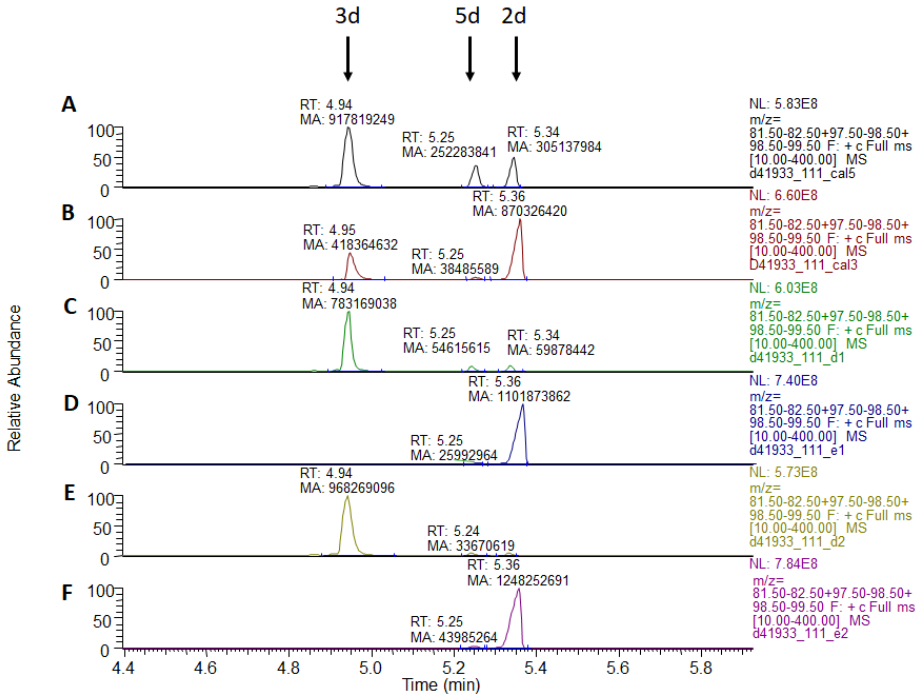

Figure S73. GC-MS chromatogram of **A**) calibration point in 2M NH_4HCO_2 pH 8.0 with 1 mM of **5d**, 8 mM of **3d** and 2 mM of **2d**, **B**) calibration point in NH_4HCO_2 pH 8.0 with 0.3 mM of **5d**, 4 mM of **3d** and 6 mM of **2d**, **C**) reaction mixture with **2d** and MATOUAmDH2 in 2 M NH_4HCO_2 pH 8.0, **D**) reaction mixture without AmDH in 2 M NH_4HCO_2 pH 8.0, **E**) reaction mixture with **2d** and MATOUAmDH2 in 2 M NH_4HCO_2 pH 10.0, **F**) reaction mixture without AmDH in 2 M NH_4HCO_2 pH 10.0.

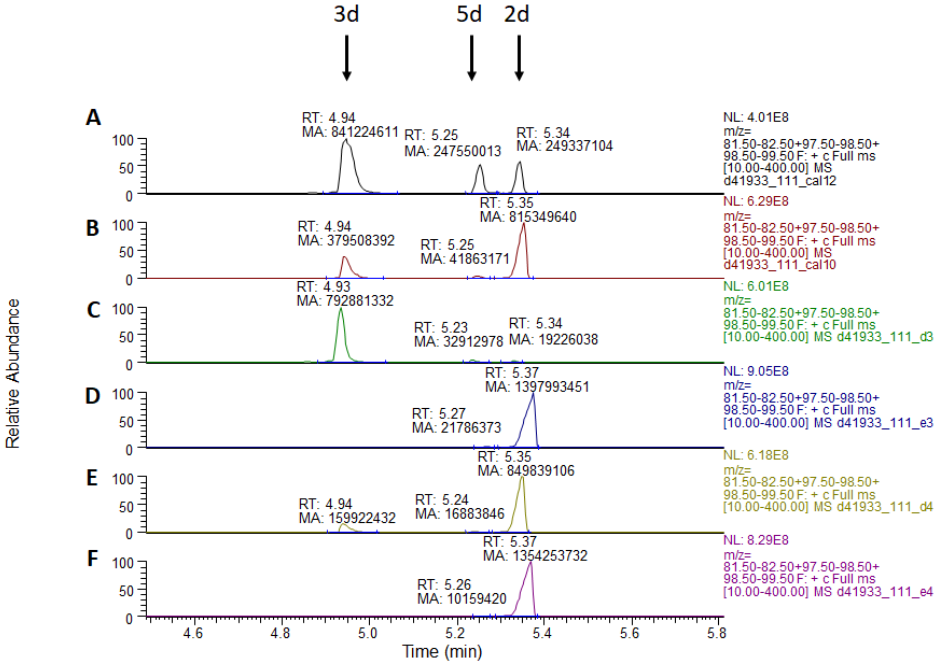

Figure S74. GC-MS chromatogram of **A**) calibration point in 2 M NH_4Cl/NH_4OH pH 8.0 with 1 mM of **5d**, 8 mM of **3d** and 2 mM of **2d**, **B)** calibration point in NH_4Cl/NH_4OH pH 8.0 with 0.3 mM of **5d**, 4 mM of **3d** and 6 mM of **2d**, **C**) reaction mixture with **2d** and MATOUAmDH2 in 2 M NH_4HCO_2 pH 8.0, **D**) reaction mixture without AmDH in 2 M NH_4Cl/NH_4OH pH 8.0, **E**) reaction mixture with **2d** and MATOUAmDH2 in 2 M NH_4Cl/NH_4OH pH 10.0, **F**) reaction mixture without AmDH in 2 M NH_4HCO_2 pH 10.0.

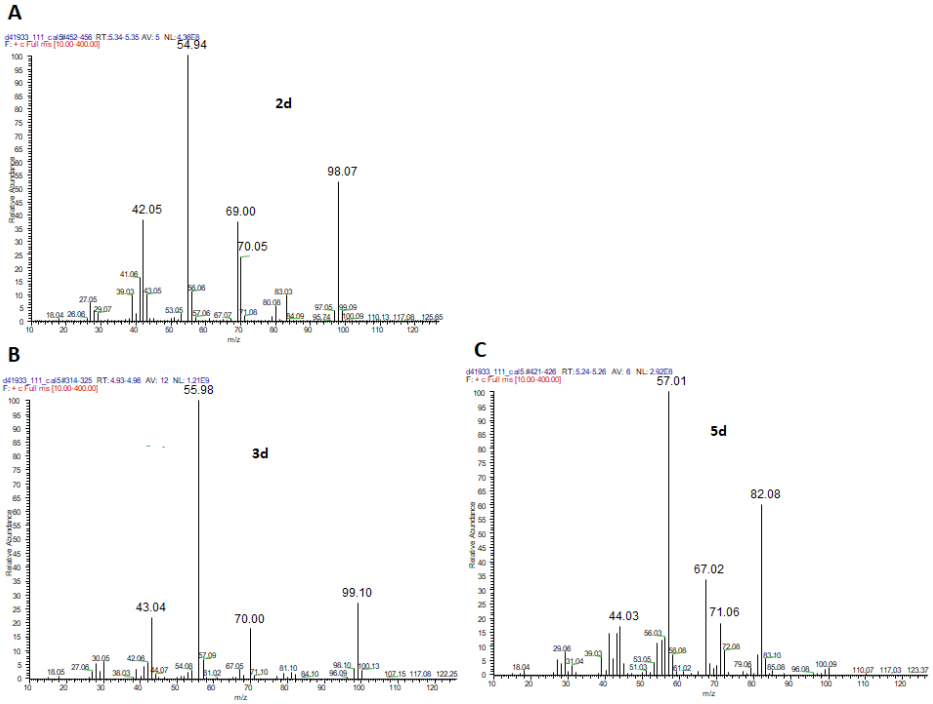

Figure S75. Spectrum of compounds A) 2d, B) 3d, C) 5d.

References

[1] T. C. Nugent, M. El-Shazly, *Adv. Synth. Catal.* **2010**, *352*, 753-819.
[2] C. Wang, J. Xiao, in *Stereoselective Formation of Amines* (Eds.: W. Li, X. Zhang), Springer Berlin Heidelberg, Berlin, Heidelberg, **2014**, pp. 261-282.
[3] G. Grogan, *Curr. Opin. Chem. Biol.* **2018**, *43*, 15-22.
[4] H. Gröger, *Appl. Microbiol. Biotechnol.* **2019**, *103*, 83-95.
[5] O. Mayol, K. Bastard, L. Beloti, A. Frese, J. P. Turkenburg, J. L. Petit, A. Mariage, A. Debard, V. Pellouin, A. Perret, V. de Berardinis, A. Zaparucha, G. Grogan, C. Vergne-Vaxelaire, *Nat. Catal.* **2019**, *2*, 324-333.
[6] A. A. Caparco, E. Pelletier, J. L. Petit, A. Jouenne, B. R. Bommarius, V. de Berardinis, A. Zaparucha, J. A. Champion, A. S. Bommarius, C. Vergne-Vaxelaire, *Adv. Synth. Catal.* **2020**, *362*, 2427-2436.
[7] J. H. Schrittwieser, S. Velikogne, M. Hall, W. Kroutil, *Chem. Rev.* **2018**, *118*, 270-348.
[8] J. I. Ramsden, R. S. Heath, S. R. Derrington, S. L. Montgomery, J. Mangas-Sánchez, K. R. Mulholland, N. J. Turner, *J. Am. Chem. Soc.* **2019**, *141*, 1201-1206.
[9] F. G. Mutti, T. Knaus, N. S. Scrutton, M. Breuer, N. J. Turner, *Science* **2015**, *349*, 1525-1529.
[10] W. Bohmer, T. Knaus, F. G. Mutti, *ChemCatChem* **2018**, *10*, 731-735.
[11] M. Tavanti, J. Mangas-Sánchez, S. L. Montgomery, M. P. Thompson, N. J. Turner, *Org. Biomol. Chem.* **2017**, *15*, 9790-9793.
[12] H. L. Yu, T. Li, F. F. Chen, X. J. Luo, A. T. Li, C. Yang, G. W. Zheng, J. H. Xu, *Metab. Eng.* **2018**, *47*, 184-189.
[13] T. Knaus, F. G. Mutti, L. D. Humphreys, N. J. Turner, N. S. Scrutton, *Org. Biomol. Chem.* **2015**, *13*, 223-233.
[14] E. Brenna, F. G. Gatti, D. Monti, F. Parmeggiani, A. Sacchetti, *ChemCatChem* **2012**, *4*, 653-659.
[15] E. Brenna, F. G. Gatti, L. Malpezzi, D. Monti, F. Parmeggiani, A. Sacchetti, *J. Org. Chem.* **2013**, *78*, 4811-4822.
[16] E. Brenna, M. Crotti, F. G. Gatti, D. Monti, F. Parmeggiani, A. Pugliese, S. Santangelo, *J. Mol. Catal. B: Enzym.* **2015**, *114*, 37-41.
[17] L. Skalden, C. Peters, L. Ratz, U. T. Bornscheuer, *Tetrahedron* **2016**, *72*, 7207-7211.
[18] D. Monti, M. C. Forchin, M. Crotti, F. Parmeggiani, F. G. Gatti, E. Brenna, S. Riva, *ChemCatChem* **2015**, *7*, 3106-3109.
[19] L. Ducrot, M. Bennett, G. Grogan, C. Vergne-Vaxelaire, *Adv. Synth. Catal.* **2021**, *363*, 328-351.
[20] D. J. Opperman, B. T. Sewell, D. Litthauer, M. N. Isupov, J. A. Littlechild, E. van Heerden, *Biochem. Biophys. Res. Commun.* **2010**, *393*, 426-431.
[21] K. Stott, K. Saito, D. J. Thiele, V. Massey, *J. Biol. Chem.* **1993**, *268*, 6097-6106.
[22] T. B. Fitzpatrick, N. Amrhein, P. Macheroux, *J. Biol. Chem.* **2003**, *278*, 19891-19897.
[23] N. Richter, H. Gröger, W. Hummel, *Appl. Microbiol. Biotechnol.* **2011**, *89*, 79-89.
[24] M. Schittmayer, A. Glieder, M. K. Uhl, A. Winkler, S. Zach, J. H. Schrittwieser, W. Kroutil, P. Macheroux, K. Gruber, S. Kambourakis, J. D. Rozzell, M. Winkler, *Adv. Synth. Catal.* **2011**, *353*, 268-274.
[25] C. E. Paul, S. Gargiulo, D. J. Opperman, I. Lavandera, V. Gotor-Fernandez, V. Gotor, A. Taglieber, I. W. Arends, F. Hollmann, *Org. Lett.* **2013**, *15*, 180-183.
[26] A. Scholtissek, D. Tischler, A. H. Westphal, W. J. H. van Berkel, C. E. Paul, *Catalysts* **2017**, *7*, 130.
[27] N. Nett, S. Duewel, A. A. Richter, S. Hoebenreich, *ChemBioChem* **2017**, *18*, 685-691.

[28] M. Pesic, E. Fernández-Fueyo, F. Hollmann, *ChemistrySelect* **2017**, *2*, 3866-3871.
[29] H. Bisswanger, *Perspectives in Science* **2014**, *1*, 41-55.
[30] R. M. Kohli, V. Massey, *J. Biol. Chem.* **1998**, *273*, 32763-32770.
[31] T. Knaus, C. E. Paul, C. W. Levy, S. de Vries, F. G. Mutti, F. Hollmann, N. S. Scrutton, *J. Am. Chem. Soc.* **2016**, *138*, 1033-1039.
[32] V. Tseliou, D. Schilder, M. F. Masman, T. Knaus, F. G. Mutti, *Chem. Eur. J.* **2021**, *27*, 3315-3325.
[33] V. Tseliou, M. F. Masman, W. Bohmer, T. Knaus, F. G. Mutti, *ChemBioChem* **2019**, *20*, 800-812.
[34] A. Fossey-Jouenne, L. Ducrot, E. P. J. Jongkind, E. Elisée, A. Zaparucha, G. Grogan, C. E. Paul, C. Vergne-Vaxelaire, *Front. Catal.* **2023**, *3*, 1105948.
[35] C. E. Paul, M. Rodríguez-Mata, E. Busto, I. Lavandera, V. Gotor-Fernández, V. Gotor, S. García-Cerrada, J. Mendiola, O. de Frutos, I. Collado, *Org. Process Res. Dev.* **2014**, *18*, 788-792.
[36] M. Pesic, E. Fernandez-Fueyo, F. Hollmann, *ChemistrySelect* **2017**, *2*, 3866-3871.
[37] A. Vorster, M. S. Smit, D. J. Opperman, *Org. Lett.* **2019**, *21*, 7024-7027.
[38] J. Ziegenhorn, M. Senn, T. Bucher, *Clin. Chem.* **1976**, *22*, 151-160.
[39] E. P. J. Jongkind, A. Fossey-Jouenne, O. Mayol, A. Zaparucha, C. Vergne-Vaxelaire, C. E. Paul, *ChemCatChem* **2022**, *14*, e202101576.

Chapter 3: Native amine dehydrogenases can catalyze the direct reduction of carbonyl compounds to alcohols in the absence of ammonia

Aurélie Fossey-Jouenne[1], Laurine Ducrot[1], **Ewald P.J. Jongkind[2]**, Eddy Elisée[1], Anne Zaparucha[1], Gideon Grogan[3], Caroline E. Paul[2], Carine Vergne-Vaxelaire[1*]

[1] Génomique Métabolique, Génoscope, Institut François Jacob, CEA, CNRS, Univ Evry, Université Paris-Saclay, 91057 Evry, France
[2] Biocatalysis, Department of Biotechnology, Delft University of Technology, Van der Maasweg 9, 2629 HZ Delft, The Netherlands
[3] York Structural Laboratory, Department of Chemistry, University of York, Heslington, York, YO10 5DD, UK

Based on *Front. Catal.*, **2023**, *3*, 1105948. doi: 10.3389/fctls.2023.1105948

Contributions: writing manuscript, screening cyclohexanone in absence of ammonia, GC analysis of chiral compounds.

Summary

Native amine dehydrogenases (nat-AmDHs) catalyze the (*S*)-stereoselective reductive amination of various ketones and aldehydes in the presence of high concentrations of ammonia. Based on the structure of *CfusAmDH* from *Cystobacter fuscus* complexed with nicotinamide adenine dinucleotide phosphate ($NADP^+$) and cyclohexylamine, we previously hypothesized a mechanism involving the attack at the electrophilic carbon of the carbonyl by ammonia followed by delivery of the hydride from the reduced nicotinamide cofactor on the *re*-face of the prochiral ketone. The direct reduction of carbonyl substrates into the corresponding alcohols requires a similar active site architecture and was previously reported as a minor side reaction of some native amine dehydrogenases and variants. Here we describe the ketoreductase (KRED) activity of a set of native amine dehydrogenases and variants, which proved to be significant in the absence of ammonia in the reaction medium but negligible in its presence. Conducting this study on a large set of substrates revealed the heterogeneity of this secondary ketoreductase activity, which was dependent upon the enzyme/substrate pairs considered. *In silico* docking experiments permitted the identification of some relationships between ketoreductase activity and the structural features of the enzymes. Kinetic studies of *Msme*AmDH highlighted the superior performance of this native amine dehydrogenases as a ketoreductase but also its very low activity towards the reverse reaction of alcohol oxidation.

Introduction

To address some of the Sustainable Development Goals to be achieved by 2030 according to the United Nation, biocatalysis, *i.e.* the use of enzymes for synthetic purposes, appeared as a valid contributor for seven of them.[1] Many of the benefits offered by biocatalysis over conventional chemistry have been reviewed. [2-4] Among the biocatalysts studied closely, NAD(P)H-dependent oxidoreductases performing reductive amination are established enzymes for the biocatalytic formation of amines. Facing the importance of sustainable access to amino compounds such as bulk chemicals and high value-added products, both the discovery of efficient enzymes and the deep understanding of their potential, have been studied by several research teams.[5] Besides requiring simple starting materials (carbonyl compound, amine source), these enzymes have the major advantage of depending on an easily recyclable nicotinamide cofactor (NAD(P)H). Currently, these enzymes include amine dehydrogenases (AmDHs) from engineered L-amino acid dehydrogenases (AADHs) including an ε-deaminating L-lysine dehydrogenase (LysEDH), native amine dehydrogenases (nat-AmDHs) identified among biodiversity by (meta)genome-mining approaches and some variants, imine reductases (IREDs) and reductive aminases (RedAms).[6-31] Mechanistically, the C4 atom of NAD(P)H that donates a hydride is in close proximity to the electrophilic carbon of the iminium intermediate that is formed from both substrates. Thanks to crystal structures, residues have been identified that interact with the carbonyl and/or with the amine function of the substrate/product, thus ensuring effective binding and catalysis. Therefore, theoretically, in the absence of an amine source, a similar binding of the carbonyl substrate might lead to its direct reduction into an alcohol as catalyzed by ketoreductases (KREDs). This ketone reduction is already known to be catalyzed by widely used alcohol dehydrogenases (ADHs) or KREDs, which harbor the same core Rossmann-type fold shared by the whole NAD(P)binding domain superfamily (InterPro entry IPR036291).[32, 33]

The dual reductive amination and direct ketoreduction activities of carbonyl compounds has been reported for few NAD(P)H dependent oxidoreductases. Recently, Tseliou *et al.* enhanced the direct ketoreduction of aromatic aldehydes observed with LysEDH from *Geobacillus stearothermophilus*, through targeted protein engineering. They extensively studied the dual KRED and AmDH activity of these engineered LysEDHs and identified a dependence of this dual activity on the substrate structure with variability according to the variants. Notably, high alcohol yields were obtained for reduction of benzaldehyde and derivatives and 3-phenylpropanal, even in the presence of ammonium buffers. The wildtype LysEDH and variants LE-AmDH-v24 and LE-AmDH-v27, harboring an F173S mutation, produced the highest alcohol yields, both in

ammonium and ammonium-free buffers. Interestingly, some good substrates for the AmDH reaction were poor substrates for ketoreduction in ammonia-free solution, highlighting the crucial positioning of the substrate in the active site with respect to the C4 atom of the NADH.[34] Interestingly, no KRED activity has been described thus far with other AmDHs engineered from AADHs. However, secondary carbonyl reductase activities were reported with enzymes known to reduce C=N bonds, namely IREDs, and RedAms, but only with highly activated fluorinated acetophenones.[35, 36] This specific behavior, surely dependent on the higher redox potential of the carbonyl carbon, appears to be assisted by a shift of the substrate positioning resulting from an interaction of fluorine atoms with hydroxy groups of the ribose of the NADPH, thus generating the required distance from the C4 atom of NADPH to the carbonyl carbon, and so a possible direct reduction. [34, 37] The dual AmDH/IRED-KRED activity of such enzymes seems to be restricted to very particular cases. By contrast, secondary C=N bond reductive activity has been reported for some enzymes of the short-chain dehydrogenases/reductases enzyme superfamily (SDR), or has been introduced through protein engineering.[38, 39] For enzymes active towards acyclic imines, and even more towards carbonyl compounds undergoing both catalyzed imine formation and reduction, this particular feature of dual AmDH-KRED activity is thus far limited and has not been studied for a wider set of enzymes.

We have recently reported the discovery of nat-AmDHs among biodiversity and detected KRED secondary activity for several of them.[17, 18, 21, 40] Biocatalytic amination with MATOUAmDH2 gave rise to small amounts of alcohols (<2% of cyclohexanol at pH 8 at 1 M ammonium formate buffer) and, with the variant IGCAmDH1-W144A, 4% of octan-1-ol from octanal were detected.[21] These results encouraged us to study this feature more specifically. Indeed, on the one hand, it is important to know whether the alcohol products can be formed in the reductive amination reactions of different types of substrates and with different nat-AmDHs, as this potentially might complicate the synthesis. On the other hand, the use of these enzymes as KREDs, or in redox-neutral cascades if a dual-active enzyme is available, can be interesting applications [34]. Here we report the results and analysis of the KRED and AmDH activities of many nat-AmDHs and some of their already described variants. Using nineteen enzymes, we have studied the correlations between their structural features and promiscuous KRED activity, while also providing some complementary kinetic studies.

Results and Discussion

Conversion data in alcohols and amines

We conducted this study with 12 characterized nat-AmDHs, i.e. *Chat*AmDH, IGCAmDH1, *Rgna*AmDH, MATOUAmDH2, *Cfus*AmDH, *Apau*AmDH, *Porti*AmDH, *Micro*AmDH, *Msme*AmDH, *Sgor*AmDH, IGCAmDH5 and AcolAmDH, in addition to the recently described seven variants corresponding to *Cfus*AmDH-W145A.[21] We tested these nineteen enzymes toward a large panel of carbonyl substrates at 10 mM concentration (**Figure 1**). Group A comprises alkyl aldehydes (isobutyraldehyde **1a**, butanal **2a**, hexanal **3a**, heptanal **4a** and octanal **5a**), group B substituted aldehydes (furfural **6a**, cyclopentanecarbaldehyde **7a** and benzaldehyde **8a**), group C linear ketones (pentan-2-one **9a**, hexan-2-one **10a**, heptan-2-one **11a**, hexan-3-one **12a**, acetophenone **13a** and 4-phenylbutan-2-one **14a**) and group D cyclic ketones (cyclohexanone **15a** and 2-methylcyclohexanone **16a**). The alcohol **1c**-**16c** and / or amine **1b**-**16b** products were semi-quantified in two reaction conditions (condition a: buffer with ammonia/ammonium species; conditions b: buffer without ammonia) by GC-FID monitoring, with a mix of NAD^+ and $NADP^+$ cofactors, internally recycled with glucose dehydrogenase GDH-105. The specific activities of some of the enzyme/substrate pairs were also determined (**Table 4**).

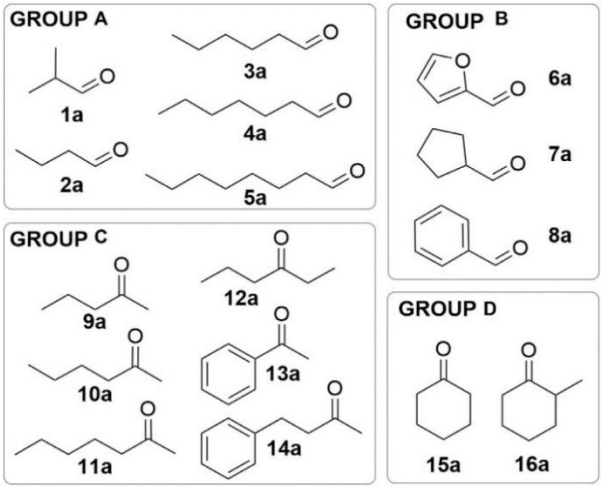

Figure 1. List of substrates used in this study.

For ammonia-free reactions, previous data reported by Tseliou *et al.* demonstrated higher apparent rates of reduction at pH 7.0 compared to higher pH, and no preferred type of buffer in cofactor-recycling conversion studies. With the objective of achieving the best conversions into alcohols in condition b, we studied the effect of pH on the alcohol formation with the couple **15a**/*Msme*AmDH

in sodium phosphate buffer. The reaction conditions (quantity of enzymes and duration) were deliberately adapted to deviate from quantitative conversions and thus to better visualize the differences according to the pH. As depicted in **Figure 2**, the alcohol amount **15c** was quite similar in the pH range 6.0–7.5 and decreased progressively above pH 8.0. The screening for KRED activity was also done at pH 7.5 unlike the one for AmDH activity performed at pH 8.5 as already published.[17]

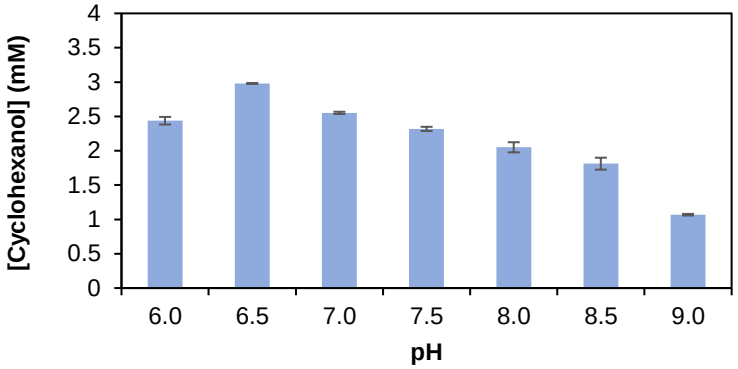

Figure 2. pH effect on the conversion of cyclohexanone 15a into cyclohexanol 15c in ammonia-free buffer. Conditions: 100 mM NaPi buffer pH 6.0–9.0, 12 mM glucose, 6 U/mL GDH-105, 0.2 mM NADP+, 0.1 mg/mL MsmeAmDH, 10 mM cyclohexanone 15a, 1% v/v DMSO, 25 °C, 400 rpm, 4 h. Cyclohexanol is quantified with calibration curves by GC-FID 1. Error bars represent standard deviations of two independent experiments.

All the conversions deduced from calibration curves of standard alcohols and amines are presented in **Figure 3**. Despite alcohol peaks observed in blank reactions lacking enzymes, especially with aldehydes, the alcohol formations are enzymatic and present after subtraction of these blank controls. Importantly, in 2 M ammonium buffer (conditions a), the AmDH activity strongly outperformed the KRED one, as, in most cases, no or only traces of alcohol could be detected (<1% conversion). The saturated ammonia / ammonium concentration promotes the amination reaction, presumably minimizing the “free” carbonyl substrate in the active site and so its direct reduction.[17] This KRED activity, specific to ammonia-free buffer, differs from the KRED side activity of wild-type or some engineered LysEDHs observed in ammonium buffer for some substrates. For example, **8a** was converted into 17% of **8b** and 23% of **8c** in 2 M ammonium formate buffer with wild-type LysEDH.[34] Here, none of the tested enzymes was revealed to display higher promiscuous KRED activity than AmDH one in ammonium buffer, except *Porti*AmDH, which displayed 3.4% conversion of **5a** into **5c** but no conversion into **5b**. More notable KRED activities (conversions of 3.1–9.3%) were reached with variants, even if they were still lower than the AmDH ones.

On the contrary, in ammonia-free buffer (condition b), alcohols were detected, even up to significant amounts. It appeared that, in general, the amounts of alcohol formed were very variable. This was not only linked to the identity of the enzyme itself, but also to the enzyme/substrate couple. Among all the tested substrates, each enzyme displayed notable KRED activity (>0.5 mM of alcohol formed) with at least one substrate. Higher alcohol formation and a higher number of accepted substrates were obtained with some enzymes compared with others. *Rgna*AmDH, MATOUAmDH2, *Porti*AmDH, *Micro*AmDH and *Msme*AmDH display high promiscuous KRED activity in ammonium-free buffer, with up to 96% of alcohols formed. Generally, for wildtype enzymes, we observed much higher AmDH activity in ammonia-rich buffer than ketoreduction in ammonia-free buffer, but with variabilities depending on the type of substrate. For the short substrates **1a** and **2a** of group A, the conversions into alcohols under condition b were at least twice lower than the conversions into amines under condition a. Up to around conversions of 40% were nevertheless obtained, for example for **1a** into **1c** with *Msme*AmDH, *Rgna*AmDH and *Cfus*AmDH. For enzymes active toward longer aldehydes, the AmDH activity was 6–20 times higher than the KRED one; no more than 10% of alcohol **3c** were obtained in condition b. For group B, unsaturated aldehydes **6a** and **8a** were not reduced, or only in very low amounts, despite many of the tested enzymes displayed high conversions to the corresponding amines **6b** and **8b** in ammonia-rich buffer. Specific activities towards **6a** were all below 0.6 mU/mg, thus in accordance with conversion results (SI **Table S4**). The KRED activity was observed only for cyclopentanecarbaldehyde **7a**, with differing AmDH/KRED activity ratios dependent on the enzymes. *Rgna*AmDH and MATOUAmDH2 appeared as the enzymes with the higher KRED promiscuous activity for this substrate with 16–32% and 23–27% conversions of **7a** into **7c** respectively, and IGCAmDH1 and *Chat*AmDH the less active ones for the direct reduction while forming 63–76% of cyclopentanecarbamine **7b**. The specific activities determined with **7a** in ammonia-free buffer correlates with such KRED activity data, with 0.4 and 14.6/ 58.4 mU/mg measured for IGCAmDH1 and *Rgna*AmDH/ MATOUAmDH2, respectively. In group C, for **9a**, the KRED activity was significant in the cases of enzymes displaying high conversions in reductive amination, with AmDH/KRED activity ratios of around 4/1 for *Cfus*AmDH and *Micro*AmDH to 2/1–1/1 for *Porti*AmDH and *Msme*AmDH, respectively. For example, 53% conversion into **9b** vs. 54% into **9c**, in the respective ammonia-rich and ammonia-free conditions, were obtained with the couple **9a**/*Porti*AmDH. This trend was not shared for hexan-3-one (**12a**), for which no alcohol **12c** was detected despite high amine **12b** formation for *Porti*AmDH, *Micro*AmDH, and *Msme*AmDH. For the other substrates of this group displaying activities only with variants, the amounts of alcohol were only significant with *Cfus*AmDH-W145A, with 17–36% of **11c** and

14c, when 54% and 53–70% of corresponding amines **11b** and **14b** were formed. For *Apau*AmDH-W141A and *Micro*AmDH-W141A, no or only low amounts of these alcohols were detected, while the AmDH activities induced conversions above 20%. For cyclic ketones of group D, all the highly active AmDHs displayed high promiscuous KRED activity, giving particularly nearly total conversion in cyclohexanol **15c** with *Cfus*AmDH, *Micro*AmDH, *Msme*AmDH and *Porti*AmDH in ammonia-free buffer. These results were in line with the high KRED specific activities of 39.4, 510.6 and 235.2 mU/mg measured in ammonia-free buffer with **15a** for the first three, respectively (SI **Table S4**).

Stereochemistry

In the case of prochiral substrates (group C and D except **15a**), the enantiomeric excesses (*ee*) were measured when >1 mM of alcohols (>10% conversion) were formed. As for the AmDH activity, the (*S*)-configuration was obtained with *ee* of (*S*)-alcohols **9c** and **11c** >99%. We can conclude a high (*S*)-selectivity for the promiscuous KRED activity of these AmDHs. In the case of the chiral substrate **16a**, the *cis*-configuration was the major but not exclusive form (*cis*:*trans* ratio from 60:40 to 82:18) of the alcohol product **16c**, with a moderate to high preference for the (*S*)-configuration at the tertiary carbon created (*ee* (*S*,*R*) = 73–83%; *ee* (*S*,*S*) = 80–97%)) (**Figure 3; SI Table S6**).

The Michaelis-Menten parameters were determined for *Msme*AmDH for the reduction of cyclohexanone **15a** to cyclohexanol **15c** to provide a comparison to the values previously reported for its reductive amination into **15b** (**Table 1**; **Figure S5**).[17] Indeed, *Msme*AmDH was able to catalyze the conversion of this substrate for both reactions in high yields. In the absence of ammonia and at pH 7.5, the K_M for cyclohexanone **15a** was slightly lower than in amination condition (0.25 and 0.55 mM, respectively). A similar observation was made for the K_M of the cofactor NADPH (0.04 and 0.06, respectively). The k_{cat} being seven times lower, the resulting catalytic efficiency was approximately two times lower for **15a** for the KRED activity over the AmDH one, and nearly identical for NADPH. *Msme*AmDH displayed very slow catalysis of oxidation with a specific activity for **15c** reaching only 0.4 mU/mg, preventing any accurate determination of kinetic parameters. No oxidation activity could even be detected for **7c**, whose corresponding ketone **7a** nevertheless emerged as a very good substrate in reduction condition.

Table 1. Kinetic parameters of *Msme*AmDH for the KRED activity[a]

	k_{cat} (s^{-1})	K_M (mM)	k_{cat}/K_M (s^{-1}/M^{-1})
cyclohexanone **15a**	0.17	0.25	667
NADPH	0.14	0.04	4155

[a] on Hydrodex β-TBDM Kinetic parameters were measured in a 100 µL final volume in 100 mM KPi buffer at pH 7.5 at concentrations of 0.05-2 mM **15a** and 0.005-0.3 mM NADPH.

Group	product	Chat	IGC1		Rgna		MATOU		Cfus		Apau		Porti	Micro		Msme		Sgor	IGC	Acol
		WT	WT	W144A	WT	W155A	WT	C148A	WT	W145A	WT	W141A	WT	WT	W141A	WT	W141A	WT	WT	WT
A	1b (a)	62.5	51.7		65.9		61.4		63.1		60.0		44.7	34.7		58.6		41.0	54.3	57.6
	1c (a)	nd	nd		nd		nd		nd		nd		nd	nd		nd		nd	nd	nd
	1c (b)	12.1; 11.4	12.2 ; 8.7		39.8 ; 29.0		35.4 ; 27.9		38.8 ; 23.4		27.7 ; 26.3		24.7;20.0	21.3 ; 18.6		40.9; 26.1		18.2 ; 12.6	27.5 ; 11.1	25.3 ; 10.5
	2b (a)	45.7	53.5		54.7		51.9		49.0		40.3		35.8	33.1		46.9		38.0	44.3	39.0
	2c (a)	nd	nd		nd		nd		nd		nd		nd	nd		nd		nd	nd	nd
	2c (b)	7.0 ; 5.0	10.9 ; 2.9		29.9 ; 24.6		32.2 ; 25.5		27.4 ; 15.0		13.5 ; 9.9		22.7 ; 19.5	18.8 ; 14.3		30.8 ; 18.2		12.2 ; 5.6	8.7 ; 3.2	7.6 ; 4.9
	3b (a)	4.6	2.4	29.7	12.5	85.6	72.7	79.2	39.9	99.5	5.3	59.6	60.8	65.1	2.0	54.9	3.0	4.2	2.0	1.2
	3c (a)	nd	nd	1.8	< 1	nd	nd	nd	nd	nd	nd	nd	nd	nd	< 1	nd	nd	< 1	< 1	< 1
	3c (b)		4.8	9.0 ; 5.0	5.5	5.2	5.2	1.3	2.8	3.8 ; 5.0		11.6 ; 8.8	2.9	6.0		4.0		4.8	2.5	6.9
	4b (a)	0.1	0.1	26.9	0.6	36.6	26.9	32.5	2.3	40.4	0.1	34.4	7.9	18.1	0.6	6.0	2.0			
	4c (a)	2.00	1.6	3.2	2.7	0.8	0.8	0.9	1.2	0.5	1.4	0.8	3.1	1.5	3.3	1.3	2.1			
	4c (b)																			
	5b (a)	nd	nd	32.3	nd	39.1	13.8	21.5	nd	38.8	nd	34.9	nd	3.1	5.2	nd	6.5			
	5c (a)	< 1	< 1	4.0	3.2	< 1	< 1	1.2	< 1	nd	< 1	< 1	3.4	< 1	2.8	< 1	1.4			
	5c (b)			16.4 ; 5.4		5.5				34.6 ; 8.2		23.9 ; 9.0			4.9		4.7			
B	6b (a)	76.3	62.7	< 1	68.2	3.2	79.7	72.4	83.5	13.3	77.3	1.5	44.5	37.2	< 1	78.9	< 1	27.0	28.9	16.9
	6c (a)	nd	nd	nd	nd	nd	nd	nd	nd	nd	nd	nd	nd	nd	nd	nd	nd	nd	nd	nd
	6c (b)	nd	nd	nd	nd	nd	nd		nd	nd	nd	nd	nd	nd	nd	nd		nd	nd	nd
	7b (a)	41.1	44.6	1.3	47.1	25.8	49.2	54.3	51.3	18.6	43.7	12.3	49.4	48.3	47.5	56.0	21.8	16.8	62.3	48.7
	7c (a)	< 1	< 1	1.0	nd	5.8	nd	nd	nd	1.7	< 1	6.6	nd	nd	< 1	nd	9.3	nd	nd	nd
	7c (b)	4.8	4.4	6.6	31.7 ; 15.7	4.1	27.1 ; 23.2		11.7 ; 10.6	4.1	7.6 ; 6.2	6.1	29.7 ; 13.2	29.4 ; 15.4	5.3	19.6 ; 16.0	4.5	4.0	3.3	4.3
	8b (a)	9.7	14.7	3.7	76.5	2.6	56.9	55.3	79.0	14.8	22.2	1.7	23.5	14.5	nd	37.2	nd	30.9	12.7	nd
	8c (a)	1.2	< 1	2.9	< 1	3.3	< 1	< 1	< 1	< 1	< 1	2.7	< 1	1.1		< 1		nd	nd	nd
	8c (b)	nd	nd	nd	nd	nd	nd		nd	nd	nd	nd	nd	nd	nd	nd	nd	nd	nd	nd

C	**9b (a)**	nd	nd		9.2		20.6		43.0		< 1		53.5		50.8		43.8							
	9c (a)	nd	nd		nd		nd		nd		nd		1.4		nd		< 1							
	9c (b)	nd	nd		< 1		1.6		9.6 ; 9.5 (>99)		nd		54.2 ; 39.2 (>99)		11.5 ; 11.4 (>99)		31.6 ; 22.6 (>99)							
	10b (a)	nd	nd	nd	< 1	< 1	2.0 (77.5)	3.0 (91.8)	3.1(94.7)	39.7 (99.3)	nd	4.0 (99.2)	26,5 (79.4)		22.6 (94.6)	1.2 (>99.9)	8.4 (98.8)	< 1	nd	nd	nd			
	10c (a)	nd	nd	nd	nd	nd	nd	nd	nd	nd	nd	nd	nd		nd	nd	nd		nd	nd	nd			
	10c (b)									2.9			6.9		< 1		2.3		nd	nd	nd			
	11b (a)	< 1	< 1	< 1	< 1	< 1	< 1	< 1	< 1	53.7 (99.7)	< 1	18.5 (99.3)	4.2 (33.0)		1.5	< 1	< 1	4.6 (>99.9)						
	11c (a)	nd	nd	nd	nd	nd	nd	nd	nd	< 1	nd	nd	< 1		nd	nd	nd	nd						
	11c (b)			nd		nd				33.2 ; 16.9 (>99)		< 1				nd		< 1						
	12b (a)	nd	nd	nd	nd	< 1	12.4 (38.2)	9.0 (12.1)	5.8 (29.1)	1.7 (91.3)	< 1	nd	46.5 (13.9)		51.2 (87.6)	4.4 (>99.9)	39.1 (88.4)	< 1	nd	nd	nd			
	12c (a)	nd	nd	nd	nd	nd	nd	nd	nd	nd	nd	nd	1.20		nd	nd	nd		nd	nd	nd			
	12c (b)						nd		nd		nd		nd		nd		nd		nd	nd	nd			
	13b (a)						< 1	< 1	< 1	2.2 (96.9)	< 1	< 1	7.4 (97.0)		13.9 (99.1)	< 1	1.9 (96.5)	< 1	nd	nd	nd			
	13c (a)						nd	nd	nd	nd	nd	nd	nd		nd	nd	nd		nd	nd	nd			
	13c (b)														< 1				nd	nd	nd			
	14b (a)						< 1	< 1	< 1	69.5 ; 52.5 (99.6)	< 1	31.2 ; 22.2 (99.2)	2.4 (49.6 R)		< 1	42.1 ; 28.1 (95.5)	< 1	46.4 ; 34.1 (99.9)						
	14c (a)									nd		nd				nd		nd						
	14c (b)									35.8 ; 24.1 (99.5)		nd				nd		6.0						

D	**15b (a)**	19.3	19.5	89.2	87.4	86.7	44.7	86.0	88.5	87.8	25.8	33.5	9.2
	15c (a)	nd	nd	nd	nd	nd	nd	nd	nd	nd	nd	nd	nd
	15c (b)	< 1	nd	17.2 ; 15.5	30.5 ; 27.5	>99 ; 80.5	11.4 ; 11.1	>99 ; 77.9	>99 ; 78.9	>99 ; 78.7	1.7	2.8	< 1
	16b (a)	< 1	< 1	5.7	52.9	55.9	5.4	62.5	62.6	61.7	< 1	< 1	nd
	16c (a)	nd	nd	nd	< 1	< 1	nd	nd	nd	nd	nd	nd	nd
	16c (b)	nd	nd	< 1	24.8 ; 40.0 (78(83):22(92))	15.0 ; 28.0 (60(81):40(80))	nd	70.0 ; 96.0 (75(73):25(88))	69.3 ; 87.0 (80(74):20(97))	75.3 ; 90.0 (82(83):18(80))	nd	nd	nd

Figure 3. Conversion of carbonyl substrates **1a-16a** into amines **1b-16b** and alcohols **1c-16c** in ammonium buffer, and in alcohols **1c-16c** in ammonium buffer and ammonia-free buffer, with described AmDHs. Conditions: 10 mM carbonyl substrate, 0.5 mg/mL AmDH, 0.2 mM NAD^+, 0.2 mM $NADP^+$, 3 U mL^{-1} GDH-105, 12 mM glucose in 2 M ammonium formate buffer pH 8.5 (condition a) or in 100 mM sodium phosphate buffer pH 7.5 (condition b). Reactions were performed in 100 µL final volume in 500 µL Eppendorf tubes for 24 h at 25 °C at 400 rpm and analyzed by GC-FID (GC-FID 2). Yields (%) provided were deduced from calibration curves with reference standards. Duplicated experiments in condition b were performed when conversions into alcohols **1b-16c** were >7% in the first screening. Both values are indicated. Color code from dark green (high conversions) to light green (low conversions) helps for reading. a = conditions a; b = conditions b. nd = not detected (<0.1% *i.e.,* 0.01 mM). Empty boxes = not tested. Enantiomeric excesses (*ee*) of alcohols are provided between brackets in case of prochiral substrates, for conversions >10% (after analyses by GC-FID (GC-FID 1)). For **16c**, *cis* ($ee_{(S,R)}$) : *trans* ($ee_{(S,S)}$) ratios are indicated.

***In silico* analysis**

In an attempt to link the *in vitro* data to the active-site characteristics of the enzymes, some structural analysis and docking experiments were performed on the closed conformations of structures of MATOUAmDH2-NADP, *Msme*AmDH-NADP and *Cfus*AmDH-NADP, and on energy minimized models of *Rgna*AmDH-NAD, *Micro*AmDH-NAD(P), IGCAmDH1-NAD and *Rgna*AmDH-NADNH$_4^+$ for studies in presence of ammonia/ammonium species (see Material and methods). We confirmed the energy minimization step by comparing the conformations before and after energy minimization for the X-ray structure of *Cfus*AmDH with NADP$^+$. The greatest difference was seen for the ribose of NADP$^+$ with a shift of 1.2 Å, but more importantly, no shift in orientation of all the residues involved in the pocket and the nicotinamide part were observed (**Figure S6**). In addition, the energy minimized model of MATOUAmDH2 was compared to its X-ray structure (PDB ID: 7ZBO) recently published.[20] Some important shifts were observed in the more flexible part such as Y176, residue too far from the reacting part to be discussed in this paper. For the residues surrounding the substrate/product, no drastic shifts were generated, the notable depicted ones (0.7–1.5 Å) must be considered for discussion results (**Figure S7**). The following molecules were docked: **6a–c**, **7a–c**, and **15a–c**; and the top ten conformations were considered (**Table 2**; **Figure S8**). We noticed that the docked aldehydes or ketones should be analyzed more carefully, as the obtained conformations were often not in agreement with the conformations of the corresponding products and mechanism. For example, the docked conformations of **15a** displayed the carbonyl function “in the lower front” of the pocket, certainly due to interactions with the NH backbone of Q137 (*Msme*AmDH numbering) and amide of the cofactor. In these conformations, the distances between the reactive carbon and the C4 of the nicotinamide are in the 4.6–5.1 Å range, therefore in disagreement with observed reduction (**Figure S9**). We can notice that in the case of MATOUAmDH2, the docked **7a** and **15a** were flipped, with the carbonyl oriented to the “right” of the pocket, i.e., to His184 and Tyr171. The higher space available in this bigger pocket enables such orientation, in a conformation more similar to the one of the alcohol product, which may induce higher efficiency of MATOUAmDH2 for the reduction compared to other enzymes such as *Msme*AmDH (**Figure S10**).[20] Precisely for cyclopentanecarbaldehyde **7a**, KRED specific activities were ten-fold higher for MATOUAmDH2 compared to *Msme*AmDH (58.4 *vs* 5.2 mU/mg, **SI Table S4**).

First, looking at the distance between the carbon bearing either the alcohol or the amine and the C4 atom of the nicotinamide (hydride donor), we noticed that they are quite similar for a couple alcohol/ amine and in an appropriate range for hydride delivery in many cases (3.3–4.2 Å).[41] The main

interaction promoting lower energy conformations is indeed the hydrogen bond between labile hydrogen of alcohol or amine with the oxygen atom of the catalytic residue Glu104 (*Msme*AmDH numbering), which "sticks" the carbon atom carrying this function at a very similar position, and therefore at a similar distance with the NADPH C4 atom hydride. Despite being in the same range, notable trends can be established from slight differences for this key distance, all the more so if we coupled the criterion of calculated energies of the top conformations (**Table 2**; **Figure S8**). Globally, the alcohol conformations were of higher energies than the amine ones, and the gain of energies between carbonyl substrates and alcohol *vs* amine were lower (0.05 – -0.22 *vs* -2.05 – -2.29 kJ/mol), which could be in agreement with the higher amount of amine formed compared to alcohol. In the case of **7c**, lower average distances of 3.90 and 3.91 Å were measured for the favored “up” conformations for *Msme*AmDH and *Rgna*AmDH respectively, enzymes with high promiscuous KRED activities, whereas slightly higher distances (3.8–4.6 Å, average value = 4.11 Å) were measured for IGCAmDH1 displaying very low conversion and specific activity toward **7a** (**Table 3**; **SI Table S4**). Bearing in mind that a distance of 4.3 Å is already too distant to postulate a direct hydride transfer, most of the conformations obtained with the latter were not in accordance with a possible reduction. Moreover, for the enzyme IGCAmDH1 with low promiscuous KRED activity, energies were all higher than -4.97 kJ/mol, unlike the others which were below -5.1 kJ/mol, reaching -5.46 kJ/mol for *Msme*AmDH with good promiscuous KRED activity. For MATOUAmDH2, and to a lesser extent *Micro*AmDH, bearing bigger catalytic pockets, these relationships were not found. Such observation could also be made for cyclohexanol (**15c**) where distances of 3.6-3.8 Å, associated with lower energies (-5.42 – -5.83 kJ/mol), were calculated for nearly all the top ten conformations for *Micro*AmDH, *Msme*AmDH, *Cfus*AmDH displaying high promiscuous KRED activities, whereas longer distances (3.9–4.6 Å) with higher energy (-5.19 – -5.15 kJ/mol[1]) were measured for IGCAmDH1, for which only traces of **15c** and specific activity of 0.5 mU/mg were obtained in *in vitro* experiments (**Figure 4**; **Figure S8**). In the case of *Rgna*AmDH, five of the ten top conformations of **15c** displayed distances of 3.4–3.5 Å whereas only 15.5-17.2% alcohol were formed experimentally and a moderate specific activity of 2.6 mU/mg was calculated with **15a**. The remaining other five conformations were inappropriately flipped which may reflect an inferior suitability of this active site for **15c**, as observed for *Cfus*AmDH for **7c**. Interestingly, the average energy for **7c** (-4.71, -5.41 and -5.23 kJ/mol) and **15c** (-5.00, -5.82 and -5.53 kJ/mol) were much lower than the ones for **6c** (-3.67, -4.23 and -4.21 kJ/mol) with respectively MATOUAmDH2, *Msme*AmDH and *Cfus*AmDH. Combined with the fact that the energy difference between ketone/aldehyde substrates and alcohol products are negative for **7** and **15** (-0.07 – -0.21 kJ/mol), while being positive for **6** (0.05 kJ

mol^{-1}) unlike the furfural **6a**/furfurylamine **6b** one (-2.05 kJ/mol), this trend can be linked to the low specific activities with **6a** compared to **7a** and **15a** and the absence of **6c** in conversion experiments, compared to notable amounts of **7c** and **15c** (conversions of 10.6–23.2% of **7a** and 30.5–>99% of **15a** into **7c** and **15c** respectively).

Table 2 C4N-C(OH) distances and related energies of the corresponding top 10 docked conformations of alcohols **6c**, **7c** and **15c** into some studied nat-AmDHs.

	6c	**7c**	**15c**
*Rgna*AmDH		3.91 (-5.18)	3.66 (-5.51)
MATOUAmDH2	4.27 (-3.67)	4.12 (-4.71)	3.80 (-5.00)
*Micro*AmDH		4.59 (-5.08)	3.98 (-5.42)
*Msme*AmDH	3.77 (-4.23)	3.90 (-5.40)	3.64 (-5.82)
*Cfus*AmDH	3.52 (-4.21)	3.64 (-5.24)	3.78 (-5.53)
IGCAmDH1		4.11 (-4.97)	4.14 (-5.17)

Distances are expressed in Å. Energy are expressed in kJ/mol and indicated in brackets. [a] flipped conformations. Average values are provided. For detailed results for each ten conformations and results on **6a**-**6b**, **7a**-**7b**, **15a**-**15b**, see Figure S8.

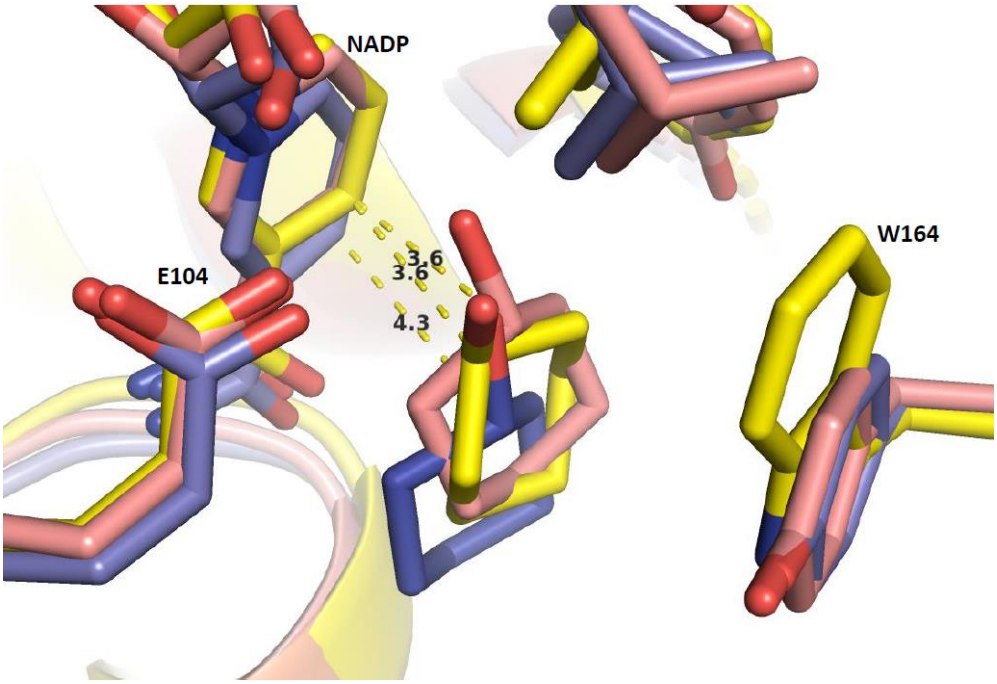

Figure 4. C4N-C(OH) distances for *Msme*AmDH (yellow), *Cfus*AmDH (pink) and IGCAMDH1 purple) with selected conformations of docked cyclohexanol (**15c**). Distances are in Å. Surrounding residues are labelled only for *Msme*AmDH for clarity.

To give some insights into the differences observed in conversions into alcohol in the presence or absence of ammonia, docking experiments were performed on *Rgna*AmDH with **6a** and **7a**, with or without NH_4^+ docked inside the active site, using the model of *Cfus*AmDH-15a-NH_4^+, already published, as a template.[17] With docked NH_4^+, the reactive carbon of **7a** was too far from the C4 nicotinamide in all the conformations (4.4–5.1 Å) to allow reduction, whereas these distances (3.7 Å for correct conformations) in absence of NH_3 were in accordance with experimentally observed KRED activity (conversion 32%) and specific activities (14.6 mU/mg). For **6a**, the calculated distances (4.3–4.4 Å) were in each case incompatible with KRED activity both in ammonia-free or ammonia-rich conditions, as observed in the in vitro experiments (**Figures 3** and **5**; **Figure S4**).

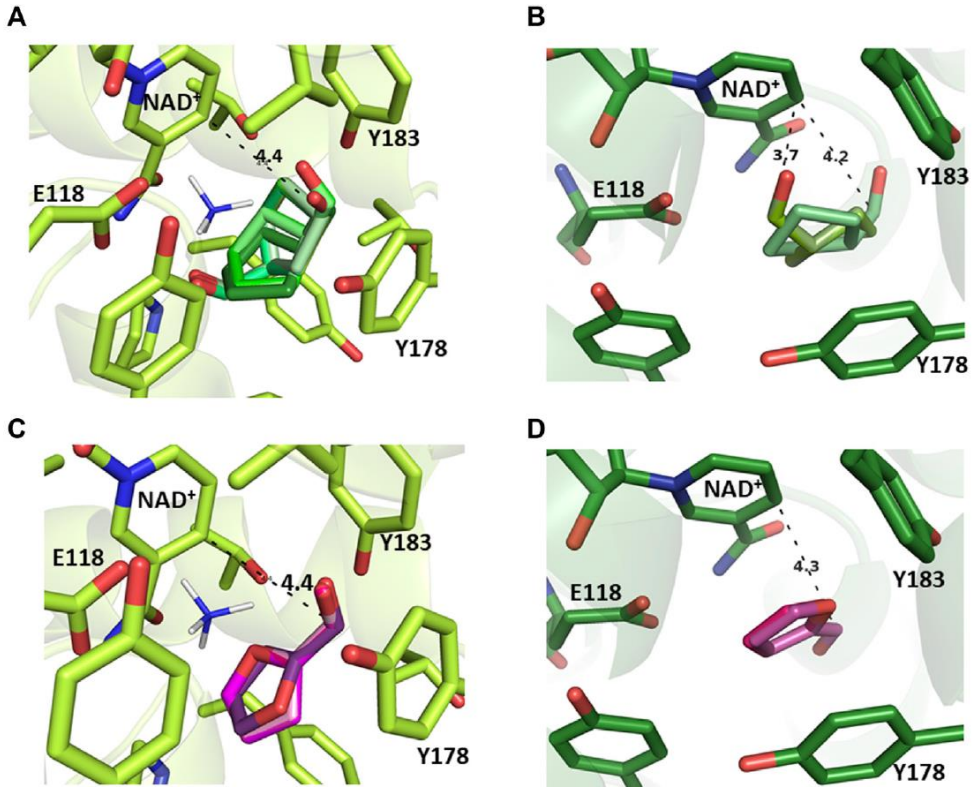

Figure 5. Active sites of *Rgna*AmDH docked (A) with NH_4^+ and **7a**; (B) without NH_3 and **7a**; (C) with NH_4^+ and **6a**; (D) without NH_3 and **6a**. Distances are in Å. For clarity, only one conformation is shown in the case of several almost identical conformations.

Conclusion

Based on the determined kinetic parameters, *Msme*AmDH performs both carbonyl reduction and reductive amination in the same range, in absence or

presence of ammonia source, respectively. It differs from LE-AmDH-v1, which was reported to act preferentially as an AmDH with benzaldehyde, mainly due to a much higher k_{app}.[34] However, the effect on K_M was similar as LE-AmDH-v1 also exhibited four-fold better K_{Mapp} for the reduction, as for *Msme*AmDH. Compared to the well described alcohol dehydrogenase (ADH) from *Ralstonia* sp. (RADH), which was shown to prefer aromatic and cyclic aliphatic compounds, the K_M for **15a** was 60 times lower for *Msme*AmDH than for RADH (10.8 mM for RADH at the same pH 7.5). The K_M for the NADPH cofactor was more in the same range (0.008 mM for RADH). The affinity of *Msme*AmDH for cyclohexanone **15a** in the reduction condition at pH 7.5 was also higher than for other ADHs/KREDs, such as that of *Methanobacterium palustre* (K_M = 6.5 mM), despite a much lower velocity (V_{max} = 30 U/mg; k_{cat} = 86 s^{-1}).[42] The catalysis is extremely less reversible for *Msme*AmDH than for both RADH and ADH from *Mb. Palustre,* reported to catalyze both the reduction of **15a** and the oxidation, even if the reduction was faster (2.5-fold at pH 9.0 in Tris-HCl buffer and 18-fold at pH 7.5 respectively).[43] *Msme*AmDH, and by extension the nat-AmDHs, therefore appear as good enzymes for the reduction of ketones to alcohols with the particularity of having almost no activity in the reverse direction of oxidation. The docking experiments carried out in this study allowed to formulate hypotheses for the KRED promiscuous activity of some nat-AmDHs with a few substrates, based on distance and energy differences. But highlighting some key residues responsible for variations in AmDH/KRED activity ratios, *via* different product positioning, remains a challenge because the first layer in enzymes with either low or high promiscuous KRED activities are all similar. Further analysis such as molecular dynamics at different pH could provide clues. The dual activity shown in this study raises the question of whether there is a link between the two families of enzymes nat-AmDHs and KREDs. Nevertheless, the demonstrated catalytic glutamate, not present in KREDs and not required in the ketoreduction mechanism, does not point to an evolutionary relationship. This hypothesis will perhaps be clarified when the metabolic role of nat-AmDHs will be elucidated, which is not currently the case for *Cfus*AmDH and *Msme*AmDH homologs .

This study highlights a key feature of the native AmDH family, i.e., the potential of some of these enzymes to perform ketoreduction, even quite efficiently for some substrate/enzyme couples. Such behavior is not detrimental for their use as biocatalysts for amine synthesis as no, or only traces, of the corresponding alcohols could be detected in the presence of excess of ammonia, required for the amination reaction. On the contrary, this dual activity can be beneficial in some synthetic schemes where the AmDH and KRED activities could be alternatively turned off or turned on depending on the reaction conditions. Nevertheless, their very low activity in the oxidative direction would prevent their

use in one pot neutral hydrogen borrowing cascades with a single enzyme, as already reported with LysEDH variants.

Materials and Methods

Chemicals and Materials

All chemicals were obtained from commercial suppliers Sigma Aldrich, Acros Organics, Supelco, Thermo Scientific and CombiBlocks with the highest purity available. Glucose dehydrogenase GDH-105 was generously donated by Codexis®. GC-FID analysis were performed either on a Shimadzu GC-2010 gas chromatographs (Shimadzu, Japan) with an AOC-20i Auto injector equipped with a flame ionization detector (FID) and using nitrogen as the carrier gas (GC-FID 1), either on a Gas Chromatograph Trace 1,300 (Thermo Scientific) equipped with an autosampler injector AI/ AS1310, a Flame Ionization Detector (FID) and a H_2 Generator Alliance (F-DGSi) (GC-FID 2). All samples were injected with GC quality solvents. The AmDHs used in this study have already been described.[18, 20, 21, 31, 40] New batches were produced, according to the protocol already described, for IGCAmDH1, IGCAmDH1-W144A, *Rgna*AmDH, *Rgna*AmDHW155A, MATOUAmDH2, *Apau*AmDH, *Apau*AmDH-W141A, *Porti*AmDH, *Porti*AmDH-W140A, *Micro*AmDH, *Msme*AmDHW141A, *Sgor*AmDH, IGCAmDH5 and AcolAmDH (SI **Figure S1**). For *Cfus*AmDH, *Cfus*AmDH-W145A, *Chat*AmDH, MATOUAmDH2-C148A and *Msme*AmDH, previous batches obtained from previous studies and stored at −80˚C were used.[21, 40] Spectrophotometric assays were recorded on a Safas UVMC2 (Safas, Monaco) thermostated at 30 °C with a refrigerated/heating circulator Corio CD-200F (Jubalo®, Seelbach, Germany) using microcells high precision cell quartz with 10-mm light path (Hellma Analytics, Müllheim, Germany).

GC-FID conditions

On GC-FID 1, the samples were injected on a CP-Sil 5 CB (25 m × 0.25 mm × 1.20 µm) with the following parameters: Injection at 340 °C, split ratio 100, linear velocity 30 cm/s, column flow 4 mL/min, nitrogen as carrier gas. Details on the oven temperature program and retention times are given in **Figure S1**. For chiral GC-FID analyses, the samples were injected on CP-Chirasil Dex CB (Agilent J&W) (25 m × 0.32 mm × 0.25 µm, injection at 250 °C, split ratio 25, linear velocity 30 cm/s, column flow 1.68 mL/min, helium as carrier gas) for compounds **9a**, **9c**, **16a**, and **16c** and on Hydrodex β-TBDM (50 m × .25 mm × 0.15 µm, injection at 250 °C split ratio 25, linear velocity 38 cm/s, column flow 2.35 mL/min, helium as carrier gas) for **11a** and **11c**. Details on the oven temperature program and retention times are described in SI **Table S2**. On GC-FID 2, samples were injected on TG-35MS AMINE column (30 m × 0.25 mm × 1 µm; Thermo

Scientific), TG-624SILMS column (30 m × 0.25 mm × 1.4 µm; Thermo Scientific), ZB-XLB column (20 m × 0.18 mm × 0.18 µm; Phenomenex) or CP-Chirasil Dex-CB column (25 m × 0.32 mm × 0.25 µm; Agilent) with H_2 as carrier gas (30 mL/min). Details on the oven temperature programs, split ratio, detector and inlet temperature and retention times are detailed in **Table S3**.

pH study of ketoreductase activity with *Msme*AmDH

The reactions were performed in 100 mM NaPi buffer at pH ranging from 6.0 to 9.0 in a final volume of 1.0 mL. A solution of 10 mM substrate **15a**, 0.2 mM $NADP^+$, 12 mM glucose, 3 U/mL glucose dehydrogenase (GDH-105), 0.1 mg/mL *Msme*AmDH, 1% v/v DMSO was stirred in a thermomixer at 400 rpm and 25 °C for 4 h. Extraction was carried out with 1 mL of ethyl acetate (EtOAc), the organic layer was dried over $MgSO_4$, and analyzed on GC-FID 1. Cyclohexanol **15c** concentrations were deduced from a calibration curve equation using 5 mM dodecane as an internal standard and **15c** reference standards. GC-FID chromatograms of reference standards, control reaction and one example of reaction with *Msme*AmDH are provided in **Figure S2**.

Conversion, *ee* and *de* analysis for reductive amination and ketoreductase activities (GC-FID monitoring)

All the selected AmDHs were screened for conversion of a range of carbonyl-containing substrates to corresponding amines and alcohols as follows. To a reaction mixture (200 µL in 500 µL Eppendorf tubes) containing 10 mM carbonyl-containing substrate (for substrates 3, 4, 8, 11, 13, and 14, 200 mM stock solutions were prepared in DMSO rather than H_2O, with 5% v/v in the final reaction mixture), 0.2 mM NAD^+, 0.2 mM $NADP^+$, 3 U/mL GDH-105, 12 mM glucose in the appropriate buffer (for reaction with ammonia/ammonium species: 2 M NH_4HCO_2/NH_4OH buffer at pH 8.5, for ammonia-free reactions: 100 mM sodium phosphate buffer at pH 7.5), was added 0.5 mg/mL of purified enzymes. For each substrate, a blank mixture was prepared in the same manner but lacking the enzyme replaced by an appropriate volume of desalting buffer used for protein purification. The reaction mixtures and the calibration points were stirred at 25 °C for 24 h at 400 rpm. To 80 µL of mix reaction were added 20 µL of 10 M NaOH and an extraction with 200 µL was performed with solvent (EtOAc or methyl tert-butyl ether (MTBE)) containing known amount of internal standard (1.5 mM dodecane or toluene) related in SI **Table S3**. The organic layers were then analyzed on GC-FID 2 according to conditions detailed in SI **Table S3**. Product **b** and **c** concentrations were deduced from calibration curves equation prepared with various ratio of ketone/alcohol/amine (or ketone/alcohol in the case of ammonia-free reactions) in the corresponding buffer and in presence of an

appropriate volume of desalting buffer. Examples of GC-FID chromatograms are provided in **Figure S3**. In addition, the organic layers were analyzed on GC-FID 1 according to conditions detailed in Supplementary **Table S2**, with chiral columns to determine the enantiomeric and diastereomeric excesses of chiral alcohols.

Determination of kinetic parameters

Kinetic parameters were determined by spectrophotometric NADPH-monitoring in the forward ketoreduction direction at 340 nm. The reactions were performed in 100 mM potassium phosphate buffer pH 7.5 in a final volume of 100 µL at 30 °C in a spectrophotometer cell with optical paths of 1 cm. Initial rates of the reaction were measured after addition of the purified enzyme (0.1 mg/mL) with various concentrations of **15a** (or NADPH) and saturated concentrations of NADPH at 0.2 mM (or **15a** at 2 mM). The uncertainties are those generated by the fitting and the data are averages of three independent experiments. The conditions, fitting and determination of kinetic parameters were performed with Sigma Plot software and plots are provided in Supplementary **Figure S5**.

Specific activities in ketoreduction and alcohol oxidation catalysis

The reactions were conducted in duplicate at 30 °C in a thermostated spectrophotometric cell (10 mm light path) in a final reaction volume of 100 µL. For the KRED activity, the reactions were performed in potassium phosphate buffer pH 7.5 with 0.2 mM of NADPH and 0.1-0.3 mg/mL of enzyme (*Msme*AmDH, MATOUAmDH2, *Cfus*AmDH, IGCAmDH1, *Micro*AmDH). Initial rates of the reaction were measured at 340 nm after addition of 2-10 mM of substrate (**6a**, **7a**, **15a**) to determine the specific activity of the enzyme according to Beer–Lambert's law and the molar absorptivity of β-NADPH (ε = 6,220 M^{-1} cm^{-1}) after subtraction of the slope obtained under the same conditions except without enzyme. The calculated specific activities are detailed in SI **Table S4**. For alcohol oxidation activity, the reactions were performed in 100 mM Tris-HCl pH 8.6 buffer with 0.2 mM of $NADP^+$ and 2 mM of **7c** or **15c**. Initial rates of the reactions were measured at 340 nm after addition of 1 mg/mL of *Msme*AmDH to determine the specific activity as mentioned above after subtraction of the slope obtained under the same conditions but lacking substrate.

Docking experiments

For study cases in ammonia-free buffer, the products **6a**, **6c**, **7a**, **7c** and **15c** were docked into the closed conformations of structures of MATOUAmDH2-NADP (PDB ID: 7ZBO), *Msme*AmDH-NADP (PDB ID: 6IAQ) and *Cfus*AmDH-NADP-**15b** (PDB ID: 6IAU) after removal of the amine **15b**, and on models of

*Rgna*AmDH-NAD, *Micro*AmDH-NAD(P) and IGCAmDH1-NAD,[17, 18] energy minimized beforehand to obtain the more favored positioning of the nicotinamide cofactor from its copied position in the *Cfus*AmDH-NADP structure. The latter were previously energy minimized without restraints, using the YASARA2 force field within YASARA, after addition of the nicotinamide cofactor copied from the *Cfus*AmDH-NADP structure.[44] For study cases in presence of ammonia/ammonium with *Rgna*AmDH, the model of *Cfus*AmDH-**15a**-NH_4, already published, was used as a template to paste the ammonium molecule, after alignment of models using PyMOL Molecular Graphics System (Version 2.0 Schrödinger, LLC).[17] NAD cofactor was built from the *Cfus*AmDH-NADP structure by replacing the phosphate group (P2B, O1X, O2X and O3X atoms) with a hydrogen atom. The ligand PDB files were generated using the CORINA Molecular Online Tool (https://demos.mn-am.com/corina.html). With AutoDockTool, the docking simulations were performed on rigid structures, with no flexibility given to any catalytic pocket residues.[45] The box was centered in the active site with the following size: 34, 36, 30 (36, 38, 30 in the case of dockings in presence of NH_3) (Autodock parameters). The number of Genetic Algorithm (GA) runs was fixed at 10 using the Lamarckian GA (4.2). The 10 ligand conformations obtained were then analyzed on PyMOL Molecular Graphics System (Version 2.0 Schrödinger, LLC).

Supporting information

The complete supporting information of this article, including Supplementary **Figures S2**, **S3**, **S4** and **S8** can be found at the following doi: 10.3389/fctls.2023.1105948.

Supplementary figures

IGCAmDH1 4.10 mg/mL	IGCAmDH1 W144A 3.06 mg/mL	RgnaAmDH 10.16 mg/mL	RgnaAmDH W155A 7.61 mg/mL	MATOUAmDH2 6.74 mg/mL
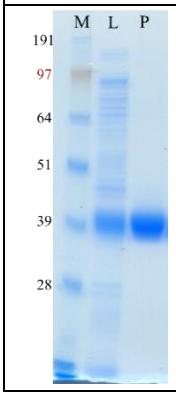	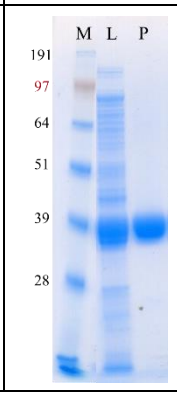	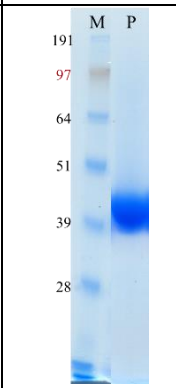	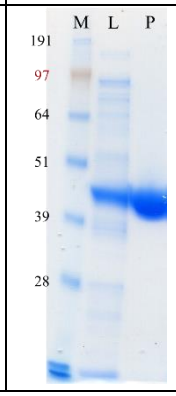	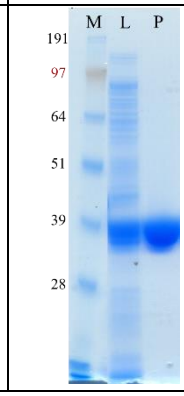

ApauAmDH 3.70 mg/mL	ApauAmDH W141A 2.84 mg/mL	PortiAmDH 2.10 mg/mL	PortiAmDH W140A 4.69 mg/mL	MicroAmDH 2.97 mg/mL
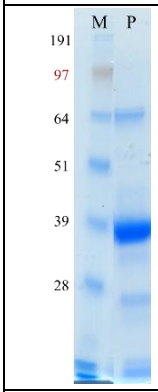	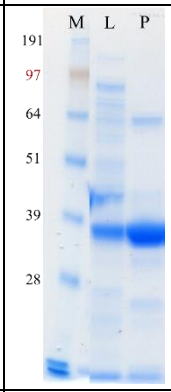	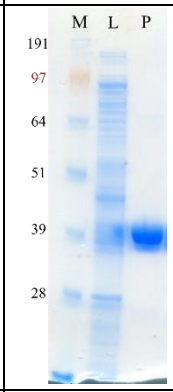	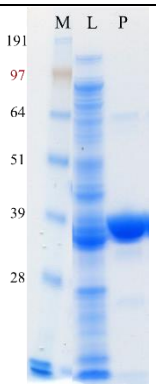	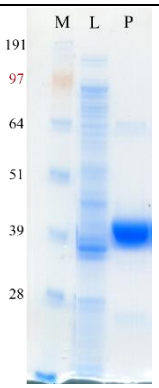
MsmeAmDH W141A 5.37 mg/mL	SgorAmDH 2.49 mg/mL	IGCAmDH5 5.52 mg/mL	AcolAmDH 4.60 mg/mL	
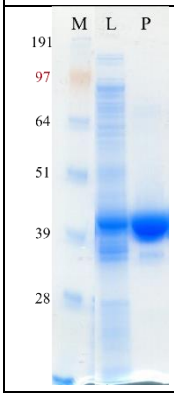	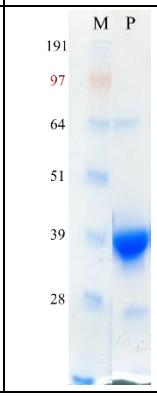	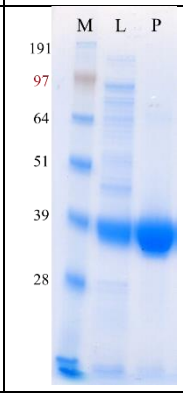	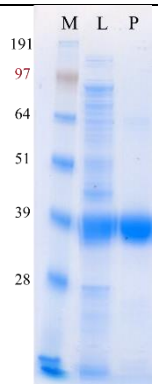	

Figure S1. SDS-PAGE gels of enzymes obtained according to the protocol already described for *Cfus*AmDH and *Cfus*AmDH-W145A.[21] M = molecular marker SeeBlue® Plus2 pre-strained standard (5 µg deposited), L = cell-free extracts (15 µg deposited) and P = purified enzymes (5 µg deposited).

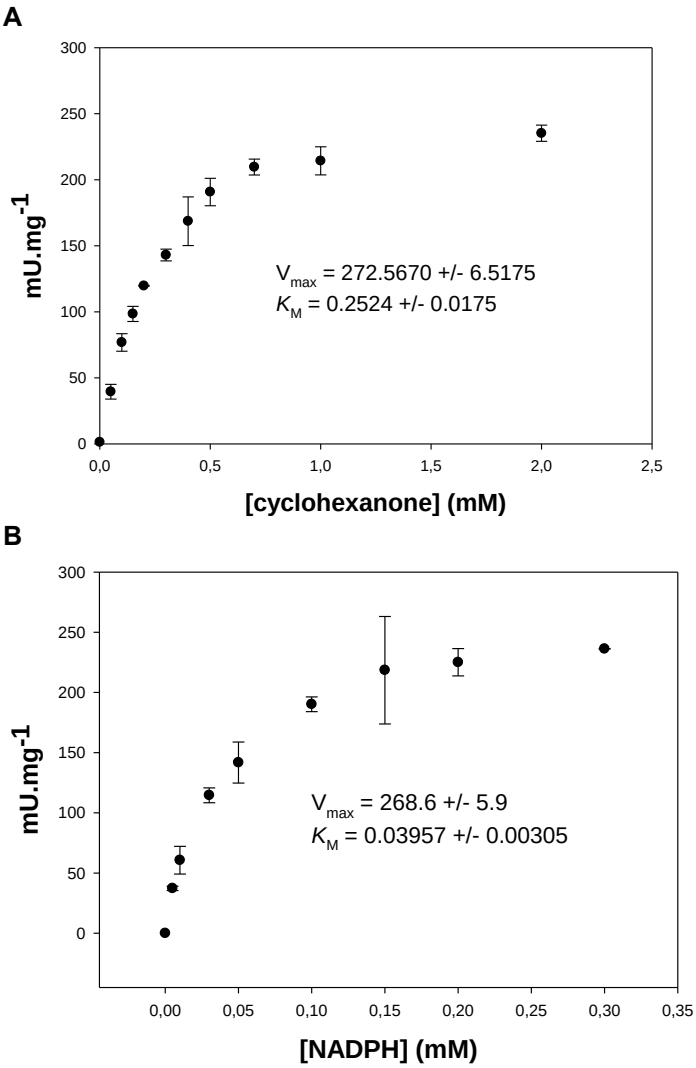

Figure S5. Plots for kinetic parameter determination of *Msme*AmDH for the ketoreductase activity toward **15a** for A) cyclohexanone (conditions: 100 mM KPi buffer pH 7.5, 0.2 mM NADPH, 30 °C, 0.1 mg/mL *Msme*AmDH) and B) NADPH (conditions: 100 mM potassium phosphate buffer pH 7.5, 2 mM cyclohexanone, 30 °C, 0.1 mg/mL *Msme*AmDH). Error bars represent the standard deviation of three independent experiments. The uncertainties of the kinetic parameters values are those generated by the fitting.

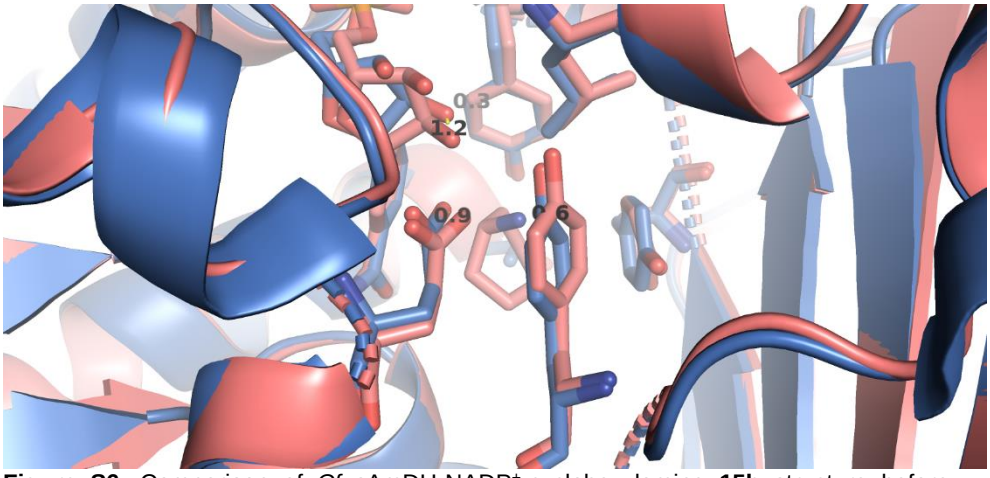

Figure S6. Comparison of *Cfus*AmDH-NADP$^+$-cyclohexylamine **15b** structure before (blue) and after (pink) energy minimization from X-ray structure (PDB ID: 6IAU).

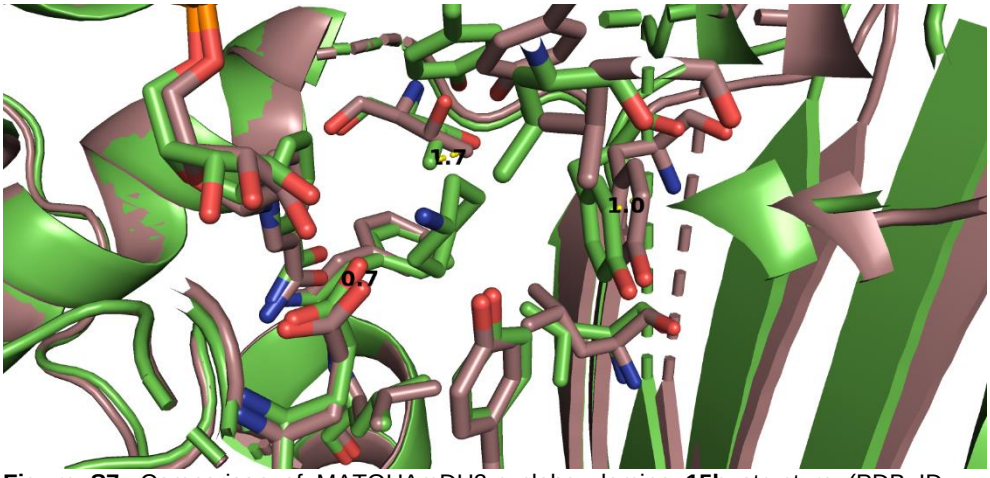

Figure S7. Comparison of MATOUAmDH2-cyclohexylamine **15b** structure (PDB ID: 7ZBO) (green) and energy minimized model of MATOUAMDH2 built from *Cfus*AmDH template.[18] Some distances (Å) between two identical residues in each model are indicated.

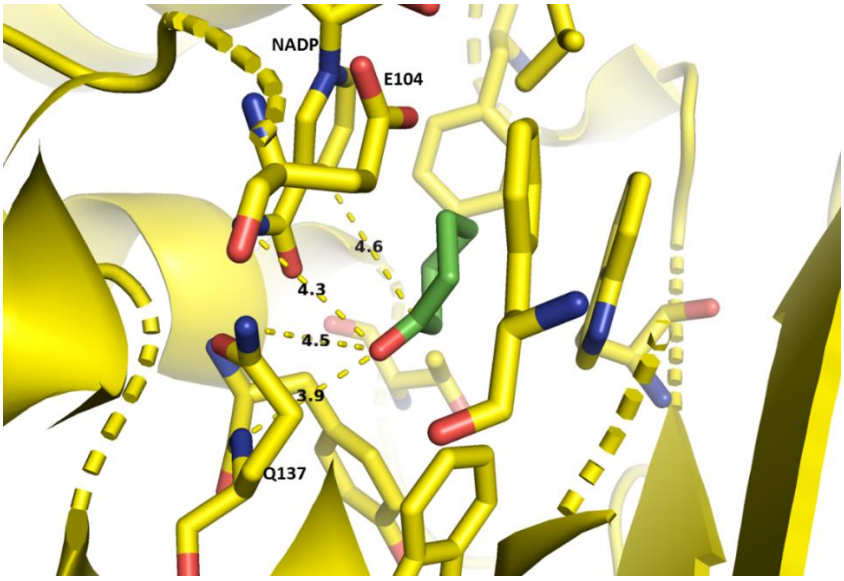

Figure S9. Positioning of cyclohexanone **15a** docked into *Msme*AmDH (only one conformation is presented for clarity, but all the docked conformations were the same). Distances (Å) leading to potential H bonds with NH backbone Q137, NH_2 amide Q137 and NH_2 amide nicotinamide are represented in dashed lines, in addition to the distance between the reactive carbon of **15a** and C4 nicotinamide.

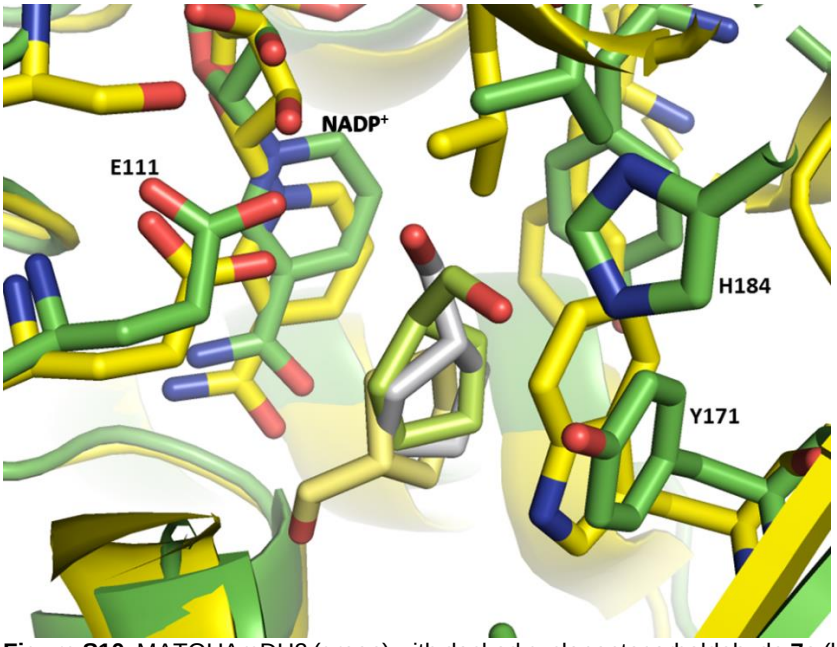

Figure S10. MATOUAmDH2 (green) with docked cyclopentacarbaldehyde **7a** (lime green) flipped compared to docked cyclopentacarbaldehyde **7a** (pale yellow) in *Msme*AmDH (yellow), in addition to docked cyclopentanecarbanol **7c** (grey) in MATOUAmDH2.

Supplementary tables

Table S1. GC method on the CP-Sil 5 CB column with oven program and compound retention times (GC-FID 1)

GC oven program	Retention time (min)
80 °C hold 3 min	cyclohexanone 10.0
5 °C/min to 100 °C hold 4 min	cyclohexanol 9.5
25 °C/min to 345 °C hold 1 min	dodecane (IS) 16.2

Table S2. Chiral GC methods with oven program and compound retention times (GC-FID 1).

GC column	GC oven program			Retention time (min)
CP-Chirasil Dex CB	°C/min	°C	hold (min)	
	-	50	2	
	5	55	2	
	5	60	2	
	5	65	2	2-pentanone **4.2**
	5	70	2	(*R*)-2-pentanol **8.4**
	5	75	2	(*S*)-2-pentanol **8.6**
	5	80	2	DMSO **12.1**
	5	95	2	
	5	100	2	
	5	105	2	
	20	220	1.25	
CP-Chirasil Dex CB	°C/min	°C	hold (min)	
	-	50	15.1	
	1.02	55	2	
	2	60	2	
	2	65	2	(*S*)-2-methylcyclohexanone **36.6**
	2	70	2	(*R*)-2-methylcyclohexanone **37.4**
	2	75	2	*trans*-2-methylcyclohexanol **49.5, 49.8**
	2	80	2	*cis*-2-methylcyclohexanol **51.6, 51.9**
	2	95	2	DMSO **16.7**
	2	100	2	
	2	105	2	
	20	220	1.25	
Hydrodex β-TBDM	°C/min	°C	hold (min)	
	-	50	24	
	5	55	2	
	5	60	2	
	5	65	2	2-heptanone **33.9**
	5	70	2	(*S*)-2-heptanol **46.3**
	5	75	2	(*R*)-2-heptanol **46.5**
	5	80	2	DMSO **39.5**
	5	95	2	
	5	100	2	
	5	105	2	
	20	220	1.25	

Table S3. GC methods on the TG-35MS AMINE column with oven program, split ratio, extracting solvent and compound retention times (GC-FID 2).

Mol ID	Retention time (min)		Extrac-tion	GC conditions					
	a	c	solvent/IS (internal standard)	column	T°C inlet	flow (ml/min)	split flow	split ratio	temperature gradient
1	1.8	2.9	MTBE/ toluene	TG-624 Sil	180	2	80	40	55 °C (0.5 min); 1 °C/min to 62 °C; 30 °C/min to 200 °C (3 min).
2	2.3	3.7	MTBE/ toluene	TG-624 Sil	180	2	80	40	55 °C (0.5 min); 1 °C/min to 60 °C; 30 °C/min to 200 °C (2 min).
3	4.3	5.7	EtOAc/ dodecane	TG-35MS Amine	220	2	20	10	70 °c (0.5 min); 9.73 °C/min to 80 °C (5 min); 10 °C/min to 130 °C; 30 °C/min to 200 °C (5 min).
4	5.7	6.9	EtOAc/ dodecane	TG-35MS Amine	220	2	20	10	80 °C (0.5 min); 10 °C/min to 115 °C (0.15 min); 2 °C/min to 125 °C; 20 °C/min to 200 °C (5 min).
6	4.2	5.2	EtOAc/ toluene	ZB-XLB	220	2	20	10	85 °C (0.5 min); 9.73 °C/min to 100 °C; 1 °C/min to 105 °C; 20 °C/min to 200 °C (5 min).
7	3.9	4.7	EtOAc/ toluene	TG-35MS Amine	220	2	20	10	85 °C (0.5 min); 9.73 °C/min to 100 °C; 1 °C/min to 105 °C ; 20 °C/min to 200 °C (5 min).
8	3.8	4.3	EtOAc/ toluene	TG-35MS Amine	220	2	20	10	95 °C (0.5 min); 20 °C/min to 200 °C (12 min).
13	2.7	2.5	EtOAc/ dodecane	TG-35MS Amine	250	2	20	10	100 °C (0.5 min); 1 °C/min to 105 °C; 20 °C/min to 220 °C (5 min).
9	2.9	2.7	EtOAc/ toluene	TG-35MS Amine	180	1.5	20	13	80 °C (3 min); 2 °C/min to 90 °C; 30 °C/min to 200 °C (0.5 min).
10	3.5	3.3	EtOAc/ toluene	TG-35MS Amine	220	2	20	10	80 °C (0.5 min); 2 °C/min to 90 °C ; 30 °C/min to 200 °C (5 min).
11	4.9	4.7	EtOAc/ toluene	TG-35MS Amine	220	2	20	10	80 °C (0.5 min); 9.73 °C/min to 90 °C (2 min); 10°C/min to 130 °C; 30°C/min to 200 °C.
12	3.3	4.9	EtOAc/ toluene	TG-35MS Amine	220	2	20	10	82 °C (0.5 min); 2 °C/min to 87 °C; 30 °C/min to 200 °C (5 min).
14	6.4	6.7	EtOAc/ dodecane	TG-624 Sil	200	2	20	10	110 °C (0.5 min); 15 °C/min to 150 °C ; 3 °C/min to 165 °C ; 15 °C/min to 200 °C (1 min).
14	3.5	3.6		TG-35MS Amine	250	2	20	10	110 °C (0.5 min); 5 °C/min to 120 °C ; 20 °C/min to 250 °C (3 min).
14		(S) : 23.7 (R) : 24.7		CP-Chirasil Dex-CB	225	2	20	10	85 °C (0.5 min); 1 °C/min to 113 °C; 10 °C/min to 200 °C (3 min).
15	6.8	6.1	EtOAc/ toluene	TG-35MS Amine	180	2	20	10	80 °C (0.5 min); 2 °C/min to 90 °C; 30 °C/min to 200 °C (5 min).
16	7.3	6.8/6.9	EtOAc/ dodecane	TG-35MS Amine	180	2	20	10	80 °C (0.5 min); 2 °C/min to 90 °C; 30°C/min to 200 °C (3 min).

Table S4. Specific activities of *Msme*AmDH, MATOUAmDH2, *Micro*AmDH, *Cfus*AmDH, *Rgna*AmDH, IGCAmDH1 for the ketoreduction of **6a**, **7a** and **15a**

	Specific activities (mU/mg)					
	*Msme*AmDH	MATOUAmDH2	*Cfus*AmDH	*Micro*AmDH	IGCAmDH1	*Rgna*AmDH
6a	0.2 ± 0.0	0.2 ± 0.0	0.5 ± 0.0	0.6 ±0.2	0.4 ± 0.0	0.5 ± 0.1
7a	5.2 ± 0.2	58.4 ± 1.1	2.4 ± 0.3	22.8 ± 3.5	0.4 ± 0.0	14.6 ± 1.1
15a	235.2 ± 4 .3	9.7 ± 0.9	39.4 ± 0.4	510.6 ± 7.2	0.5 ± 0.0	2.6 ± 0.1

Conditions: Ketone substrate **6a**, **7a**, **15a** at 2 or 10 mM, potassium phosphate buffer pH 7.5, 0.2 mM NADPH, 0.1-1.0 mg/mL of enzyme (*Msme*AmDH, MATOUAmDH2, *Cfus*AmDH, IGCAmDH1, *Micro*AmDH). Specific activities were determined according to the protocol described in Materials and Methods.

References

[1] K. L. J. Prather, *Nat. Catal.* **2020**, *3*, 181-183.

[2] S. K. Wu, R. Snajdrova, J. C. Moore, K. Baldenius, U. T. Bornscheuer, *Angew. Chem. Int. Ed.* **2021**, *60*, 88-119.

[3] S. Simic, E. Zukic, L. Schmermund, K. Faber, C. K. Winkler, W. Kroutil, *Chem. Rev.* **2022**, *122*, 1052-1126.

[4] F. Hollmann, D. J. Opperman, C. E. Paul, *Angew. Chem. Int. Ed.* **2021**, *60*, 5644-5665.

[5] L. Ducrot, M. Bennett, G. Grogan, C. Vergne-Vaxelaire, *Adv. Synth. Catal.* **2021**, *362*, 328-351.

[6] M. J. Abrahamson, E. Vazquez-Figueroa, N. B. Woodall, J. C. Moore, A. S. Bommarius, *Angew. Chem. Int. Ed.* **2012**, *51*, 3969-3972.

[7] M. J. Abrahamson, J. W. Wong, A. Bommarius, *Adv. Synth. Catal* **2013**, *355*, 1780-1786.

[8] L. J. Ye, H. H. Toh, Y. Yang, J. P. Adams, R. Snajdrova, Z. Li, *ACS Catal.* **2015**, *5*, 1119-1122.

[9] T. Knaus, W. Böhmer, F. G. Mutti, *Green Chem.* **2017**, *19*, 453-463.

[10] F. F. Chen, G. W. Zheng, L. Liu, H. Li, Q. Chen, F. L. Li, C. X. Li, J. H. Xu, *ACS Catal.* **2018**, *8*, 2622-2628.

[11] F. F. Chen, S. C. Cosgrove, W. R. Birmingham, J. Mangas-Sánchez, J. Citoler, M. P. Thompson, G. W. Zheng, J. H. Xu, N. J. Turner, *ACS Catal.* **2019**, *9*, 11813-11818.

[12] R. D. Franklin, C. J. Mount, B. R. Bommarius, A. S. Bommarius, *ChemCatChem* **2020**, *12*, 2436-2439.

[13] L. Liu, D. H. Wang, F. F. Chen, Z. J. Zhang, Q. Chen, J. H. Xu, Z. L. Wang, G. W. Zheng, *Catal. Sci. Technol.* **2020**, *10*, 2353-2358.

[14] J. Lu, Z. J. Wang, Y. Jiang, Sun, Z., W. Luo, *Syst. Microbiol. Biomanuf.* **2022**, *3*, 384-392.

[15] V. Tseliou, T. Knaus, M. F. Masman, M. L. Corrado, F. G. Mutti, *Nat. Commun.* **2019**, *10*, 3717.

[16] O. Mayol, S. David, E. Darii, A. Debard, A. Mariage, V. Pellouin, J. L. Petit, M. Salanoubat, V. de Berardinis, A. Zaparucha, C. Vergne-Vaxelaire, *Catal. Sci. Technol.* **2016**, *6*, 7421-7428.

[17] O. Mayol, K. Bastard, L. Beloti, A. Frese, J. P. Turkenburg, J.-L. Petit, A. Mariage, A. Debard, V. Pellouin, A. Perret, V. de Berardinis, A. Zaparucha, G. Grogan, C. Vergne-Vaxelaire, *Nat. Catal.* **2019**, *2*, 324-333.

[18] A. A. Caparco, E. Pelletier, J. L. Petit, A. Jouenne, B. R. Bommarius, V. de Berardinis, A. Zaparucha, J. A. Champion, A. S. Bommarius, C. Vergne-Vaxelaire, *Adv. Synth. Catal.* **2020**, *362*, 2427-2436.

[19] R. F. Cai, L. Liu, F. F. Chen, A. T. Li, J. H. Xu, G. W. Zheng, *ACS Sust. Chem. Eng.* **2020**, *8*, 17054-17061.

[20] M. Bennett, L. Ducrot, C. Vergne-Vaxelaire, G. Grogan, *ChemBioChem* **2022**, *23*.

[21] L. Ducrot, M. Bennett, G. André-Leroux, E. Elisée, S. Marynberg, A. Fossey-Jouenne, A. Zaparucha, G. Grogan, C. Vergne-Vaxelaire, *ChemCatChem* **2022**.

[22] D. Wetzl, M. Gand, A. Ross, H. Müller, P. Matzel, S. P. Hanlon, M. Müller, B. Wirz, M. Höhne, H. Iding, *ChemCatChem* **2016**, *8*, 2023-2026.

[23] G. A. Aleku, S. P. France, H. Man, J. Mangas-Sánchez, S. L. Montgomery, M. Sharma, F. Leipold, S. Hussain, G. Grogan, N. J. Turner, *Nat. Catal.* **2017**, *9*, 961-969.

[24] G. D. Roiban, M. Kern, Z. Liu, J. Hyslop, P. L. Tey, M. S. Levine, L. S. Jordan, K. K. Brown, T. Hadi, A. F. Ihnken, M. J. B. Brown, *ChemCatChem* **2017**, *9*, 4475-4479.

[25] M. Sharma, J. Mangas-Sánchez, S. P. France, G. A. Aleku, S. L. Montgomery, J. I. Ramsden, N. J. Turner, G. Grogan, *ACS Catal.* **2018**, *8*, 11543-11541.
[26] J. R. Marshall, P. Yao, S. L. Montgomery, J. D. Finnigan, T. W. Thorpe, R. B. Palmer, J. Mangas-Sánchez, R. A. M. Duncan, R. S. Heath, K. M. Graham, D. J. Cook, S. J. Charnock, N. J. Turner, *Nat. Chem.* **2021**, *13*, 140-148.
[27] S. L. Montgomery, A. Pushpanath, R. S. Heath, J. R. Marshall, U. Klemstein, J. L. Galman, D. Woodlock, S. Bisagni, C. J. Taylor, J. Mangas-Sánchez, J. I. Ramsden, B. Dominguez, N. J. Turner, *Sci. Adv.* **2020**, *6*, eaay9320.
[28] E. J. Ma, E. Siirola, C. Moore, A. Kummer, M. Stoeckli, M. Faller, C. Bouquet, F. Eggimann, M. Ligibel, D. Huynh, G. Cutler, L. Siegrist, R. A. Lewis, A. C. Acker, E. Freund, E. Koch, M. Vogel, H. Schlingensiepen, E. J. Oakeley, R. Snajdrova, *ACS Catal.* **2021**, *11*, 12433-12445.
[29] Z. Y. Yang, Y. C. Hao, S. Q. Hu, M. H. Zong, Q. Chen, N. Li, *Adv. Synth. Catal.* **2021**, *363*, 1033-1037.
[30] J. Zhang, D. Liao, R. Chen, F. Zhu, Y. Ma, L. Gao, G. Qu, C. Cui, Z. Sun, X. Lei, S. S. Gao, *Angew. Chem. Int. Ed.* **2022**, *61*, e202201908.
[31] L. Ducrot, M. Bennett, A. A. Caparco, J. A. Champion, A. S. Bommarius, A. Zaparucha, *Front. Catal.* **2021**, *363*, 328-351.
[32] J. An, Y. Nie, Y. Xu, *Crit. Rev. Biotechnol.* **2019**, *39*, 366-379.
[33] G. De Gonzalo, C. E. Paul, *Curr. Opin. Green. Sust.* **2021**, *32*.
[34] V. Tseliou, D. Schilder, M. F. Masman, T. Knaus, F. G. Mutti, *Chem. Eur. J.* **2021**, *27*, 3315-3325.
[35] M. Lenz, J. Meisner, L. Quertinmont, S. Lutz, J. Kästner, B. M. Nestl, *ChemBioChem* **2017**, *18*, 253-256.
[36] D. González-Martínez, A. Cuetos, M. Sharma, M. García-Ramos, I. Lavandera, V. Gotor-Fernández, G. Grogan, *ChemCatChem* **2020**, *12*, 2421-2425.
[37] M. Lenz, S. Fademrecht, M. Sharma, J. Pleiss, G. Grogan, B. M. Nestl, *Protein Eng. Des. Sel.* **2018**, *31*, 109-120.
[38] S. Roth, A. Präg, C. Wechsler, M. Marolt, S. Ferlaino, S. Lüdeke, N. Sandon, D. Wetzl, H. Iding, B. Wirz, M. Müller, *ChemBioChem* **2017**, *18*, 1703-1706.
[39] S. Roth, P. Stockinger, J. Steff, S. Steimle, V. Sautner, K. Tittmann, J. Pleiss, M. Müller, *ChemBioChem* **2020**, *21*, 2615-2619.
[40] E. P. J. Jongkind, A. Fossey-Jouenne, O. Mayol, A. Zaparucha, C. Vergne-Vaxelaire, C. E. Paul, *ChemCatChem* **2022**, *14*, e202101576.
[41] P. K. Agarwal, S. P. Webb, S. Hammes-Schiffer, *J. Am. Chem. Soc.* **2000**, *122*, 4803-4812.
[42] K. Bleicher, J. Winter, *Eur. J. Biochem.* **1991**, *200*, 43-51.
[43] J. Kulig, A. Frese, W. Kroutil, M. Pohl, D. Rother, *Biotechnol. Bioeng.* **2013**, *110*, 1838-1848.
[44] E. Krieger, K. Joo, J. Lee, J. Lee, S. Raman, J. Thompson, M. Tyka, D. Baker, K. Karplus, *Proteins* **2009**, *77*, 114-122.
[45] G. M. Morris, R. Huey, W. Lindstrom, M. F. Sanner, R. K. Belew, D. S. Goodsell, A. J. Olson, *J. Comput. Chem.* **2009**, *30*, 2785-2791.

Chapter 4: Mechanistic insights in *Lactobacillus brevis* alcohol dehydrogenase: stability and active site role of Ser143 and Tyr156

E.P.J. Jongkind,[1] W.J. Kools,[1] M. Pareek,[2] S.C.L. Kamerlin,[2,3] C.E. Paul*,[1]

[1] *Biocatalysis section, Department of Biotechnology, Delft University of Technology, Van der Maasweg 9, 2629 HZ Delft, The Netherlands.*
[2] *Department of Chemistry-BMC, Uppsala University, BMC Box 576, S-751 23 Uppsala, Sweden*
[3] *School of Chemistry and Biochemistry, Georgia Institute of Technology, 901 Atlantic Drive NW, Atlanta, GA 30332, USA*

Manuscript in preparation

Summary

Alcohol dehydrogenases are currently industrially applied for their exquisite selectivity for asymmetric reduction of carbonyls to potent chiral alcohols. In particular, *Lactobacillus brevis* alcohol dehydrogenase (*Lb*ADH) is known for its high activity and stability, although this data has been inconsistent in literature. We determined the specific activity with acetophenone to be 96 U/mg after two months of storage at 4°C in 10% v/v glycerol and 50 mM NaCl. Previous work showed the possibility to engineer an amino acid dehydrogenase to an amine dehydrogenase (AmDH) to synthesize valuable chiral amines. Therefore, we envisioned to repurpose *Lb*ADH to an AmDH through rational design with single variants Y156E and S143E, inspired by the active site of AmDH. Further amino acid substitutions were predicted using the FuncLib algorithm to ensure stable and active variants. Despite promising molecular dynamics predictions, no amine dehydrogenase activity was observed but 4% of 10 mM imine was reduced by *Lb*ADH-Y156E. This work shows the surprising variation in activity and stability of *Lb*ADH along with the essential role of Tyr156 and Ser143 in its catalytic active site and provides insights on further amino acids positions and predictions. This study also highlights the complexity of rationally re-purposing *Lb*ADH, despite promising computational predictions, and highlights the need for further studies on the *Lb*ADH activity and storage conditions.

Introduction

Alcohol dehydrogenases (ADHs) are ubiquitous in nature and catalyze the reversible asymmetric reduction of carbonyl substrates into corresponding chiral alcohols. Large panels of ADHs are characterized and available to be used in industry with their exquisite activity and enantioselectivity.[1] Chiral alcohols are essential for the synthesis of fine chemicals or active pharmaceutical ingredients (APIs), with recent examples including an engineered alcohol dehydrogenase from *Paraburkholderia hospita* to obtain (*S*)-3-cyclopentyl-3-hydroxypropanenitrile, a precursor for ruxolitinib.[2] Another example is an engineered ADH from *Kluyveromyces marxianus*, which is capable of forming the precursor of atorvastatin (*tert*-butyl 6-cyano-(3*R*,5*R*)-dihydroxyhexanoate [3, 4] In parallel, the chiral amine moiety is highly valuable and found in *ca.* 40% of pharmaceutical ingredients.[5, 6] Besides enzymes from the hydrolase[7, 8] and transferase classes[9], many enzyme families have been discovered from the oxidoreductase class.[10] Previous work on amino acid dehydrogenases (AADH) demonstrated the possibility to engineer these enzymes to gain amine dehydrogenase (AmDH) activity.[11, 12] However, these engineered AmDHs are mostly active on aromatic substrates.[13] later, native AmDH (nat-AmDH) were discovered, and mostly accepted smaller, aliphatic aldehydes and ketones.[14-16] Further discoveries of imine reductases (IREDs)[17] and reductive aminases (RedAms)[18] expanded the biocatalytic toolbox to access chiral amines, but these enzymes are plagued by low stability. Applications of IREDs in industry rely on protein engineering to obtain stability.[19-21] Besides stability, broadening the substrate scope was also a target for these enzymes, proving how protein engineering and mutagenesis are essential approaches in industrial applications.[22, 23]

The *anti*-Prelog *R*-selective ADH from *Lactobacillus brevis* (*Lb*ADH)[24] is a short-chain reductase (SDR) that is known for its high activity and stability.[25] In this work, we envisioned to engineer *Lb*ADH to gain AmDH activity to harness the stability and large substrate scope of *Lb*ADH.[14] AmDHs show specific activities in the range of 1 U/mg, whilst *Lb*ADH displays over 100-fold towards multiple ketone substrate.[26] Therefore, *Lb*ADH as a backbone of a new reductive aminating enzyme could combat the main challenges known for AmDHs.

*Lb*ADH requires two magnesium ions for each tetramer,[27] and the active site contains a proton relay system, formed by the residues from asparagine, lysine, tyrosine and serine. Y156 is the catalytic proton donor, S143 binds the substrate in the active site, and both residues stabilize the alkoxide intermediate formed after reduction by the nicotinamide adenine dinucleotide cofactor NADPH. *Lb*ADH also contains residues S142, Y189, E145 and M206 that engage in conformational changes to the holo-enzyme.[27-29]

In Chapters 2 and 3, we observed ketoreduction activity with AmDHs,[30, 31] therefore we compared their active sites and determined relevant residues that would be needed for reductive amination (**Figure 1**). Both enzymes are NADP-dependent oxidoreductases, containing a Rossmann fold domain to bind and position the nicotinamide cofactor in the active site, which contains a proton donating tyrosine residue. We used a computationally guided, semi-rational design approach to create AmDH activity in an ADH (**Figure 2**). The main difference between the active site of the ADH and AmDH is the conserved negatively charged glutamate E108 in the AmDH active site. Therefore, we aimed for mutations in the active site of *Lb*ADH: Y156E and S143E. In this way, the ADH activity would be suppressed while a negative charge, crucial in AmDHs to catalyze reductive amination,[14, 32] is present in the active site. Since function-enhancing mutations may destabilize a protein, we additionally added multiple mutations using the FuncLib algorithm[33] and screened the variants for ketoreduction and reductive amination of different substrates.

Although *Lb*ADH was discovered over 25 years ago and is being used extensively in research and industry, the stability and activity of this enzyme varied drastically in literature. Reported specific activities range from 89 U/mg[26] to 455 U/mg, although conditions are unclear how to reach this activity.[34] To ensure our reaction or storage conditions are not limiting the potential AmDH activity of the *Lb*ADH-mutants, we first determined the specific activity with acetophenone under different conditions. We also assessed several storage conditions to maintain stability of the enzyme.

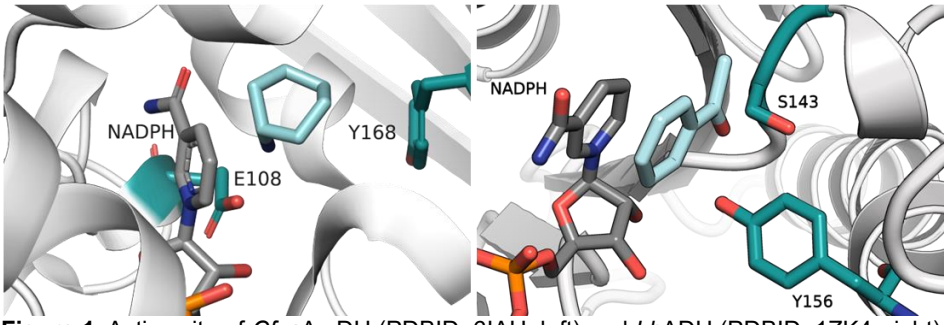

Figure 1. Active site of *Cfus*AmDH (PDBID: 6IAU, left) and *Lb*ADH (PDBID: 1ZK4, right), highlighting the nicotinamide cofactor and catalytic residues in both enzymes. In the active site of *Cfus*AmDH, cyclohexylamine is present, whereas in *Lb*ADH acetophenone is present.

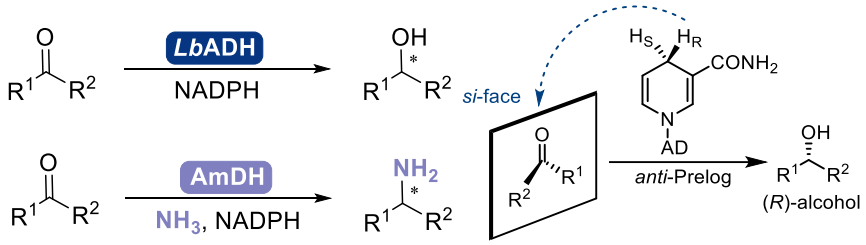

Figure 2. Schematic overview of reactions catalyzed by the *Lb*ADH (top) and amine dehydrogenase (AmDH, bottom). Hydride attack on the *si*-face of the ketone substrate by NADPH (right).

Results and Discussion

Specific activity and stability of *Lb*ADH-wt

After successful expression and purification of the *Lb*ADH-wt (see SI), we determined its specific activity with acetophenone to be 43 U/mg for acetophenone, when measured directly after purification (**Table 1**, entry 3). The specific activity of *Lb*ADH was further measured in different buffers (**Table 1**). Tris-HCl and sodium or potassium phosphate buffers without DMSO as co-solvent resulted in comparable specific activities of *ca.* 40 U/mg. Because of the pH-stability and similarity to storage conditions of the purified *Lb*ADH, KP_i buffer was chosen for further activity measurements and screenings. The *Lb*ADH activity decreased drastically in presence of 5% v/v DMSO, whereas 1% showed no significant activity loss. Likewise, the activity was drastically reduced in 1 M NH_4HCO_2 buffer pH 8.0 and 9.0, which agrees well with the known pH-dependence of ADH activity wherein reduction (comprising hydride and proton transfer to the substrate) is favored at neutral to slightly acidic pH values, whereas oxidation is favored at mildly alkaline pH values.

Table 1. Specific activity of *Lb*ADH in different buffers [a]

Buffer	[Buffer] (mM)	pH	DMSO (% v/v)	Spe. activity (U/mg)
Tris-HCl	50	7.5	0	40.3 ± 1.5
NaH_2PO_4	50	7.5	0	41.0 ± 2.8
KH_2PO_4	50	7.5	1	43.0 ± 1.6
KH_2PO_4	50	7.5	5	4.7 ± 0.1
NH_4HCO_2	1000	8.0	0	16.9 ± 1.1
NH_4HCO_2	1000	9.0	0	0.2 ± 0.1

[a] Conditions: 11 mM acetophenone, 0.2 mM NADPH, varying buffer and DMSO composition, 1 mM $MgCl_2$, 30 °C. Average of triplicates.

The addition of 10% glycerol and 50 mM NaCl improved the retention of activity, especially when the protein was stored at -80 °C or 4 °C (SI Section 4). Storage at -20 °C showed no difference with respect to initial activity. Storage at

4 °C with 10% v/v glycerol and 50 mM NaCl resulted in the highest measured specific activity on day 1 (54.9 U/mg). We also measured the specific activity of *Lb*ADH aliquots stored at -80 °C and 4 °C at various time points over a period of 59 days (**Figure 3**). Again, the specific activity is higher when stored at 4 °C. Moreover, the activity increased over time with storage at 4 °C, reaching a plateau between 90 and 100 U/mg. At -80 °C the activity remained around the starting level (34-50 U/mg).

The highest specific activity we measured for *Lb*ADH was 96 U/mg, which is close to values reported by Kulishova (112.9 U/mg; 10 mM acetophenone, 50 mM Tris-HCl pH 7.5, 1 mM $MgCl_2$, 30 °C)[35] and Kulig (89.6 U/mg; 10 mM acetophenone, 50 mM TEA-HCl pH 7.0, 0.8 mM $CaCl_2$, 30 °C).[26] However, with only 1.5 mM acetophenone, well below the K_M of *Lb*ADH for acetophenone (2.8 mM)[27], a surprisingly high activity of 450 U/mg was reported by Hummel.[34] Reaction conditions were not reported to reach this activity. Machielsen *et al.* also reported high activity with the same acetophenone concentration (355 U/mg; 1.5 mM acetophenone, 100 mM NaP_i pH 6.5, 1 mM $MgCl_2$,30 °C).[36] Regarding the half-life of the *Lb*ADH, storage at 4 °C provided high stability with a half-life of at least two months. At 30 °C, Hildebrand *et al.* reported a half-life of 20 h,[37] Kulishova of 63 h[35] and Machielsen *et al.* of 160 h.[36] With a bi-phasic system in MTBE in a 50:50 ratio, Villela Filho *et al.* reached a half-life of 1400 h. [38] Because the activity assays and storage conditions are either different or unclear, the reported activities and half-life values of *Lb*ADH have ranged drastically in literature.[25] Despite this unclarity, this work shows how storing with 10% v/v glycerol and 50 mM NaCl will increase the stability of *Lb*ADH.

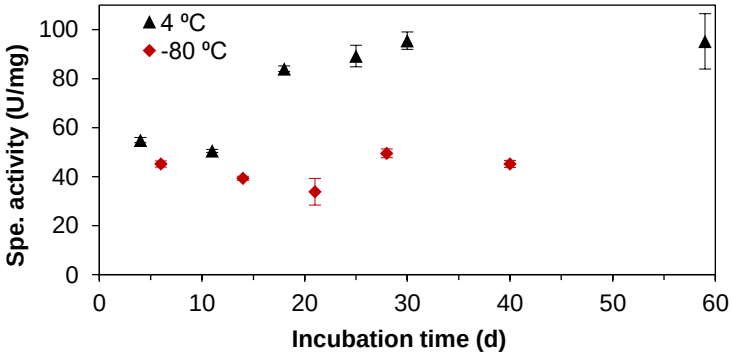

Figure 3. Stability of *Lb*ADH after storage in 4 °C (black triangles) and -80 °C (red diamonds). The enzyme was stored with 10% v/v glycerol and 50 mM NaCl. Conditions: 11 mM acetophenone, 0.2 mM NADPH, 50 mM KP_i buffer pH 7.5, 1 mM $MgCl_2$, 30 °C. Average of duplicates or triplicates.

*Lb*ADH variants selection

After manually changing the active site of *Lb*ADH with either Y156E or S143E in YASARA[39] (PDB: 1ZK4),[27] we explored each amino acid present in the active site near these residues. We discarded the amino acids present in the catalytic tetrad or involved in the folding into the *holo*-structure. We then used the algorithm FuncLib[33] (SI Section 2.3) to create a library for the following positions: I93, A94, V95, N96, L110, I144, L153, A155, N157, A158, S159, G189, V196, L199. We created libraries with both *Lb*ADH-Y156E and *Lb*ADH-S143E and selected the hits with the lowest Rosetta energy from each library.

In case the single mutant from the catalytic tetrad would prevent amine reduction activity, we also focused on residues more distant from the active site. The alanine on position 94 (A94) is positioned on the outside border of the active site, and by replacing A94 with an acidic amino acid on this position, it could potentially be more accessible for the ammonia to bind. Because the MD-simulations showed good binding of the iminium ion in the active site after replacing the A94 with either aspartic acid (D) or glutamic acid (E), we engineered the single variants A94E and A94D (SI, section 2.3). All *Lb*ADH variants were obtained in high purity and yield (**Table 2**, see SI). Under the same conditions as described above, none of the purified *Lb*ADH-Y156E and *Lb*ADH-S143E variants displayed ketoreduction activity. Activity measurements of *Lb*ADH-A94D and *Lb*ADH-A94E cell-free extracts (CFE) gave a specific activity of 55 and 23 U/mL, respectively.

Table 2. *Lb*ADH variants with corresponding labels used in this work.

***Lb*ADH variant**	**Label**
Y156E	*Lb*ADH-Y156E
A94F/N96P/L110V/Y156E/N157H/L199I	*Lb*ADH-YF1
A94F/N96P/Y156E/S159A	*Lb*ADH-YF2
A94Y/N96P/L110V/Y156E/S159A	*Lb*ADH-YF3
S143E	*Lb*ADH-S143E
A94Y/N96P/S143E/N157A/S159A/L199I	*Lb*ADH-SF1
N96P/L110V/S143E/N157Q/S159A/L199I	*Lb*ADH-SF2
A94D	*Lb*ADH-A94D
A94E	*Lb*ADH-A94E

Screening of *Lb*ADH variants

After purifying our designed *Lb*ADH variants (**Table 2**), we screened the enzymes for ketoreduction of our substrate scope (**Figure 4**). As expected, *Lb*ADH-wt afforded almost complete conversion of all tested ketones to the corresponding chiral alcohols. The Y156E series of variants showed a significantly impacted activity, with only 0 to 11% ketoreduction. The substrate 2-methylcyclohexanone **1d** was the only exception, as we observed up to 56% conversion by *Lb*ADH-YF2. The S143E series of variants showed lower

conversions to the alcohols (0-7%) than the Y156E series. Contrary to our expectations, none of the overexpressed mutants showed amine product formation under reductive amination conditions (ammonium formate buffer pH 8.0) (**Figure 5**). Under reductive amination conditions, we observed that the wild-type enzyme still converted the ketone into the corresponding alcohol. Whereas some of the tyrosine variants showed little to no conversion into the alcohol (up to 13%), the serine variants showed no alcohol formation for any substrate. Remarkably, all tyrosine variants were still able to reduce 2-methylcyclohexanone **1d** into the corresponding alcohol under reductive amination conditions. Because the mutation for A94D and *Lb*ADH-A94E was not within the catalytic tetrad, alcohol formation would still be possible. When we performed reaction screening under reductive amination conditions, neither A94D nor A94E displayed reductive amination activity. Instead, these enzymes showed up to full ketoreduction of the carbonyl substrate into the corresponding alcohol product.

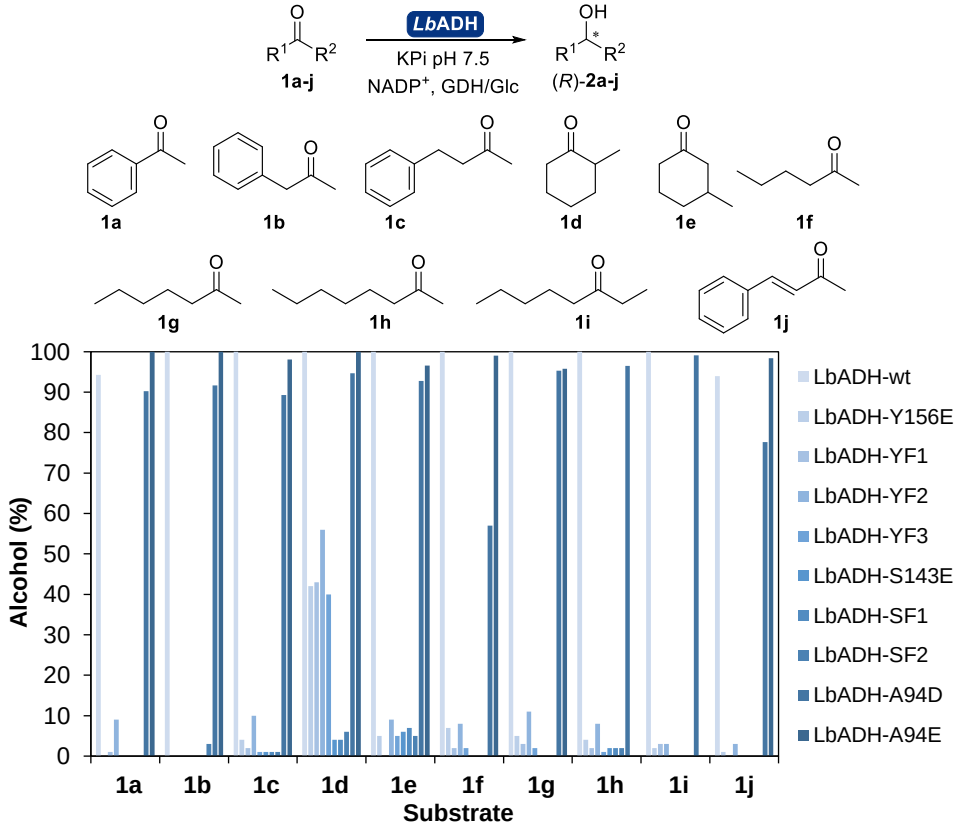

Figure 4. Ketone reduction catalyzed by *Lb*ADH-wt and variants in reaction conditions for ketoreduction. Conditions: 50 mM KPi buffer pH 7.5, 1 mM $MgCl_2$, 0.2 mM $NADP^+$, 6 U/mL *Bs*GDH, 20 mM glucose (Glc), 10 mM substrate, 2 µM enzyme unless stated otherwise, 0.5 mL reaction volume, 24 h at 500 rpm and 30 °C. *Lb*ADH-A94D CFE: 4.4% v/v. *Lb*ADH-A94E CFE: 2.2%v/v.

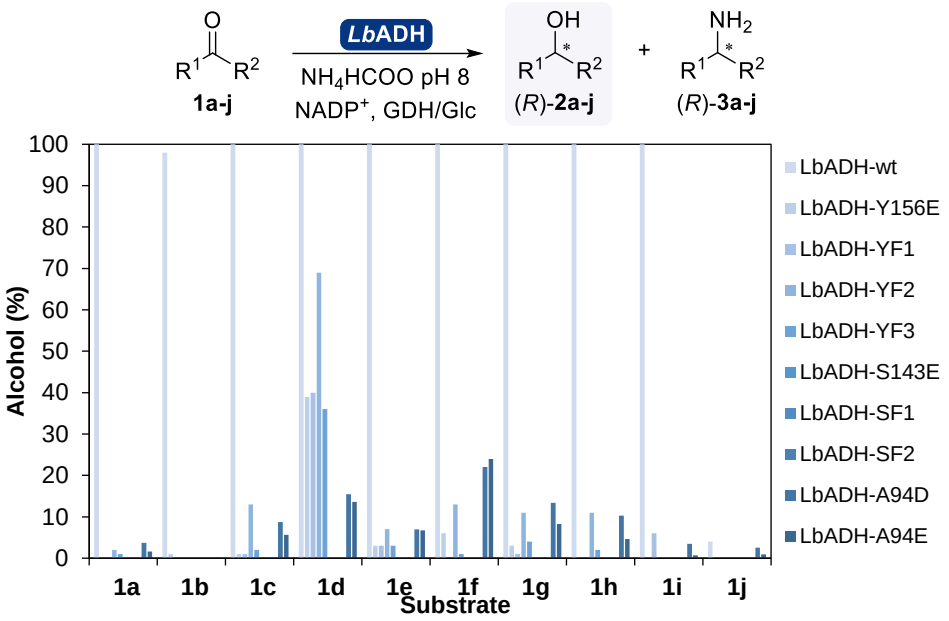

Figure 5. Ketone reduction catalyzed by *Lb*ADH wt and variants in reaction conditions for reductive amination with excess ammonia. Amine products **3a-j** were not observed. Conditions: 1 M NH_4HCOO^- buffer, pH 8.0, 0.2 mM $NADP^+$, 6 U/mL *Bs*GDH, 20 mM Glc, 10 μM enzyme unless stated otherwise, 0.5 mL reaction volume, 24 h at 500 rpm and 30 °C. *Lb*ADH-A94D CFE: 22.2% v/v. *Lb*ADH-A94E CFE: 11.4% v/v.

MD simulations of *Lb*ADH in complex with substrate 1a

In addition to our biochemical characterization, we conducted molecular dynamics (MD) simulations of wild-type (wt), and all the variants derived from *Lb*ADH in complex with the substrates acetophenone **1a** and 2-methylcyclohexanone **1d** (see SI). Specifically, we initiated simulations of the Michaelis complex of *Lb*ADH-wt with **1a** bound in an initial productive mode. This associated chemical reaction involves the transfer of the hydride group from the C-4 atom of the nicotinamide group of NADPH to the carbonyl carbon of **1a**. The enzyme exhibits *anti*-Prelog stereopreference, with the small methyl group in a pocket formed by residues E145, D150, L153 and Y190, whereas the larger phenyl group interacts with the A94 and L195 sidechains. Furthermore, according to our simulations, the motion of active site loops plays a crucial role in determining whether the substrate remains bound to the active site or dissociates (see SI). Given the *R*-specificity of the enzyme, *si* face addition to the carbonyl group results in the formation of *R*-alcohol (**Figure 6A**). The addition to other prochiral face *re*, results into the formation of *S*-alcohol.

This distinction between addition to the *re* and *si* faces was determined by Cahn-Ingold-Prelog priority-based improper dihedral angle distributions during the MD simulation, where the *re* face (clockwise) is marked by a negative dihedral

angle and the *si* face (counterclockwise) by a positive dihedral angle (**Figure 6B**). The frames are separated based upon this improper dihedral angle distribution throughout the simulation. The overall product formation depends upon the two steps: (1) hydride transfer from C-4 atom of the nicotinamide ring of NADPH to the carbonyl carbon of the substrate, and (2) the proton transfer from Y156 to the alkoxide of the substrate. After sorting the frames based on this improper dihedral angle distribution, we have further filtered out the frames by setting the criteria on both the reactive distance and proton transfer as less than 3.5 Å and less than 3.0 Å, respectively, and then back-calculated this to get a predicted % *ee* (**Figure 6C**). Using this definition, our MD simulations predicted the wild-type enzyme, and the A94D, A94E and to a lesser extent the YF3 variant to have a higher % *ee* compared to the other tested variants.

A similar approach was extended to the iminium intermediate to compare the relationship between the catalytic distances and the performance of *Lb*ADH as an amine dehydrogenase. Notably, the Y156E-*Lb*ADH was the only variant showing a slightly lower average distance between the hydride transfer from C-4 atom of the nicotinamide ring of NADPH to the iminium carbon than and between the cofactor and acetophenone (**Figure 6C**). However, this data falls within the calculated error range, so no clear conclusions can be made on the differences between the *Lb*ADH variants. The increased distances with the iminium ion are in line with the experimental characterization of the poor performance of the enzymes as AmDHs.

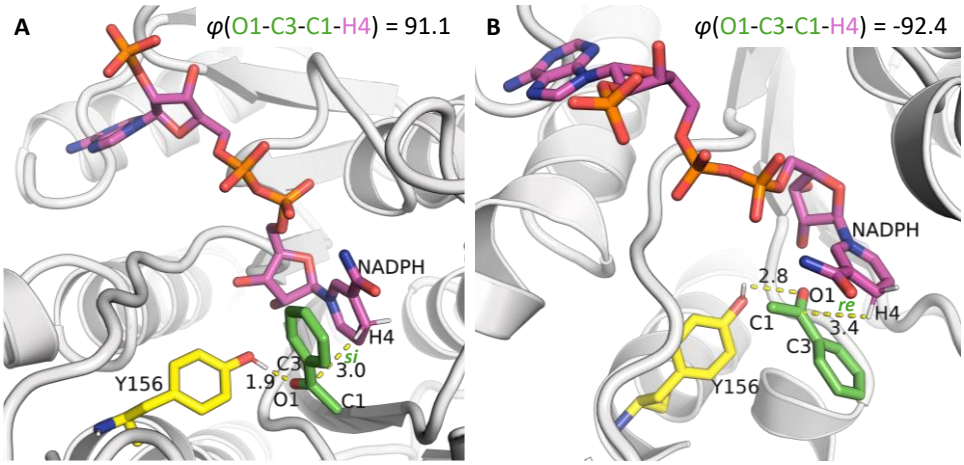

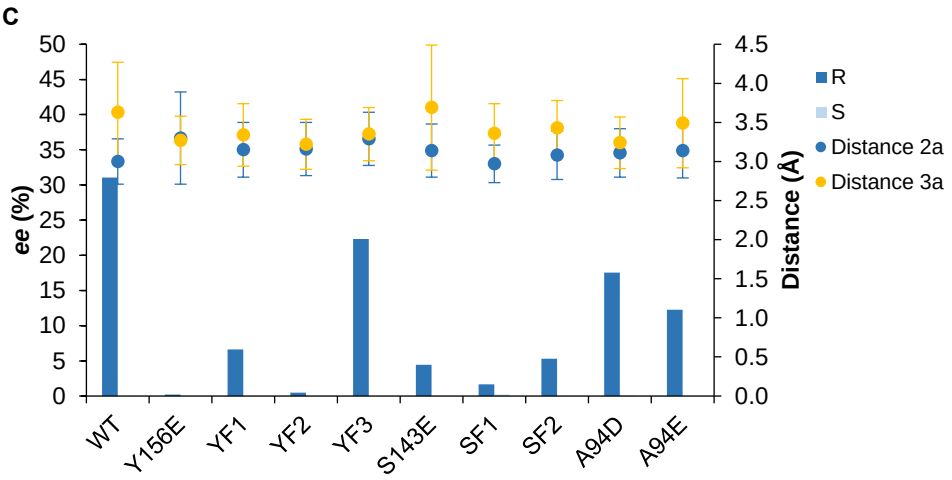

Figure 6. MD predictions of the expected ketone reduction selectivity by *Lb*ADH in complex with acetophenone (**1a**). Shown here are representative structures of the *si* prochiral face addition (**A**) and *re* prochiral face addition (**B**). **C**: *ee* distribution across all the variants based on 5 × 100ns simulations of each variant (blue bars), with average values and standard deviation of the reactive distance between transferrable hydride atom and carbonyl carbon (blue circles for the alcohol, yellow circles for the iminium).

Selectivity towards 2-methylcyclohexanone

Surprisingly, although the designed variants led to significant loss in conversion for most substrates, the mutants Y156E, YF1, YF2 and YF3 still displayed conversion of a mixture of *cis*- and *trans* 2-methylcyclohexanone **1d** into 2-methylcyclohexanol (**Figure 7**). Because this product contains two chiral centers, we investigated the impact of the tyrosine mutation and FuncLib algorithm on the selectivity of the *Lb*ADH (**Figure 8**). It is known that the *Lb*ADH-wt follows the *anti*-Prelog rule,[1, 40] hence the expected product is the *R*-alcohol. The *Lb*ADH-wt shows full ketoreduction of the carbonyl substrate, and showed high enantioselectivity towards the *trans*-product, but not the *cis*-product. The mutants showed a much lower conversion to the *cis*-product while the conversion to the *trans*-product remained largely intact, greatly increasing the *de* (**Table 3**). Especially *Lb*ADH-YF3 showed a high preference for the *trans*-product (94%). The *Lb*ADH-YF2 mutant showed the highest conversion into the alcohol product, at the expense of the *de*. Remarkably, YF3 showed the highest *de,* demonstrating an increased selectivity compared to the other variants. In reductive amination conditions, no corresponding amine was formed, but the *de* was lower (**see SI**).

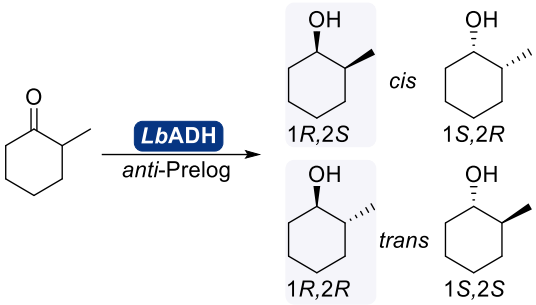

Figure 7. Expected diastereoisomeric products obtained with *Lb*ADH from 2-methylcyclohexanone **1d** (highlighted in light blue).

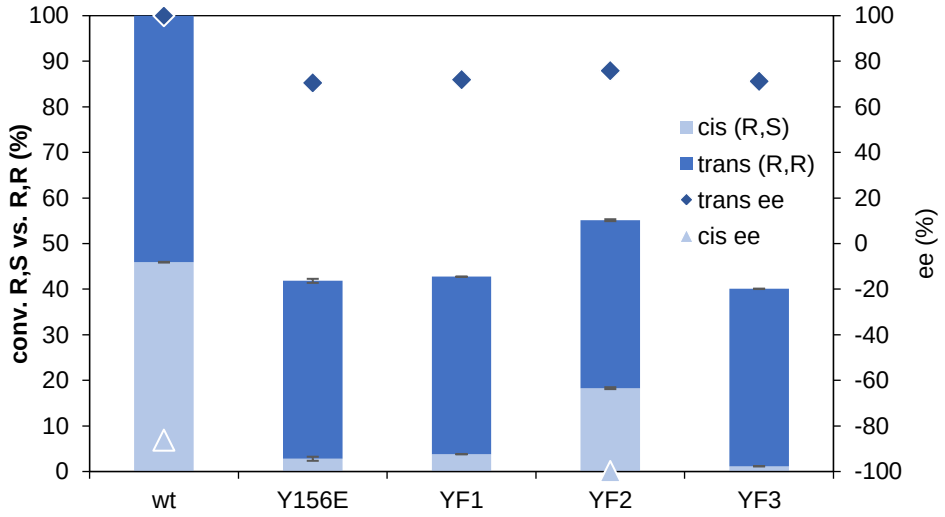

Figure 8. Ketoreduction of 2-methylcyclohexanone **1d** to 2-methylcyclohexanol, and the corresponding *ee* of either *trans*- (diamonds) or *cis*-product (triangles). *ee* was not determined for conversions under 10%. Conditions: 50 mM KP_i pH 7.5, 1 mM $MgCl_2$, 12 mM Glc, 0.2 mM $NADP^+$, 6 U/mL *Bs*GDH, 2 µM *Lb*ADH, 10 mM **1d**, 24 h at 500 rpm, 30 °C. Average of duplicates.

Table 3. Diastereomeric excess (*de*) of the *trans*-2-methylcyclohexanol catalyzed by the *Lb*ADH variants from screening in ketoreduction.

***Lb*ADH**	***de* (%)**
wt	8
Y156E	86
YF1	82
YF2	33
YF3	94

MD simulations of *Lb*ADH in complex with substrate 1d

Corresponding simulations were also conducted of different *Lb*ADH variants in complex with 2-methylcyclohexanone **1d**, with separate simulations

being performed for each of the *S* (**Figure 9A**) and *R* (**Figure 9B**) enantiomers of the substrate in each system. Given the *R*-specificity of the enzyme, only the *R*-configuration of the alcohol is considered among the four possible diastereomers that can be formed. The *R*-enantiomer of **1d** resulted in the formation of the *trans* diastereomer (1*R*,2*R*) as the major stereoisomer whereas the *S*-enantiomer of 2-methylcyclohexanone led to the formation of the *cis* diastereomer (1*R*,2*S*) as the major product. Based on initial studies, all variants preferred the ketoreduction into the *trans* diastereomer (1*R*,2*R*). Throughout the simulations, we monitored the reactive distance between the hydride of the C-4 atom of the nicotinamide group of NADPH and the C-1 carbonyl carbon of 2-methylcyclohexanone **1d** and predicted the selectivities (**Figure 9C**). Interestingly, some of the variants (Y156E and YF3) showed a preference for the *cis*-product, contradicting our experimental data. However, the distance between the cofactor and ketone substrate for all *Lb*ADH-variants is within the standard deviations. The enantioselectivity of the *cis*- and *trans*-products were higher in our experiments than we obtained from our simulations. From the racemic substrate mixture, the *Lb*ADH probably reduced the (*R*)-2-methylcyclohexanone with a high selectivity to get the *trans*-product with high *ee*, but accepted the (*S*)-2-methylcyclohexanone with lower enantioselectivity after the (*R*)-substrate was depleted.

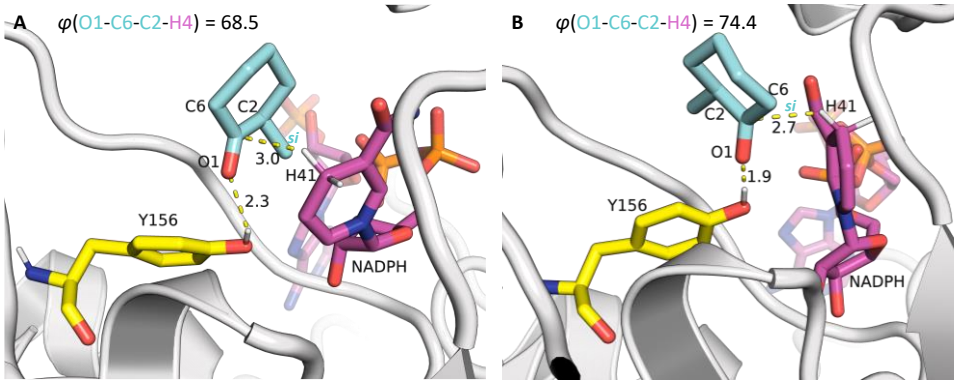

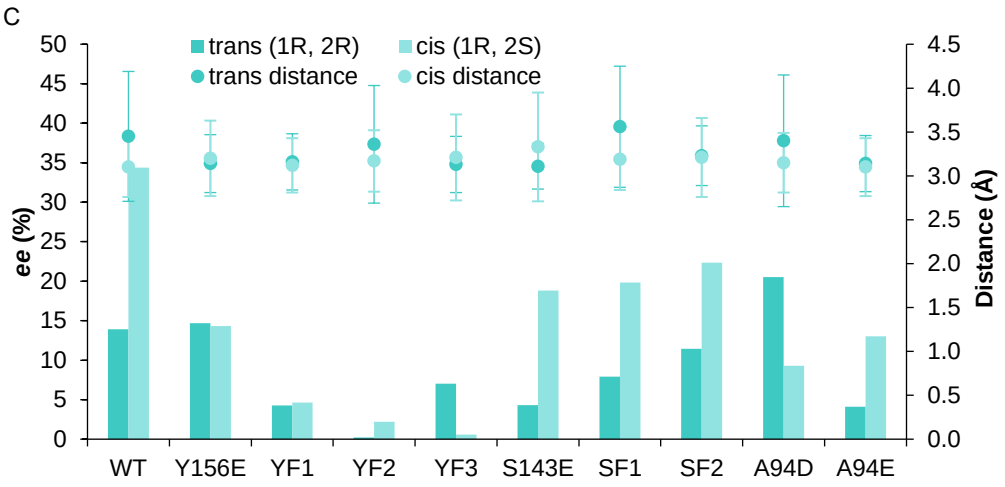

Figure 9. MD predictions of the expected ketone reduction selectivity by *Lb*ADH in complex with 2-methylcyclohexanone **1d**. Shown here are representative structures of the *si* prochiral face addition with (*R*)-**1d** (A) or (*S*)-**1d** (B). The *ee* distribution across all the variants with either the *trans* or *cis* product (C) based on 5 × 100 ns simulations of each variant (bars), with average values and standard deviation of the reactive distance between transferrable hydride atom and carbonyl carbon (circles).

IRED and ER conditions screening

We initially aimed for AmDH activity, hence we used ammonium or methylamine as potential amine donors in our initial screening. Because this activity was not present, we also screened for amine formation under conditions where the imine intermediate is formed (**Table 4**, **Figure 10**).[41] We combined hexanal or benzaldehyde with either cyclopropylamine or allylamine and ran the reactions at pH 9. In this way, we screened for promiscuous imine reductase (IRED) activity, which was realized in previous works.[42, 43] The serine variants showed no amine formation under these conditions. Only the single mutant *Lb*ADH-Y156E afforded the amine product formed from hexanal and cyclopropylamine (4% from 10 mM, see SI), aside from formation of the corresponding alcohol. Benzaldehyde with both amine donors and hexanal with allylamine were not accepted as a substrate (data not shown). From this data, we conclude that *Lb*ADH-Y156E gained IRED activity towards the specific substrate combination of hexanal and cyclopropylamine. In the initial studies of the simulation on the Michaelis complex derived from hexanal and cyclopropylamine, all data is within the error range, therefore no conclusions can be made based on these MD predictions (**Figure 10**).

We also screened the variants *Lb*ADH-Y156E, *Lb*ADH-YF1, *Lb*ADH-YF2 and *Lb*ADH-YF3 for double bond reduction of cinnamaldehyde, as this switch in reactivity was previously reported to promote ADH activity from an ene reductase

with a single mutation.[44] We observed no alkene reduction activity with this substrate, nor aldehyde reduction to the corresponding alcohol (data not shown).

Table 4. *Lb*ADH-catalyzed reaction with IRED reaction conditions starting from hexanal and cyclopropylamine.

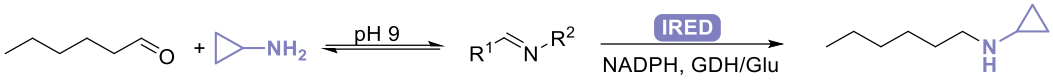

***Lb*ADH**	**hexanal (%)**	**hexanol (%)**	**imine (%)**	***N*-hexylcyclo-propanamine (%)**
wt	0	100	0	0
Y56E	3	28	65	4
YF1	2	26	71	0
YF2	3	36	61	0
YF3	3	26	72	0
S143E	6	29	65	0

Conditions: 50 mM Tris-HCl buffer pH 9.0, 1 mM $MgCl_2$, 30 mM Glc, 10 U/mL *Bs*GDH, 0.2 mM $NADP^+$, 10 mM hexanal, 100 mM cyclopropylamine, 10 µM *Lb*ADH variant. Average of duplicates.

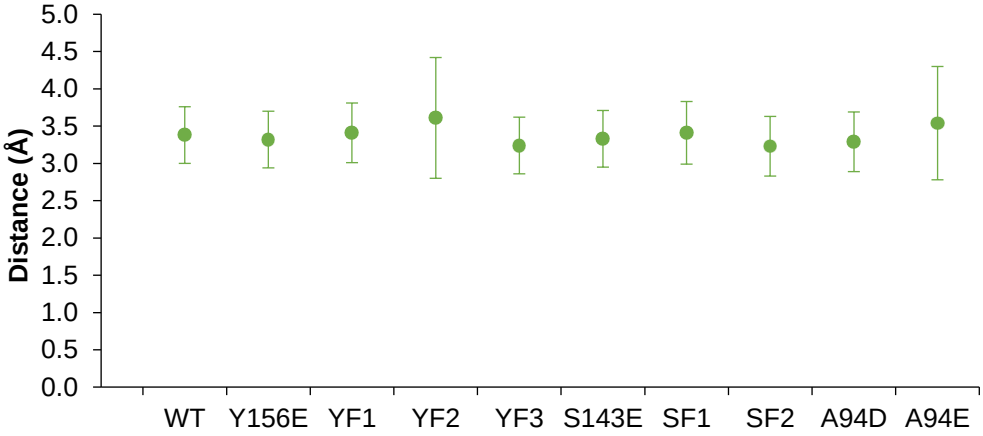

Figure 10. MD predictions of the expected IRED reduction by *Lb*ADH in complex with iminium intermediate derived from hexanal and cyclopropylamine, with average values and standard deviation of the reactive distance between transferrable hydride atom and iminium carbon.

Conclusions

We aimed to re-purpose the enzyme *Lb*ADH to catalyze reductive amination instead of ketoreduction. After engineering, the variants displayed no reductive amination activity in the presence of ammonium or methylamine. The catalytic tetrad is probably affected by our engineering to such extent that no reduction or reductive amination is possible. Both S143 and Y156 are essential for such activity and should be kept intact if *Lb*ADH re-purposing is investigated

further. Adding mutations on the A94 position created no AmDH activity either, so other positions should be targeted to possibly reach such activity.

Although the results from our engineering and screening efforts are not what we hoped for, we can still draw some interesting conclusions. Firstly, the stability of *Lb*ADH combined with glycerol causes the enzyme to maintain its activity over time after storing the enzyme at -80 °C. Four weeks after storing the enzyme at 4 °C, *Lb*ADH activity was at its highest activity (96 U/mg), and was retained for another four weeks. The reported *Lb*ADH activities of over 200 U/mg could not be reproduced from literature, therefore clearer storage and reaction conditions should be reported for this enzyme in future works. Secondly, engineering on the Y156 position has a drastic effect on *Lb*ADH, but the enzyme still displays ketoreduction activity. Thirdly, the impact on engineering S143 was more destructive than Y156, proving the higher importance of the serine in the proton relay system than the tyrosine. Finally, *Lb*ADH-Y156E displayed slight IRED promiscuous activity to reduce the imine formed from hexanal and cyclopropylamine. Based on these observations, this work contributes to the knowledge about the *Lb*ADH storage and stability properties.

Acknowledgements

This project received funding from the Department of Biotechnology, Delft University of Technology, and from the Swedish Research Council (2019-03499). The simulations were enabled by resources provided by the National Academic Infrastructure for Supercomputing in Sweden (NAISS), partially funded by the Swedish Research Council through grant agreement n° 2022-06725. The authors thank L. Koekkoek, M. Strampraad and R. van Oosten for technical support.

Materials and methods

Chemicals were purchased from Sigma-Aldrich (Merck, Darmstadt, Germany), Janssen Chimica (Geel, Belgium), Fluka Chemica (Buchs, Switzerland), Acros organics (ThermoFisher Scientific, Ward Hill, MA, USA), Thermo Fisher Scientific (Ward Hill, MA, USA) and Enamine (Riga, Latvia). HPLC-grade ethyl acetate (EtOAc) was used as solvent for gas chromatography. HPLC-grade dimethylsulfoxide (DMSO) was used as a co-solvent. Lyophilized glucose dehydrogenase 105 (GDH-105) was purchased from Codexis (Redwood City, CA, USA). Crude lyophilized DNaseI, lyophilized lysozyme from chicken egg white and cOmplete™EDTA-free Protease I inhibitor were purchased from Sigma-Aldrich (Merck, Darmstadt, Germany).

Ketoreduction conditions

To 50 mM KP_i buffer with 1 mM $MgCl_2$ and pH 7.5 in a glass GC vial, glucose (20 mM), GDH-105 (6 U/mL), $NADP^+$ (0.2 mM), *Lb*ADH (2 µM) and

ketone substrate (10 mM) were added. Products were extracted with 0.5 mL EtOAc. The isolated organic layer was dried with $MgSO_4$, centrifuged at 10,000 × *g* for 1 min, decanted to a GC vial and injected onto the GC-FID.

Reductive amination conditions

To 1 M NH_4HCOO buffer (titrated to pH 8.0 or 9.0 with 4 M NH_4OH), glucose (20 mM), GDH-105 (6 U/mL), $NADP^+$ (0.2 mM), ketone substrate (10 mM) and *Lb*ADH (10 µM) were added. In case of reactions with methylamine, 250 mM methylamine was added to 50 mM Tris-HCl buffer with 1 mM $MgCl_2$ at pH 9.0. The reaction mixtures of 0.5 mL were incubated for 24 h at 30 °C and 500 rpm. For reductive amination conditions, 0.4 mL 10 M NaOH was added, and the reactions were extracted twice with 0.5 mL EtOAc. The isolated organic layers were combined, dried with $MgSO_4$, centrifuged at 10,000 × *g* for 1 min, decanted to a GC vial and injected onto the GC-FID.

Supporting Information

Complete data from Supporting Information, including GC chromatograms in **Figures S12-S22** van be found at doi: 10.4121/af778919-5f7a-4b39-ae6d-92b563d44063.v1. The synthesis of 3-octanamine was performed according to Mangas-Sánchez *et al.*,[45] with the following deviations. 35 mmol ammonium acetate and 7 mmol sodium cyanoborohydride were added to 3.5 mmol of ketone in 11 mL methanol. The reaction was stirred for 4 h and was quenched with 12.6 mL 1 M NaOH. The mixture was then concentrated by rotary evaporation. The product was analysed on proton and carbon NMR (400 MHz). The spectrum of the product was in accordance with literature.[45]

***Lb*ADH production and purification**

Sequence of *Lactobacillus brevis* alcohol dehydrogenase (*Lb*ADH). UniProt: Q84EX5 Genbank: AJ544275.1.

MGSSHHHHHHSSGLVPRGSHMSNRLDGKVAIITGGTLGIGLAIATKFVEEGAK
VMITGRHSDVGEKAAKSVGTPDQIQFFQHDSSDEDGWTKLFDATEKAFGPVS
TLVNNAGIAVNKSVEETTTAEWRKLLAVNLDGVFFGTRLGIQRMKNKGLGASII
NMSSIEGFVGDPSLGAYNASKGAVRIMSKSAALDCALKDYDVRVNTVHPGYIK
TPLVDDLPGAEEAMSQRTKTPMGHIGEPNDIAYICVYLASNESKFATGSEFVVD
GGYTAQ

Induced fit docking of iminium in *Lb*ADH active site

The crystal structure of the alcohol dehydrogenase from *Lactobacillus brevis* (*Lb*ADH, PDB ID: 1zk4) was loaded in YASARA (20.8.23). The docked acetophenone was removed from the crystal structure, and the *Lb*ADH was

mutated either on position Y156 or S143 to glutamate. The energy was minimized, and the positively charged iminium ion formed from acetophenone was docked into the *Lb*ADH active site by induced fit docking (VINA). The YASARA sessions were saved as .pdb to be used as described below.

FuncLib library

The following parameters were used for the generation of variants with the FuncLib algorithm (URL: https://funclib.weizmann.ac.il/bin/steps)[33]. Amino acid positions to diversify: 92A, 93A, 94A, 95A, 109A, 143A, 152A, 154A, 156A, 157A, 158A, 188A, 195A, 198A. Min ID: 35. Max targets: 4000. Coverage: 75. E value: 0.0001. A PDB file of *Lb*ADH-Y156E (**Table S1**) or *Lb*ADH-S143E (**Table S2**) with the docked iminium intermediate of acetophenone as described above was used as input. Essential amino acid residue positions were: 113A, 141A, 142A, 144A, 155A, 159A, 189A, 205A. Ligands to keep during simulations were: 1270A (nicotinamide cofactor), 1682A (iminium intermediate). The single mutant and the three hits from the FuncLib algorithm with the highest predicted stability were selected for expression in the lab.

Table S1 List of the 50 most stable hits from Y156E-*Lb*ADH generated by FuncLib.

Label	92	93	94	95	109	143	152	154	156	157	158	188	195	198	ΔΔG (kJ/mol)
Y156E	I	A	V	N	L	I	L	A	N	A	S	G	V	L	-744
YF1	I	F	V	P	V	I	L	A	H	A	S	G	V	I	-760
YF2	I	F	V	P	L	I	L	A	H	A	S	G	L	Y	-759
YF3	I	Y	V	P	V	I	L	A	N	A	A	G	V	L	-759

Table S2. List of the 50 most stable hits from S143E-*Lb*ADH generated by FuncLib.

Label	92	93	94	95	109	143	152	154	156	157	158	188	195	198	ΔΔG (kJ/mol)
S143E	I	A	V	N	L	I	L	A	N	A	S	G	V	L	-741
SF1	I	Y	V	P	L	I	L	A	A	A	A	G	V	I	-760
SF2	I	A	V	P	V	I	L	A	Q	A	A	G	V	I	-760
SF3	I	A	I	N	V	I	L	A	Q	A	A	G	V	I	-760

Production of *Lb*ADH-wt and variants

The gene sequences for the *Lb*ADH-wt, the serine and tyrosine variants were ordered in a pET28a(+) vector from SynBio (Monmouth Junction, NJ, USA). The corresponding plasmids were transformed in *E. coli* C43(DE3) competent cells. The transformed cells were grown on selective LB-agar plates (50 µg/mL kanamycin) overnight at 37 °C. TB-medium (500 mL in 2L baffled flask) was inoculated with 1% overnight LB preculture of the transformed cells and incubated for 3-5 h at 37 °C, 180 rpm. After reaching an OD_{600} of 0.6-0.8, 0.5 mM IPTG was added, followed by overnight incubation at 22 °C. Cells were harvested (17,000 × *g*, 20 min, 4 °C) and stored at -80 °C.

For *Lb*ADH-A94D and *Lb*ADH-A94E, primers were ordered from BaseClear (Leiden, The Netherlands). Site-directed mutagenesis was performed *via* PCR using a Q5® High-Fidelity 2X Master Mix (NEB M0492) from New England Biolabs (Ipswich, MA, USA). The produced plasmids were purified using a Monarch® Plasmid Miniprep Kit (NEB T1010) from New England Biotech and were sequenced by Macrogen (Amsterdam, The Netherlands) (Appendix C.2). The mutated genes were confirmed with an alignment with CloneManager Professional Suite (**Figure S1**).
Primer sequences:

A94E forward: CGC TGG GAT CGA GGT TAA GA
A94E reverse: TTA TTA ACT AAT GTA GAA ACT GGG CC
A94D forward: CGC TGG GAT CGA CGT TAA CAA GAG
A94D reverse: TTA TTA ACT AAT GTA GAA ACT GG

```
lb-adh co       241 tttggcccagtttctacattagttaataacgctgggatcgcggttaacaagagtgtcgaag
lb-adh co A9    241 tttggcccagtttctacattagttaataacgctgggatcgacgttaacaagagtgtcgaag
lb-adh coA94    241 tttggcccagtttctacattagttaataacgctgggatcgaggttaacaagagtgtcgaag
```

Figure S1. Alignment of gene fraction encoding for *Lb*ADH-wt (top), *Lb*ADH-A94D (middle) and *Lb*ADH-A94E (bottom). Prepared with Clone Manager.

Affinity chromatography purification of *Lb*ADH-wt and variants

Two buffers were prepared for each purification: a 20 mM sodium phosphate (NaP_i) buffer with 0.5 M NaCl, 1 mM $MgCl_2$, pH 7.4, titrated with 3 M NaOH (referred to as 'binding buffer') and a 20 mM NaP_i buffer with 0.5 M NaCl, 250 mM imidazole, 1 mM $MgCl_2$, pH 7.4, titrated with 3 M HCl (referred to as 'elution buffer'). For preparation of the cell-free extracts the cells were resuspended in 20 mM NaP_i buffer pH 7.5, 0.5 M NaCl, 1 mM $MgCl_2$. To the buffer, EDTA-free protease inhibitor, lysozyme and DNaseI were added. After 10 min incubation, the suspension was passed through a cell disruptor at 22 kpsi with 50 mM KP_i buffer pH 7.5 with 1 mM $MgCl_2$ and clarified by centrifugation (32,000 × *g*, 30 min, 4 °C). After filtering the CFE (0.2 µm), IMAC was performed with 5 mL HisTrap™ FF crude column (GE Healthcare, Chicago, Illinois, U.S.). These columns were attached into a Bio-Rad NGC Chromatography system.

Protein fractions were concentrated with Amicon® Ultra-15 10 K Centrifugal Filter Devices at 4,000 rcf. Desalting was performed using PD10 desalting columns (52-1308-00 AP) from GE Healthcare (Chicago, IL, USA), equilibrated with 50 mM potassium or sodium phosphate buffer, pH 7.4, with 1 mM $MgCl_2$. 10% glycerol and 50 mM NaCl were added to the pure protein fraction which was then stored at -80°C. When comparing storage conditions, stocks were placed either at 4 °C and -20 °C. Total protein amounts were determined by BC

Assay (Uptima Protein Quantitation Kit UP40840A, Interchim, Montlucon, France).

Sodium dodecyl sulphate polyacrylamide gel electrophoresis (SDS-PAGE) was run to show gene expression and enzyme purity levels (**Figure S2 - Figure S8**). Samples were prepared by mixing with one equivalent of Laemmli buffer and 5% v/v dithiothreitol (DTT), heated to 95 °C for 5 min, then centrifuged at 9,000 × *g* for 2 min. From these samples, 10 µL was loaded onto the gel, whereas 5 µL of protein ladder was loaded onto a Criterion TGX Stain-Free Precast Gel. Imaging was performed with a ChemiDoc MP imaging system (Bio-Rad Laboratories, Hercules, California, U.S.).

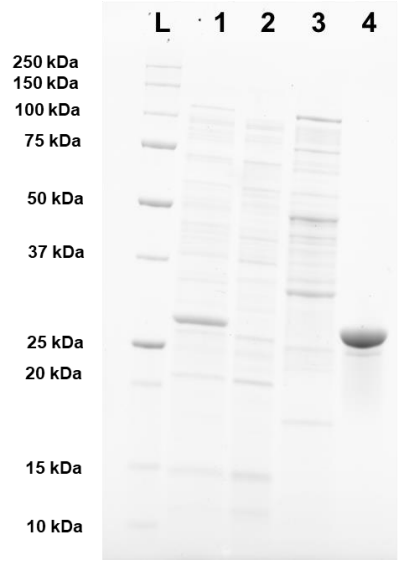

Figure S2. SDS-PAGE gel of the purification of the *Lb*ADH-wt IMAC purification. L: protein ladder. 1: cell-free extract. 2: flowthrough after loading on Histrap colum. 3: washing fraction. 4: eluted *Lb*ADH-wt.

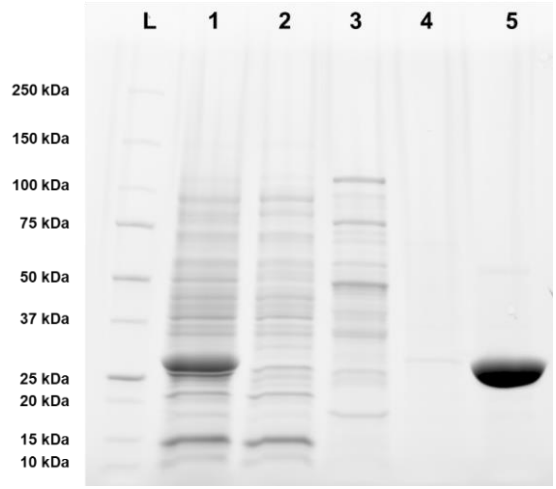

Figure S3. SDS-PAGE gel of the purification of the *Lb*ADH-Y156E IMAC purification 1: cell-free extract. 2: flowthrough after loading on Histrap column. 3-4: washing fractions. 5: eluted *Lb*ADH-Y156E.

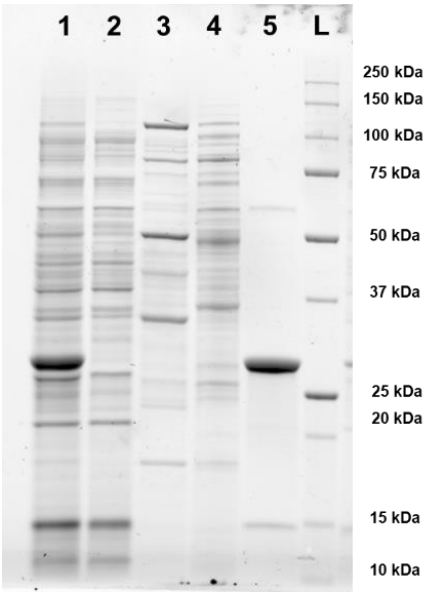

Figure S4. SDS-PAGE gel of the purification of *Lb*ADH-YF1 IMAC purification. 1: cell-free extract. 2: flowthrough after loading on Histrap column. 3-4: washing fractions. 5: eluted *Lb*ADH-YF1. L: protein ladder.

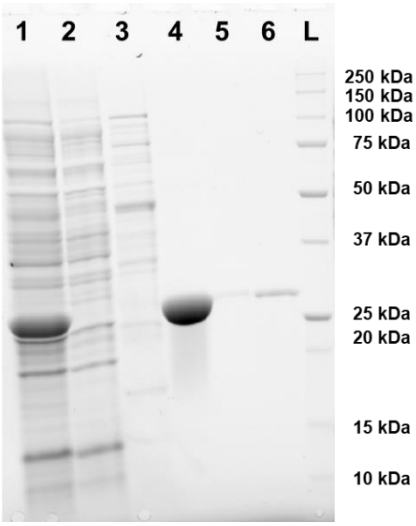

Figure S5. SDS-PAGE gel of the purification of *Lb*ADH-YF2 IMAC purification. 1: cell-free extract. 2: flowthrough after loading on Histrap column. 3: washing fractions. 4-6: eluted *Lb*ADH-YF2. L: protein ladder.

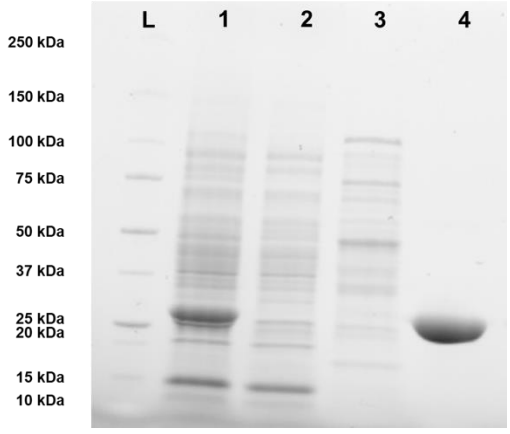

Figure S6. SDS-PAGE gel of the purification of *Lb*ADH-YF3 IMAC purification. L: protein ladder. 1: cell-free extract. 2: flowthrough after loading on Histrap column. 3: washing fractions. 4: eluted *Lb*ADH-YF3.

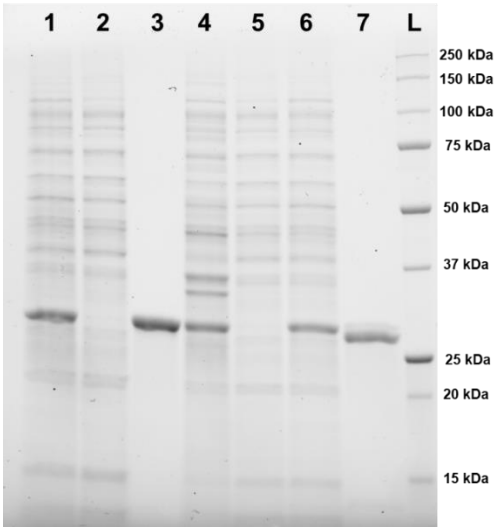

Figure S7. SDS-PAGE gel of the purification of *Lb*ADH-S143E (1-3) and *Lb*ADH-SF1 (4-7) IMAC purifications. 1: cell-free extract. 2: flowthrough after loading on Histrap column. 3: eluted *Lb*ADH-S143E. 4: cell-free extract. 5: flowthrough after loading on Histrap column. 6: elution fraction with *Lb*ADH-SF1. 7: pure fraction with *Lb*ADH-SF1.

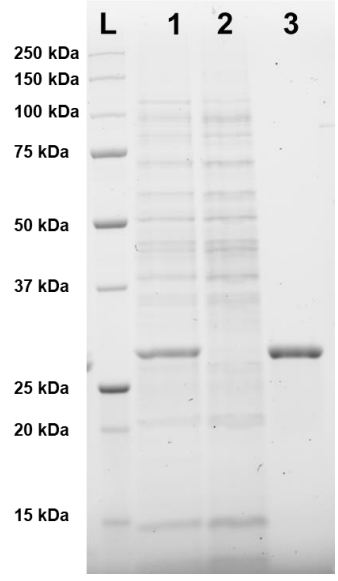

Figure S8. SDS-PAGE gel of the purification of *Lb*ADH-SF2 IMAC purification. L: protein ladder. 1: cell-free extract. 2: flowthrough after loading on Histrap column. 3: eluted *Lb*ADH-SF2.

Carbonyl substrates and corresponding products

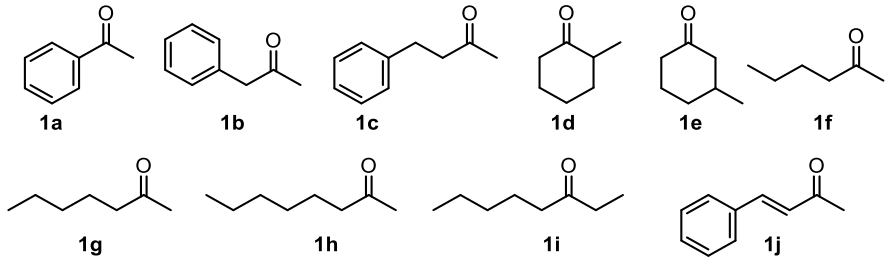

Figure S9. Panel of ketone substrates used in screening of *Lb*ADH variants towards ketoreduction or reductive amination.

Table S3. List of carbonyl substrates, original alcohol products and targeted amine products with the corresponding labels used in this work.

Label	Carbonyl substrates	Label	Alcohol product	Label	Amine product
1a	acetophenone	**2a**	phenylethanol	**3a**	phenylethylamine
1b	phenylacetone	**2b**	1-phenyl-2-propanol	**3b**	1-phenylpropan-2-amine
1c	4-phenyl-2-butanone	**2c**	4-phenyl-2-butanol	**3c**	4-phenylbutan-2-amine
1d	2-methylcyclohexanone	**2d**	2-methylcyclohexanol	**3d**	2-methylcyclohexanamine
1e	3-methylcyclohexanone	**2e**	3-methylcyclohexanol	**3e**	3-methylcycolhexanamine
1f	2-hexanone	**2f**	2-hexanol	**3f**	2-hexanamine
1g	2-heptanone	**2g**	2-heptanol	**3g**	2-heptanamine
1h	2-octanone	**2h**	2-octanol	**3h**	2-octanamine
1i	3-octanone	**2i**	3-octanol	**3i**	3-octanamine
1j	hexane-2,3-dione	**2j**	hexane,2-3-diol	**3j**	2-aminohexan-3-one
1k	hexanal	**2k**	1-hexanol	**3k**	1-hexanamine
1l	benzaldehyde	**2l**	benzyl alcohol	**3l**	benzylamine

Activity assays

Specific activity measurements were carried out with a volume of 2 mL in a 4 mL UV cuvette monitoring the consumption of NADPH at a wavelength of 340 nm on a Cary 60 UV-Vis spectrophotometer. The extinction coefficient of NAD)H was assumed to be 6220 $M^{-1}cm^{-1}$.[46] Carbonyl substrates were prepared as a 1 M stock solution in DMSO. NAD(P)H stock solution was prepared in the mentioned buffer as a 10 mM concentration (confirmed by UV spectroscopy).

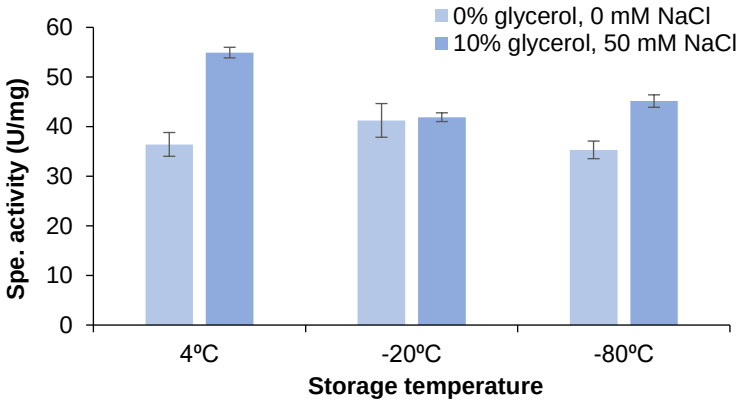

Figure S10. Specific activity of *Lb*ADH-wt after storage in 4, -20 and -80 °C, without (light blue) and with (dark blue) 10% glycerol and 50 mM NaCl. Conditions: 11 mM acetophenone, 0.2 mM NADPH, 50 mM KP_i buffer pH 7.5, 1 mM $MgCl_2$, 30 °C. Averages of triplicates.

The specific activity of *Lb*ADH-wt and *Lb*ADH-YF2 was measured with the best performing substrate 2-methylcyclohexanone from the previous screening (**Table S4**). For *Lb*ADH-wt, the specific activity towards 2-methylcyclohexanone was 137 U/mg, compared with 22.6 U/mg for acetophenone in similar conditions (1% v/v DMSO as co-solvent). *Lb*ADH-YF2 gave a specific activity of 20 mU/mg.

Table S4. Specific activities of *Lb*ADH-wt and *Lb*ADH-YF2 with 2-methylcyclohexanone.

***Lb*ADH**	**Specific activity (U/mg)**
wt	137 ± 3.3
YF2	0.02 ± 0.00

Conditions: 0.2 mM $NADP^+$, 50 mM KP_i buffer pH 7.5, 1 mM $MgCl_2$, 30 °C. Average of duplicates.

Biocatalytic reactions

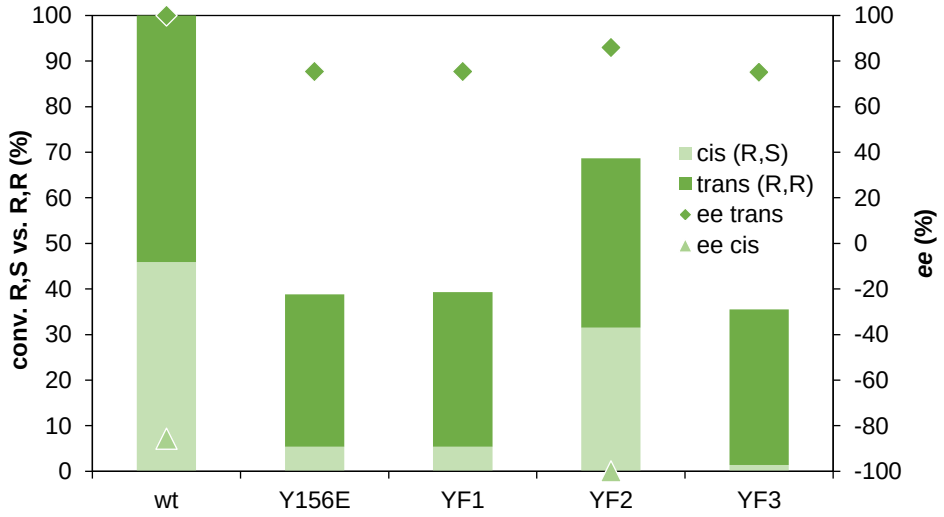

Figure S11. Ketoreduction of 2-methylcyclohexanone in 2-methylcyclohexanol under reductive amination conditions, and the corresponding enantiomeric excess of either the *trans*- (diamonds) or *cis*-product (triangles). *ee* was not determined for conversions under 10%. Conditions: 1 M NH_4HCOO buffer, pH 8.0, 0.2 mM $NADP^+$, 6 U/mL *Bs*GDH, 10 µM *Lb*ADH, 20 mM glucose, 24 h at 500 rpm, 30 °C. Average of duplicates.

Table S5. Diastereomeric excess (*de*) of the *trans*-2-methylcyclohexanol catalysed by the *Lb*ADH variants from screening in reductive amination conditions.

***Lb*ADH**	***de* (%)**
wt	8
Y156E	73
YF1	72
YF2	10
YF3	91

Imine reductase conditions

To 50 mM Tris-HCl buffer pH 9.0, 1 mM $MgCl_2$ glucose (20 mM), GDH-105 (6 U/mL), $NADP^+$ (0.2 mM), aldehyde substrate (either hexanal or benzaldehyde 10 mM), amine donor (either cyclopropylamine or allylamine, 100 mM) and *Lb*ADH (10 µM) were added. The reaction mixtures of 0.5 mL were incubated for 24 h at 30 °C and 500 rpm. For reductive amination conditions, 0.4 mL 10 M NaOH was added, and the reactions were extracted with 0.5 mL EtOAc. The isolated organic layer was dried with $MgSO_4$, centrifuged at 10,000 × *g* for 1 min, decanted to a GC vial and injected onto the GC-FID.

GC analyses

Samples were measured on Shimadzu GC-2010 gas chromatographs (Kyoto, Japan) with an AOC-20i Auto injector equipped with a flame ionization detector (FID), using nitrogen or helium as the carrier gas. Products were confirmed by reference standards. Product concentrations were obtained with a calibration curve equation using 5 mM dodecane or tridecane as an internal standard. All samples were injected with GC quality ethyl acetate (EtOAc), except where specified with diethyl ether (Et_2O) or methyl *tert*-butyl ether (MTBE). Columns used in this work:

A: CP-Wax 52 CB (Agilent Technologies, Santa Clara, California, United States) (25 m × 0.53 mm × 2.0 µm), injection at 250 °C, split ratio 100, flow 4 mL/min, nitrogen as carrier gas.

B: CP Chirasil-DEX CB 1a, 25 m x 0.32 mm x 0.25 µm, injection at 250 °C, split ratio 100, flow 4 mL/min, helium as carrier gas.

C: Hydrodex β-TBDM (Macherey-Nagel, Düren, Germany), 50 m × 0.25 mm × 0.15 µm, heptakis-(2,3-di-O-methyl-6-O-*t*-butyldimethyl-silyl)-β-cyclodextrin, injection at 250 °C split ratio 50, linear velocity 38 cm/s, column flow 2.23 mL/min, helium as carrier gas.

D: CP Sil 5 CB Split, 25 m x 0.25 mm x 1.20 µm, injection at 250 °C, split ratio 50, flow 4 mL/min, nitrogen as carrier gas.

Table S6. Overview of GC methods and retention times for ketone substrates **1a-k** and aldehyde substrates **1l-o**.

No.	Column	Parameters	Ramp (°C/min)	Temp. (°C)	Hold time (min)	Compound	Ret. time (min)
1	**A**	Split ratio: 50 Linear velocity: 30.0 cm/s	- 10 10 10 20	100 140 175 190 250	3 1 4 1 1	tridecane phenylethylamine **3a** DMSO acetophenone **1a** phenylethanimine[a] phenylethanol **2a**	7.4 12.5 13.0 14.4 16.4 17.4
2	**A**	Split ratio: 50 Linear velocity: 30.0 cm/s	- 10 10 10 10	80 145 190 205 245	3 1 1 4 1	tridecane DMSO phenylacetone **1b** 1-phenyl-2-propanol **2b**	9.8 15.6 18.2 19.7
3	**A**	Split ratio: 50 Linear velocity: 30.0 cm/s	- 10 10 10 10	80 145 190 230 245	3 1 1 4 1	tridecane DMSO 4-phenyl-2-butanone **1c** 4-phenyl-2-butanol **2c**	9.8 15.6 20.2 21.9
4	**B**	Split ratio: 100 Linear velocity: 30.0 cm/s	- 5 5 5 10	70 80 90 100 220	2 3 3 2 1	DMSO 2-methylcyclohexanamine **3d** 2-methylcyclohexanone **1d** 2-methylcyclohexanol **2d** tridecane	6.3 11.2, 13.4 11.5, 11.8 16.1, 16.2, 17.1, 17.2 20.5
5	**B**	Split ratio: 50 Linear velocity: 38.0 cm/s	- 1.02 2	50 55	15.1 2	DMSO 2-methylcyclohexanone **1e** 2-methylcyclohexanol **2e**	12.4 19.1, 19.6 23.2, 23.5, 23.9

			2	60	2	dodecane	25.6
			2	75	2	tridecane	30.7
			2	80	2		
			2	95	2		
			2	100	2		
			20	105	2		
				220	1.25		
		Split ratio: 50	-	80	5	DMSO	12.4
		Linear velocity:	5	100	10	3-methylcyclohexanamine **3e**	13.9, 14.2, 15.8,
		38.0 cm/s	5	120	5	3-methylcyclohexanone **1e**	16.1
6	**C**		20	240	1	3-methylcyclohexanol **2e**	19.1, 19.6
						dodecane	23.2, 23.5, 23.9
						tridecane	25.6
							30.7
		Split ratio: 50	-	80	3	2-hexanamine **3f**	5.6
		Linear velocity:	5	150	1	2-hexanone **1f**	6.8
		30.0 cm/s	20	250	1	2-heptanamine **3g**	7.8
7	**A**					2-heptanone **1g**	9.4
						tridecane	12.1
						2-heptanol **2g**	12.8
						2-hexanol **2f**	13.9
						DMSO	17.6
		Split ratio: 50	-	100	3	2-octanamine **3h**	6.5
		Linear velocity:	10	130	7	tridecane	7.9
8	**A**	30.0 cm/s	10	165	2	2-octanone **1h**	8.2
			30	250	1	2-octanone **2h**	11.3
						DMSO	18.0
		Split ratio: 50	-	80	3	DMSO	10.7
		Linear velocity:	5	110	3	3-octanone **1i**	11.4
9	**C**	38.0 cm/s	5	125	3	3-octanamine **3i**	11.5, 11.6
			10	180	1.5	3-octanol **2i**	15.4
			20	220	1	tridecane	22.0
		Split ratio: 50	-	80	3	hexane-2,3-dione **1j**	5.8
		Linear velocity:	5	220	2	DMSO	10.6
10	**C**	38.0 cm/s				hexane-2,3-diol **2j**	17.8
						2-hydroxy-3-hexanone	11.6
						tridecane	18.9
		Split ratio: 100	-	50	4	hexanal **1l**	7.7
		Linear velocity:	5	60	2	1-hexanamine **3l**	9.7
		30.0 cm/s	5	65	4	1-hexanol **2l**	11.3
11	**D**		20	340	1	benzaldehyde **1m**	13.6
						DMSO	14.7
						tridecane	22.0
		Split ratio: 50	-	80	3	hexanal	6.8
		Linear velocity:	5	150	1	dodecane	9.2
12	**A**	30.0 cm/s	20	250	1	imine[a]	11.8
						N-hexylcyclopropanamine	11.3
						DMSO	20.3

[a] hypothesized

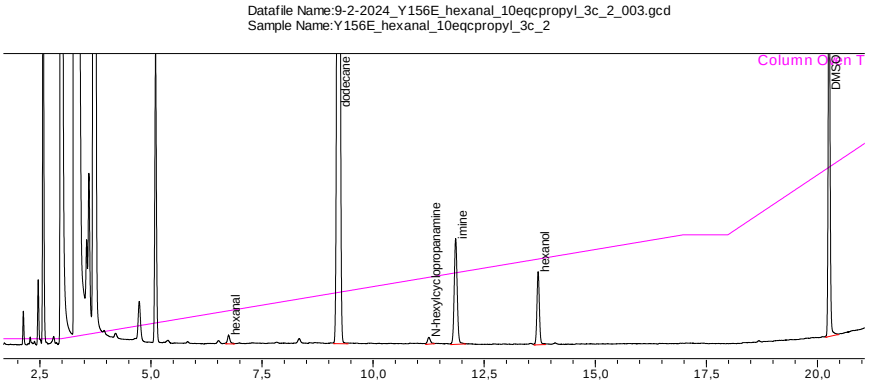

Figure S23. Gas chromatogram of reaction mixture with *Lb*ADH-Y156E, hexanal (6.8 min), hexanol (13.7 min) and the corresponding imine formed with cyclopropylamine (11.8 min) and amine product *N*-hexylcyclopropanamine (11.3 min) (Method 12).

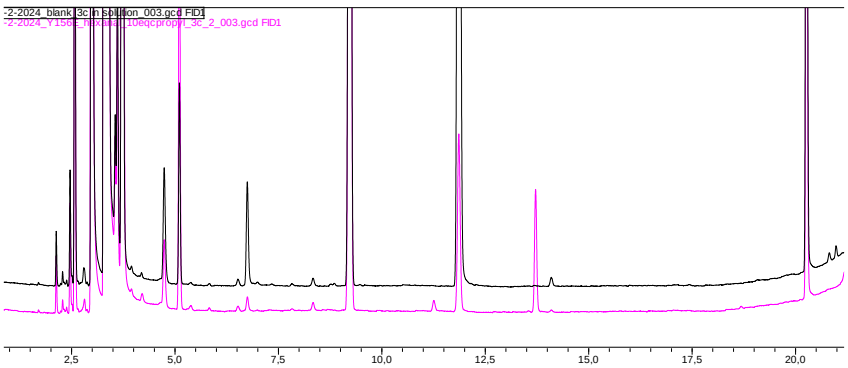

Figure S24. Overlay of reaction mixture with *Lb*ADH-Y156E with hexanal and cyclopropylamine (pink) and a negative control of extracted hexanal and cyclopropylamine in buffer (black) (Method 12).

Molecular dynamics simulations

Molecular dynamics (MD) simulations were performed using the crystal structures of *Lb*ADH (PDB ID: 1ZK4)[27] from the Protein Data Bank[47] to describe the wild-type enzyme, with mutant forms of *Lb*ADH generated using the Dunbrack 2010 Rotamer library as implemented in Chimera.[48] *Lb*ADH is a homotetrameric enzyme whose quaternary structure is stabilized by the presence of two divalent magnesium ions at the dimerization interface. The structure of the homotetramer was generated in PyMOL[49] using the symmetry matrix, and protonation states of all titratable residues were assigned to their predicted states at physiological pH based on predictions using PROPKA v 3.1.[50] Histidine side-chain protonation states were assigned based on a visual inspection of their local environment to maintain optimal hydrogen bonding networks.

One limitation of the *Lb*ADH structure used in these simulations is that in this structure, a critical substrate binding loop (Thr192 – Lys210)[27] is found in an open conformation. This results in substrate dissociation from the active site when attempting simulations from this starting structure. In contrast, the crystal structure of a different ADH *from Lactobacillus kefir* (*Lk*ADH, PDB ID: 4RF2) presents this loop in a closed conformation, and as these two enzymes share both 70% sequence identity and high structural homology in this region (**Figure S24**), we grafted the closed loop onto the *Lb*ADH structure in our simulations, thus allowing us to retain the substrate in the active site.

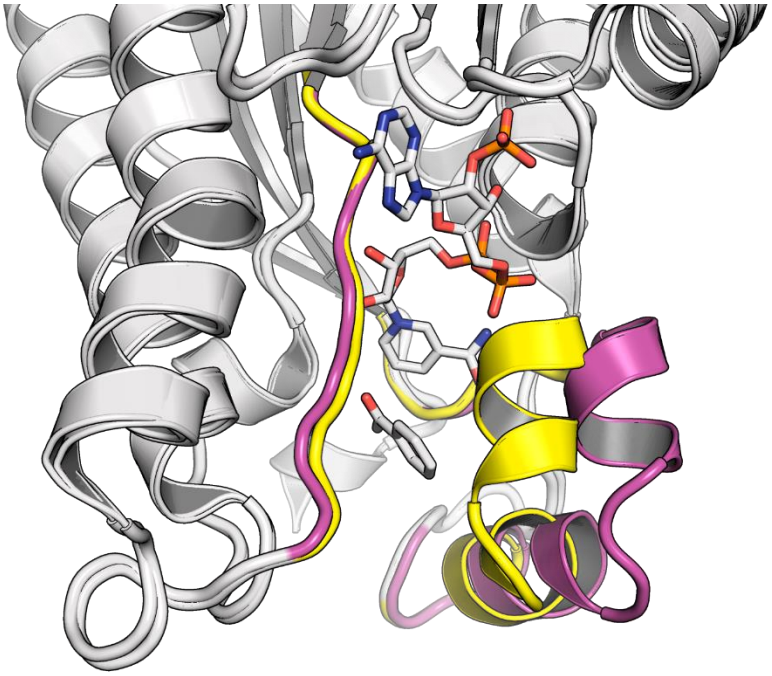

Figure S25. Overlay of the structures of the ADHs from *Lactobacillus brevis* (*Lb*ADH, PDB ID: 1ZK4[27]) and *Lactobacillus kefir* (*Lk*ADH, PDB ID: 4RF2), with the active site loop in open (pink) and closed (yellow) conformations, respectively.

The substrate molecules, acetophenone (**1a**) and the corresponding iminium intermediate derived from **1a**, the (*R*) and (*S*) enantiomers of 2-methylcyclohexanone (**1d**) and the iminium intermediate formed from hexanal and cyclopropylamine for IRED activity were parametrized using Antechamber[51] and the General AMBER Force Field (GAFF)[52]. Partial charges were calculated at the HF/6-31G* level of theory using Gaussian16 Rev.[53] and fitted using the standard RESP protocol.[54] NADPH parameters were adopted from the literature[55], and an octahedral cationic dummy model was used to describe Mg^{2+}.[56, 57]

The simulations were performed using the GPU version of the AMBER20 simulation package[58] with the ff14SB force field[59] and TIP3P[60] water model. All systems were solvated in an octahedral box of water molecules extending to 10 Å from the closest solute atom. Sodium and chloride ions were added for overall charge neutrality.

The preparation for production MD simulations involved a series of steps, including energy minimization, system heating, and equilibration. All hydrogen atoms and solvent molecules were first minimized using 100 steps of steepest descent, followed by 900 steps of conjugate gradient minimization. A 100 kcal mol^{-1} $Å^{-2}$ positional restraint was placed on all heavy (non-hydrogen) protein and ligand atoms during this process. The positional restraints of 25 kcal mol^{-1} $Å^{-2}$ were applied as the system was heated from 50 to 300 K in an NVT ensemble over 50 ps of simulation time using a 2fs time step and Langevin thermostat[61] (collision frequency of 1 ps^{-1}). After the initial steps of energy minimization, the subsequent phase involved another round of energy minimization with 5 kcal mol^{-1} $Å^{-2}$ positional restraints specifically applied to the C_α-atoms. This process consisted of 1000 steps of steepest descent minimization. Following this, the system underwent a heating process from 25 K to 300 K over a period of 20 picoseconds (ps) in an NVT ensemble, maintaining constant volume and temperature. Following the preparatory phases, the simulations progressed into the NPT ensemble at 300 K and 1 atm pressure, employing Langevin thermostat with a collision frequency of 1 ps^{-1} and a Berendsen barostat[62] with a 1 ps pressure relaxation time. A simulation time step of 2 femtoseconds (fs) was utilized during the NPT simulations. During these simulations, four quasi-harmonic distance restraints of 20 kcal mol^{-1} $Å^{-2}$ were implemented strategically. The first restraint targeted the reactive distance between the substrate and the transferrable hydride of NADPH. The remaining three restraints were crucial for maintaining specific structural features: one between the C_α-atoms of amino acid residues A94 and L195, another between N96 and L199, and the fourth between D63 and the amino group of the adenine ring of NADPH. These restraints were helpful in preventing the substrate from escaping the active site throughout the MD simulations. Gradual release of the 5 kcal mol^{-1} $Å^{-2}$ positional restraints occurred in increments of 1 kcal mol^{-1} $Å^{-2}$ every 10 picoseconds (ps) during 40 ps of simulation time. Subsequently, a 7 nanosecond (ns) MD simulation was conducted for further equilibration. During this phase, the distance restraints were reduced from 20 kcal mol^{-1} $Å^{-2}$ to 5 kcal mol^{-1} $Å^{-2}$, decreasing incrementally every 1 ns simulation time while maintaining the NPT conditions.

The final production runs consisted of 100 ns simulations (5 replicas per system) using a 2fs time step. The SHAKE[63] algorithm was employed to constrain all bonds containing hydrogen atoms. Temperature and pressure were

controlled by the Langevin thermostat with a collision frequency of 1 ps^{-1} and the Berendsen barostat with a 1 ps coupling constant. A cutoff of 8 Å was applied to all non-bonded interactions, and long-range electrostatic interactions were evaluated using the particle mesh Ewald (PME)[64] approach. Analysis of the MD simulations was performed using CPPTRAJ.[65]

References

[1] M. M. Musa, *ChemistryOpen* **2022**, *11*, e202100251.
[2] Y. Cui, L. Zhu, X. Chen, J. Feng, Q. Wu, D. Zhu, *ChemBioChem* **2022**, *23*, e202100589.
[3] F. Cheng, Y. Chen, S. Qiu, Q.-Y. Zhai, H.-T. Liu, S.-F. Li, C.-Y. Weng, Y.-J. Wang, Y.-G. Zheng, *ACS Catal.* **2021**, *11*, 2572-2582.
[4] A. Chadha, S. K. Padhi, S. Stella, S. Venkataraman, T. Saravanan, *Org. Biomol. Chem.* **2024**, *22*, 228-251.
[5] D. Ghislieri, N. J. Turner, *Top. Catal.* **2014**, *57*, 284-300.
[6] S. M. Hoy, G. M. Keating, *Drugs* **2012**, *72*, 643-669.
[7] M. T. Reetz, K. Schimossek, *Chimia* **1996**, *50*, 668-669.
[8] M. Höhne, U. T. Bornscheuer, *ChemCatChem* **2009**, *1*, 42-51.
[9] C. E. Paul, M. Rodríguez-Mata, E. Busto, I. Lavandera, V. Gotor-Fernández, V. Gotor, S. García-Cerrada, J. Mendiola, Ó. de Frutos, I. Collado, *Org. Process Res. Dev.* **2014**, *18*, 788-792.
[10] M. D. Patil, G. Grogan, A. Bommarius, H. Yun, *ACS Catal.* **2018**, *8*, 10985-11015.
[11] M. J. Abrahamson, J. W. Wong, A. Bommarius, *Adv. Synth. Catal* **2013**, *355*, 1780-1786.
[12] M. J. Abrahamson, E. Vazquez-Figueroa, N. B. Woodall, J. C. Moore, A. S. Bommarius, *Angew. Chem. Int. Ed.* **2012**, *51*, 3969-3972.
[13] V. Tseliou, T. Knaus, M. F. Masman, M. L. Corrado, F. G. Mutti, *Nat. Commun.* **2019**, *10*, 3717.
[14] O. Mayol, K. Bastard, L. Beloti, A. Frese, J. P. Turkenburg, J.-L. Petit, A. Mariage, A. Debard, V. Pellouin, A. Perret, V. de Berardinis, A. Zaparucha, G. Grogan, C. Vergne-Vaxelaire, *Nat. Catal.* **2019**, *2*, 324-333.
[15] E. Elisée, L. Ducrot, R. Méheust, K. Bastard, A. Fossey-Jouenne, G. Grogan, E. Pelletier, J.-L. Petit, M. Stam, V. de Berardinis, A. Zaparucha, D. Vallenet, C. Vergne-Vaxelaire, *Nat. Commun.* **2024**, *15*, 4933.
[16] T. Knaus, W. Böhmer, F. G. Mutti, *Green Chem.* **2017**, *19*, 453-463.
[17] J. Mangas-Sánchez, S. P. France, S. L. Montgomery, G. A. Aleku, H. Man, M. Sharma, J. I. Ramsden, G. Grogan, N. J. Turner, *Curr. Opin. Chem. Biol.* **2017**, *37*, 19-25.
[18] G. A. Aleku, S. P. France, H. Man, J. Mangas-Sánchez, S. L. Montgomery, M. Sharma, F. Leipold, S. Hussain, G. Grogan, N. J. Turner, *Nat. Catal.* **2017**, *9*, 961-969.
[19] A. K. Gilio, T. W. Thorpe, N. J. Turner, G. Grogan, *Chem. Sci.* **2022**, *13*, 4697-4713.
[20] M. Schober, C. MacDermaid, A. A. Ollis, S. Chang, D. Khan, J. Hosford, J. Latham, A. F. Ihnken, M. J. B. Brown, D. Fuerst, M. J. Sanganee, G. D. Roiban, *Nat. Catal.* **2019**, *2*, 909-915.
[21] J. Zhang, D. Liao, R. Chen, F. Zhu, Y. Ma, L. Gao, G. Qu, C. Cui, Z. Sun, X. Lei, S. S. Gao, *Angew. Chem. Int. Ed.* **2022**, *61*, e202201908.
[22] F. Leipold, S. Hussain, D. Ghislieri, N. J. Turner, *ChemCatChem* **2013**, *5*, 3505-3508.
[23] B. Yuan, D. Yang, G. Qu, N. J. Turner, Z. Sun, *Chem. Soc. Rev.* **2024**, *53*, 227-262.
[24] W. Hummel, *Adv. Biochem. Eng./Biotechnol.* **1997**, *58*, 145-184.
[25] S. Leuchs, L. Greiner, *Chem. Biochem. Eng. Q.* **2011**, *25*, 267-281.
[26] J. Kulig, R. C. Simon, C. A. Rose, S. M. Husain, M. Häckh, S. Lüdeke, K. Zeitler, W. Kroutil, M. Pohl, D. Rother, *Catal. Sci. Technol.* **2012**, *2*, 1580-1589.
[27] N. H. Schlieben, K. Niefind, J. Muller, B. Riebel, W. Hummel, D. Schomburg, *J. Mol. Biol.* **2005**, *349*, 801-813.
[28] J. An, Y. Nie, Y. Xu, *Crit. Rev. Biotechnol.* **2019**, *39*, 366-379.

[29] C. Filling, K. D. Berndt, J. Benach, S. Knapp, T. Prozorovski, E. Nordling, R. Ladenstein, H. Jornvall, U. Oppermann, *J. Biol. Chem.* **2002**, *277*, 25677-25684.
[30] A. Fossey-Jouenne, L. Ducrot, E. P. J. Jongkind, E. Elisée, A. Zaparucha, G. Grogan, C. E. Paul, C. Vergne-Vaxelaire, *Front. Catal.* **2023**, *3*, 1105948.
[31] E. P. J. Jongkind, A. Fossey-Jouenne, O. Mayol, A. Zaparucha, C. Vergne-Vaxelaire, C. E. Paul, *ChemCatChem* **2022**, *14*, e202101576.
[32] L. Ducrot, M. Bennett, G. Grogan, C. Vergne-Vaxelaire, *Adv. Synth. Catal.* **2021**, *362*, 328-351.
[33] O. Khersonsky, R. Lipsh, Z. Avizemer, Y. Ashani, M. Goldsmith, H. Leader, O. Dym, S. Rogotner, D. L. Trudeau, J. Prilusky, P. Amengual-Rigo, V. Guallar, D. S. Tawfik, S. J. Fleishman, *Mol. Cell.* **2018**, *72*, 178-186 e175.
[34] W. Hummel, *Trends Biotechnol.* **1999**, *17*, 487-492.
[35] K. Kulishova, Heinrich-Heine-Universität Düsseldorf **2010**.
[36] R. Machielsen, L. L. Looger, J. Raedts, S. Dijkhuizen, W. Hummel, H. G. Hennemann, T. Dausmann, B. van der Oost, *Eng. Life Sci.* **2009**, *9*, 38-44.
[37] F. Hildebrand, S. Lütz, *Tetrahedron: Asymmetry* **2006**, *17*, 3219-3225.
[38] M. Villela Filho, T. Stillger, M. Müller, A. Liese, C. Wandrey, *Angew. Chem. Int. Ed.* **2003**, *42*, 2993-2996.
[39] E. Krieger, G. Vriend, *Bioinform.* **2014**, *30*, 2981-2982.
[40] V. Prelog, *Pure Appl. Chem.* **1962**, *9*, 119-130.
[41] P. N. Scheller, M. Lenz, S. C. Hammer, B. Hauer, B. M. Nestl, *ChemCatChem* **2015**, *7*, 3239-3242.
[42] S. Roth, M. B. Kilgore, T. M. Kutchan, M. Müller, *ChemBioChem* **2018**, *19*, 1849-1852.
[43] S. Roth, P. Stockinger, J. Steff, S. Steimle, V. Sautner, K. Tittmann, J. Pleiss, M. Müller, *ChemBioChem* **2020**, *21*, 2615-2619.
[44] A. Lygidakis, V. Karuppiah, R. Hoeven, A. Ní Cheallaigh, D. Leys, J. M. Gardiner, H. S. Toogood, N. S. Scrutton, *Angew. Chem. Int. Ed.* **2016**, *55*, 9596-9600.
[45] J. Mangas-Sánchez, M. Sharma, S. C. Cosgrove, J. I. Ramsden, J. R. Marshall, T. W. Thorpe, R. B. Palmer, G. Grogan, N. J. Turner, *Chem. Sci.* **2020**, *11*, 5052-5057.
[46] J. Ziegenhorn, M. Senn, T. Bucher, *Clin. Chem.* **1976**, *22*, 151-160.
[47] H. M. Berman, J. Westbrook, Z. Feng, G. Gilliland, T. N. Bhat, H. Weissig, I. N. Shindyalov, P. E. Bourne, *Nucleic Acids Res.* **2000**, *28*, 235-242.
[48] M. V. Shapovalov, R. L. Dunbrack, Jr., *Structure* **2011**, *19*, 844-858.
[49] L. Schrödinger Inc., *The PyMOL Molecular Graphics System,* Version 1.2r3pre*, LLC*.
[50] C. R. Søndergaard, M. H. Olsson, M. Rostkowski, J. H. Jensen, *J. Chem. Theory Comput.* **2011**, *7*, 2284-2295.
[51] J. Wang, W. Wang, P. A. Kollman, D. A. Case, *J. Mol. Graph. Model.* **2006**, *25*, 247-260.
[52] J. Wang, R. M. Wolf, J. W. Caldwell, P. A. Kollman, D. A. Case, *J. Comput. Chem.* **2004**, *25*, 1157-1174.
[53] M. J. Frisch, G. W. Trucks, H. B. Schlegel, G. E. Scuseria, M. A. Robb, J. R. Cheeseman, G. Scalmani, V. Barone, G. A. Petersson, H. Nakatsuji, X. Li, M. Caricato, A. V. Marenich, J. Bloino, B. G. Janesko, R. Gomperts, B. Mennucci, H. P. Hratchian, J. V. Ortiz, A. F. Izmaylov, J. L. Sonnenberg, Williams, F. Ding, F. Lipparini, F. Egidi, J. Goings, B. Peng, A. Petrone, T. Henderson, D. Ranasinghe, V. G. Zakrzewski, J. Gao, N. Rega, G. Zheng, W. Liang, M. Hada, M. Ehara, K. Toyota, R. Fukuda, J. Hasegawa, M. Ishida, T. Nakajima, Y. Honda, O. Kitao, H. Nakai, T. Vreven, K. Throssell, J. A. Montgomery Jr., J. E. Peralta, F. Ogliaro, M. J. Bearpark, J. J. Heyd, E. N. Brothers, K. N. Kudin, V. N. Staroverov, T. A. Keith, R. Kobayashi, J. Normand, K. Raghavachari, A. P. Rendell, J. C. Burant, S. S. Iyengar, J. Tomasi, M. Cossi, J. M. Millam, M. Klene,

C. Adamo, R. Cammi, J. W. Ochterski, R. L. Martin, K. Morokuma, O. Farkas, J. B. Foresman, D. J. Fox, *Gaussian 09*, Gaussian, Inc., Wallingford, CT, **2019**.
[54] P. Cieplak, W. D. Cornell, C. Bayly, P. A. Kollman, *J. Comput. Chem.* **1995**, *16*, 1357-1377.
[55] N. Holmberg, U. Ryde, L. Bülow, *Protein Eng.* **1999**, *12*, 851-856.
[56] F. Duarte, P. Bauer, A. Barrozo, B. A. Amrein, M. Purg, J. Aqvist, S. C. Kamerlin, *J. Phys. Chem. B* **2014**, *118*, 4351-4362.
[57] Q. Liao, A. Pabis, B. Strodel, S. C. L. Kamerlin, *J. Phys. Chem. Lett.* **2017**, *8*, 5408-5414.
[58] D. A. B. Case, K.; Ben-Shalom, I. Y.; Brozell, S. R.; Cerutti, D. S.; Cheatham, T. E., III; Cruzeiro, V. W. D.; Darden, T. A.; Duke, R. E.; Giambasu, G.; Gilson, M. K.; Gohlke, H.; Goetz, A. W.; Harris, R.; Izadi, S.; Izmailov, S. A.; Kasavajhala, K.; Kovalenko, A.; Krasny, R.; Kurtzman, T.; Lee, T. S.; LeGrand, S.; Li, P.; Lin, C.; Liu, J.; Luchko, T.; Luo, R.; Man, V.; Merz, K. M.; Miao, Y.; Mikhailovskii, O.; Monard, G.; Nguyen, H.; Onufriev, A.; Pan, F.; Pantano, S.; Qi, R.; Roe, D. R.; Roitberg, A.; Sagui, C.; Schott-Verdugo, S.; Shen, J.; Simmerling, C. L.; Skyrnnikov, N. R.; Smith, J.; Swails, J.; Walker, R. C.; Wang, J.; Wilson, L.; Wolf, R. M.; Wu, X.; Xiong, Y.; Xue, Y.; York, D. M.; Kollman, P. A., *AMBER 2020*, University of California, San Francisco, **2020**.
[59] J. A. Maier, C. Martinez, K. Kasavajhala, L. Wickstrom, K. E. Hauser, C. Simmerling, *J. Chem. Theory Comput.* **2015**, *11*, 3696-3713.
[60] W. L. Jorgensen, J. Chandrasekhar, J. D. Madura, R. W. Impey, M. L. Klein, *J. Chem. Phys.* **1983**, *79*, 926-935.
[61] R. W. Pastor, B. R. Brooks, A. Szabo, *Mol. Phys.* **1988**, *65*, 1409-1419.
[62] H. J. C. Berendsen, J. P. M. Postma, W. F. Vangunsteren, A. Dinola, J. R. Haak, *J. Chem. Phys.* **1984**, *81*, 3684-3690.
[63] J. P. Ryckaert, G. Ciccotti, H. J. C. Berendsen, *J. Comput. Phys.* **1977**, *23*, 327-341.
[64] T. Darden, D. York, L. Pedersen, *J. Chem. Phys.* **1993**, *98*, 10089-10092.
[65] D. R. Roe, T. E. Cheatham, *J. Chem. Theory Comput.* **2013**, *9*, 3084-3095.

Chapter 5: Discovery and synthetic applications of a NAD(P)H-dependent reductive aminase from *Rhodococcus erythropolis*

Ewald P.J. Jongkind,[1] Jack Domenech,[2] Arthur Govers, [1] Marcel van den Broek, [1] Jean-Marc Daran, [1] Gideon Grogan, [2] Caroline E. Paul[1,*]

[1] Department of Biotechnology, Delft University of Technology, van der Maasweg 9, 2629 HZ Delft, The Netherlands

[2] York Structural Biology Laboratory, Department of Chemistry, University of York, Heslington, York YO10 5DD, UK

Based on *ACS Catal.,* **2024***, 15,* 211-219. doi: 10.1021/acscatal.4c04935

Summary

Reductive amination is one of the most synthetically direct routes to access chiral amines. Several Imine Reductases (IREDs) have been discovered to catalyze reductive amination (Reductive Aminases or RedAms), yet are dependent on the expensive phosphorylated nicotinamide adenine dinucleotide cofactor NADPH and usually more active at basic pH. Here we describe the discovery and synthetic potential of an IRED from *Rhodococcus erythropolis* (*Ryt*RedAm) that catalyzes reductive amination between a series of medium to large carbonyl and amine compounds with conversions of up to >99% and 99% enantiomeric excess at neutral pH. *Ryt*RedAm catalyzes the formation of a substituted γ-lactam and *N*-methyl-1-phenylethanamine with opposite stereochemistry to that of fungal RedAms, giving the (*S*)-enantiomer. This enzyme remarkably uses both NADPH and NADH cofactors with K_M values of 15 and 247 μM, and turnover numbers k_{cat} of 3.6 and 9.0 s^{-1}, respectively, for the reductive amination of hexanal with allylamine. The crystal structure obtained provides insights in the flexibility to also accept NADH, with residues R35 and I69 diverging from that of other IREDs/RedAms in the otherwise conserved Rossmann fold. *Ryt*RedAm thus represents a subfamily of enzymes that enable synthetic applications using NADH-dependent reductive amination to access complementary chiral amine products.

Introduction

Chiral amines are valuable for applications in the pharmaceutical and agrochemical industries, representing *ca.* 40% of FDA-approved small molecule drugs.[1, 2] Besides metallo-[3] and organocatalysts,[4] biocatalysts have been used for the asymmetric production of chiral amines from prochiral substrates since the early 2000s.[5-11] Within the oxidoreductase class of enzymes,[12, 13] herein we focus on the family of nicotinamide adenine dinucleotide (phosphate) NAD(P)-dependent imine reductases (IREDs) that catalyze the asymmetric reduction of imines to amines,[14, 15] and its subfamily of reductive aminases (RedAms) that catalyze the full reductive amination reaction from carbonyls and alkyl amines (**Figure 1**),[16-19] in contrast to amine dehydrogenases, which mostly accept ammonia and methylamine.[10, 20] IREDs are homodimeric enzymes that contain a Rossmann-fold and prefer NADPH over NADH.[21] In general, their active site harbors a negatively charged residue, usually aspartate, which has been proposed to stabilize the positively charged iminium substrate, and a proton donor such as tyrosine is often present as well.[22] IREDs show highest activity toward imine substrates at neutral pH,[23] however with imines being prone to hydrolysis in water,[24, 25] a carbonyl substrate with an excess of amine donor at a basic pH are usually applied to favor imine formation. The discovery of a 'Reductive Aminase' from *Aspergillus oryzae* (*Asp*RedAm) and other IREDs enabled some reductive aminations to be performed with one molar equivalent of amine donor at neutral pH (**Figure 1**).[18, 19, 26, 27]

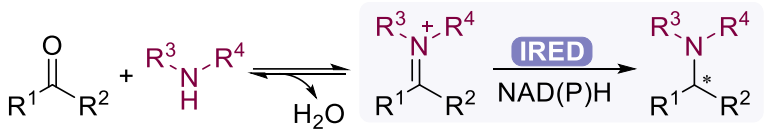

Figure 1. Reductive amination of carbonyls with alkylated amines, and imine reduction (in light blue), catalyzed by IREDs.

Several IREDs with the ability to enable reductive aminations at equimolar concentrations of carbonyl and amine at neutral pH have been identified in fungi,[22, 28] bacteria[19, 29] and from wide panels of IREDs that were screened for this property at neutral pH.[18, 27] While the active sites in fungal enzymes contains several conserved amino acids,[26] RedAm activity has also been demonstrated in enzymes with a range of active site residues.[30] In most cases, however, the majority of enzymes favor the phosphorylated cofactor NADPH over NADH.

In this work, we describe the discovery and characterization of a bacterial enzyme from *Rhodococcus erythropolis* (*Ryt*RedAm), which accepts both NADPH and NADH as nicotinamide cofactors. The gene encoding for this

enzyme was discovered based on a sequence alignment with the *Asp*RedAm, from a database from the *Rhodococcus* genome via a Hidden-Markov Model (HMM).[28]

Results and Discussion

Discovery of *Ryt*RedAm

We started our search for bacterial reductive aminases with *Asp*RedAm (accession number Q2TW47) as the query sequence, based on its three catalytic active site residues N93, D169 and Y177, and the other three residues W210, M239 and Q240 reported for substrate binding (**Table 1**).[26] With the National Center for Biotechnology Information (NCBI) database, we used two bioinformatics tools. First, EnzymeMiner identified putative sequences by filtering hits containing either all six or only the three catalytic residues.[31] Several enzyme sequences were selected for production, some did not express, or the protein precipitated after overexpression. Of the seven soluble enzymes obtained (SI Table S1), five gave activity with cell-free extracts (CFE) and three were screened for conversions with different substrates (**Figure 2**, SI Figures S9-S11, S14). *Pih*RedAm (from *Paenibacillus ihbetae*), *Shy*RedAm (from *Streptomyces hygroscopicus*), and *Bac*RedAm (from *Bacillus* sp. J13) gave low to high conversions. *Shy*RedAm was the most promising, as it converted ketones such as cyclohexanone (with cyclopropylamine, propargylamine and allylamine) and 2-hexanone (with cyclopropylamine and propargylamine) in a 1:1 ratio of carbonyl: amine (**Figure 2**). *Shy*RedAm displayed the same (*R*)-enantioselectivity as with *Asp*RedAm (**2c**, **2d**, **10c**), and accepted methyl amine to produce *N*-methylcyclohexylamine **1b**. *Pih*RedAm also displayed the same enantiopreference as *Asp*RedAm for **10c**, but with higher selectivity, >99% ee.

In parallel, we used the basic local alignment search tool (BLAST)[32] to download all hits with a sequence identity of more than 50%, cumulating to 100 sequences. A multiple sequence alignment was extrapolated from a multiple sequence comparison by log-expectation (MUSCLE),[33] and a HMM database was created with the HMMer tool, resulting in a database with conserved domains of 101 protein sequences. With the HMM we searched in the genome databases of 43 different *Rhodococcus* strains as reported in Busch *et al*.[28] The output list of sequences was ranked based on the E-value.

We selected the most significant hits with the following restrictions: the host organism should be known, and each sequence should originate from a different bacterial organism. Four hits from *Rhodococcus rhodochrous* (*Roc*RedAm), *Rhodococcus opacus* (*Rop*RedAm), *Nocardia seriolae* (*Noc*RedAm), and *Rhodococcus erythropolis* (*Ryt*RedAm) were selected based on the six active site residues from the *Asp*RedAm query sequence (**Table 1**,

sequence identity and solubility factor predicted by SoluProt (between 0 and 1)[34]. Two of the three catalytic residues in the *Asp*RedAm active site D169 and Y177 are similar to the hit sequences except for *Noc*RedAm. The asparagine N93, shown to have a role in the catalytic activity,[22] is replaced by a threonine or serine. The substrate active site residues at positions 210, 239 and 240 showed variances that could possibly result in a different substrate scope.

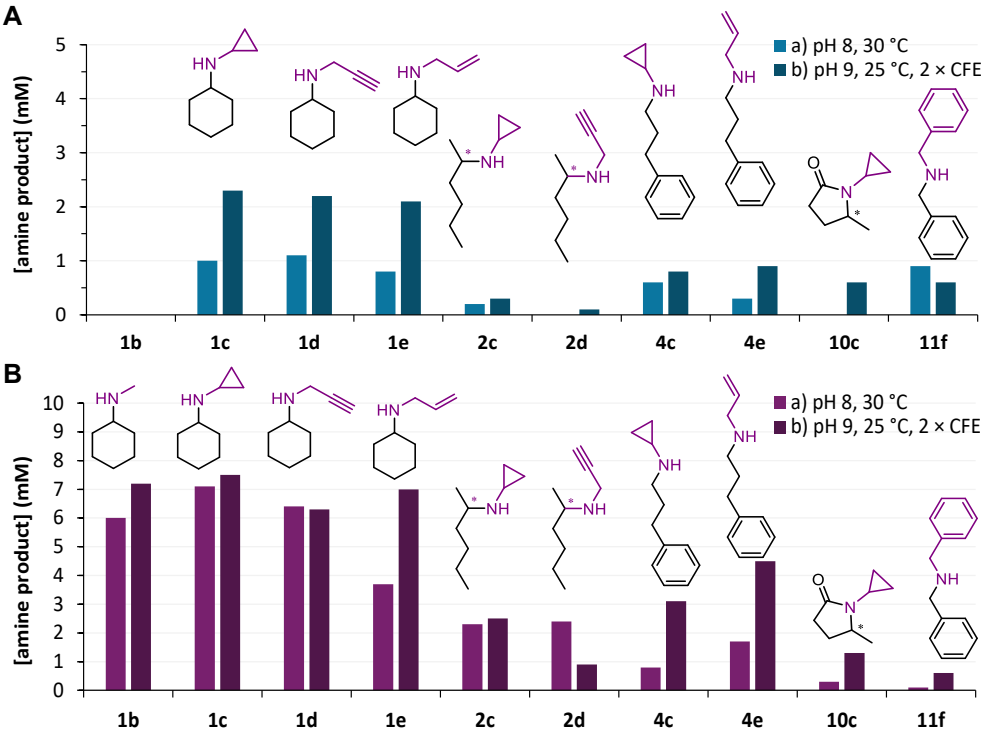

Figure 2. CFE-catalyzed reductive amination under reaction conditions a) and b) of **(A)** *Pih*RedAm and **(B)** *Shy*RedAm. *Absolute configuration aligned with that of *Asp*RedAm. Conditions: a) 100 mM Tris-HCl pH 8.0, 0.2 mM NADP, 12 mM Glc, 6 U/mL GDH, 50 µL CFE, 10 mM carbonyl, 1-20 equivalents amine: **1c**, **1d**, **1e**, **2c** and **2d** with a 1:1 ratio, **1b** 1:2 ratio, **4c**, **4e** and **11f** 1:4 ratio, **10c** 1-20 ratio, 30 °C, 500 rpm, 24 h; b) 100 mM Tris-HCl pH 9.0, 0.4 mM NADP, 30 mM Glc, 10 U /mL GDH, 100 µL CFE, 10 mM carbonyl, 1-20 equivalents amine as above, 25 °C, 500 rpm, 24 h.

Table 1. Active site residues of sequences obtained from the *Rhodococcus* database, and corresponding positions of hit sequences compared with *Asp*RedAm.[21] Sequence identity and solubility factor predicted by SoluProt (between 0 and 1).[27]

RedAm	93	169	177	210	239	240	Identity	Solubility
*Asp*RedAm	N	D	Y	W	M	Q	100	0.76
*Roc*RedAm	T	D	Y	F	L	E	39	0.47
*Rop*RedAm	T	D	Y	F	F	T	35	0.13
*Noc*RedAm	S	Y	H	F	M	M	32	0.34
*Ryt*RedAm	T	D	F	W	V	Y	31	0.36

The potential bacterial RedAms were recombinantly produced in *E. coli* and their activity was tested with hexanal and allylamine at neutral pH (SI Figures S4, S10). The gene encoding for *Noc*RedAm did not over-express and *Roc*RedAm resulted in insoluble protein (Figures S4). *Rop*RedAm was poorly active at pH 7, whereas *Ryt*RedAm showed highly promising activity from the CFE, more than with *Shy*RedAm (SI Figures S10-S11), and thus was further characterized.

*Ryt*RedAm was purified by affinity chromatography in high yield, with 250 mg pure *Ryt*RedAm/6 g wet cell weight (SI Figure S5). *Ryt*RedAm was further characterized in different buffer salts, measuring activity with hexanal and allylamine across a pH range of 5.0-10.0 (**Figure 3A**). MOPS-NaOH buffer caused lower activity compared with KP_i and Tris-HCl. KP_i buffer showed the highest activity within the range pH 6.0-7.0 (6.1 U/mg at 25 °C), and was therefore used as a reaction and storage buffer. The specific activity was systematically higher at neutral pH than at pH 9 by a factor of 0.4. In comparison, *Asp*RedAm has a 0.8 fold lower activity at pH 7 compared with pH 9.[26] Certain IREDs were also reported to have a broad pH range and active at neutral pH, indicating the formation of the iminium.[23, 27, 35] Therefore, we hypothesize that *Ryt*RedAm acts as a reductive aminase at neutral pH with 1:1 ratio for several carbonyl:amine partners (shown further below in **Figure 6**). The activity at different pH for cyclohexanone and cyclopropylamine was also measured and provided the highest activity at pH 7 (**Figure 3B**).

With the ideal neutral pH at hand, *Ryt*RedAm activity was measured at varying temperatures (**Figure 3C**). The activity increased along with higher temperatures, reaching a maximum at 50 °C, and dropping at 60 °C. In terms of stability, *Ryt*RedAm displayed 20-35% loss of activity after a one-hour incubation at 20-30 °C, and complete loss of activity at 40 °C (**Figure 3D**). Therefore, a temperature of 30 °C was used for further reaction screenings.

Considering the key amino acids involved in the active site, we propose the following mechanism based on previous observations with *Asp*RedAm (**Figure 7**).[22] Y235 would be involved as a proton donor, while D166 and T90 would coordinate the protonated amine donor. A nucleophilic attack of the amine on the carbonyl substrate can lead to the iminium ion intermediate and the release of water. NAD(P)H then can reduce the iminium intermediate, resulting in amine formation and release.

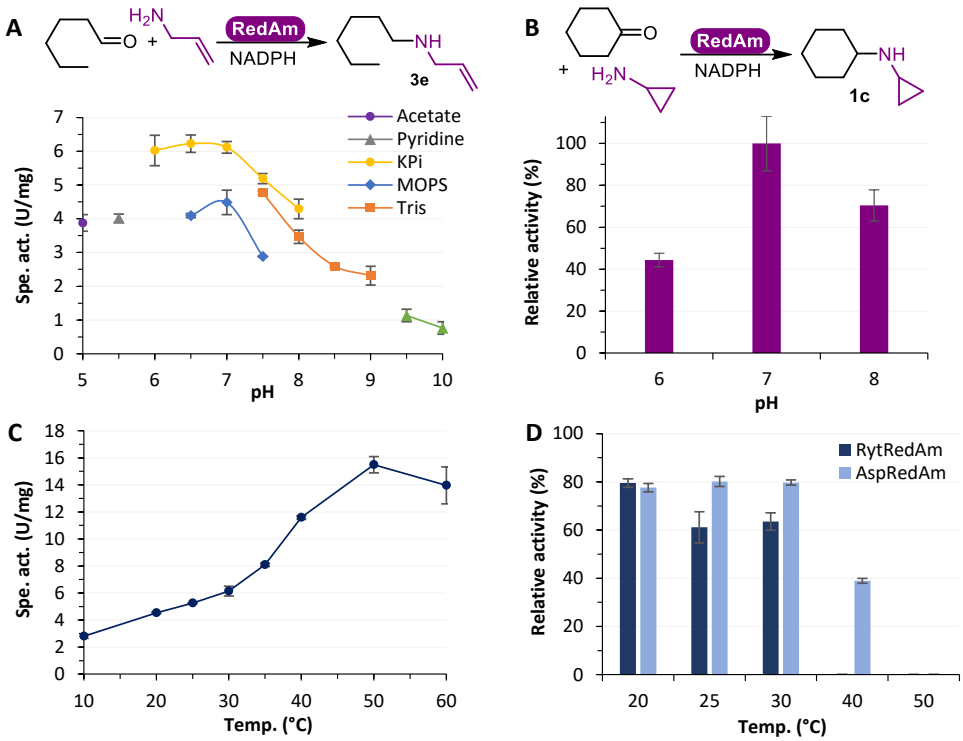

Figure 3. Effect of pH and temperature on activity. **A)** Conditions: 50 mM buffer: acetate pH 5.0 (●), pyridine pH 5.5 (▲), KPi pH 6.0-8.0 (●), MOPS-NaOH pH 6.5-7.5 (◆), Tris-HCl pH 7.5-9.0 (■), glycine-NaOH pH 9.5-10.0 (▲), 10 mM hexanal, 100 mM allylamine, 1% v/v DMSO, 0.2 mM NADPH, *Ryt*RedAm, 25 °C. **B)** Conditions: 50 mM KP_i pH 6.0-8.0, 10 mM cyclohexanone, 100 mM cyclopropylamine, 0.2 mM NADPH, *Ryt*RedAm, 25 °C; 100% corresponds to 23 mU/mg. **C)** Conditions: 100 mM KPi pH 7.0, 10 mM hexanal, 100 mM allylamine, 1% v/v DMSO, 0.2 mM NADPH, *Ryt*RedAm, 10-60 °C. **D)** Conditions: *Ryt*RedAm or *Asp*RedAm incubated 1 h in 100 mM KP_i pH 7.0 at 20-50 °C, activity measured at 30 °C with 10 mM hexanal, 100 mM allylamine, 1% v/v DMSO, 0.2 mM NADPH; 100% corresponds to 6.7 U/mg for *Ryt*RedAm, 0.97 U/mg for *Asp*RedAm. Average of duplicates.

Evaluation of *Ryt*RedAm substrate scope

*Ryt*RedAm activity was highest with aldehydes, hexanal and benzaldehyde, coupled with allyl amine, followed by cyclopropyl amine and methylamine (**Figure 5**). With ketones, cyclohexanone and acetophenone gave activities of 23-65 mU/mg with allyl amine and cyclopropyl amine, and no observable initial activity with methylamine.

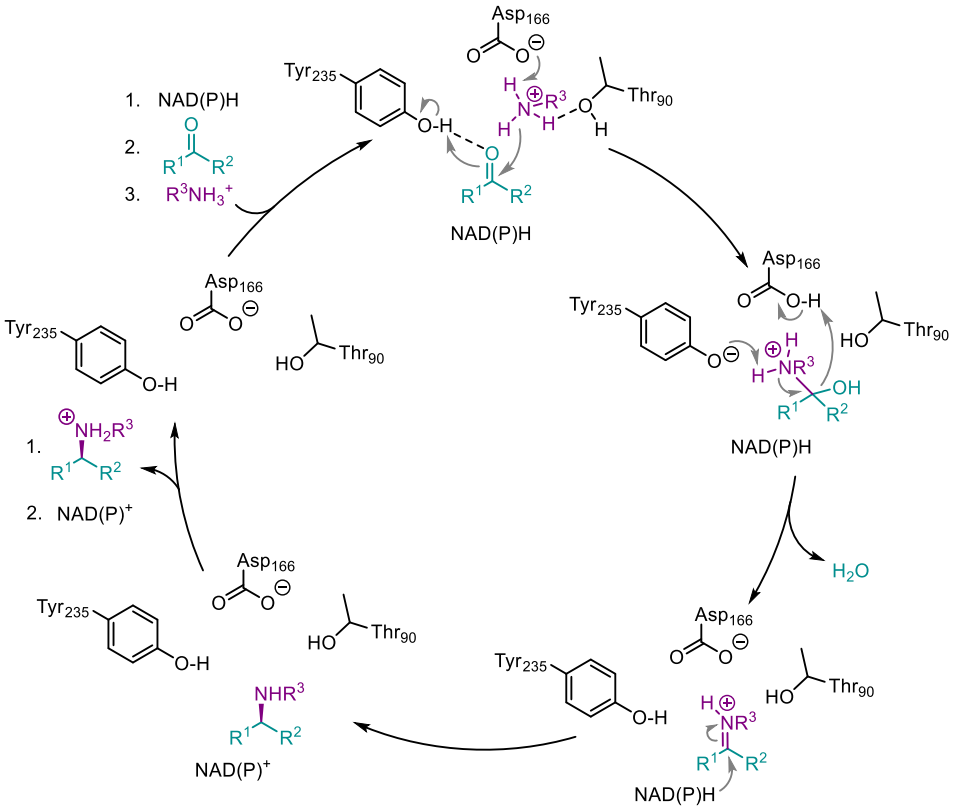

Figure 4. Proposed reaction mechanism of *Ryt*RedAm for reductive amination, involving key residues T90, D166 and Y235.

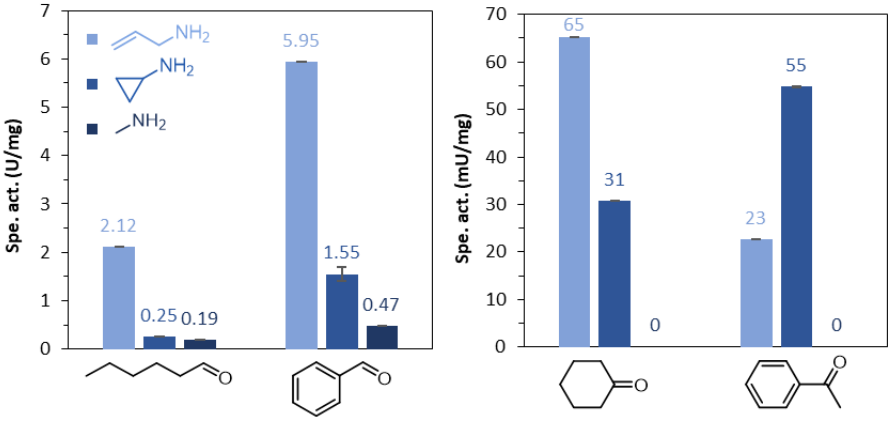

Figure 5. Specific activity of *Ryt*RedAm toward aldehyde (left) or ketone (right) substrates with 10 molar eq. of amine donor. Conditions: 100 mM KPi pH 7.0, 10 mM hexanal, benzaldehyde, cyclohexanone or acetophenone, 100 mM allylamine, cyclopropylamine or methylamine, 0.2 mM NADPH, *Ryt*RedAm, 30 °C. Average of duplicates.

The conversion rate of *Ryt*RedAm with two different substrate-amine combinations over time showed full conversion in under 30 min for the most favored combination of hexanal and allylamine (**Figure 6**). The reductive amination of cyclohexanone with cyclopropylamine to **1c** was clearly slower over time. A scale-up with 50 mM hexanal and 100 mM allylamine afforded 65 mg of pure **3e** (52% isolated yield), confirmed by NMR (SI Figures S47-S48).

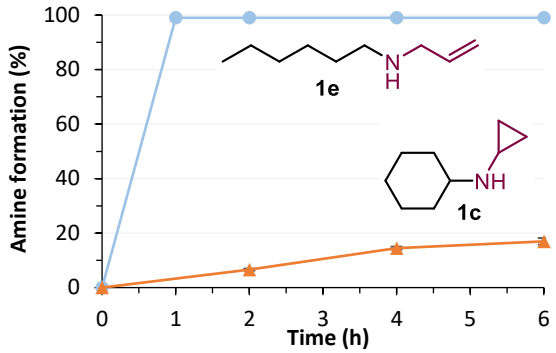

Figure 6. Reductive amination of hexanal with allylamine (●), and cyclohexanone with cyclopropylamine (▲). Conditions: 100 mM KPi pH 7.0, 30 mM Glc, 6 U/mL *Bs*GDH E170K/Q252L, 10 mM carbonyl, 25 mM amine, 0.2 mM NADP, 0.25 mg/mL *Ryt*RedAm, 500 rpm, 30 °C, 24 h. Average of duplicates.

Bioconversions were carried out with a panel of carbonyl substrates and amine donors to establish a wider substrate scope (**Figure 7**, SI). Starting from 10 mM carbonyl, excellent conversions were obtained with aldehydes such as hexanal (>99% **3c**-**e**) and benzaldehyde (89->99% **11c**-**11e**) with only one molar equivalent of amine donor, and moderate to high conversions with hydrocinnamaldehyde (59-67% **4c-e**), combined with four molar equivalent of the best amine donors cyclopropylamine, propargylamine and allylamine. Methyl amine gave 43-55% conversion with aldehydes (**3b**, **11b**) and 7-12% with ketones (**1b**, **7b** with >99% *ee S*). Benzyl amine gave 80% conversion with benzaldehyde (**11f**) and 4% conversion with cyclohexanone (**1f**). Reductive amination was not observed with ammonia (**1a**, Figure S15), nor with 2-hexanone (Figure S8).

Previous work showed that more equivalents of amine donor increased conversion. A conversion of 98% **1c** was achieved with 20 equivalent cyclopropyl amine, compared with 24% when using equimolar amounts (see SI Figure S15). Imine reduction with 2-methyl-1-pyrroline was attempted, but less than 2% conversion was obtained after 24 h (SI Figure S39). This displays the lack of IRED activity in contrast with the reported *Asp*RedAm v_{max} of 0.24 U/mg.[26]

Interestingly, ethyl levulinate combined with cyclopropylamine produced the chiral γ-lactam product 1-cyclopropyl-5-methyl-2-pyrrolidinone **10c**. A scale-up provide 11 mg of pure **10c** (confirmed by NMR, Figures S50-51) with 95% *ee*, the opposite enantiomer to that formed by *Asp*RedAm, which provides only 74%

ee (Figures S33 and S49). The opposite enantioselectivity is also seen with **7b** (>99% *ee* (*R*)- for *Asp*RedAm and (*S*)- for *Ryt*RedAm, Figure S30). This complementarity enables further opportunities for product scope with RedAms, which are otherwise engineered to access the desired enantiomer.[36]

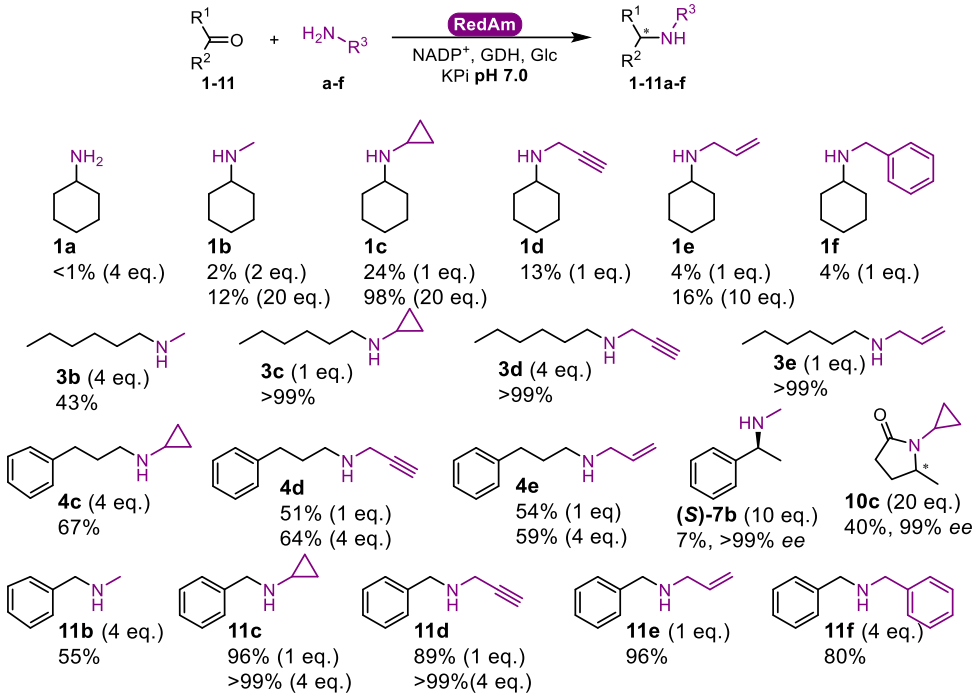

Figure 7. Reductive amination of carbonyl:amine combinations catalyzed by *Ryt*RedAm. Conditions: 100 mM KPi pH 7.0, 0.5 mg/mL *Ryt*RedAm, 30 mM Glc, 6 U/mL *Bs*GDH E170K/Q252L, 10 mM carbonyl, 10-200 mM amine (equivalents of amine donor in brackets), 0.2 mM NADP, 500 rpm, 30 °C, 24 h. Average of duplicates. * Absolute configuration not assigned, opposite to that obtained with *Asp*RedAm.

Evaluation of *Ryt*RedAm cofactor specificity

*Ryt*RedAm specific activity was measured with each NADPH and NADH cofactors, and was surprisingly slightly higher with NADH (7.6 U/mg, **Figure 8A**), which has been so far unreported for RedAms and IREDs,[37, 38] and would significantly increase the economic and synthetic potential of these enzyme families, allowing for NAD-dependent biocatalytic processes. Conversions of one hour were run with varying combinations of carbonyls and amines with each $NADP^+$ or NAD^+ with a GDH/Glc recycling system (**Figure 8B**). Full conversion was obtained for **3e** with both cofactors, whereas **11e** and **1c** with lower conversions showed the slight preference for NADPH over NADH, which may also be ascribed to the GDH employed for cofactor recycling (*Bacillus subtilis* *Bs*GDH E170K/Q252L, SI section 1)[39].

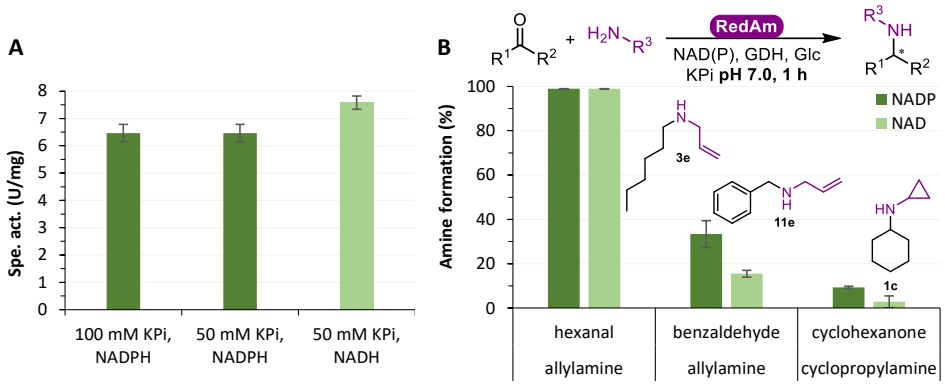

Figure 8. Cofactor specificity. **A)** Specific activity with NADPH and NADH. Conditions: 100 or 50 mM KPi pH 7.0, 10 mM hexanal, 100 mM allylamine, 1% v/v DMSO, 0.2 mM NAD(P)H, *Ryt*RedAm, 25 °C. **B)** One-hour conversions of carbonyl substrates with 10 eq. of amine donor with NADP (dark green) and NAD (light green). Conditions: 100 mM KPi pH 7.0, 10 mM carbonyl, 100 mM amine, 30 mM Glc, 12 U/mL *Bs*GDH E170K/Q252L, 0.2 mM NAD(P), 0.5 mg/mL *Ryt*RedAm, 500 rpm, 30 °C, 1 h.

At first glance, the cofactor binding motif in the *Ryt*RedAm sequence is similar to other IREDs/RedAms that have strong NADPH preference.[21, 38] However, when measuring the kinetic parameters (**Table 2**, SI Figures S12-S13), the catalytic efficiency k_{cat}/K_M with NADH was only seven times lower than that with NADPH. Noticeably, the k_{cat} for NADH is three-fold higher, which explained the higher specific activity observed earlier. Kinetic parameters of *Asp*RedAm with NADH are not known, but it is reported that *Asp*RedAm is approximately 150 times more active with NADPH than with NADH.[26] When measuring the activity with cyclohexanone and methylamine, Aleku *et al.* reports a K_M of 120 µM for NADPH, which is ten times higher than that of the *Ryt*RedAm K_M of 15 µM. One IRED from *Myxococcus stipitatus* was engineered using the Cofactor Specificity Reversal Structural Analysis and Library Design (CSR-SALAD) to change cofactor specificity from NADPH to NADH, resulting in an V10 mutant with an overall k_{cat}/K_M of 7.9 $min^{-1}mM^{-1}$, with a K_M of 11 mM. [37, 38] In our study, *Ryt*RedAm gave a catalytic efficiency of 2187 $min^{-1}mM^{-1}$ with NADH, with a K_M of 0.25 mM (**Table 2**). One recent report from Ward and co-workers describes a range of IREDs accepting both NADH and NADPH as cofactors for reductive amination at pH 7 and 9, but no kinetic data is reported.[40] *Ryt*RedAm displays significant activity for NADH that is uncommon in RedAms and IREDs, including engineered variants. This enzyme model enables opportunities for protein engineering of other RedAms and IREDs, and the further discovery of other 'cofactor-flexible' enzymes.

Table 2. *Ryt*RedAm kinetic parameters K_M and k_{cat} for NADPH and NADH.[a]

Cofactor	K_M (μM)	k_{cat} (s^{-1})	k_{cat}/K_M ($s^{-1}mM^{-1}$)
NADPH	15 ± 4	3.6 ± 0.2	241
NADH	247 ± 50	9.0 ± 0.3	36

[a] Conditions, 100 mM KPi pH 7.0, 10 mM hexanal, 100 mM allylamine, NADPH or NADH, *Ryt*RedAm, 30 °C (see SI).

Crystal structure and mechanism

In an effort to shed light on the determinants of cofactor binding by *Ryt*RedAm, its structure was determined by X-ray crystallography in two forms. Each structure was obtained in space group $P3_221$ with one molecule in the asymmetric unit, so the IRED dimer was constructed using the symmetry neighbor. The first, an apo-structure, was determined in the absence of cofactor (PDB 9FM8). While co-crystallization with NAD^+ or $NADP^+$ failed to give a structure with a fully intact cofactor, crystals obtained with the latter gave an ADP-2'-ribose phosphate (ADP-2RP) complex (density for the nicotinamide ring and ribose sugar of $NADP^+$ being absent) that revealed the residues involved in cofactor binding. A search of the structural databases with the *Ryt*RedAm monomer using DALI [41] revealed fairly low sequence homology with determined structures, including IREDs from *Streptomyces albidoflavus* (PDB 7XE8,[42] 33% sequence id; Z-score 32.8; rmsd 1.3 Å over 284 Ca atoms) and *Mycobacterium smegmatis* (6SMT;[43] 30%; 32.7; 2.6 Å over 283 Ca atoms). Neither of these enzymes was reported to use NADH as the cofactor in addition to NADPH. The structure of the reconstituted dimer of the *Ryt*RedAm ADP-2RP complex is shown in **Figure 9A** (PDB 9FM7) and the residues involved in cofactor binding are shown in **Figure 9B**.

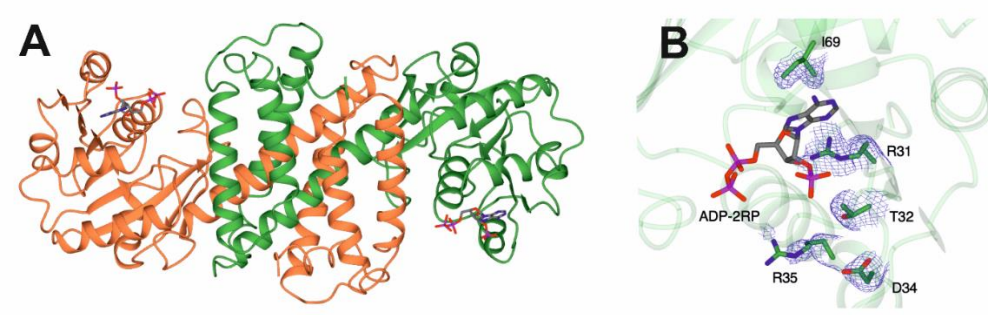

Figure 9. Crystal structure and active site residues of *Ryt*RedAm. **A**: Structure of dimer of *Ryt*RedAm (PDB 9FM7) with subunits in coral and green; **B**: Cofactor binding site of *Ryt*RedAm showing selected side chains and ADP-2RP with carbon atoms in green and grey respectively. The electron density map shown is the 2*Fo*-*Fc* map at a level of 0.6 σ clipped to the side chains to show R35 pointing away from the cofactor binding site.

A consideration of the residues involved in cofactor binding is revealing when compared with natural IREDs with NADPH specificity and especially those that have been engineered previously for NADH recognition. These include the enzyme from *Myxococcus stipitatus*,[38] for which crystal structures of both the NADPH-dependent wild-type (6TO4) and NADH-dependent mutant (6TOE) have both been presented by one of our groups.[44] An alignment of selected cofactor binding regions for a range of IREDs is shown in **Figure 10**.

```
6TO4            TTTVWNRTKAKSEPLAK----------NVLDYDTSDQ
6TOE            TTTVWEYEKARSEPLAK----------NVIDYDVSDQ
3ZHB            PTTVWNRTAAKAEPLVA----------CVSDYDAVHA
5G6R            KTSVWNRTTAKAIPLVE----------CLLNNQVVED
7XE8            STTVWNRTPGKADELAA----------CVADDEAVHQ
6SMT            TVTVWNRTESKAQALRD----------NVVDHDAVDA
RytRedAm        KVTVWNRTADRALPLAA----------SLLNYEIAKD
                  .:**:    :: *:.           : : :  .
```

Figure 9. Sequence alignment of selected IREDs in cofactor binding regions. 3ZHB and 5G6R are NADPH-specific IREDs. 6TO4 is the NADPH-specific IRED from *Myxococcus stipitatus* that was engineered into 6TOE, a variant with improved NADH specificity through, among others, mutation of K37 (red) to R and T71 to V (blue). Natural *Ryt*RedAm is seen to have R35 and hydrophobic I69 in these positions.

The alignment reveals that, although many residues are involved in cofactor binding, two of the most effective mutations for increasing NADH binding in 6TO4 were at positions K37 and T71 to R and V, respectively. K37 is also present in enzymes of established NADPH specificity including 3ZHB, *Asp*RedAm 5G6R and also the closest extant structural homologs of *Ryt*RedAm, 7XE8 and 6SMT. *Ryt*RedAm already has an R in position 35 equivalent to 37; in the structure of *Ryt*RedAm in complex with ADP-2RP, the side chain had incomplete density for the terminal guanidinium group, but the map at a level of 0.6 σ indicates that the side chain is pointing away from the phosphate binding site. Ward, Hailes and co-workers[40] suggest that this K to R substitution does not always have to be present for IREDs to display at least some NADH-dependent activity. In 6TO4 position T71, *Ryt*RedAm has hydrophobic I69, which stacks against the adenine ring of ADP-2RP in the structure, and is closer in chemical character to the valine in the NADH dependent 6TOE variant. A consideration of the variant data suggests that preference for either cofactor is a complicated phenomenon with synergistic input from a number of residues, but the

observations for *Ryt*RedAm may provide useful indicators for the mutations of other IREDs to alter cofactor specificity.

Conclusions

We discovered bacterial reductive aminases via EnzymeMiner and HMM approaches, in particular, *Ryt*RedAm represents another family of RedAms that catalyze reductive amination at neutral pH and accepts both NADPH and NADH cofactors. It is active on a panel of carbonyl substrates, especially aldehydes, to produce secondary amines and provides a chiral γ-lactam with 95% *ee* and (*S*)-*N*-methyl-1-phenylethylamine, opposite selectivity to that of fungal RedAms. The higher activity at pH 7 compared to pH 9 shows this enzyme catalyzes the formation of the iminium ion.

*Ryt*RedAm displays an interesting profile regarding substrate preference, enantioselectivity, cofactor specificity and reaction conditions. The crystal structure obtained provides insights for its NADH acceptance. Because of its complementarity with previously characterized RedAms and IREDs, *Ryt*RedAm is a good model to investigate the reductive amination reaction mechanism with varying substrate combinations with NADH as a cofactor for further scale-up applications.

*Ryt*RedAm could benefit from protein engineering to obtain other chiral amine products and higher thermostability. Other optimizing strategies such as reaction temperature, amine donor equivalents and protein concentrations can be investigated. *Ryt*RedAm is a promising example of the potential undiscovered pool of bacterial reductive aminases, and further discovery of enzymes from this family is ongoing.

Acknowledgements

This project has received funding from the European Research Council (ERC) under the European Union's Horizon 2020 research and innovation programme (grant agreement n° 949910). The authors thank Prof. N.J. Turner for providing the *Asp*RedAm plasmid, M. Strampraad, L. Koekkoek-van der Weel and R.J.C. van Oosten for technical assistance, T. van ’t Riet for kinetic measurements and M. Teke for a preliminary activity screening. We also thank Mr. Sam Hart and Dr. Johan P. Turkenburg for assistance with X-ray data collection, and the Diamond Light Source for access to beamline I03 and I04 under proposal number mx37236.

Materials and methods

General information

Chemicals (aldehydes, amines, ketones) were purchased from abcr GmbH (Karlsruhe, Germany), Merck Sigma (St. Louis, Missouri, U.S.), TCI Europe (Zwijndrecht, Belgium), Thermo Fisher Scientific (Waltham, Massachusetts, U.S.) and VWR International BV (Amsterdam, the Netherlands) and were used as received without further purification. Amines were stored under nitrogen atmosphere. Aldehydes were newly bought before use and were checked by GC for purity. NADPH was bought from OYC EU B.V. (Rotterdam, The Netherlands) with a reported purity of ≥95%. NADH was purchased from Prozomix (Haltwhistle, United Kingdom).

Conversions and enantiomeric excess were measured on Shimadzu GC-2010 gas chromatographs (Kyoto, Japan) with an AOC-20i Auto injector equipped with a flame ionization detector (FID), using nitrogen or helium as the carrier gas. Products were confirmed by reference standards. Product concentrations were obtained with a calibration curve equation using 5 mM dodecane as an internal standard. All samples were injected with GC quality ethyl acetate (EtOAc), except where specified with diethyl ether (Et_2O) or methyl *tert*-butyl ether (MTBE).

Thin layer chromatography (TLC) were run on TLC polyester sheets with a silica gel layer POLYGRAM SIL G (Macherey-Nagel, Düren, Germany) and compounds were revealed using a potassium permanganate solution.

Nuclear magnetic resonance (NMR) spectra were recorded on an Agilent 400 spectrometer at 400 (^1H) and 100 (^{13}C) MHz. Chemical shifts (δ) are reported in parts per million (ppm) relative to Me_4Si (δ 0.00) in deuterated chloroform ($CDCl_3$). NMR data is reported as follows: br = broad, s = singlet, d = doublet, t = triplet, m = multiplet, coupling constant(s) (*J*) in Hz, integration.

Specific rotation measurements were performed on a Perkin Elmer Model 343 S Polarimeter at 20 °C, at a wavelength of 589 nm with the solvent and concentration stated.

*Ryt*RedAm reaction screening

Reactions were performed in GC glass vials with 100 mM KP_i buffer pH 7.0, 10 mM carbonyl substrate, 10-1000 mM amine donor, 0.2 mM NADP, 30 mM Glc, 10 U/mL *Bs*GDH, 0.5 mL purified *Ryt*RedAm, 0.5 mL total reaction volume. Reactions were stirred at 500 rpm at 30 °C for 24 h on an Eppendorf Thermomixer C. To quench the reaction, 0.8 eq. 10 M NaOH was added, and the reaction mixture was vortexed and extracted with 1 eq. EtOAc (centrifuged at 10,000 × *g* for 1 min). The isolated organic layer was dried with $MgSO_4$, centrifuged at 10,000 × *g* for 1 min, decanted to a GC vial and injected onto the GC-FID. Conversions were determined by the product peak area divided by the

sum of the substrate and product peak areas. Control reactions were run in the same conditions but without *Ryt*RedAm.

Supporting information

The complete supporting information, including Figures S16-S24, S26-S29 and S34-S38 can be found at: https://doi.org/10.4121/6fda9cb1-beb8-4985-a210-a9625eca8899

RedAm sequences and production

EnzymeMiner search: The sequence from *Asp*RedAm (Q2TW47, PDB 5G6R) was used to identify targets on the online EnzymeMiner database. Two approaches were used: protein sequences that contained the six key residues N93, D169 Y177, W210, M239 and Q240, or contained only the first three of these residues. Then, the query identity range was set to 0-50%, as all hits with higher similarity come from fungal organisms. The predicted transmembrane protein sequences were excluded. The first hit with an identified organism strain was selected from *Streptomyces hygroscopicus*. The solubility factor was set to be a minimum of 0.5, determined by SoluProt. Then, the bacterial strains were manually selected. From eight sequences, *Streptomyces* and *Bacillus* hits were selected. From the remaining six sequences, one hit was selected from each family, since there were three pairs of sequences from the same family of *Amycolatopsis*, *Paenibacillus* and *Kibdelosporangium*. The sequence from *Rhodococcus rhodnii* was rationally selected to use a broad range of bacterial strains for this work (**Table S1**).

Table S1. Amino acids on key-residue positions of selected hits from bacterial organisms, found by EnzymeMiner. Sequence identity is based on the *Asp*RedAm sequence. Solubility is calculated by SoluProt.

Organism	RedAm	93	169	177	210	239	240	Id.	Solub.
Aspergillus oryzae	*Asp*RedAm	N	D	Y	W	M	Q	100	0.76
Amycolatopsis lurida	*Alu*RedAm	N	D	Y	W	M	Q	41.3	0.54
Bacillus sp. J13	*Bac*RedAm	N	D	Y	Y	M	Q	39.5	0.66
Kibdelosporangium aridum	*Kar*RedAm	N	D	Y	W	M	Q	36.7	0.55
Paenibacillus ihbetae	*Pih*RedAm	N	D	Y	Y	M	Q	40.1	0.56
Rhodococcus rhodnii LMG 5362	*Rhod*RedAm	N	D	Y	W	L	N	35.3	0.23
Streptomyces hygroscopicus	*Shy*RedAm	N	D	Y	W	M	Q	48.1	0.23
Streptomyces sp. WAC 01529	*Strep*RedAm	N	D	Y	W	I	N	42.9	0.53

RedAm accession numbers and sequences

All gene sequences were cloned in a pET-28a(+) vector with a *N*-terminal His-tag, without codon optimization.

***Aspergillus oryzae Asp*RedAm**, GenBank accession number: KY327363.1; UniProt number: Q2TW47
MGSSHHHHHHSSGLVPRGSHMSKHIGIFGLGAMGTALAAKYLEHGYKTSVWN
RTTAKAIPLVEQGAKLASTISEGVNANDLIIICLLNNQVVEDALRDALQTLPSKTI
VNLTNGTPNQARKLADFVTSHGARYIHGGIMAVPTMIGSPHAVLLYSGESLELF
QSIESHLSLLGMSKYLGTDAGSASLHDLALLSGMYGLFSGFLHAVALIKSGQDT
STTATGLLPLLTPWLSAMTGYLSSIAKQIDDGDYATQGSNLGMQLAGVENIIRA
GEEQRVSSQMILPIKALIEQAVGEGHGGEDLSALIEYFKVGKNVD

***Amycolatopsis lurida Alu*RedAm**, GenBank accession number: WP_091600158.1
MGSSHHHHHHSSGLVPRGSHMGKALAAAFLAAGHPTTVWNRSAGKADSLVA
DGAIQAATITEAVTASPIVVVCLLDYPVLHEILEPVGDTLAGRALVNLTNGTPDQ
ARETAGWARGRGADYLDGGIMAVPAMIGRPEARVLYSGSRPVFDQYEGTLNR
LGTARYVGADHGLASLYDLALLSAMYGQFAGASHALALVRTEKADLTEFASSLL
APWLTATTVALPLLAEQNDTGTQAGEESASPPDMQAVAIANIVTASNAQNVDKA
LLSHLFVPLRDLIGRPAHDRDLAGMVDLIKKPQE

***Bacillus* sp. *Bac*RedAm**, GenBank accession number: WP_028404255.1
MGSSHHHHHHSSGLVPRGSHMVRYFFRQGKGEIKVSTDQSKNEALSPVTIIGL
GEMGQALANVFLQNGYPTTVWNRTAAKAEALVKQGAVLAATPREAIQASPVVI
LCVLDYDAVHEILDPLGDALKGRVLFNLTNGTPKQAGDTAQWAKDRGYDYIDA
GIMAVPQIIGTEDAFILYSGGNKNSFDSNKELLDVMGASTYLGEDAGLASLLDL
AMNGAMYGMLAGAMHAISVVATEGIKAQAFSSELLIPYLTAITGIIPNLARQFDT
KEFTVGVSAKLAMQQVGFRNIRQASKDQGISTELLDPIQSLMDRRVAAGFPDD
DFSAVTELFKQAKHNT

***Kibdelosporangium aridum Kar*RedAm**, GenBank accession number:
MGSSHHHHHHSSGLVPRGSHMGETLAETFVSNGHPTTVWNRTPGKVVEGAT
HAPTAAEAVAASEVVVVCVLDYKAAREVLDPIDLTGKAVVNLTNGTPAHAREFV
RGDYLDGGIMAVPQMIGTPEAIVLYSGSRTVFDNYQDTLNVLGQSRFVGEDPG
LAALYDLALLSAMYGQFAGAKHALDMVGANRGDFVETLLIPWLTSTMVAIPVLG
QSDPQSPDDMQAVAIGNIIEANEDLGLGQPGHLR

***Paenibacillus ihbetae Pih*RedAm**, GenBank accession number: WP_099476365.1
MGSSHHHHHHSSGLVPRGSHMNTDQSKRNALSPVTIIGLGEMGQALANVFLQ
NGYPTTVWNRTAAKAEALVKQGAVLAATPYEAIQASPVVILCVLDYDAVHEILD
PLGDALKGRVLFNLTNGTPKQARDTAQWAKDLGYDYMDAGIMAVPQIIGTEAA
FILYSGGNKESFNSNKELLDVMGASTYLGEDAGLASLLDLAMNGAMYGMLAG
AMHAISVVATERIKAQDFSSELLIPYLTAITGIIPNLARQFDTKEFTVGVSAKLAM

QQVGFRNIRQASKDQGISTELLDPIQSLMDRRVAAGFPDDDFSAVTELFKTPK
Q

***Rhodococcus rhodnii* *Rhod*RedAm**, GenBank accession number: EOM76188.1
MGSSHHHHHHSSGLVPRGSHMGTPIAAAFIDAGYRTIVWNRSPGKADALASR
GAEPAATAAEAVAAAPLVVAPLLDHVAVRQTLVPATAALQGRTVVNLANSTPDQ
ARDLAAWVAGHGAAYLDGAMMALPDSVATREGFFLYSGSEEAFTRYRSALEV
MAPAHYFGADPGGAEIHDLAVLGTGYGALSGFLHSLAILHGTGTSPEHFAALA
ARWLNGLAAFLPELAREIDAAHYTDGISTIDLNRAAVDGIVELGRASGVSAATH
EPLRDLLHRSSDNGRGKDSFSSVFELMRKRDDPRQ

***Streptomyces hygroscopicus* *Shy*RedAm**, GenBank accession number: WP_066027906
MGSSHHHHHHSSGLVPRGSHMSKTPVTVLGLGDMGTALARALLEGGHPTTV
WNRTAAKAEALAPEGALTAATTGEAVAASRLVVVCLLDYDSVRQVLGPLGEAL
AGRTVVNLTNGTPRQARDLAAWAAGHGAEYIDGGIMAVPPMIGTPAAFLLYSG
SPAAFAAHRSVLDLFGESHHLGEDHGRAPLYDLALLSAMYGMFSGVLHAYALV
RSDGVAAGDVAPLLGRWLTAMSGAVDGYAQRIDSGDHATGVVSTIAMQSAAF
GNFTGSARDQGISPELIAPIGALMARRVAAGHGHEDLTGLVELLTA

***Streptomyces* sp. *Strep*RedAm**, GenBank accession number: WP_125517916.1
MGSSHHHHHHSSGLVPRGSHMGSALAAALLRAGHRTTVWNRTAAKTGPLAA
QGATPAETAAEAIEASALVIVCLTTNDNVRTLLEPEAAALAGRTVVNLTNGTPAQ
ARELAHWAAEHGITYIDGGIMAVPQMIATPGAYILYSGTDEEAYETHRPTLAALA
ETKWVGKDPGAAALYDLSLLTGMYGMVMGVAQAYALIGTGGVPARDFAPLLK
EWVNAMTDGLVPGMAEALDSGQHLTDVSSLAINQAALPNFLDAFAQQGLSGA
LFEPLQALLDRSVEEGYGADGLSRLATLIKKE

***Rhodococcus rhodochrous* reductive aminase *Roc*RedAm**, GenBank accession number WP_059384799
MGSSHHHHHHSSGLVPRGSHMGSALASRLLDIGYHVTVWNRSPGRDTVLVE
SGAHPAETVAAAAGANPLIVACLLRATSVYETLTPVVEQLRGRTLINLTTTTPNE
ARALADWADRHGIAYLTGAILAVPDMIGTPAAQIFYSGPQPIYEQHHELLDTWA
TSTYDGADPGMASLVDLAMLSGMYQMFAGFFHGAAMVGSEGMTAEEFARRA
TPFLRAMTSGFREYAAVIDAGDYTAPGQQSLEFSDLGHIVSASEEQCVDPATLV
ALQGLITREIAAGHGSEGFARVFVSMRADTGDRTAERIA

***Rhodococcus opacus* reductive aminase *Rop*RedAm**, GenBank accession number: WP_064080687.1

MGSSHHHHHHSSGLVPRGSHMTGTDVTVLGLGAMGQAIAVALLRAGRTVTV
WNRTPEKADTVTKSGAHPAGSVSAAVQASPLVLVCVLDDETVHELIEPVAGDL
RGRTLVNLTTTTPEQARAMSRWAGAARVEYVDGGIMAVPDMIGGGDTFVLYS
GAAEAFDRNRPVLELFGRAVFVGDDAGAAAMYDLALLGAMYAMFAGFEQGA
AMVRGAGGTAGELAAMAAPFLQAMTGSFEEFAVGIDTPAQYEPVQSAEFTAA
AIDTVARAGAEAGVPTALPIAVRAVLAGSIDAACP

Rhodococcus erythropolis **reductive aminase** ***Ryt*****RedAm**, GenBank accession number: WP_020971038.1
MGSSHHHHHHSSGLVPRGSHMDVSILGTGLMGTALAQALIRSGTKVTVWNRT
ADRALPLAAAGATVAESPQSAIAASPLIVISLLNYEIAKDVVTEADSIAGKIIVNTA
TGTPEEANQFAEWIAGRGARYLDGAIAAYPEDIGTESSGINYSGDEDVWEDVQ
SLLTPIAAQSRYVGARPGAANVIDAAMAGAFFNVALGAFHEAAAYVRSEDVAIA
EMRHSLHLWTDKLLELLHEALKAFESGEYETDQATLNVYAAAVEAWQQSMQR
AGQRAALMTANLDNLQRACAAGHGDKGIFAQIETLSANPQSAI

Nocardia seriolae **reductive aminase** ***Noc*****RedAm,** GenBank accession number: WP_033085900
MGSSHHHHHHSSGLVPRGSHMSEPRRSVTVIGLGPMGRAMVKAFLAAGVEV
TVWNRSPEKADAMAESGAKRAGTVAEALDANEVIVVSLTHYAAMYDVLEPVA
DRLRGKVIANLSSDSPENARKGAASVRSFGARFLSGGCMTVSDDILHPASYIF
YSGPREVFDAHAELLRPLSPQEYLGADDGLSQVYYQALLTIFHSWMLALDQAF
ALIVNSGNEIGHFLPYALRSQTPFADFMANFAAAAEAGGWGDLANLRMMDAG
AQHVIEASEDAGVDASLAHAAQALWRKAIAASETAGAPVPVFRILKGTAA

Bacillus subtilis **glucose dehydrogenase E170K/Q252L** ***Bs*****GDH**, UniProt number: P12310
MGSSHHHHHHSSGLVPRGSHMYPDLKGKVVAITGAASGLGKAMAIRFGKEQA
KVVINYYSNKQDPNEVKEEVIKAGGEAVVVQGDVTKEEDVKNIVQTAIKEFGTL
DIMINNAGLENPVPSHEMPLKDWDKVIGTNLTGAFLGSREAIKYFVENDIKGNVI
NMSSVHEVIPWPLFVHYAASKGGIKLMTKTLALEYAPKGIRVNNIGPGAINTPIN
AEKFADPKQKADVESMIPMGYIGEPEEIAAVAAWLASKEASYVTGITLFADGGM
TLYPSFQAGRG

Enzyme production

Lyophilized plasmids of the selected sequences from EnzymeMiner and the *Rhodococcus* sequences cloned in pET-28a(+) were ordered and received from SynBio Technologies (Monmouth Junction, NJ, United States). The *Asp*RedAm plasmid was kindly provided by Prof. N.J. Turner (University of Manchester, Manchester Institute of Biotechnology, UK).

E. coli BL21(DE3) chemically competent cells were transformed with the vector containing the listed genes unless stated otherwise. The *Asp*RedAm gene was transformed in either *E. coli* BL21(DE3), C43(DE3) or BL21 Gold(DE3) competent cells. The transformed cells were grown on selective LB-agar plates (50 µg/mL kanamycin) overnight at 37 °C. TB-medium (500 mL in 2 L baffled flask) was inoculated with 1% v/v overnight LB preculture of the transformed cells and incubated for 3-5 h at 37 °C, 180 rpm. After reaching an OD_{600} of 0.6-0.8, 0.5 mM IPTG was added, followed by overnight incubation at 20 °C. Cells were harvested (17,000 × *g*, 20 min, 4 °C) and stored at -80 °C.

Sodium dodecyl sulfate polyacrylamide gel electrophoresis (SDS-PAGE) was run to show gene expression and enzyme purity levels (**Figures S1-S4**). Samples were prepared by mixing with one equivalent of Laemmli buffer and 5% v/v dithiothreitol (DTT), heated to 95 °C for 5 min, then centrifuged at 9,000 × *g* for 2 min. From these samples, 10 µL was loaded onto the gel, whereas 5 µL of protein ladder was loaded onto a Criterion TGX Stain-Free Precast Gel. Imaging was performed with a ChemiDoc MP imaging system (Bio-Rad Laboratories, Hercules, California, U.S.).

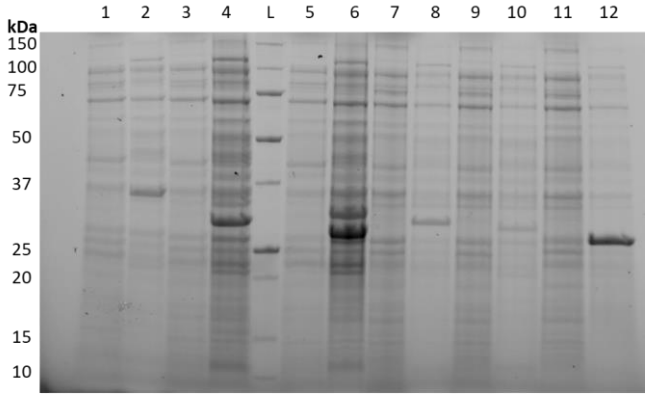

Figure S1. SDS-PAGE gel of hits from EnzymeMiner search before and after IPTG-induction. 1: *Alu*RedAm (29 kDa) before induction. 2: *Alu*RedAm after induction. 3: *Rhod*RedAm before (29 kDa) induction. 4: *Rhod*RedAm after induction. 5: *Bac*RedAm (32 kDa) before induction. 6: *Bac*RedAm after induction. 7: *Rhod*RedAm (29 kDa) before induction. 8: *Rhod*RedAm after induction. 9: *Shy*RedAm (29 kDa) before induction. 10: *Shy*RedAm after induction. 11: *Strep*RedAm before induction. 12: *Strep*RedAm after induction.

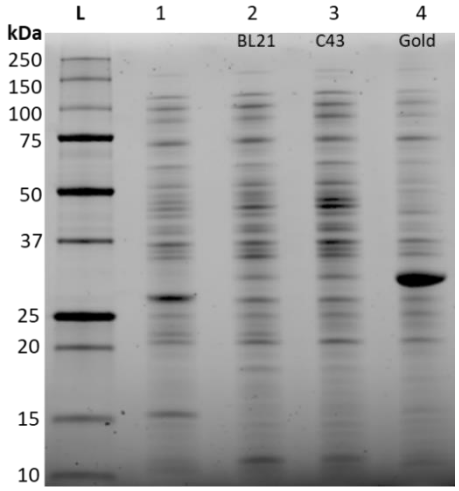

Figure S2. SDS-PAGE gel of *Asp*RedAm (32 kDa) cell-free extracts (CFE) after induction with different strains of *E. coli*. **L**: protein ladder. **1**: *Kar*RedAm (24 kDa). **2**: *Asp*RedAm in *E. coli* BL21(DE3). **3**: *Asp*RedAm in *E. coli* C43(DE3). **4**: *Asp*RedAm in *E. coli* BL21 Gold(DE3).

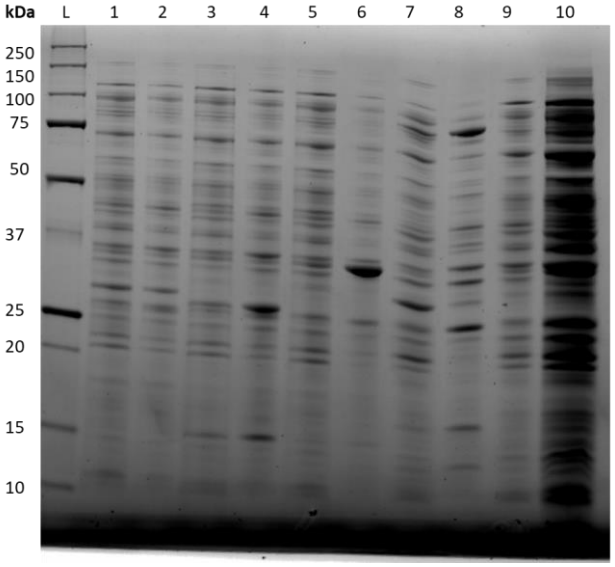

Figure S3. SDS-PAGE gel of all hits selected from EnzymeMiner after cell lysis. 1: *Shy*RedAm CFE. 2: *Shy*RedAm lysate. 3: *Kar*RedAm CFE. 4: *Kar*RedAm lysate. 5: *Alu*RedAm CFE. 6: *Alu*RedAm lysate. 7: *Pih*RedAm CFE. 8: *Pih*RedAm lysate. 9: *Strep*RedAm CFE. 10: *Strep*RedAm lysate.

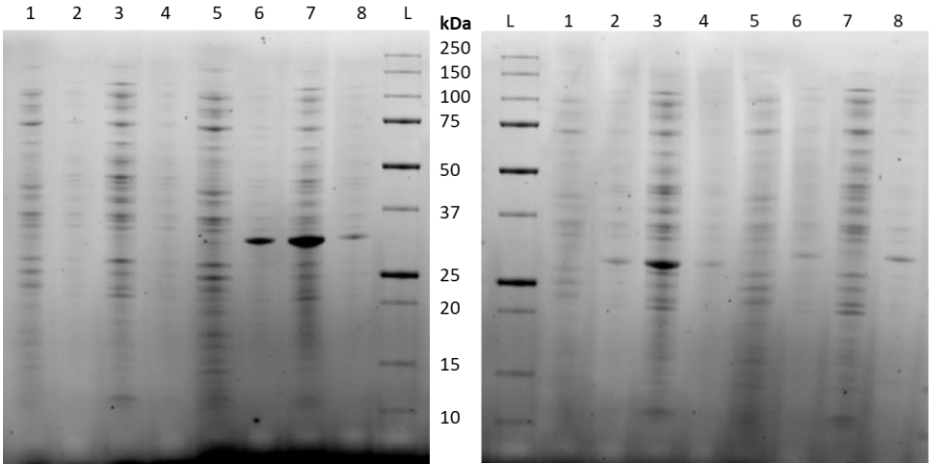

Figure S4. SDS-PAGE gels of CFE of bacterial RedAms. **Left: 1**: *Noc*RedAm before induction. **2**: *Noc*RedAm after IPTG induction. **3**: CFE. **4**: cell lysate. **L**: protein ladder. **5**: *Ryt*RedAm before induction. **6**: *Ryt*RedAm (31.4 kDa) after IPTG induction. **7**: CFE. **8**: cell lysate. **Right: 1**: *Rop*RedAm before induction. **2**: *Rop*RedAm (28.7 kDa) after IPTG induction. **3**: CFE. **4**: cell lysate. **5**: *Roc*RedAm before induction. **6**: *Roc*RedAm after IPTG induction. **7**: CFE. **8**: cell lysate. **L**: protein ladder.

Affinity chromatography purification of *Asp*RedAm and *Ryt*RedAm

Two buffers were prepared: 50 mM Tris-HCl pH 8.0, 300 mM NaCl, 1 mM $MgCl_2$ with 30 mM imidazole for the binding buffer, and with 300 mM imidazole for the elution buffer. The buffers were filtered and degassed before use. The cell pellets were thawed and suspended in 5 mL/g_{wcw} binding buffer. After adding a spatula tip of deoxyribonuclease (DNase), $MgCl_2$, lysozyme from chicken egg white (Sigma Aldrich) and a pill of cOmplete™ Mini EDTA-free Protease Inhibitor (Merck), 3 g_{wcw} of cells were disrupted using a Constant Systems Continuous Flow Cell Disrupter CF1 (22 kpsi) and clarified by centrifugation (32,000 × *g*, 30 min, 4 °C).

The cell-free extract (CFE) was then filtered (0.2 µm) and purification was performed by immobilized-metal affinity chromatography (IMAC) using a Ni-NTA 5 mL HisTrap™ FF crude column (GE Healthcare, Chicago, Illinois, U.S.) on a Bio-Rad NGC Chromatography system. After equilibrating the column with binding buffer at 5 mL/min, the CFE was loaded on the column with a velocity of 3 mL/min. Then, the column was flushed with 10 column volumes (CVs) of binding buffer at 3 mL/min. after 10 CVs, or when the absorbance at 280 nm reached near zero, 100% of the elution buffer was pumped through the column, also at 3 mL/min. Elution fractions were collected, pooled, and kept on ice until desalted with a PD10 desalting column (GE Healthcare). Enzyme concentration was determined by the Uptima bicinchoninic acid (BC) assay (Interchim, Montluçon, France).

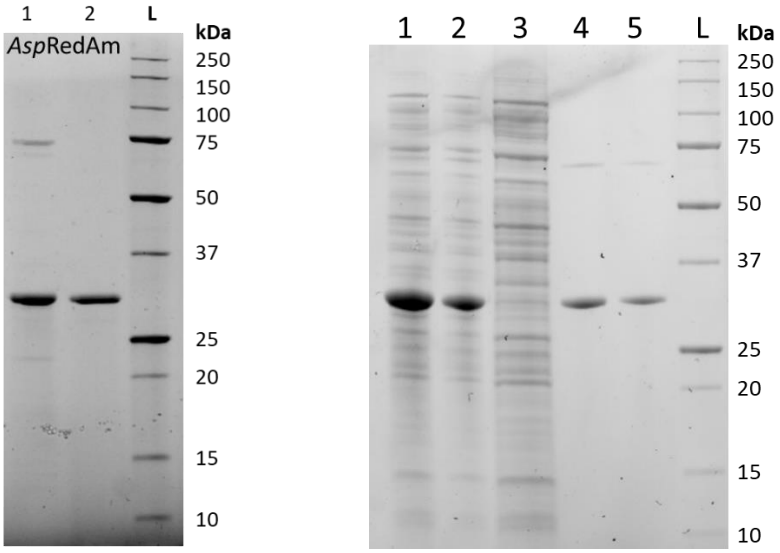

Figure S5. SDS-PAGE gels of IMAC purification of *Asp*RedAm and *Ryt*RedAm. **Left: 1**: *Asp*RedAm (32 kDa) elution, 180 mM imidazole. **2**: *Asp*RedAm elution, 300 mM imidazole. **L**: protein ladder. **Right: 1**: CFE *Ryt*RedAm. **2**: cell lysate after disruption. **3**: IMAC flowthrough. **4-5**: *Ryt*RedAm (31.4 kDa) elution, 300 mM imidazole. **L**: protein ladder.

Size exclusion chromatography purification of *Ryt*RedAm

Peak fractions after affinity chromatography containing protein of the correct molecular weight (32 kDa) were pooled. Size exclusion chromatography (SEC) was conducted on an ÄKTA pure Protein Purification System. The pooled fractions were loaded on a HiLoad 16/600 Superdex 75 pg Cytiva column and eluted using buffer containing 100 mM KP_i pH 7.0, 300 mM NaCl and 10% v/v glycerol. Peak fractions containing protein of the correct molecular weight were pooled and centrifugally concentrated, using 10 kDa MWCO concentrator (VivaSpin20™ Göttingen, Germany).

Protein concentration was determined by absorbance at 280 nm using the Beer-Lambert law. Proteins were concentrated to 13, 26, 36 and 65 mg/mL. proteins were mixed with 5 mM $NAD(P)^+$. Initial screening of crystallization conditions was performed using commercially available INDEX (Hampton Research), PACT premier and CSSI/II (Molecular Dimensions) screens in 96-well sitting drop trays.

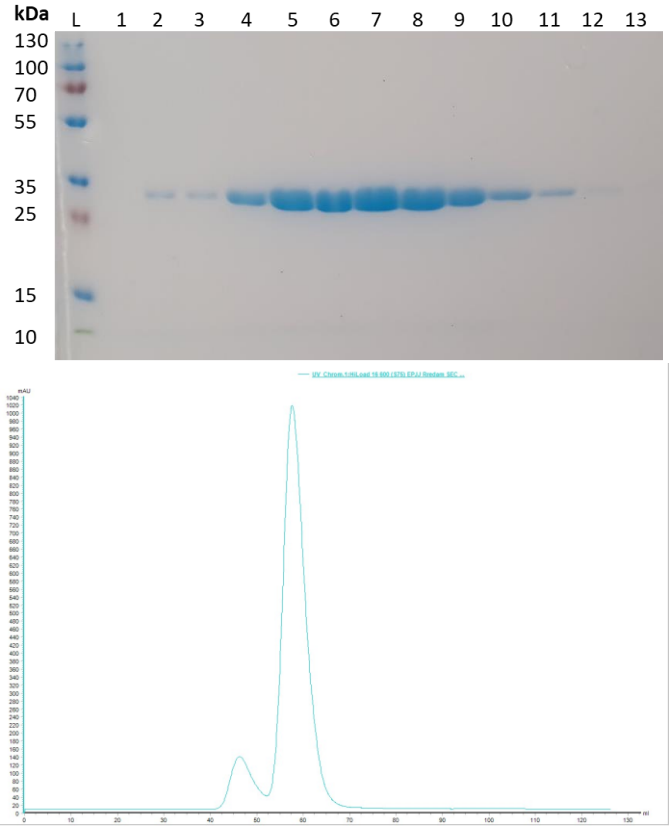

Figure S6. SDS-PAGE gel (top) and SEC chromatogram (bottom) of the SEC purification of *Ryt*RedAm. **L**: protein ladder. **1**: void volume. **2**: fraction minor peak. **3-13**: fractions major peak.

Expression and purification of *Ryt*RedAm for X-ray crystallography

The sequence encoding *Ryt*RedAm was subcloned into the pETYSBLIC-3C plasmid using established protocols.[45] The LIC3C plasmid containing the gene for *Ryt*RedAm was used to transform *E. coli* BL21(DE3) competent cells for gene expression. Pre-cultures were grown in LB-medium (10 mL) containing 30 µg/mL kanamycin for 18 h at 37 °C with shaking at 180 rpm. 0.5 L Terrific Broth cultures were inoculated with the pre-culture (10 mL) and incubated at 37 °C, with shaking at 230 rpm until an OD_{600} of 0.7 was reached. Gene expression was induced by addition of IPTG (0.5 mM) and shaking was continued overnight at 16 °C with shaking at 230 rpm. The cells were then harvested by centrifugation at 5000 × *g* for 20 min and resuspended in 0.1 M Tris-HCl buffer pH 8.0 containing 300 mM NaCl and 30 mM imidazole (His Buffer A). Cells were disrupted, and the suspension was centrifuged at 20,000 × *g* for 1 h at 4 °C to yield a clear lysate.

The *N*-terminal His6-tagged protein was purified by IMAC using Ni-NTA column, followed by size exclusion chromatography (SEC). The lysate was

loaded onto a pre-equilibrated HisTrap™ FF crude 5 mL column, followed by washing with His Buffer A. The bound protein eluted with a step profile with 500 mM imidazole. Fractions were analyzed by 12% acrylamide SDS-PAGE (**Figure S7A**). Fractions containing *Ryt*RedAm were pooled, HRV3C protease (1:50 ratio) added in order to cleave the histidine tag, and the protein dialyzed overnight against His buffer A. The cleaved *Ryt*RedAm was loaded onto the aforementioned IMAC column, with only the flow-through being collected. His-tag free *Ryt*RedAm was centrifugally concentrated (10 kDa MWCO Vivaspin) and loaded onto a HiLoad 16/600 Superdex 75 gel filtration column pre-equilibrated with buffer containing 50 mM HEPES pH 7.0 and 300 mM NaCl. Fractions were analyzed by 12% acrylamide SDS-PAGE (**Figure S7B**). The concentrated protein sample after gel filtration was used for crystallization screening.

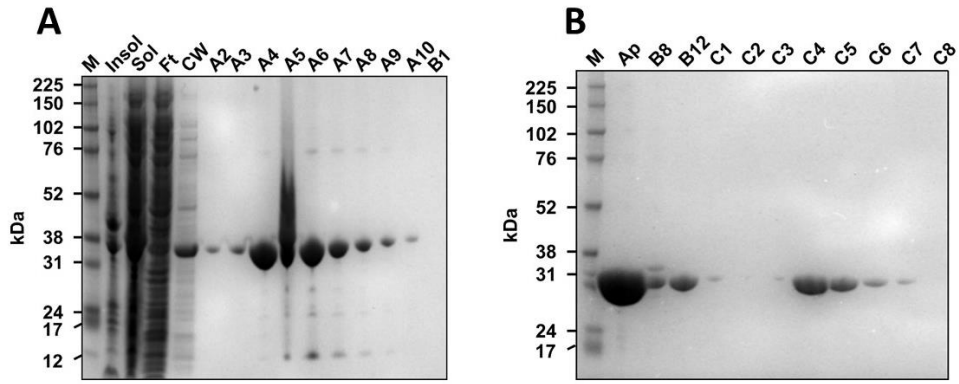

Figure S7. 12% acrylamide SDS-PAGE gels of the Ni-NTA column **A** and gel filtration column **B** showing *Ryt*RedAm at approximately 31 kDa.

Crystallization, data collection and structure solution and refinement

Initial screening of crystallization conditions was performed using commercially available INDEX (Hampton Research), PACT premier and CSSI/II (Molecular Dimensions) screens in 96-well sitting drop trays. Optimization was carried out in a 48-well sitting-drop format to obtain crystals for X-ray diffraction studies. For co-crystallization experiments, a 0.1 M stock solution of cofactor $NADP^+$ in water was prepared and cofactor added to a final concentration of 2 mM.

Crystals of both apo- *Ryt*RedAm and the ADP-2'-ribose phosphate (ADP-2RP) complex were grown using *Ryt*RedAm concentrated to 35 mg/mL in 50 mM HEPES buffer at pH 7.0 containing 300 mM NaCl. The best crystals were obtained in conditions containing 25% (w/v) PEG 3350 and 0.2 M $MgCl_2$ (hexahydrate) in bis-Tris buffer pH 6.5. Crystals for diffraction testing were

harvested directly into liquid nitrogen with nylon CryoLoops™ (Hampton Research), using the mother liquor without any further cryoprotectant.

Data collection, structure solution and refinement

The datasets described in this report were collected at the Diamond Light Source, Didcot, Oxfordshire, U.K. on beamlines I03 and I04. Data were processed and integrated using XDS[46] and scaled using [47] included in the Xia2[48] processing system. Data collection statistics are provided in **Table S2**. All crystals were obtained in space group $P3_221$, with one molecule in the asymmetric unit. The structure of *Ryt*RedAm was solved by molecular replacement using MOLREP[49] and a model generated using AlphaFold[50] as the search model. The structures were built and refined using iterative cycles in Coot[51] and REFMAC.[52] Following building and refinement of the protein and water molecules in the ADP-2RP dataset, residual density was observed in the omit maps at what would be the dimer interface. This could be clearly modelled as ADP-2RP, as no density for the nicotinamide ring and ribose of $NADP^+$ were observed.

The final structures of *Ryt*RedAm and *Ryt*RedAm-ADP-2RP exhibited % R_{cryst} /R_{free} values of 21.8/30.0 and 19.5/24.5, respectively. Refinement statistics for the structures are presented in **Table S2.** The structures of *Ryt*RedAm and *Ryt*RedAm-ADP-2RP have been deposited in the Protein Databank (PDB) with accession codes **9FM8** and **9FM7**, respectively.

Table S2. Data collection and refinement statistics for *Ryt*RedAm. Numbers in brackets refer to data for highest resolution shells.

	RytRedAm apo 21-04-24 - 0574	RytRedAm ADP-2RP 10-05-24 - 5331
Beamline	I03	I04
Wavelength (Å)	0.97627	0.95374
Resolution (Å)	53.39-2.38 (2.47-2.38)	70.78-2.00 (2.05-2.00)
Space Group	$P3_221$	$P3_221$
Unit cell (Å)	a = b = 80.66; c = 82.78; α = β = 90.00°; γ = 120.00°	a = b = 81.73; c = 83.38; α = β = 90.00°; γ = 120.00°
No. of molecules in the asymmetric unit	1	1
Unique reflections	12900 (1319)	22229 (1631)
Completeness (%)	100.0 (100.0)	100.0 (100.0)
R_{merge} (%)	0.14 (0.98)	0.07 (1.14)
$R_{p.i.m.}$	0.03 (0.22)	0.02 (0.37)
Multiplicity	19.8 (20.0)	20.3 (20.6)
$\langle I/\sigma(I) \rangle$	8.6 (0.6)	28.0 (3.1)
Overall B from Wilson plot ($Å_2$)	47	35

$CC_{1/2}$	1.00 (0.96)	1.00 (0.94)
R_{cryst}/ R_{free} (%)	21.8/30.0	19.5/24.5
r.m.s.d 1-2 bonds (Å)	0.005	0.007
r.m.s.d 1-3 angles (°)	1.44	1.65
Avge main chain B ($Å^2$)	71	48
Avge side chain B ($Å^2$)	76	55
Avge waters B ($Å^2$)	61	50
Avge ligand B ($Å^2$)	-	82

Carbonyl substrates, amine donors and products.

Substrates and amine donors

Table S3. List of carbonyl substrates and amine donors used in this study

Label	Carbonyl substrates	Label	Amine donors
1	cyclohexanone	a	ammonium chloride
2	2-hexanone	b	methylamine
3	hexanal	c	cyclopropylamine
4	hydrocinnamaldehyde	d	propargylamine
5	2,5-hexanedione	e	allylamine
6	benzylacetone	f	benzylamine
7	acetophenone		
8	1-indanone		
9	β-tetralone		
10	ethyl levulinate		
11	benzaldehyde		
12	4-fluorophenylacetone		
13	2-heptanone		

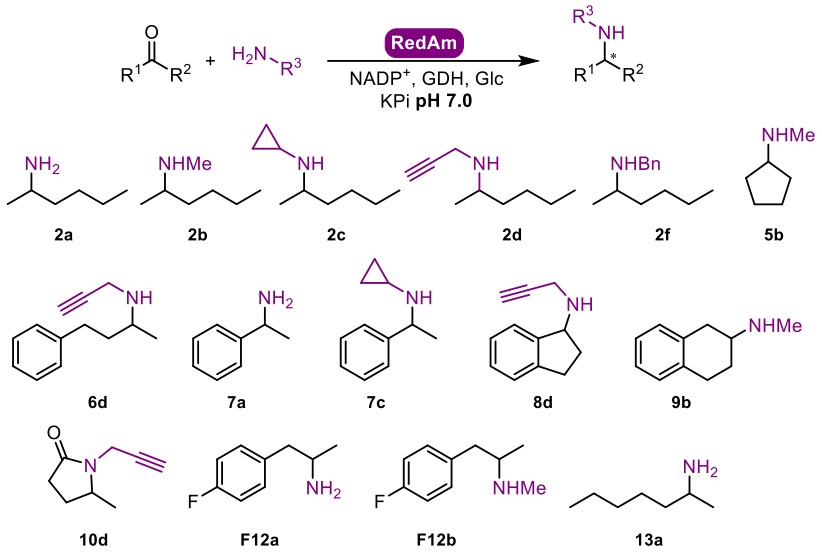

Figure S8. Targeted amine products for which the *Ryt*RedAm showed no measurable conversion.

Amine product synthesis

The synthesis of cyclopropylcyclohexanamine (**1c**, 824-82-8), *N*-2-propyn-1-ylcyclohexanamine (**1d**, 18292-76-7), *N*-cyclopropylbenzenepropanamine (**4c**, 18381-62-9), *N*-2-propyn-1-ylbenzenepropanamine (**4d**, 56862-31-8), *N*-allylbenzenepropanamine (**4e**, 528812-92-2) and 5-methyl-1-(2-propyn-1-yl)-2-pyrrolidinone (**10d**, 18327-34-9) was performed as previously reported.[53]

In dry tetrahydrofuran (THF), 2 mmol of ketone/aldehyde, 2.2 mmol amine, 3 mmol sodium triacetoxyborohydride and 2 mmol glacial acetic acid were mixed and stirred under N_2 at room temperature (20 °C) overnight. The reaction was quenched with 10 mL of 10 M NaOH. The reaction mixture was mixed with EtOAc (10 mL) and the organic phase was separated. This step was repeated, the organic phases were combined and extracted with 1M HCl (3 × 10 mL). The aqueous phase was basified to pH 12 with a 5 M NaOH solution. The product was extracted into EtOAc (2 × 20 mL), dried with $MgSO_4$ and the solvent was removed under reduced pressure on a rotary evaporator to afford the aforementioned amines.

The synthesis of 1-cyclopropyl-5-methyl-2-pyrrolidinone (**10c**, 1351473-78-3) and 5-methyl-1-(2-propyn-1-yl)-2-pyrrolidinone (**10d**, 18327-34-9) was performed based on literature.[53] In dry THF, 1 mmol of ketone, 2 mmol of amine, 2 mmol of acetic acid and 1.4 mmol of sodium triacetoxyborohydride were mixed and stirred under N_2 at room temperature overnight. The mixture was quenched with 1 M NaOH (5 mL) and extracted with EtOAc (3 × 5 mL). The organic layers

were combined, dried over $MgSO_4$ and the solvent evaporated under reduced pressure to afford crude amine products. Yields of synthesized amines varied between 30 and 50% isolated yield. The synthesized compounds were confirmed by NMR. Products *N*-methylhexylamine (**3b**, 35161-70-7), *N*-hexylcyclopropanamine (**3c**, 1040067-31-9), N-allylhexan-1-amine (**3e**, 22774-71-6), *N*-methylbenzylamine (**11b**, 103-67-3) and *N*-benzylcyclopropanamine (**11c**, 13324-66-8) were obtained via biotransformations and confirmed by GC-MS (see section 5.3).

N-methylation of (*S*)-*α*-methylbenzylamine

To assign the enantiomer obtained from product *N*-methyl-1-phenethylamine (**7b**, 32512-24-6), *N*-methylation of (*S*)-α-methylbenzylamine was performed as described by Aleku *et al.*[53] 2 mg of the primary amine was dissolved in 200 µL methanol, then 100 µL of 16% v/v formaldehyde in H_2O was added, and the mixture was shaken at room temperature (20 °C) at 800 rpm for 1 h. The reaction mixture was cooled on ice, and 5 mg of $NaBH_4$ was added slowly. 200 µL dH_2O was added, and the reaction mixture was extracted with 1 mL CH_2Cl_2. The organic layer was dried with $MgSO_4$ and the corresponding secondary amine with known configuration was analyzed by GC-FID without further purification.

RedAm activity assays

For specific activity measurements, 4 mL UV grade polymethylmethacrylate (PMMA) plastic cuvettes were used to monitor the decrease of NAD(P)H at a wavelength of 340 nm on a Cary 60 UV-Vis spectrophotometer. The extinction coefficient of NAD(P)H used was $\varepsilon_{340\,nm}$ = 6220 $M^{-1}cm^{-1}$,[54] and $\varepsilon_{370\,nm}$ = 2.216 $M^{-1}cm^{-1}$ (for kinetic parameter measurements at higher NADH concentrations).[53]

Carbonyl substrates were prepared fresh as a 1 M stock solution in DMSO. Amines were prepared fresh in 100 mM KP_i buffer pH 7.0, titrated with a solution of 6 M HCl to adjust the pH to 7.0. NAD(P)H stock solutions were prepared fresh in the mentioned buffer as a 10 mM concentration, confirmed by UV spectrophotometry at 340 nm.

For buffers at different pHs the following salts were used: sodium acetate-HCl pH 5, pyridine-HCl pH 5.5, KPi pH 6-8, MOPS-NaOH pH 6.5-7.5, Tris-HCl pH 7.5-9, glycine-NaOH pH 9.5-10. Buffer pHs were thermodynamically corrected using Buffer Calculator© (Prof. Robert J. Beynon http://phbuffers.org/BuffferCalc/Buffer.htm, checked on 22/05/2024).

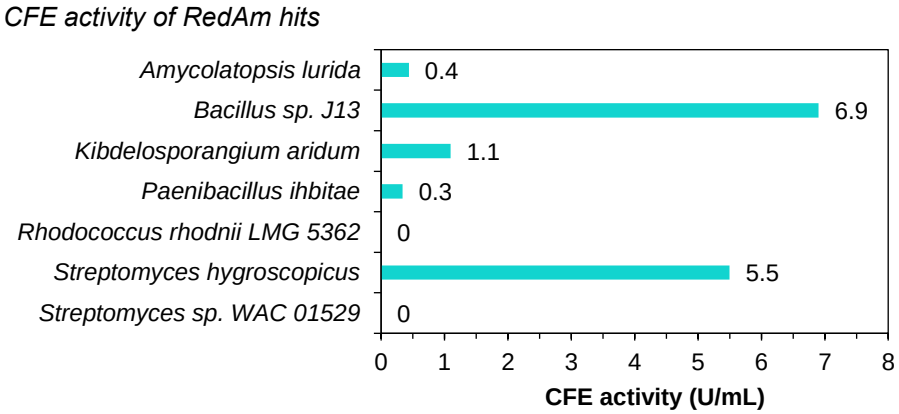

Figure S9. CFE reductive amination activity of RedAms from the EnzymeMiner search (*Alu*RedAm, *Bac*RedAm, *Kar*RedAm, *Pih*RedAm, *Rhod*RedAm, *Shy*RedAm, *Strep*RedAm). Conditions: 100 mM KP_i pH 7.0, 10 mM hexanal, 100 mM allylamine, 1% v/v DMSO, 0.2 mM NADPH, 75 µL CFE, 25 °C.

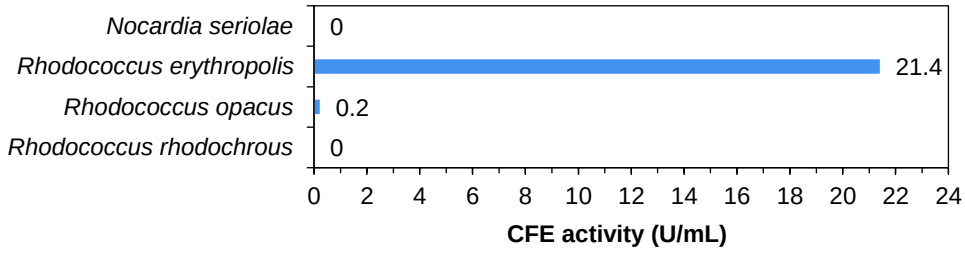

Figure S10. CFE reductive amination activity of RedAms from the HMM search in the *Rhodococcus* genome (*Noc*RedAm, *Ryt*RedAm, *Rop*RedAm, *Roc*RedAm). Conditions: 100 mM KP_i pH 7.0, 10 mM hexanal, 100 mM allylamine, 1% v/v DMSO, 0.2 mM NADPH, CFE, 25 °C.

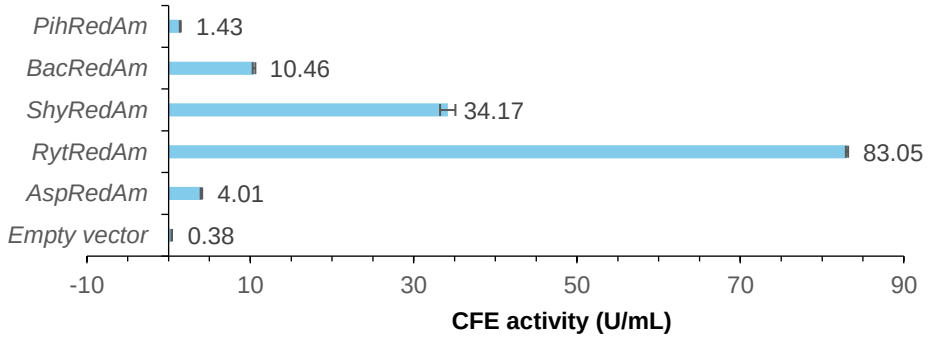

Figure S11. CFE reductive amination activity of soluble and active RedAm hits, compared with *Asp*RedAm and an empty pET28(+) vector. Conditions: 100 mM KP_i pH 7.0, 10 mM hexanal, 100 mM allylamine, 1% v/v DMSO, 0.2 mM NADPH, CFE, 25 °C.

Steady-state kinetics of RytRedAm with NADH and NADPH

Steady-state kinetics were analyzed using IGOR Pro 9 (WaveMetrics). Measurements were plotted onto the equation f(S) = v_{max} × (S/(K_M+S).

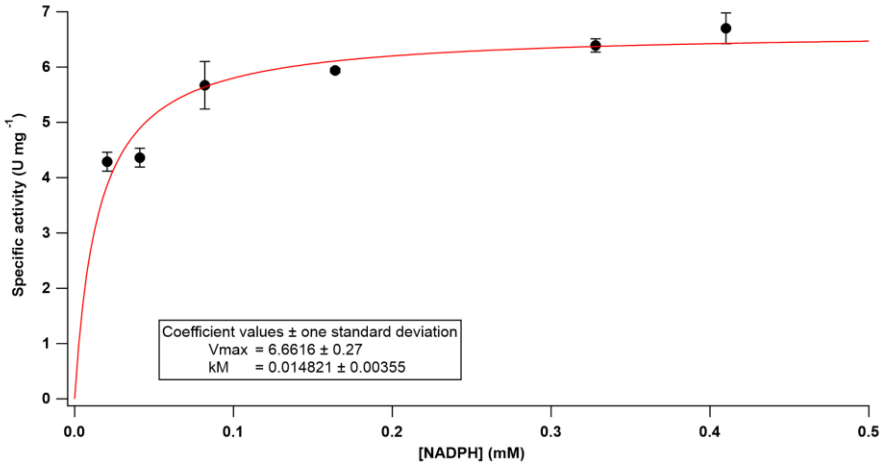

Figure S12. Steady-state kinetics for the reductive amination of hexanal and allylamine catalyzed by *Ryt*RedAm with NADPH. Conditions: 100 mM KP_i pH 7.0, 0.025-0.5 mM NADPH, 10 mM hexanal, 100 mM allylamine, 7.5 µg *Ryt*RedAm, 30 °C.

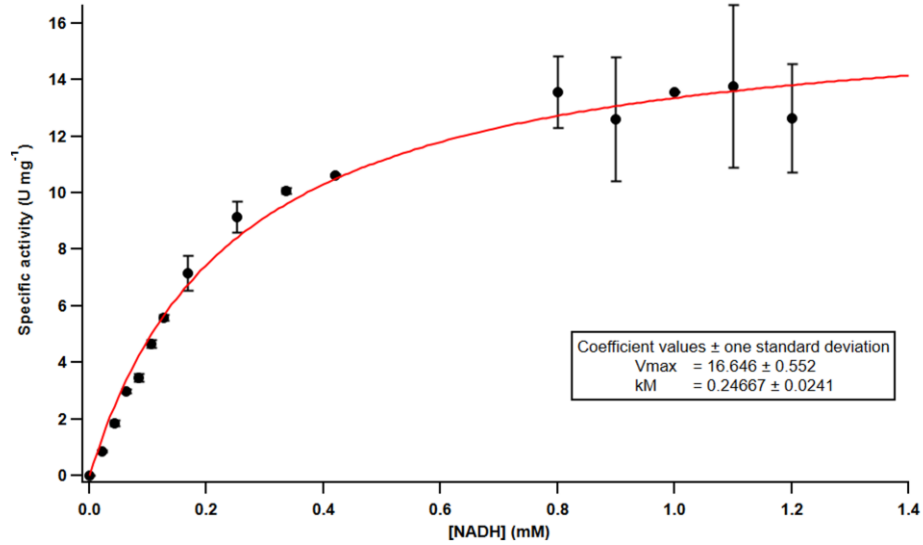

Figure S13. Steady-state kinetics for the reductive amination of hexanal and allylamine catalyzed by *Ryt*RedAm with NADH. Conditions: 100 mM KP_i pH 7.0, 0.025-0.5 mM NADH, 10 mM hexanal, 100 mM allylamine, 7.5 µg *Ryt*RedAm, 30 °C.

RedAm reactions

CFE reactions of RedAm hits

CFE screening of *Pih*RedAm, *Shy*RedAm and *Kar*RedAm (not shown) were performed under two different sets of conditions:

A: 100 mM Tris-HCl pH 8.0, 0.2 mM NADP, 12 mM Glc, 6 U/mL GDH, 50 µL CFE, 10 mM carbonyl substrate, 1-20 eq. amine donor. Stirred at 30 °C and 500 rpm for 24 h

B: 100 mM Tris-HCl pH 9.0, 0.4 mM NADP, 30 mM Glc, 10 U /mL GDH, 100 µL CFE, 10 mM carbonyl substrate, 1-20 eq. amine donor. Stirred at 25 °C and 500 rpm for 24 h.

CFE screening of *Bac*RedAm was only performed under condition set A (**Figure S14**). *Kar*RedAm displayed no reductive amination conversions in both sets of conditions for any substrate-amine combination we tried. To quench the reaction, 0.8 eq. 10 M NaOH was added to the mixtures, and vortexed thoroughly. Then, the reaction mixture was extracted twice with 0.5 µL EtOAc, vortexed, centrifuged and the organic layer separated. After drying with $MgSO_4$, the organic phase was centrifuged at 12,000 rpm for 1 min, transferred to a GC vial and injected onto the GC-FID for analysis. Conversions were calculated by the product peak area divided by the sum of the substrate and product peak areas.

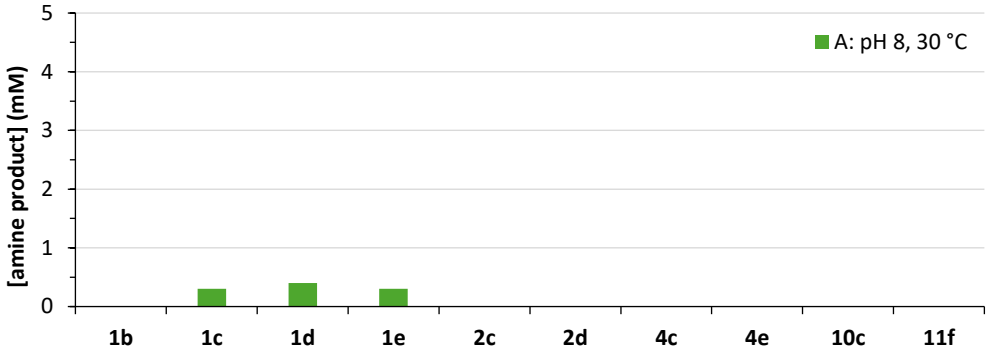

Figure S14. *Bac*RedAm CFE-catalyzed reductive amination.

RytRedAm 1-hour biotransformation

Reactions were performed in GC glass vials with 100 mM KP_i buffer pH 7.0, 10 mM carbonyl substrate, 100 mM amine donor, 0.2 mM NADP, 30 mM Glc, 12 U/mL *Bs*GDH, 0.5 mg/mL purified *Ryt*RedAm, 0.5 mL total reaction volume, stirred at 500 rpm at 30 °C for 1 h on an Eppendorf Thermomixer C.

RytRedAm imine reduction screening

Reactions were performed in GC glass vials with 10 mM 2-methyl-1-pyrroline, 0.2 mM NADP, 30 mM Glc, 10 U/mL *Bs*GDH, 100 mM KPi buffer pH

7.0, 0.5 mg/mL purified *Ryt*RedAm, 0.5 mL total reaction volume. Reactions were stirred at 500 rpm at 30 °C for 24 h on an Eppendorf Thermomixer C. The reaction mixture was quenched, extracted and analyzed as described above. Less than 1% conversion was observed (see GC section 5.2.7).

Reductive amination with cyclohexanone and different amine donor concentrations

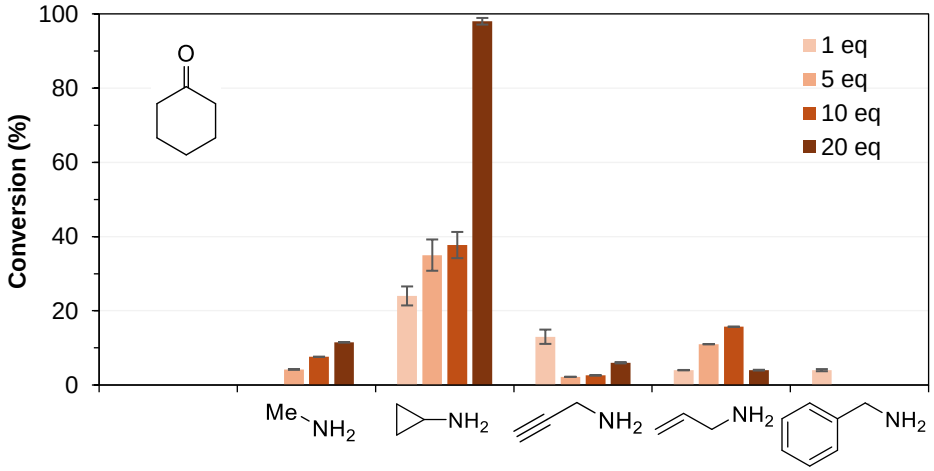

Figure S15. Influence of the amine donor concentration for the reductive amination of cyclohexanone catalyzed by *Ryt*RedAm. Conditions: 100 mM KPi pH 7.0, 30 mM Glc, 10 U/mL *Bs*GDH, 10 mM cyclohexanone, 10-500 mM amine, 0.2 mM NADP, 0.5 mg/mL *Ryt*RedAm, stirred at 500 rpm at 30 °C for 24 h.

GC analyses

GC columns and methods

The following chiral columns were used to determine enantiomeric excess of chiral products; details on the injection temperature, linear velocity, column flow, oven temperature program and retention times can be found for each compound below.

A. CP-Sil 8 CB (Agilent Technologies, Santa Clara, California, United States) (25 m × 0.25 mm × 1.20 µm), injection at 340 °C, split ratio 50, linear velocity 30 cm/sec, column flow 1.01 mL/min, nitrogen as carrier gas.

B. CP-Wax 52 CB (Agilent Technologies, Santa Clara, California, United States) (25 m × 0.53 mm × 2.0 µm), injection at 250 °C, split ratio 50, flow 4 mL/min, nitrogen as carrier gas.

C. Hydrodex β-TBDM (Macherey-Nagel, Düren, Germany), 50 m × 0.25 mm × 0.15 µm, heptakis-(2,3-di-O-methyl-6-O-*t*-butyldimethyl-silyl)-β-cyclodextrin, injection at 250 °C split ratio 50, linear velocity 38 cm/s, column flow 2.23 mL/min, helium as carrier gas.

Table S4. List of GC methods, with corresponding methods and retention times.

GC column	Mthd	GC oven program: rate (°C/min), temp. (°C), hold (min)			Compound	ret. time (min)
A CP-Sil 8 CB	A1	- 5 25	80 100 345	3 4 1	Methylamine b DMSO cyclohexylamine 1a cyclohexanol (side product) cyclohexanone 1 *N*-methylcyclohexylamine 1b dodecane	7.8 8.3 9.9 10.8 11.4 12.5 16.8
A	A2	- 5 10 25	80 100 200 345	3 4 2.2 1	DMSO cyclohexanol (side product) cyclohexanone 1 benzylamine f *N*-2-propyn-1-ylcyclohexanamine 1d [a] *N*-allylcyclohexanamine 1e *N*-cyclopropylcyclohexanamine 1c [a] dodecane *N*-benzylcyclohexanamine 1f	8.3 10.8 11.4 16.0 18.6 [a] 17.9 18.6 [a] 20.3 27.3
A	A3	- 5 20	100 250 345	3.25 1 0	DMSO benzaldehyde 11 benzyl alcohol *N*-methylbenzylamine 11b [b] dodecane *N*-allylbenzylamine 11e [c] *N*-benzylcyclopropanamine 11c [b] *N*-benzylpropargylamine 11d [b] dibenzylamine 11f	5.9 9.7 11.7 12.6 [b] 16.9 17.8 [c] 18.6 [b] 18.7 [b] 32.6
A	A4	- 10 5 20	100 140 180 345	1.75 2 5 1	DMSO dodecane hydrocinnamaldehyde 4 *N*-allylbenzenepropanamine 4e [a] *N*-2-propyn-1-ylbenzenepropanamine 4d [a] *N*-cyclopropylbenzenepropanamine 4c [a]	5.1 13.8 13.2 21.8 [a] 22.6 [a] 22.7 [a]
B CP-Wax 52 CB	B1	- 5	80 150	3 1	hexanal 3 dodecane	6.7 9.2 11.2 [b]

		20	250	1	*N*-hexylcyclopropanamine 3c [b] *N*-methylhexylamine 3b [b] *N*-(prop-2-yn-1-yl)hexan-1-amine 3d [c] *N*-allylhexan-1-amine 3e [b] DMSO	13.6 [b] 16.8 [c] 11.2 [b] 20.2
C Hydrodex β-TBDM	C1	- 5	100 220	2 1	DMSO *N*-Methyl-1-phenylethylamine 7b ethyl levulinate 10 acetophenone 7 1-cyclopropyl-5-methyl-2-pyrrolidinone 10c dodecane	6.8 9.5, 9.6 9.8 10.5 16.7, 16.8 [a] 10.7
C	C2	- 5	80 220	2 1	2-methyl-1-pyrroline 2-methylpyrrolidine *(R)*-2-methylpyrrolidine DMSO	10.7 20.1, 20.5 20.1 17.7

[a] Based on products of amine synthesis
[b] Based on comparison with negative control, confirmed on GC-MS
[c] Based on negative control

*N-allylhexan-1-amine **3e***

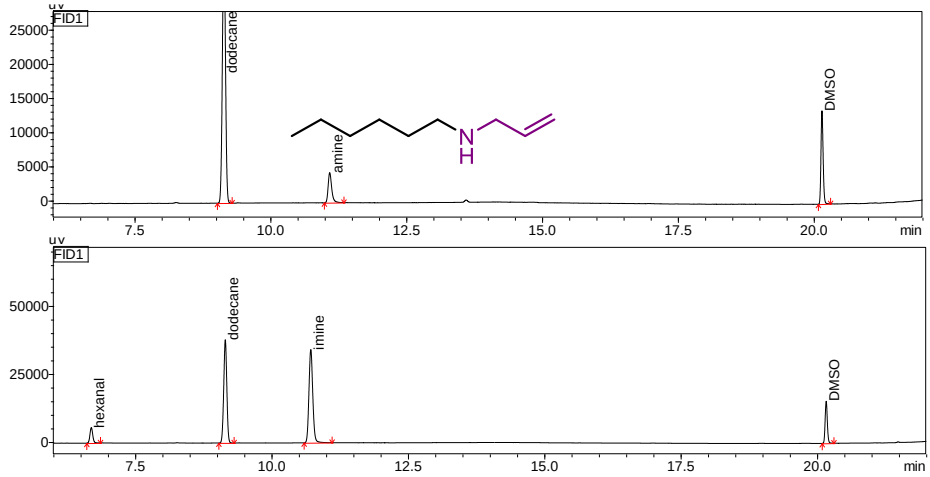

Figure S25. GC chromatogram of reaction mixture with *Ryt*RedAm to produce *N*-allylhexan-1-amine **3e** (top) and control reaction without enzyme (bottom); on column CP-Wax 52 CB method B. Expected amine product at 11.2 min.

Amine products from acetophenone 7

N-methyl-1-phenylethylamine **7b**

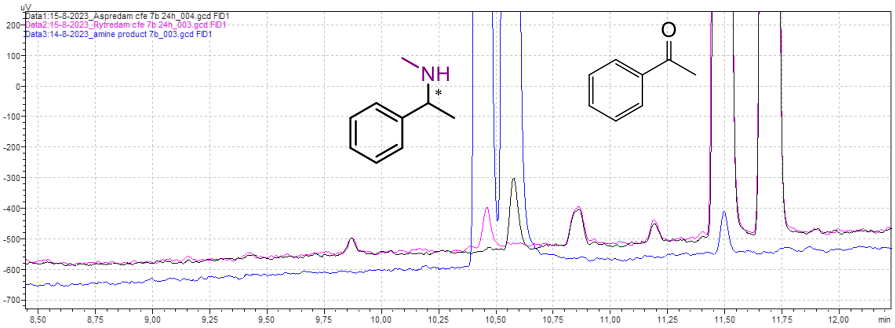

Figure S30. GC chromatogram of reaction mixture with *Ryt*RedAm to produce *N*-methyl-1-phenylethylamine **7b** by *Ryt*RedAm (black), and the enantiomers of **7b** (pink) on Hydrodex β-TBDM.

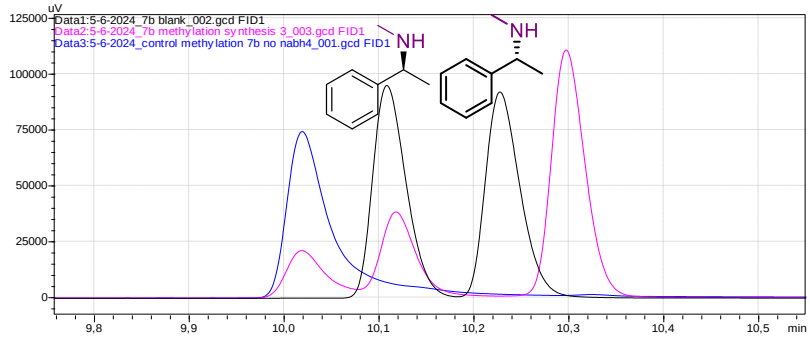

Figure S31. GC Chromatogram of racemic standard of N-methyl-1-phenylethylamine (black), *(S)*-N-methyl-1-phenylethylamine after methylation of *(S)*-α-methylbenzylamine (pink), and control reaction without $NaBH_4$. Expected imine at 10.0 min, expected dimethylated product at 10.3 min; on Hydrodex β-TBDM.

Amine products from ethyl levulinate 10

1-cyclopropyl-5-methyl-2-pyrrolidinone **10c**

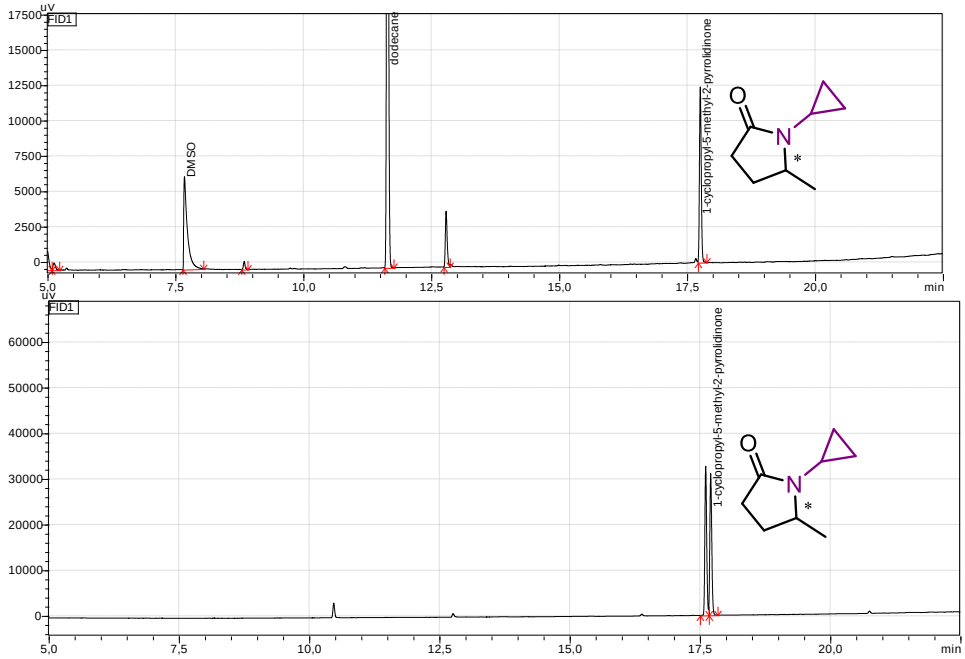

Figure S32. GC chromatogram of *Ryt*RedAm reaction product 1-cyclopropyl-5-methyl-2-pyrrolidinone **10c** (top), unknown side-product formed at 12.8 min; bottom: synthesized amine product 1-cyclopropyl-5-methyl-2-pyrrolidinone **10c;** on Hydrodex β-TBDM.

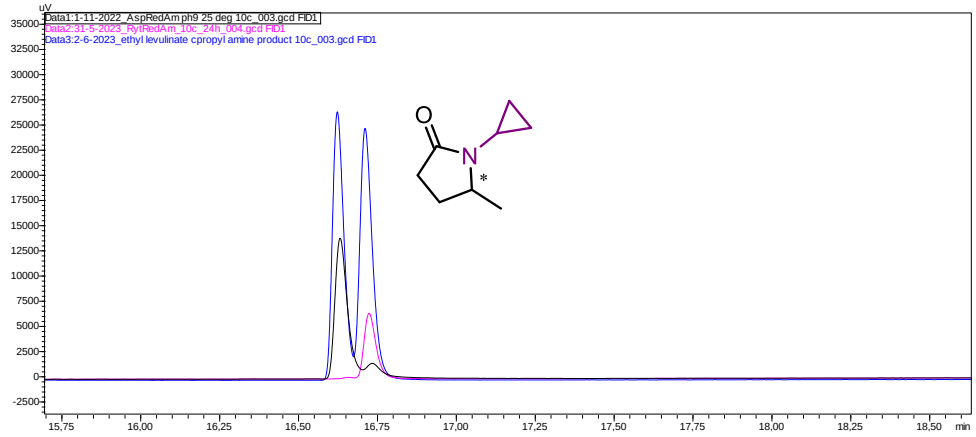

Figure S33. Chiral GC chromatograms of the reaction mixture to produce 1-cyclopropyl-5-methyl-2-pyrrolidinone **10c** with *Asp*RedAm (black), *Ryt*RedAm (pink), and the synthesized racemic product (blue); on Hydrodex β-TBDM.

Imine reduction by RytRedAm

2-methyl-1-pyrroline reduction by *Ryt*RedAm.

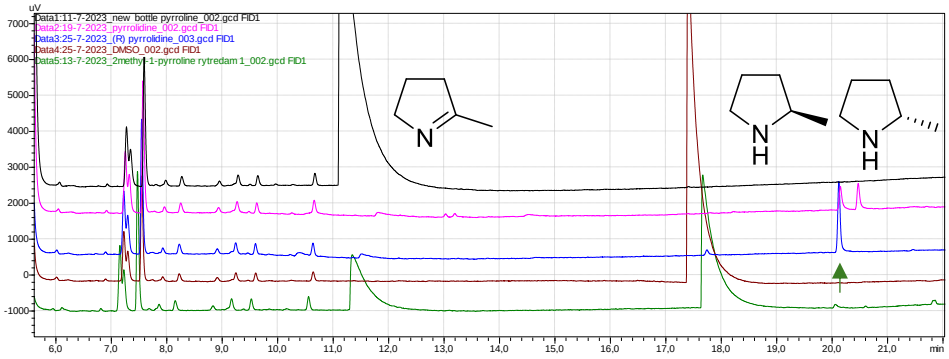

Figure S39. GC chromatograms of 2-methyl-1-pyrroline (black), 2-methylpyrrolidine (pink), (*R*)-2-methylpyrrolidine (blue), DMSO (brown) and a reaction mixture with the *Ryt*RedAm (green); on Hydrodex β-TBDM method C2.

GC-MS column and chromatograms

When the expected amine product was not commercially or synthetically available, extracted reaction samples were injected and analyzed on a GC-MS-QP2010 SE from Shimadzu.

Column D: CP-Sil-5 VF-1ms, 25 m × 0.25 mm × 0.4 µm, split ratio 50, injection temperature 340 °C, helium as carrier gas.

Table S5. GC-MS method and retention times of products which were commercially unavailable.

		GC oven program				
GC column	Method	rate (°C/min), temp. (°C), hold (min)			Compound	Ret. time (min)
D CP-Sil-5 VF-1ms	D1	-	80	3	*N*-methylhexylamine 3b	3.4
					N-allylhexan-1-amine 3e	5.5
		5	100	4	*N*-methylbenzylamine 11b	5.9
					N-hexylcyclopropanamine 3c	6.0
		25	345	1	*N*-benzylpropargylamine 11d	8.9
					dodecane	9.0
					N-benzylcyclopropanamine 11c	9.5

N-methylhexylamine 3b

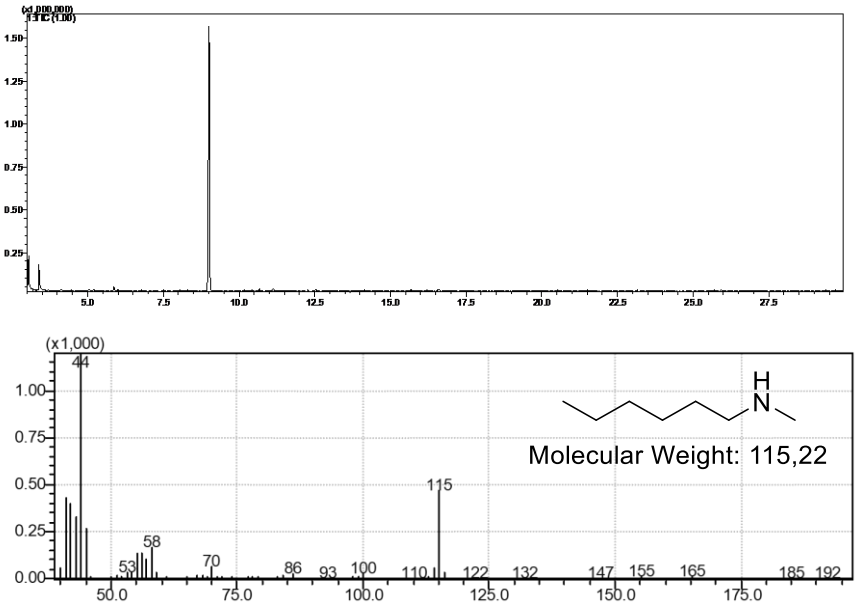

Figure S40. GC-MS chromatogram (top) and mass spectrum (bottom) of N-methylhexylamine 3b (3.4 min) on CP-Sil-5 VF-1ms method D1.

N-hexylcyclopropanamine 3c

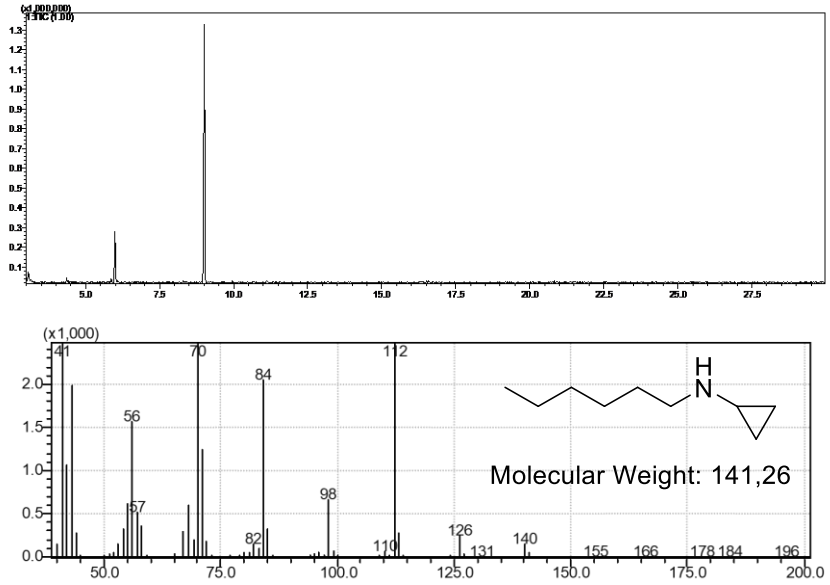

Figure S41. GC-MS chromatogram (top) and mass spectrum (bottom) of *N*-hexylcyclopropanamine **3c** (6.0 min) on CP-Sil-5 VF-1ms method D1.

N-allylhexan-1-amine 3e

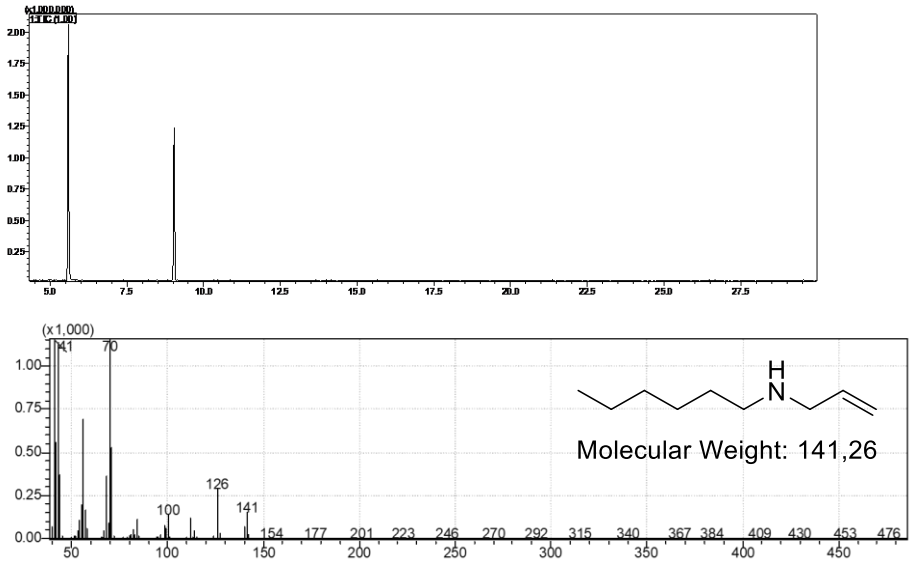

Figure S42. GC-MS chromatogram (top) and mass spectrum (bottom) of *N*-allylhexan-1-amine **3e** (5.5 min) on CP-Sil-5 VF-1ms method D1.

N-methylbenzylamine 11b

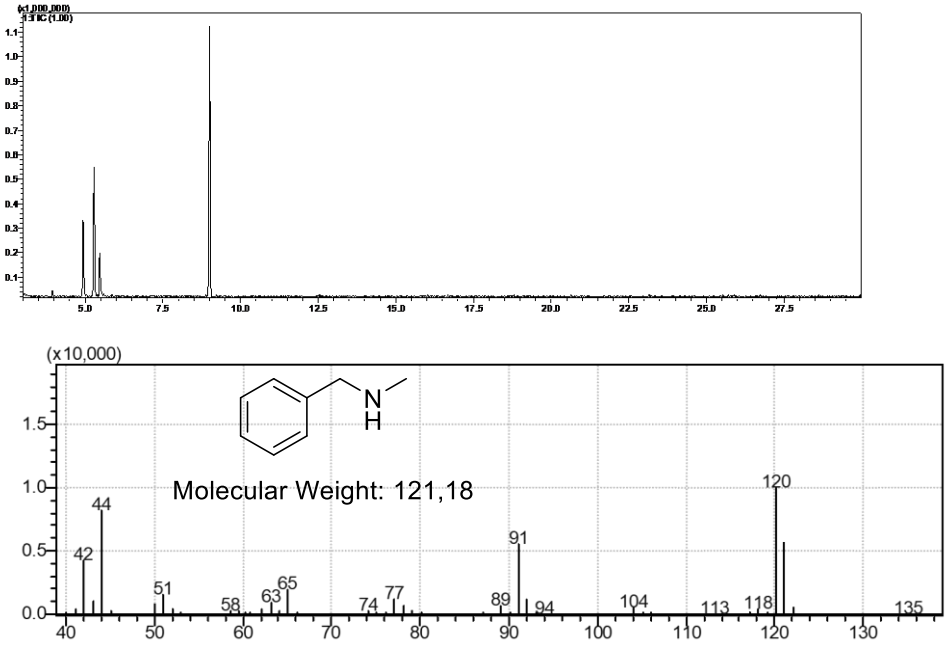

Figure S43. GC-MS chromatogram (top) and mass spectrum (bottom) of *N*-methylbenzylamine **11b** (6.0 min) on CP-Sil-5 VF-1ms method D1. Corresponding alcohol present at 4.9 min, corresponding imine present at 5.3 min.

N-benzylcyclopropanamine 11c

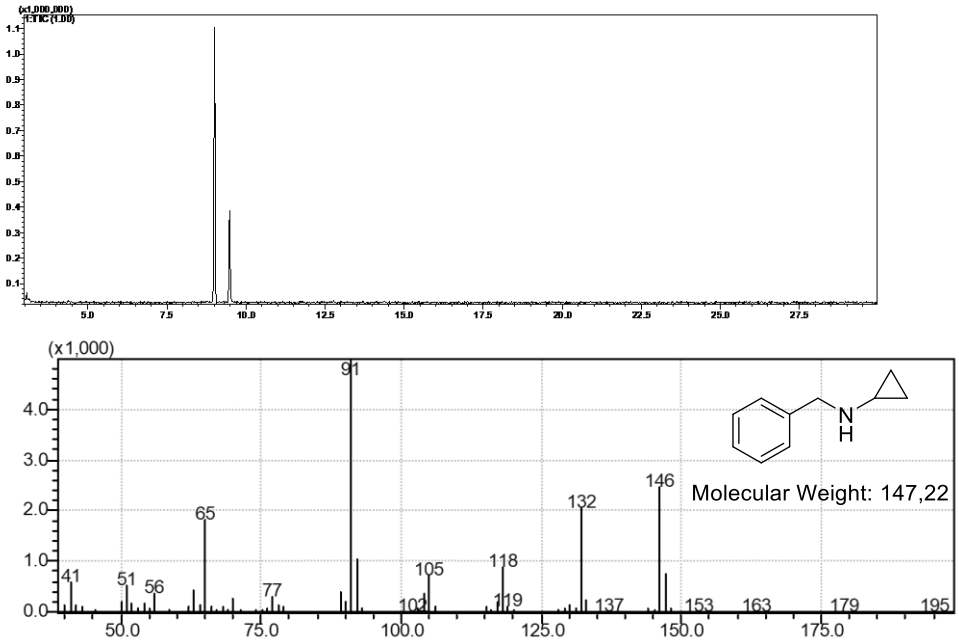

Figure S44. GC-MS chromatogram (top) and mass spectrum (bottom) of *N*-benzylcyclopropanamine **11c** (9.5 min) on CP-Sil-5 VF-1ms method D1.

N-benzylpropargylamine 11d

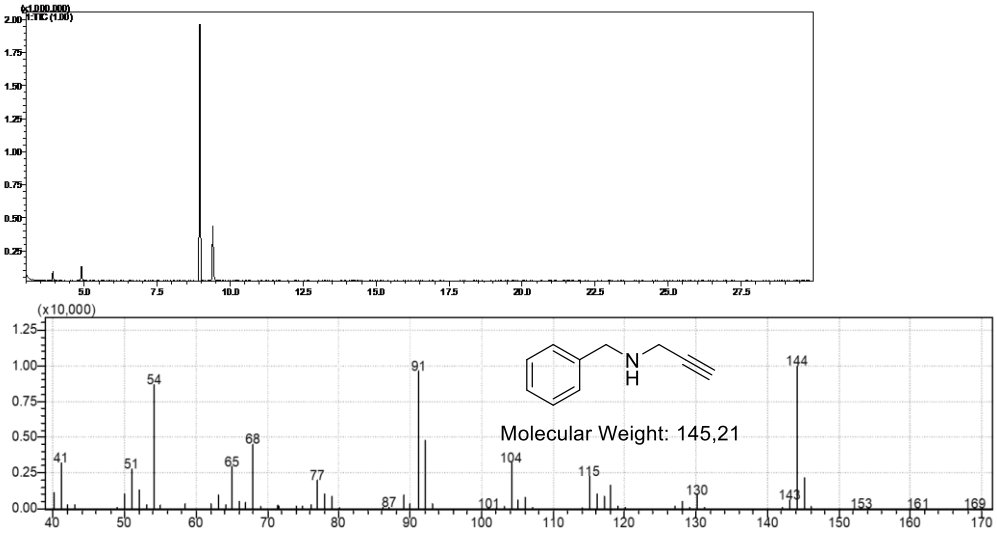

Figure S45. GC-MS chromatogram (top) and mass spectrum (bottom) of *N*-benzylpropargylamine **11d** (8.9 min) on CP-Sil-5 VF-1ms method D1.

RytRedAm scale-up reactions

Biotransformation to N-allylhexan-1-amine 3e

In a 50 mL falcon tube were added 100 mM KP_i buffer pH 7.0, 50 mM hexanal, 200 mM allylamine, 150 mM Glc, 0.2 mM NADP, 12 U/mL *Bs*GDH, and 1.0 mg/mL *Ryt*RedAm in a total volume of 14 mL. The reaction mixture was shaken at 350 rpm at 20 °C for 24 h. The workup was done as described by Mayol *et al.*,[55] After 24 h, the mixture was basified with 10 M NaOH until pH was 12.0. Then, the product was extracted with 3 × 20 mL Et_2O. A solution of 2 M HCl in Et_2O was added (2 mmol) to the combined organic layers. Then, 10 mL of distilled water was added and the corresponding amine hydrochloride salt was extracted with 2 × 20 mL water. The combined aqueous phase was washed with 3 × 10 mL Et_2O. The aqueous phase was lyophilized to obtain *N*-allylhexan-1-amine hydrochloride salt **3e** (65 mg, 52% yield) as pale-yellow crystals.

^{1}H NMR 400 MHz, $CDCl_3$) 9.58 (br s, 2H), 6.14-6.03 (m, 1H), 5.46 (m, 2H), 3.59 (m, 2H), 2.88 (m, 2H), 1.89-1.81 (m, 2H), 1.38-1.29 (m, 6H), 0.87 (t, *J* = 6.7 Hz, 3H); **^{13}C NMR** (100 MHz, $CDCl_3$) 127.8, 123.9, 49.4, 46.4, 31.1, 26.4, 25.8, 22.4, 13.9.

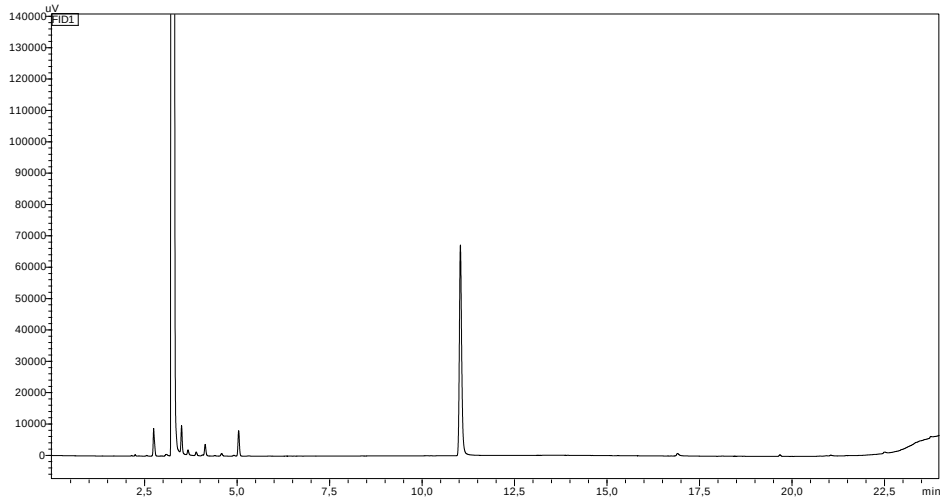

Figure S46. GC chromatogram of isolated *Ryt*RedAm reaction product *N*-allylhexan-1-amine **3e**. Product was solubilized in water before extraction in EtOAc and analysis by GC-FID.

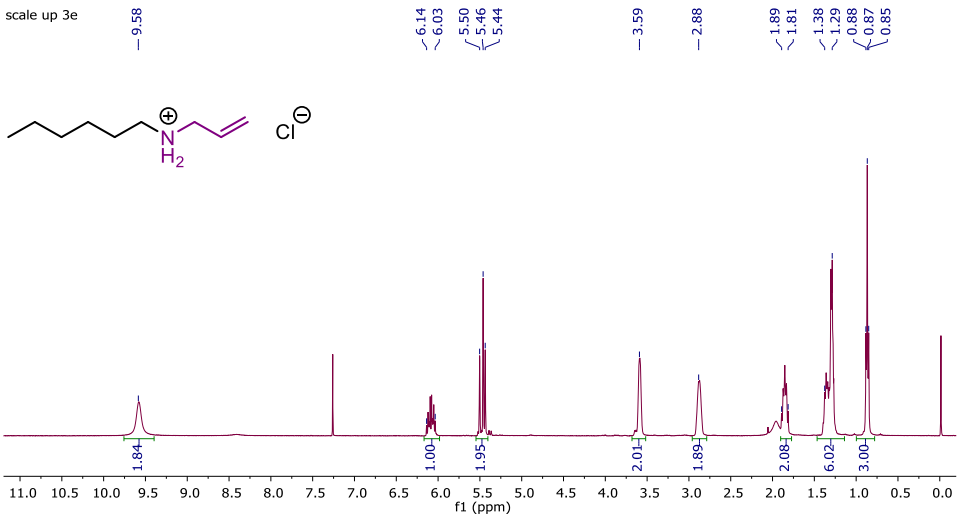

Figure S47. ^{1}H NMR spectrum in $CDCl_3$ of isolated *Ryt*RedAm reaction product *N*-allylhexan-1-amine hydrochloride salt **3e**-HCl.

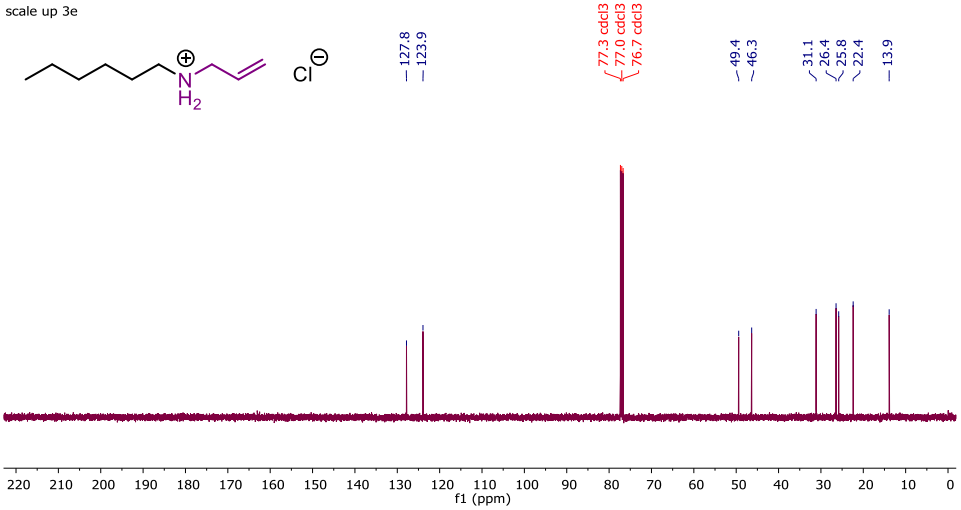

Figure S48. ^{13}C NMR spectrum in $CDCl_3$ of isolated *Ryt*RedAm reaction product *N*-allylhexan-1-amine hydrochloride salt **3e**-HCl.

Biotransformation to 1-cyclopropyl-5-methyl-2-pyrrolidinone 10c

In a 50 mL falcon tube were added 100 mM KP_i buffer pH 7.0, 50 mM ethyl levulinate, 250 mM cyclopropylamine, 150 mM Glc, 0.2 mM NADP, 12 U/mL *Bs*GDH, and 1.0 mg/mL *Ryt*RedAm in a total volume of 14 mL. The reaction mixture was shaken at 350 rpm at 20 °C for 24 h. The workup was done as described by Aleku *et al*.[53] After 24 h, the mixture was basified with 10 M NaOH until pH was 12.0. The product was extracted with 3 × 20 mL dichloromethane (CH_2Cl_2). The organic layers were pooled, and the CH_2Cl_2 was removed under

reduced pressure until a small volume remained. The remaining oil was subjected to column chromatography (silica, 100% EtOAc, R_f = 0.20) to afford the corresponding product as a colorless oil (11 mg, 95.3% *ee,* 11% isolated yield).

^{1}H NMR δ (400 MHz, $CDCl_3$) 3.60-3.52 (m, 1H), 2.43-2.35 (m, 2H), 2.31-2.23 (m, 1H), 2.14-2.05 (m, 1H), 1.61-1.53 (m, 1H), 1.26 (d, *J* = 6.3 Hz, 3H), 0.97-0.90 (m, 1H), 0.83-0.76 (m, 1H), 0.71-0.62 (m, 1H), 0.55-0.48 (m, 1H). **^{13}C NMR** δ (100 MHz $CDCl_3$) 175.8 (C=O), 55.0 (CH), 30.7 (CH_2), 26.3 (CH_2), 23.0 (CH), 20.0 (CH_3), 7.4 (CH_2), 4.1 (CH_2).

The isolated 1-cyclopropyl-5-methyl-2-pyrrolidinone (**10c**) was dissolved in $CHCl_3$ to a concentration of 10 mg/mL. Specific rotation was determined using a Perkin Elmer Model 343 S Polarimeter at 20 °C, at a wavelength of 589 nm, $[\alpha]_D^{20}$= –69° (*c* = 1.0, $CHCl_3$).

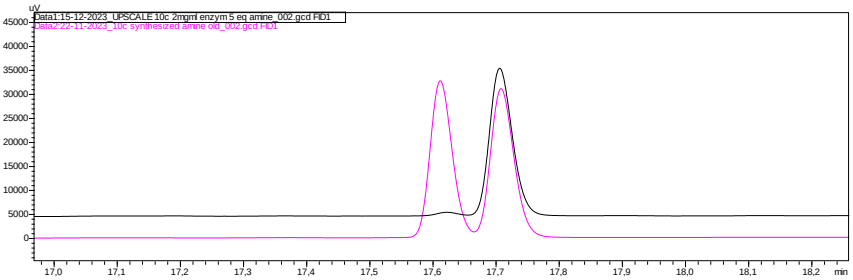

Figure S49. GC chromatograms of reaction product 1-cyclopropyl-5-methyl-2-pyrrolidinone **10c** obtained with *Ryt*RedAm (black) and by chemical synthesis (pink); on Hydrodex β-TBDM.

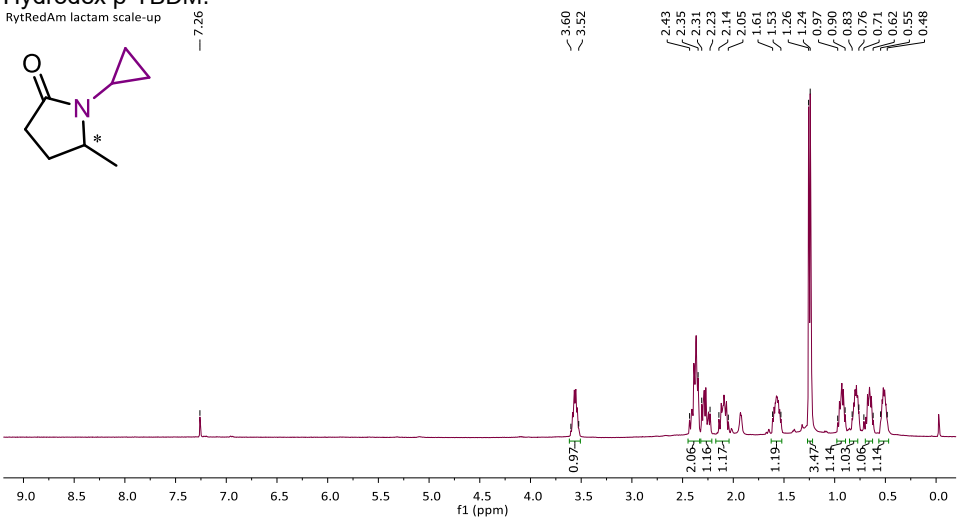

Figure S50. ^{1}H NMR spectrum in $CDCl_3$ of isolated *Ryt*RedAm reaction product 1-cyclopropyl-5-methyl-2-pyrrolidinone **10c**.

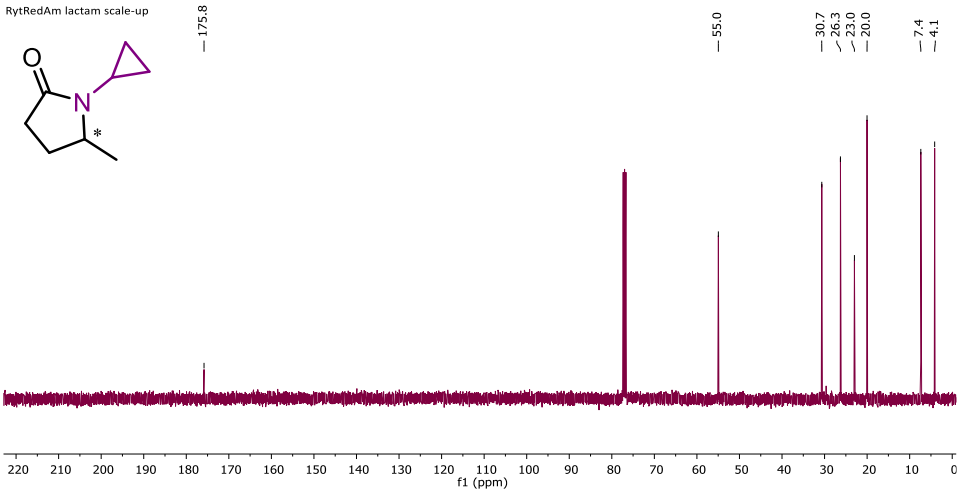

Figure S51. ^{13}C NMR spectrum in $CDCl_3$ of isolated *Ryt*RedAm reaction product 1-cyclopropyl-5-methyl-2-pyrrolidinone **10c**.

References

[1] D. Ghislieri, N. J. Turner, *Top. Catal.* **2014**, *57*, 284-300.
[2] N. A. McGrath, M. Brichacek, J. T. Njardarson, *J. Chem. Educ.* **2010**, *87*, 1348-1349.
[3] A. Cabré, X. Verdaguer, A. Riera, *Chem. Rev.* **2022**, *122*, 269-339.
[4] A. J. Burke, *Expert Opin. Drug Discov.* **2023**, *18*, 37-46.
[5] D. Koszelewski, I. Lavandera, D. Clay, D. Rozzell, W. Kroutil, *Adv. Synth. Catal.* **2008**, *350*, 2761-2766.
[6] M. Hohn, U. T. Bornscheuer, *ChemCatChem* **2009**, *1*, 42-51.
[7] C. E. Paul, M. Rodríguez-Mata, E. Busto, I. Lavandera, V. Gotor-Fernández, V. Gotor, S. García-Cerrada, J. Mendiola, O. de Frutos, I. Collado, *Org. Process Res. Dev.* **2014**, *18*, 788-792.
[8] M. D. Patil, G. Grogan, A. Bommarius, H. Yun, *ACS Catal.* **2018**, *8*, 10985-11015.
[9] S. P. France, R. D. Lewis, C. A. Martinez, *JACS Au* **2023**, *3*, 715-735.
[10] L. Ducrot, M. Bennett, G. Grogan, C. Vergne-Vaxelaire, *Adv. Synth. Catal.* **2021**, *363*, 328-351.
[11] S. K. Wu, R. Snajdrova, J. C. Moore, K. Baldenius, U. T. Bornscheuer, *Angew. Chem. Int. Ed.* **2021**, *60*, 88-119.
[12] S. Roth, R. Niese, M. Müller, M. Hall, *Angew. Chem. Int. Ed.* **2024**, *63*, e202314740.
[13] G. Grogan, *Curr. Opin. Chem. Biol.* **2018**, *43*, 15-22.
[14] D. Wetzl, M. Berrera, N. Sandon, D. Fishlock, M. Ebeling, M. Muller, S. Hanlon, B. Wirz, H. Iding, *ChemBioChem* **2015**, *16*, 1749-1756.
[15] D. Wetzl, M. Gand, A. Ross, H. Müller, P. Matzel, S. P. Hanlon, M. Müller, B. Wirz, M. Höhne, H. Iding, *ChemCatChem* **2016**, *8*, 2023-2026.
[16] A. K. Gilio, T. W. Thorpe, A. Heyam, M. R. Petchey, B. Pogranyi, S. P. France, R. M. Howard, M. J. Karmilowicz, R. Lewis, N. Turner, G. Grogan, *ACS Catal.* **2023**, *13*, 1669-1677.
[17] J. Mangas-Sánchez, S. P. France, S. L. Montgomery, G. A. Aleku, H. Man, M. Sharma, J. I. Ramsden, G. Grogan, N. J. Turner, *Curr. Opin. Chem. Biol.* **2017**, *37*, 19-25.
[18] B. Yuan, D. M. Yang, G. Qu, N. J. Turner, Z. T. Sun, *Chem. Soc. Rev.* **2024**, *53*, 227-262.
[19] A. K. Gilio, T. W. Thorpe, N. Turner, G. Grogan, *Chem Sci* **2022**, *13*, 4697-4713.
[20] T. Knaus, W. Bohmer, F. G. Mutti, *Green Chem.* **2017**, *19*, 453-463.
[21] S. Fademrecht, P. N. Scheller, B. M. Nestl, B. Hauer, J. Pleiss, *Proteins* **2016**, *84*, 600-610.
[22] M. Sharma, J. Mangas-Sánchez, S. P. France, G. A. Aleku, S. L. Montgomery, J. I. Ramsden, N. J. Turner, G. Grogan, *ACS Catal.* **2018**, *8*, 11534-11541.
[23] K. Mitsukura, M. Suzuki, S. Shinoda, T. Kuramoto, T. Yoshida, T. Nagasawa, *Biosci. Biotechnol. Biochem.* **2011**, *75*, 1778-1782.
[24] P. N. Scheller, M. Lenz, S. C. Hammer, B. Hauer, B. M. Nestl, *ChemCatChem* **2015**, *7*, 3239-3242.
[25] V. Saggiomo, U. Lüning, *Tetrahedron Lett.* **2009**, *50*, 4663-4665.
[26] G. A. Aleku, S. P. France, H. Man, J. Mangas-Sánchez, S. L. Montgomery, M. Sharma, F. Leipold, S. Hussain, G. Grogan, N. J. Turner, *Nat. Chem.* **2017**, *9*, 961-969.
[27] G. D. Roiban, M. Kern, Z. Liu, J. Hyslop, P. L. Tey, M. S. Levine, L. S. Jordan, K. K. Brown, T. Hadi, L. A. F. Ihnken, M. J. B. Brown, *ChemCatChem* **2017**, *9*, 4475-4479.
[28] H. Busch, F. Tonin, N. Alvarenga, M. van den Broek, S. Lu, J. M. Daran, U. Hanefeld, P.-L. Hagedoorn, *Appl. Microbiol. Biotechnol.* **2020**, *104*, 5801-5812.

[29] P. R. Beynon, J. Easterby, *Buffer solutions*, 1st ed., Taylor & Francis, London, **1996**.
[30] D. Ribeaucourt, G. T. Höfler, M. Yemloul, B. Bissaro, F. Lambert, J.-G. Berrin, M. Lafond, C. E. Paul, *ACS Catal.* **2022**, *12*, 1111-1116.
[31] J. Hon, S. Borko, J. Stourac, Z. Prokop, J. Zendulka, D. Bednar, T. Martinek, J. Damborsky, *Nucleic Acids Res.* **2020**, *48*, W104-W109.
[32] S. F. Altschul, W. Gish, W. Miller, E. W. Myers, D. J. Lipman, *J. Mol. Biol.* **1990**, *215*, 403-410.
[33] R. C. Edgar, *Nucleic Acids Res.* **2004**, *32*, 1792-1797.
[34] J. Hon, M. Marusiak, T. Martinek, A. Kunka, J. Zendulka, D. Bednar, J. Damborsky, *Bioinformatics* **2021**, *37*, 23-28.
[35] S. Velikogne, V. Resch, C. Dertnig, J. H. Schrittwieser, W. Kroutil, *ChemCatChem* **2018**, *10*, 3236-3246.
[36] A. R. Casamajo, Y. Q. Yu, C. Schnepel, C. Morrill, R. Barker, C. W. Levy, J. Finnigan, V. Spelling, K. Westerlund, M. Petchey, R. J. Sheppard, R. J. Lewis, F. Falcioni, M. A. Hayes, N. J. Turner, *J. Am. Chem. Soc.* **2023**, *145*, 22041-22046.
[37] M. Gand, C. Thole, H. Muller, H. Brundiek, G. Bashiri, M. Hohne, *J. Biotechnol.* **2016**, *230*, 11-18.
[38] N. Borlinghaus, B. M. Nestl, *ChemCatChem* **2018**, *10*, 183-187.
[39] E. Vazquez-Figueroa, J. Chaparro-Riggers, A. S. Bommarius, *ChemBioChem* **2007**, *8*, 2295-2301.
[40] M. Cárdenas-Fernandez, R. Roddan, E. M. Carter, H. C. Hailes, J. M. Ward, *ChemCatChem* **2023**, *15*, e202201126.
[41] L. Holm, A. Laiho, P. Törönen, M. Salgado, *Protein Sci.* **2023**, *32*, e4519.
[42] J. Zhang, X. Li, R. Chen, X. Tan, X. Liu, Y. Ma, F. Zhu, C. An, G. Wei, Y. Yao, L. Yang, P. Zhang, Q. Wu, Z. Sun, B. G. Wang, S. S. Gao, C. Cui, *Commun. Chem.* **2022**, *5*, 123.
[43] T. Meyer, N. Zumbragel, C. Geerds, H. Groger, H. H. Niemann, *Biomolecules* **2020**, *10*, 1130.
[44] P. Stockinger, N. Borlinghaus, M. Sharma, B. Aberle, G. Grogan, J. Pleiss, B. M. Nestl, *ChemCatChem* **2021**, *13*, 5210-5215.
[45] K. E. Atkin, R. Reiss, N. J. Turner, A. M. Brzozowski, G. Grogan, *Acta Crystallogr. Sect. F Struct. Biol. Cryst. Commun.* **2008**, *64*, 182-185.
[46] W. Kabsch, *Acta Crystallogr. D. Biol. Crystallogr.* **2010**, *66*, 125-132.
[47] P. Evans, *Acta Crystallogr. D Biol. Crystallogr.* **2006**, *62*, 72-82.
[48] G. Winter, *J. Appl. Crystallogr.* **2010**, *43*, 186-190.
[49] A. Vagin, A. Teplyakov, *J. Appl. Crystallogr.* **1997**, *30*, 1022-1025.
[50] J. Jumper, R. Evans, A. Pritzel, T. Green, M. Figurnov, O. Ronneberger, K. Tunyasuvunakool, R. Bates, A. Žídek, A. Potapenko, A. Bridgland, C. Meyer, S. A. A. Kohl, A. J. Ballard, A. Cowie, B. Romera-Paredes, S. Nikolov, R. Jain, J. Adler, T. Back, S. Petersen, D. Reiman, E. Clancy, M. Zielinski, M. Steinegger, M. Pacholska, T. Berghammer, S. Bodenstein, D. Silver, O. Vinyals, A. W. Senior, K. Kavukcuoglu, P. Kohli, D. Hassabis, *Nature* **2021**, *596*, 583-589.
[51] P. Emsley, K. Cowtan, *Acta Crystallogr. D. Biol. Crystallogr.* **2004**, *60*, 2126-2132.
[52] G. N. Murshudov, A. A. Vagin, E. J. Dodson, *Acta Crystallogr. D. Biol. Crystallogr.* **1997**, *53*, 240-255.
[53] G. A. Aleku, S. P. France, H. Man, J. Mangas-Sánchez, S. L. Montgomery, M. Sharma, F. Leipold, S. Hussain, G. Grogan, N. J. Turner, *Nat. Catal.* **2017**, *9*, 961-969.
[54] J. Ziegenhorn, M. Senn, T. Bucher, *Clin. Chem.* **1976**, *22*, 151-160.
[55] O. Mayol, K. Bastard, L. Beloti, A. Frese, J. P. Turkenburg, J.-L. Petit, A. Mariage, A. Debard, V. Pellouin, A. Perret, V. de Berardinis, A. Zaparucha, G. Grogan, C. Vergne-Vaxelaire, *Nat. Catal.* **2019**, *2*, 324-333.

Chapter 6: Discovery and synthetic applications of thermostable NAD(P)H-dependent reductive aminases

Ewald P.J. Jongkind,[1] Mees de Jong,[1] Giang-Son Nguyen,[2] Caroline E. Paul[1,*]

[1] Department of Biotechnology, Delft University of Technology, van der Maasweg 9, 2629 HZ Delft, The Netherlands
[2] Department of Biotechnology and Nanomedicine, SINTEF Industry, P.O. Box 4760 Torgard, N-7465 Trondheim, Norway

Manuscript in preparation

Summary

Chiral amines are valuable building blocks that are accessible via reductive amination. Their formation can be catalyzed by reductive aminases (RedAms), a subfamily of imine reductases (IREDs), showing great potential using a 1:1 ratio of carbonyl: amine at pH 7. However, most characterized RedAms display poor thermostability, making industrial applications challenging. In this work, we discovered and characterized three thermostable RedAms from *Streptosporangium roseum* (*Stro*RedAm), *Pseudonocardia aurantiaca* (*Pau*RedAm) and *Streptomyces griseus* (*Strep*RedAm). We observed a K_M in the micromolar range for NADPH and in the millimolar range for NADH. All three RedAms retained most of their activity after 24 h incubation in 30 °C, and *Stro*RedAm retained 83% of its relative activity after 48 h at 40 °C. Besides a broad substrate scope of aldehydes, cyclic ketones, enones and amine donors (up to >99% conversion), *Stro*RedAm and *Pau*RedAm were used in multi-enzymatic cascades with different OYEs, yielding chiral amine products with high purity (*ee* and *de* up to 99%). First scale-up reactions show promise to proceed further with assessing these enzymes for applications on a larger scale, eventually contributing to the panel of chiral amines produced by IREDs and RedAms.

Introduction

Chiral amines are highly targeted products because of their use as building blocks in the pharmaceutical industry.[1, 2] Approximately 40% of all FDA approved drugs contain a chiral amine within its structure. The demand for high enantiopurity makes enzymes interesting catalysts for this purpose, because of their high enantioselectivity. In particular, imine reductases (IRED), NADP-dependent oxidoreductases, catalyze the asymmetric reduction of imines to the corresponding amine products.[3, 4] Besides the reduction of cyclic imines,[5] reductive amination of carbonyl substrates has also been achieved with IREDs. Due to the poor stability of imines in solution, a basic pH and a large excess of amine donor are usually used as reaction conditions.[6-8] Recently, Turner and co-workers discovered an enzyme from a subfamily of IREDs, a reductive aminase from *Aspergillus oryzae* (*Asp*RedAm), capable of reductive amination of carbonyl substrates with low mol equivalents of amine donor at neutral pH (**Figure 1**).[9] In the active site of *Asp*RedAm, N93 and D169 are hypothesized to coordinate the amine donor in the active site, whereas Y177 acts as a proton donor. Other amino acids in the active site, M210, W239 and W240, form the hydrophobic pocket for the substrates.[9] Since the discovery of the *Asp*RedAm, many characterization studies were done with RedAms from fungi,[9-11] and bacteria.[12, 13] Both IREDs and RedAms have a Rossmann-fold domain, and contain the NADP cofactor binding motif, showing the preference of NADP over NAD.[14] Furthermore, both enzymes are homodimers, forming two active sites by domain swapping.

Because of the high similarity between IREDs and RedAms, the distinction between the two has been challenging to establish. The active site residues of *Asp*RedAm indicate RedAm activity but are not required to name an enzyme a RedAm instead of an IRED. In previous research, some reductive aminating enzymes were described as IREDs, while others were described as IREDs facilitating reductive amination,[6] IREDs with reductive amination activity,[15] or IREDs that switch into RedAms dependent on the substrate.[16] In other cases, the distinction is made after RedAm activity was observed.[17-19] Another challenge with the use of RedAms and IREDs is their poor stability and low to no tolerance to higher temperatures, apart from a few exceptions.[20-22] Therefore, the discovery of RedAms requires a well-described strategy, and finding thermostable RedAms with this strategy would be beneficial for making pharmaceuticals by biocatalysis.

In Chapter 5, we searched and discovered bacterial RedAms using the public database NCBI. In this work, we further explored the diversity of bacterial RedAms using the database from SINTEF (Trondheim, Norway). We discovered and characterized three thermostable RedAms from the following organisms: *Streptosporangium roseum* (*Stro*RedAm), *Pseudonocardia aurantiaca*

(*Pau*RedAm) and *Streptomyces griseus subsp. griseus* (*Strep*RedAm), and used these in multi-enzymatic cascades and larger scale biotransformations.

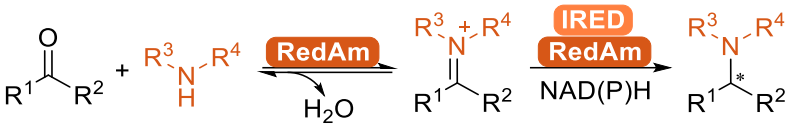

Figure 1. Imine reduction and reductive amination catalysed by RedAms, whereas IREDs only catalyse imine reduction.

Results and Discussion

RedAm discovery

We selected five potential reductive aminases from the database of SINTEF (see SI) coming from the following organisms: *Streptosporangium roseum* (*Stro*RedAm and *Stro*RedAm2), *Pseudonocardia aurantiaca* (*Pau*RedAm and *Pau*RedAm2) and *Streptomyces griseus subsp. griseus* (*Strep*RedAm) (**Table 1**). Mining of the RedAm sequences from SINTEF internal sequence databases were carried out by homology search approaches using the BLAST software (version 2.7.1+) and HMMER suite (version 3.1b2) with a set of reference RedAm sequences. The set includes *Asp*RedAm (accession number Q2TW47) and other characterized sequences reported in literature.[9] The reported catalytic active site residues, N93, D169 and Y177 were required to be present in all hits, whereas we allowed variety in the pocket residues (positions 210, 239 and 240 in *Asp*RedAm). From this search, five of the hits ranked the highest based on similarity were selected. Sequences that were too similar to each other were skipped to increase our chances of finding good hits. Because the hits were found in a genome database, the start of the sequence was rationally determined by finding a methionine followed up with a Rossmann-fold domain (recognized by the GxGxxG motif).

All hits were successfully transformed and expressed in *Escherichia coli* (*E. coli*), although *Pau*RedAm2 precipitated after cell lysis (see SI). After cell lysis, we determined the activity of the cell-free extracts (CFEs) and measured activity in both pH 7 and pH 9 (**Figure 2**). Scheller and co-workers showed how a basic pH increases the pre-formation of the imine in aqueous solution.[7] Whereas IREDs would rely on this imine formation, RedAms catalyze reductive amination, decreasing the reliance on the buffer pH.[9] We determined enzymatic activity of *Stro*RedAm, *Pau*RedAm and *Strep*RedAm using a range of carbonyl substrates and amine donors. The activity at pH 7 was higher for each of these RedAms than at pH 9, suggesting reductive amination activity. *Stro*RedAm2 showed no reductive amination activity for any carbonyl substrate-amine donor combination. Therefore, we discarded *Pau*RedAm2 and *Stro*RedAm2 from future studies.

Table 1. Active site residues of selected RedAms compared to the residues in *Asp*RedAm, including sequence identity, calculated mass and predicted solubility (Sol.) from SoluProt.[23]

RedAm	93	169	177	210	239	240	Seq. id (%)	length (aa)	MW (kDa)	Sol.
*Asp*RedAm	N	D	Y	W	M	Q	100	295	31.9	0.815
*Stro*RedAm	N	D	Y	W	M	Q	43	291	35.2	0.216
*Pau*RedAm	N	D	Y	W	M	Q	40	297	34.3	0.270
*Strep*RedAm	N	D	Y	W	V	N	43	328	30.6	0.189
*Pau*RedAm2	N	D	Y	W	M	Q	54	283	30.4	0.270
*Stro*RedAm2	N	D	Y	W	L	M	37	336	31.8	0.204

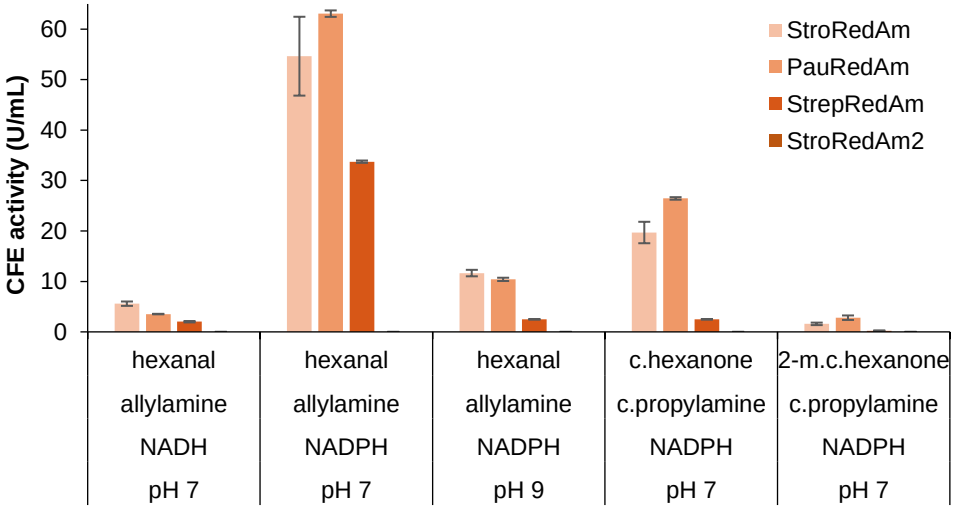

Figure 2. Activity of RedAm CFEs towards hexanal, cyclohexanone (c.hexanone) or 2-methylcyclohexanone (2-m.c.hexanone) and amine donors allylamine or cyclopropylamine (c.propylamine). Conditions: 100 mM KP_i pH 7 or Tris-HCl pH 9, 10 mM carbonyl substrate, 100 mM amine donor, 0.2 mM NAD(P)H, CFE in a total volume of 2 mL, 30 °C. Average of duplicates.

pH and temperature preferences

After reductive amination activity was detected with CFE, *Stro*RedAm, *Pau*RedAm and *Strep*RedAm were purified by affinity chromatography (see SI) and their specific activity was determined towards hexanal and allylamine (**Figure 3A**). All three RedAms showed higher reductive amination activity at pH 7 than at pH 9. The ratio of the activity pH 9 compared to pH 7 for *Stro*RedAm, *Pau*RedAm and *Strep*RedAm were 0.40, 0.23 and 0.49, respectively, whereas *Asp*RedAm is slightly more active at pH 9 (activity ratio of 1.3), probably due to promiscuous IRED activity. Therefore, these RedAms display true reductive aminase activity, and could be classified as RedAms based on this assay. *Pau*RedAm displayed the highest specific activity (5.1 U/mg), followed by *Stro*RedAm (2.9 U/mg) and *Strep*RedAm (1.1 U/mg). When determining the pH profile of *Stro*RedAm,

*Pau*RedAm and *Strep*RedAm, all RedAms displayed higher activity in KP_i over Tris-HCl buffer, with a maximum at 7.5 or 8.0 (see SI). To ensure a reductive aminase activity from our RedAms in the substrate screening, we proceeded with KP_i buffer at pH 7. Interestingly, the three RedAms preferred NADPH over NADH, yet still displayed a measurable activity with NADH (up to 0.38 U/mg for *Stro*RedAm).

IREDs and RedAms tend to precipitate at higher temperatures due to their poor stability, apart from a few exceptions.[20] We measured the activity of the RedAms at higher temperatures (**Figure 3B**), and evaluated their thermostability by incubating the enzymes at 30 and 40 °C (**Figure 3C-D**). The specific activity increased for all RedAms with a reaction temperature up to 60 °C. Whereas the activity decreased significantly for *Pau*RedAm and *Strep*RedAm at temperatures over 60 °C, *Stro*RedAm showed higher activities at 70 and 80 °C. Remarkably, *Stro*RedAm showed the most thermostability, but all three enzymes displayed a good tolerance towards higher temperatures. After incubation at 30 °C, *Pau*RedAm displayed the largest loss in activity after 48 h (51% residual activity), whereas *Stro*RedAm and *Strep*RedAm retained 87 and 83% of their activity, respectively (**Figure 3C**). Upon increasing the incubation temperature to 40 °C, both *Pau*RedAm and *Strep*RedAm showed a drastic decrease after 24 h (13% and 12% residual activity), whereas *Stro*RedAm, impressively retained 83% activity after 48 h (**Figure 3D**), making this enzyme the most thermostable RedAm from our studies.

Cofactor specificity

The kinetic properties for the RedAms were determined with both NADPH and NADH cofactors (**Table 2**, see SI), although the activity was too low to determine the k_{cat} and K_M with NADH for *Strep*RedAm. The K_M of all three enzymes was very low, (<10 μM NADPH), similar to our previously characterized *Ryt*RedAm, and thus showing better affinity compared to that of *Asp*RedAm (0.12 mM).[9] With respect to IREDs, Nestl and co-workers engineered the cofactor specificity from NADPH to NADH, producing a variant V10 with a K_M of 11 mM and a k_{cat} of 1.5 s^{-1}, which is the only other example currently known.

When comparing the k_{cat} values of the RedAms with NADPH and NADH, we observed a decrease of 1.9- and 13-fold for *Stro*RedAm and *Pau*RedAm, respectively. The k_{cat} is lower for *Stro*RedAm and *Pau*RedAm than for V10 in the mentioned work, yet the catalytic efficiency of the engineered V10 is lower than that of our RedAms.[24] Overall, the k_{cat}/K_M with NADH is 34 and 33 $mM^{-1}min^{-1}$ for *Stro*RedAm and *Pau*RedAm, respectively. Due to the higher activities with NADPH, we proceeded to further screening of substrates with this cofactor, however the acceptance of NADH could be further exploited for its lower cost.

It is relevant to note here that the synthetic cofactor 1-benzyl-1,4-dihydronicotinamide (BNAH) is not accepted by these Rossmann-fold containing enzymes (data not shown), and care must be taken to ensure purified enzymes do not contain trace amounts of NAD(P) before making such a claim.[25, 26] Extensive protein engineering would be needed to reach such activities.

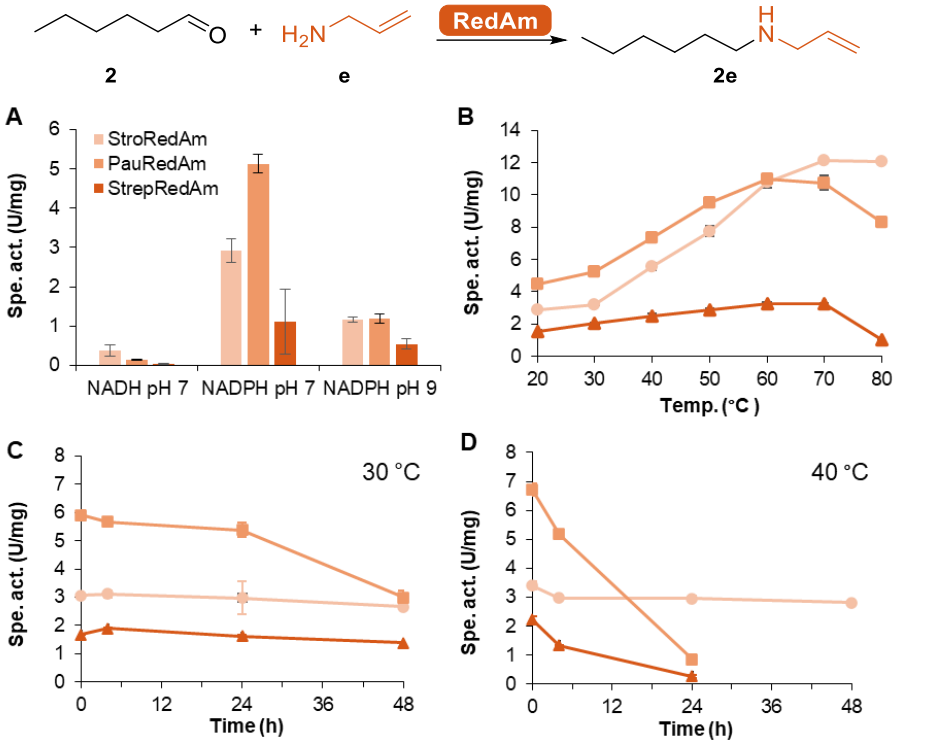

Figure 3. Effect of cofactor, pH and temperature on RedAm activity. **A and B)** Conditions: 100 mM KP_i pH 7 or Tris-HCl pH 9, 10 mM hexanal, 100 mM allylamine, 0.2 mM NAD(P)H, purified RedAm, 2 mL volume, **A)** measured at 30 °C, **B)** measured at 20-80 °C with 0.2 mM NADPH; **C** and **D)** Conditions: 100 mM KP_i pH 7, 10 mM hexanal, 100 mM allylamine, 0.2 mM NADPH, RedAm, 2 mL volume **C)** incubation of 0.5 mg/mL enzyme in 100 mM KP_i pH 7 at 30 °C, **D)** at 40 °C. Average of duplicates.

Table 2. Observed estimated kinetic data of *Stro*RedAm, *Pau*RedAm and *Strep*RedAm with NADPH and NADH.[a]

	NADPH			**NADH**	
Enzyme	***Stro*RedAm**	***Pau*RedAm**	***Strep*RedAm**	***Stro*RedAm**	***Pau*RedAm**
K_M (μM)	6.7	9.4	6.1	1600	550
k_{cat} (s^{-1})	1.7	4.0	0.7	0.9	0.3
k_{cat}/K_M ($mM^{-1}\,s^{-1}$)	254	425	115	0.56	0.55
k_{cat}/K_M ($mM^{-1}\,min^{-1}$)	15200	25500	6890	34	33

[a] Conditions: 100 mM KP_i pH 7, 10 mM hexanal, 100 mM allylamine, NAD(P)H, RedAm, 30 °C (see SI). Kinetic data of *Strep*RedAm with NADH was not determined.

Substrate scope

We proceeded to screen a range of carbonyl substrates and amine donors (**Figure 4**). We used 1.0 mg/mL of purified *Strep*RedAm because of its lower activity, and 0.5 mg/mL for *Stro*RedAm and *Pau*RedAm. Especially cyclohexanone, hexanal, hydrocinnamaldehyde and benzaldehyde (**1**-**4**) were well-accepted substrates, with up to 98% conversion into the amine product starting from 10 mM carbonyl substrate. Cyclopropylamine **c** and propargylamine **d** were the best accepted amine donors from our scope. Remarkably, we obtained high conversions after only 4 h, whilst most literature reports data with RedAms after 24 h.[9, 13, 20, 27]

The ketone-amine combinations (**5**-**13**) yielding chiral products were screened after 24 h. Unfortunately, we were unable to obtain any reductive amination of several chiral amine products we screened for (see SI). Although ethyl levulinate with cyclopropylamine showed poor conversions, *Pau*RedAm showed moderate conversion of ethyl levulinate with propargylamine with good *ee* (56%, *ee* 89%). According to our chiral GC-analysis, we obtained **5d** in the same configuration of *Asp*RedAm as with *Pau*RedAm. In our screening efforts we observed no differences in enantioselectivity between the three RedAms. Therefore, we assumed the three RedAms in this work are (*R*)-selective, as reported for the *Asp*RedAm.[9] We screened the RedAms for EneIRED activity, another subfamily of enzymes previously discovered by Turner and co-workers.[28, 29] Starting from 2-cyclohexen-1-one **12**, the enzymes produced the corresponding unsaturated amines **12c** and **12d**, and no trace of over reduction to the saturated products (see SI). Only work from the Turner group showed the EneIRED asymmetric reduction of the double bond in addition to reductive amination of saturated aldehydes.[12]

Beyond cyclohexanone, we also screened 2-methyl- and 3-methylcyclohexanone to obtain amines with two chiral centers (**Figure 4**, **Table 3**). Based on synthesized standards of both racemates and (*R*)-**10** and (*R*)-**11** (see SI), the *ee* (selectivity of the amine group) and diastereomeric excess (*de*) were determined. *Pau*RedAm showed full conversion to **10c**-**d** with high enantioselectivity (**Table 3**). *Stro*RedAm showed high conversion with **10d** only, and *Strep*RedAm only showed moderate conversions. Starting from *rac*-2-methylcyclohexanone, *Stro*RedAm and *Pau*RedAm produced **10c**-**d** with high conversions (>99%) and *ee* (>99% for the amine). However, both enzymes showed no selectivity to either the *cis*- or *trans*-product (*de* 4 and 3%). *Strep*RedAm showed a slight preference for the *trans*-product over *cis* (*de* 38%), but the conversion was much lower (30%). With propargylamine **d**, *Stro*RedAm and *Pau*RedAm showed high conversion compared to *Strep*RedAm (>99% versus 11%), while the *de* is much lower for *Stro*RedAm (3%) and *Pau*RedAm

(24%) compared to *Strep*RedAm (>99%). With 3-methylcyclohexanone **11** as a substrate, the enantioselectivity is low amongst all for **11c** (<17%), whilst the highest diastereoselectivity is for *Stro*RedAm (>99%). As for **11d**, *Stro*RedAm showed remarkable conversion and *ee* (>99%), although no stereoselectivity was observed. With *Pau*RedAm higher *ee* and lower *de* was observed.

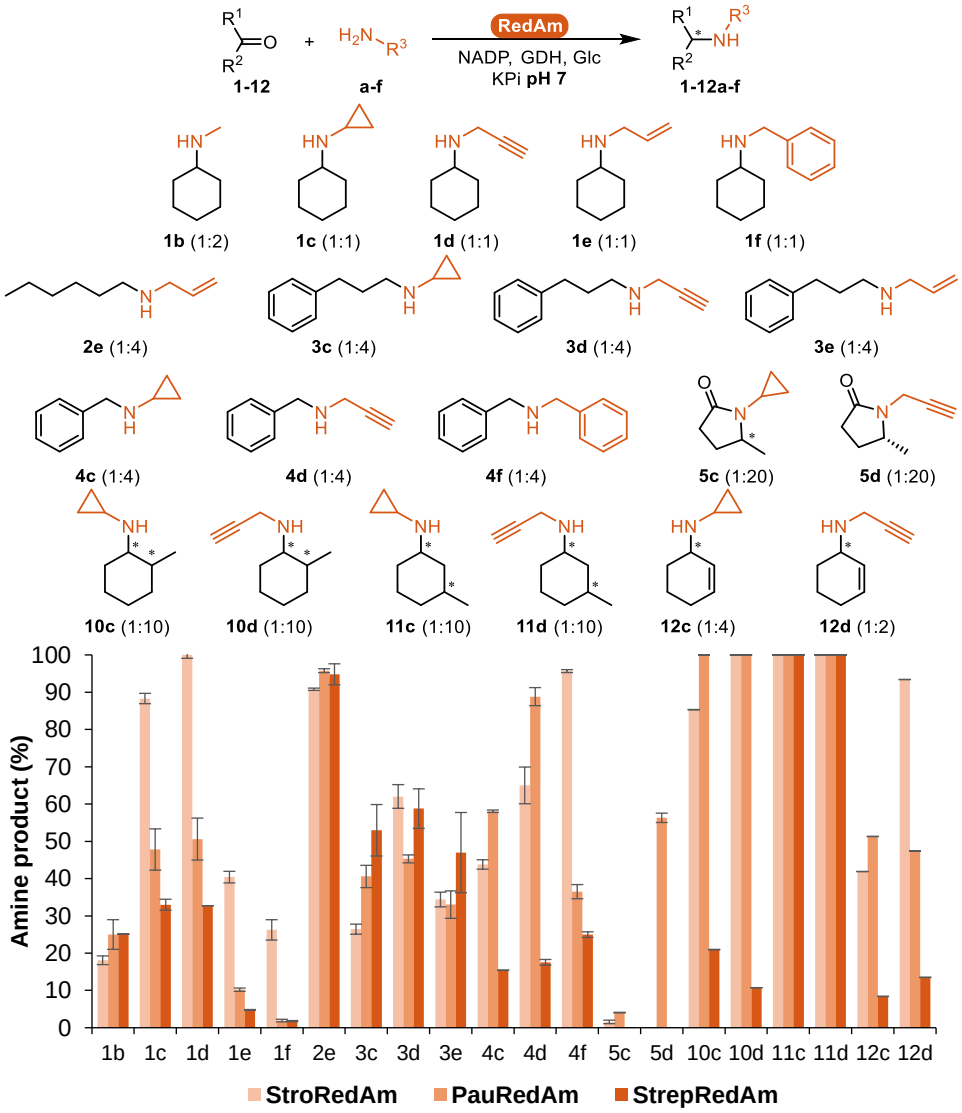

Figure 4. Conversions of carbonyl and amine donor combinations catalyzed by *Stro*RedAm, *Pau*RedAm and *Strep*RedAm. Carbonyl:amine donor ratios shown in brackets. Conditions: 100 mM KP_i buffer pH 7, 30 mM Glc, 10 U/mL *Bs*GDH, 0.2 mM NADP, 10 mM carbonyl, 10-200 mM amine donor, 0.5 mg/mL *Stro*RedAm or *Pau*RedAm or 1 mg/mL *Strep*RedAm, 30 °C, 500 rpm, 500 µL volume. Reaction time: 4 h for **1-3**, 24 h for **4-12**. Average of duplicates.

To overcome the poor stereoselectivities for products **11c** and **11d**, we screened *Stro*RedAm and *Pau*RedAm toward reductive amination of the (*R*)-2-methylcyclohexanone to make (3*R*)-**11c** and (3*R*)-**11d** (**Figure 5**). With both enzymes, full conversion to (3*R*)-**11c** and (3*R*)-**11d** was reached, and with *Stro*RedAm, *de* >99% was reached for (3*R*)-**11d**. *Pau*RedAm showed excellent selectivity for (1*R*,3*R*)-**11d** (**Figure 5**), and less for (1*R*,3*R*)-**11c** (9% *de*, 46:54 *dr* *cis*:*trans*). Based on these results, these RedAms could potentially yield enantio- and diastereomerically pure amines with two chiral centers with chiral substrate precursors.

Table 3. Conversions of substrates **10**-**11** as shown in Figure 4 and the corresponding amine products with two chiral centers, *ee*, *er*, *de* and *dr* determined by chiral GC-FID (see SI).

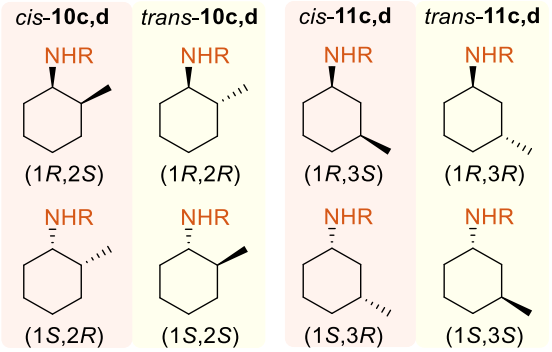

Product	Enzyme	Conv. (%)	*ee* (1*R*) (%)	*er* (1*R*:1*S*)	*de* (%)	*dr* (*cis*:*trans*)
10c	*Stro*RedAm	85	>99	>99:<1	4	48:52
	*Pau*RedAm	>99	>99	>99:<1	5	47:53
	*Strep*RedAm	30	>99	>99:<1	38	31:69
10d	*Stro*RedAm	>99	>99	>99:<1	3	48:52
	*Pau*RedAm	>99	>99	>99:<1	24	38:62
	*Strep*RedAm	11	>99	>99:<1	>99	<1:>99
11c	*Stro*RedAm	>99	2	49:51	>99	<1:>99
	*Pau*RedAm	>99	0	50:50	25	37:63
	*Strep*RedAm	>99	17	58:42	43	29:71
11d	*Stro*RedAm	>99	1	50:50	>99	<1:>99
	*Pau*RedAm	>99	64	18:82	12	44:56
	*Strep*RedAm	>99	n.d.	n.d.	n.d.	n.d.

n.d. not determined due to unclear product separation on GC-FID. *er*: enantiomeric ratio; *dr*: diastereomeric ratio.

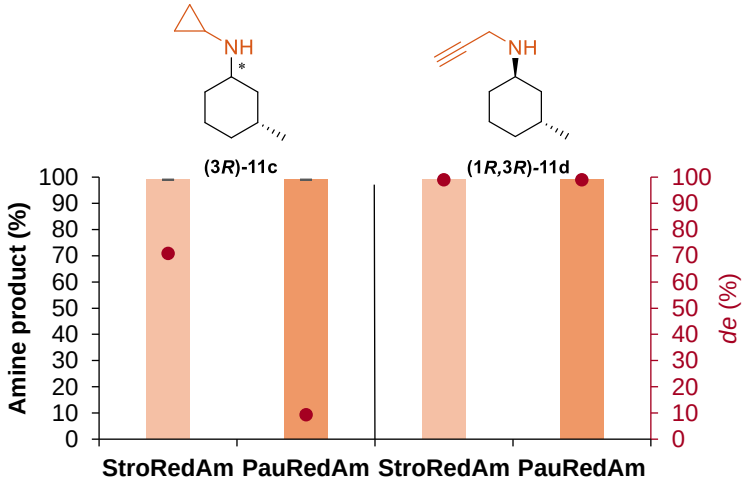

Figure 5. Reductive amination of (3*R*)-methylcyclohexanone **11** with cyclopropylamine or propargylamine to obtain (3*R*)-**11c** and (3*R*)-**11d**. Conditions: 100 mM KP_i pH 7, 30 mM glucose, 10 U/mL *Bs*GDH, 0.2 mM NADP, 10 mM (3*R*)-methylcyclohexanone **11**, 100 mM cyclopropylamine **c** or 20 mM propargylamine **d** and 0.5 mg/mL *Stro*RedAm or *Pau*RedAm at 30 °C and 500 rpm in a total volume of 500 µL. Average of duplicates.

Multi-enzymatic cascades

The conversions with substrates **10** and **11** showed potential for a multi-enzymatic cascade, as is previously described in Chapter 2 and in literature.[30-32] These substrates are formed from the unsaturated ketone by the ene-reductase family of Old Yellow Enzymes (OYEs). (*R*)-**10** can be formed by PETNR,[33] (*R*)-**11** can be formed by OYE2 and (*S*)-**11** by *Ts*OYE-C25D/I67T[34] (**Figure 6**). Because we found reductive amination activity towards enones, we applied a one-pot, two-step multi-enzymatic cascade; after incubating the enone with the OYEs for 24 h, we added the amine donor and RedAms to the reaction mixture (see SI).

We explored different reaction conditions to products (2*R*)-**10**, (3*R*)-**11** or (3*S*)-**11** (**Figure 6**). In all cascades, little to no enone was present, confirming full ketoreduction of the enones by the OYEs. With intermediate **10**, there was only moderate amine formation with *Pau*RedAm and PETNR, but with high *ee* and *de*. *Stro*RedAm gave less amine product for both **10c** and **10d**, and moderate formation of (3*R*)-**11d** with high purity (56%, *ee* and *de* >99**%**). (3*S*)-**11d** was only obtained with *Pau*RedAm (71%), albeit with a *de* of 64%. Higher purities were obtained with the (*R*)-methylated substrates, showing some selectivity towards this orientation over (*S*)-methylated substrates. Interestingly, both RedAms can be used based on the carbonyl substrate and amine donor.

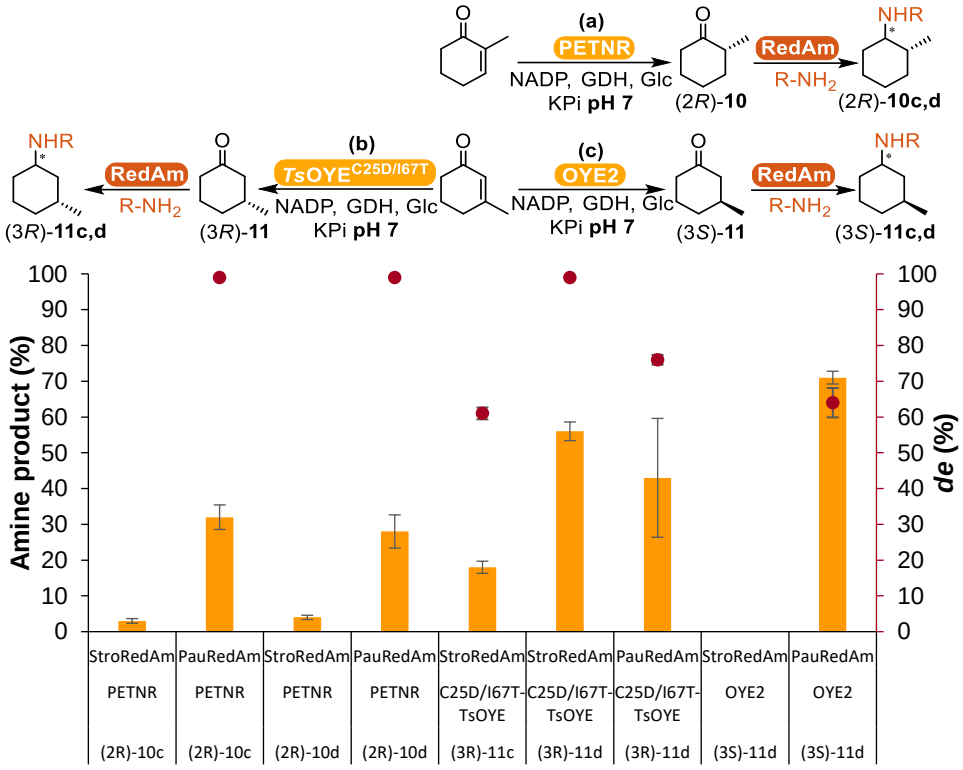

Figure 6. Reductive amination of 2-methylcyclohexenone **10** (a) and 3-methylcyclohexenone **11** (b) and (c), by *Stro*RedAm and *Pau*RedAm. Conditions: 100 mM KP_i pH 7, 60 mM Glc, 12 U/mL *Bs*GDH, 0.2 mM NADP, 10 µM OYE, 10 mM 2-methyl-2-cyclohexen-1-one or 3-methyl-2-cyclohexen-1-one, 500 rpm, 30 °C. After 24 h, 100 mM propargylamine or cyclopropylamine and 0.5 mg/mL RedAm were added to a total volume of 0.5 mL, and the reaction was mixed for another 24 h. *de* was not determined for conversions <10%. Average of duplicates.

Scale-up reactions

Scale-up reactions were performed with *Pau*RedAm and *Stro*RedAm (**Figure 7**). Full conversion to **1d** was possible with *Pau*RedAm, with an isolated yield of 65 mg (53% yield, see SI). *Stro*RedAm gave high conversion but low yield with (3*R*)-**11d** (9 mg, 7% yield), due to product loss during the work-up. The optical rotation was measured for the first time (see SI), and the configuration was assumed to be (1*R*,3*R*)-**11d**, since the selectivity is the same as with *Asp*RedAm for product **5d**, although further confirmation is needed.

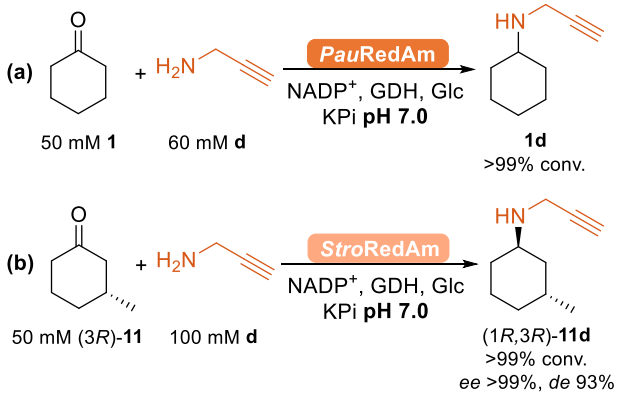

Figure 7. Scale-up reactions to produce **1d** and (1*R*,3*R*)-**11d**.

Conclusions

In this work, three thermostable RedAms were discovered and characterized. Measuring the reductive amination activity at pH 7 compared with basic pH confirmed they belong to the subfamily of RedAms. The three RedAms displayed a broad substrate scope. Especially (methylated) cyclohexanone and aldehydes showed high promise amongst all three characterized enzymes. Enones were also accepted as substrates, showing selective reductive amination compared with EneIREDs, leading to unsaturated amines. While *Pau*RedAm displays the highest specific activity, *Stro*RedAm has the best thermotolerance at 40 °C. Although *Strep*RedAm did not stand out in our characterization studies, it is worthwhile to test other ketone-amine combinations with this enzyme. Further investigation on even more ketone-amine combinations and larger scale reactions with higher temperatures could increase the amount of complex chiral amines made. Obtaining a crystal structure of the three enzymes could provide further insights in substrate preferences, cofactor specificity and thermostability. Due to their tolerance to higher temperatures and NADH activity, these RedAms are interesting targets for protein engineering. With these future steps, the RedAms from this work could contribute to eventually use these biocatalysts for industrial applications.

Acknowledgements

This project has received funding from the European Research Council (ERC) under the European Union's Horizon 2020 research and innovation program (grant n° 949910). The authors thank M. Strampraad, L. Koekkoek-van der Weel and R.J.C. van Oosten for technical assistance, and A.E. Wolder for providing the purified Old Yellow Enzymes. GSN would like to acknowledge the support from SINTEF internal projects, SEP AGREE (102029187) and POS BIOINFO 2024 (102024676-14).

Materials and methods

Chemicals (aldehydes, amines, ketones) were purchased from abcr GmbH (Kalsruhe, Germany), Merck Sigma (St. Louis, Missouri, U.S.), TCI Europe (Zwijndrecht, Belgium), Thermo Fisher Scientific (Waltham, Massachusetts, U.S.) and VWR International BV (Amsterdam, the Netherlands) and were used as received without further purification. Amines were stored under nitrogen atmosphere. Aldehydes were newly bought before use and were checked by GC for purity.

Conversions and enantiomeric excess were measured on Shimadzu GC-2010 gas chromatographs (Kyoto, Japan) with an AOC-20i Auto injector equipped with a flame ionization detector (FID), using nitrogen or helium as the carrier gas. Products were confirmed by reference standards. Product concentrations were obtained with a calibration curve equation using 5 mM dodecane as an internal standard. All samples were injected with GC quality ethyl acetate (EtOAc), except where specified with diethyl ether (Et_2O) or methyl *tert*-butyl ether (MTBE).

NMR spectra were recorded on an Agilent 400 spectrometer at 400 (^1H) and 100 (^{13}C) MHz. Chemical shifts (δ) are reported in parts per million (ppm) relative to Me_4Si (δ 0.00) in deuterated chloroform $CDCl_3$. NMR data is reported as follows: br = broad, s = singlet, d = doublet, t = triplet, m = multiplet, coupling constant(s) (*J*) in Hz, integration.

Specific rotation measurements were performed on a Perkin Elmer Model 343 S Polarimeter at 20 °C, at a wavelength of 589 nm with the solvent and concentration stated.

Biocatalytic conversions

Biotransformations

Reactions were performed in a total volume of the reaction was 500 µl and were added in 2 mL safe-lock Eppendorf tubes, containing 0.1 M KP_i buffer pH 7, 30 mM glucose, 10 U/mL *Bs*GDH, 0.2 mM $NADP^+$, 10 mM ketone/aldehyde, 10-1000 mM amine donor and 0.5 mg/mL and 0.5-1 mg/mL RedAm (0.5 mg/mL *Stro*RedAm or *Pau*RedAm, 1 mg/L *Strep*RedAm). The total reaction time was 4 or 24 h stirred at 500 rpm and 30 °C on an Eppendorf Thermomixer C. After the reaction time was reached, the Eppendorf tubes were cooled on ice for 5 minutes. Then 0.8 eq. of 10 M sodium hydroxide (NaOH) was added and vortexed to the GC samples. Next, 1 eq. of ethyl acetate (EtOAc) containing 5 mM dodecane or tridecane as internal standard was added and the mixture was vortexed. Then, the tubes were centrifuged at 10,000 × *g* for one minute and the upper organic layer was extracted from the aqueous layer. Finally, magnesium sulphate ($MgSO_4$) was added and centrifuged at 10000 × *g* for one minute to obtain a dry sample ready for gas chromatography (GC) analysis.

Reductive amination of 2-cyclohexen-1-one was carried out in 0.1 M KP_i buffer pH 7, 30 mM glucose, 10 U/mL *Bs*GDH, 0.2 mM $NADP^+$, 10 mM 2-cyclohexen-1-one, 100 mM cyclopropylamine or propargylamine and 0.5 mg/mL *Stro*RedAm. The workup was performed as described above.

$NaBH_3CN$ reactions

Sodium cyanoborohydride ($NaBH_3CN$) was used for the chemo selective reduction of the imines formed out the ketones 2-methylcyclohexanone (10), 3-methylcyclohexanone (11) and (*R*)-3-methylcyclohexanone (12) and the amine donors propargylamine and cyclopropylamine. The following compounds were used for this procedure: 0.1 M KP_i buffer pH 7, 10 mM ketone, 100 mM amine donor and 150 mM $NaBH_3CN$ dissolved in 0.1 M KP_i buffer pH 7 with a total reaction volume of 1 mL stirred at 500 rpm at 30 °C for 2 h on an Eppendorf Thermomixer C. Then, the samples were prepared for GC analysis as described before.

Multi-enzymatic cascades

To 2 mL Eppendorf tubes, 0.1 M KP_i buffer pH 7, 60 mM glucose, 12 U/mL *Bs*GDH, 0.2 mM $NADP^+$,10 µM either PETNR, C25D-I67T *Ts*OYE or OYE2, 10 mM 2-methylcyclohexenone (14) or 3-methylcyclohexenone (15) were added and stirred at 500 rpm and 30 °C for 24 h. Then, 100 mM propargylamine or cyclopropylamine and 0.5 mg/mL *Stro*RedAm or *Pau*RedAm were added to a total volume of 0.5 mL. The reactions were mixed again for another 24 h. Then, the reactions were quenched, the amines were extracted, and the samples were dried as described above.

Supporting Information

More details, including GC chromatograms (**Figure S14-S28**) and DNA sequences of used enzymes in this work can be found at doi: 10.4121/b727ca98-bdab-4434-96d5-fe3e75dee4fb.

Enzyme sequences and production

RedAm sequences

***Streptosporangium roseum* (*Stro*RedAm)**

MGSSHHHHHHSSGLVPRGSHMTTDDRPPVTVLGLGSMGRALAGAFLDNGHP
TTVWNRTAGKGGELAERGATEAATAAEAIAASPVVVVCVLDYDAVREVLGAPG
ASGLTGIEDIEDVLDTPGEAGTVSGLLAGRTLVNLTNGTPRQARELARWVSGR
GADYLDGGIMAVPPMIGNPASLVLCSGSPDAFTTHERTLSALGTISYLGEDAGR
AALYDIALLSAMYGMFGGFFQAVAMTASEKVPATEFTPLVVSWLNAMITSLPEM

AKAYDANDHSATASNLGMQAAGFVNLLETGRDQGVSTELLEPMGALLDRAVA
ANRGGDDLSALIGLLRTNPAKGAAPARDANTGSHDIGSE

***Pseudonocardia aurantiaca* (*Pau*RedAm)**
MGSSHHHHHHSSGLVPRGSHMTDDRPSVTVIGLGAMGRALAGVFLDNGHPT
TVWNRTAGKGGELTARGATEAATAAEAIAASPIVVVCVLDYDAVRSVLGAPGTS
GVSNAEGVTDVSSASGVTNVADILDPPGTSGTVTGVLAGRTLVNLTNGTPRQA
RELARWVSAQGADYLDGGIMAVPPMIGHPGSLVLYSGSTEAFTAHERTLSVM
GAANYLGEDAGRASLYDIALLSAMYGMFGGFFHAIAMVGSEKVPATEFAPLVV
SWLNAMTTSLPAMAKAYDANDHSATASNLEMQAEAYVNLLDASRDQGVSTEL
VEPMGTLLHRGVAANRGGGDLSTLIDLLRTGPV

***Streptomyces griseus subsp. griseus* (*Strep*RedAm)**
MGSSHHHHHHSSGLVPRGSHMSTNPAVSVIGLGMMGTALAAAFLKAGHPVTV
WNRSPAKTGPLVAQGATPADTAAEAVAASPLVVVCLTTYDTVRTVLEPLSGQLT
GKTVANLTNGTPEQARDLAVWAAKEGAGYLDGGIMAVPQMIAGPHAYVFYSG
AREVFDAHQETFAALGGTKYVGADPGLAALYDLALLTGMYGMIMGVMQAYALV
GTESIPATEFSELLVPWVGAMLGSAPAWAAAIDSGQHLTDVSSLAVNQEAFPNL
LETFAAQGVSGELFAPVQNLLDRAVAEGHGADGLSRLADLLRSSTS

***Streptosporangium roseum* (*Stro*RedAm2)**
MGSSHHHHHHSSGLVPRGSHMPVSVFGLGAMGTALATQFLRKGHKTTVWNR
TPAKAQPLIAIGASHAPTIDSAAAASSLLIICQLDKASVMQTLQQAPTAWAAKTIV
DLTNGTPAHARETADWALAHGARYIHGGIMAVPFMIGQPDAMILYSGPAEVFE
GVKDTLSVLGTNTYVGEDVGLASLHDLALLSGMYGLFSGFTHAVALVQSANIP
AAGFVATQLIPWLTAMTQHLNLLATQVDEKDYGDGGSSLDMQAKAAPNILEAS
QAQGVSVELIQPIFKLIERRVEEGKGSEGLAALVGMI

***Pseudonocardia aurantiaca* (*Pau*RedAm2)**
MGSSHHHHHHSSGLVPRGSHMSERAKSPVTVLGLGRMGTPIATAFLDAGHPT
TVWNRTAGKADALVARGAIRAATVTEAVATGPLVIAIPLLDQDAVRQTLGPATAA
LRGRTLVNLANSTPDHARELASWAAGHGADYLDGAMMALPQTVATPEGFFLY
SGSQDAFTTYRRELEVMAPAHYFGADPGAAEVHDLALLGTGYAALTGFLHAA
ALLDSVGTTPEVFAPLAARWLHGMAGFLPELAREAGSAAYADGVSTVDLNRA
GIDALIRLSGAHGIAADVHEPLRTLLDKRSADGHGQDSFSSVFELLRSRGTPR
R

Lyophilized plasmids of the selected sequences were cloned in pET-28a(+) with a *N*-terminal His-tag, without codon optimization and received from SynBio Technologies (Monmouth Junction, NJ, United States).

OYE sequences

***Saccharomyces cerevisiae* Old Yellow Enzyme 2 (OYE2): accession number Q03558**

MGSSHHHHHHSSGLVPRGSHMPFVKDFKPQALGDTNLFKPIKIGNNELLHRA
VIPPLTRMRAQHPGNIPNRDWAVEYYAQRAQRPGTLIITEGTFPSPQSGGYDN
APGIWSEEQIKEWTKIFKAIHENKSFAWVQLWVLGWAAFPDTLARDGLRYDSA
SDNVYMNAEQEEKAKKANNPQHSITKDEIKQYVKEYVQAAKNSIAAGADGVEI
HSANGYLLNQFLDPHSNNRTDEYGGSIENRARFTLEVVDAVVDAIGPEKVGLR
LSPYGVFNSMSGGAETGIVAQYAYVLGELERRAKAGKRLAFVHLVEPRVTNPF
LTEGEGEYNGGSNKFAYSIWKGPIIRAGNFALHPEVVREEVKDPRTLIGYGRFF
ISNPDLVDRLEKGLPLNKYDRDTFYKMSAEGYIDYPTYEEALKLGWDKN

***Enterobacter cloacae PB2* Old Yellow Enzyme (PETNR): accession number P71278**

MSAEKLFTPLKVGAVTAPNRVFMAPLTRLRSIEPGDIPTPLMGEYYRQRASAG
LIISEATQISAQAKGYAGAPGLHSPEQIAAWKKITAGVHAEDGRIAVQLWHTGRI
SHSSIQPGGQAPVSASALNANTRTSLRDENGNAIRVDTTTPRALELDEIPGIVN
DFRQAVANAREAGFDLVELHSAHGYLLHQFLSPSSNQRTDQYGGSVENRARL
VLEVVDAVCNEWSADRIGIRVSPIGTFQNVDNGPNEEADALYLIEELAKRGIAYL
HMSETDLAGGKPYSEAFRQKVRERFHGVIIGAGAYTAEKAEDLIGKGLIDAVAF
GRDYIANPDLVARLQKKAELNPQRPESFYGGGAEGYTDYPSLHHHHHH

***Thermus scotoductus* Old Yellow Enzyme C25D/I67T (*Ts*OYE C25D/I67T): wildtype accession number B0JDW3**

MALLFTPLELGGLRLKNRLAMSPM**D**QYSATLEGEVTDWHLLHYPTRALGGVG
LILVEATAVEPLGR**T**SPYDLGIWSEDHLPGLKELARRIREAGAVPGIQLAHAGRK
AGTARPWEGGKPLGWRVVGPSPIPFDEGYPVPEPLDEAGMERILQAFVEGAR
RALRAGFQVIELHMAHGYLLSSFLSPLSNQRTDAYGGSLENRMRFPLQVAQAV
REVVPRELPLFVRVSATDWGEGGWSLEDTLAFARRLKELGVDLLDCSSGGVV
LRVRIPLAPGFQVPFADAVRKRVGLRTGAVGLITTPEQAETLLQAGSADLVLLG
RVLLRDPYFPLRAAKALGVAPEVPPQYQRGF

OYEs were retrieved as pure enzymes from previous works. Production and purification were performed as previously described.[34-36]

RedAm production

E. coli BL21(DE3) chemically competent cells were transformed with the vector containing all listed genes. The transformed cells were grown on selective LB-agar plates (50 µg/mL kanamycin) overnight at 37 °C. TB-medium (500 mL in 2L baffled flask) was inoculated with 1% overnight LB preculture of the transformed cells and incubated for 3-5 h at 37 °C, 180 rpm. After reaching an

OD_{600} of 0.6-0.8, 0.5 mM IPTG was added, followed by overnight incubation at 20 °C. Cells were harvested (17,000 × *g*, 20 min, 4 °C) and stored at -80 °C.

Sodium dodecyl sulfate polyacrylamide gel electrophoresis (SDS-PAGE) was run to show gene expression and enzyme purity levels (**Figures S1-S2**). Samples were prepared by mixing with one equivalent of Laemmli buffer and 5% v/v dithiothreitol (DTT), heated to 95 °C for 5 min, then centrifuged at 9,000 × *g* for 2 min. From these samples, 10 µL was loaded onto the gel, whereas 5 µL of protein ladder was loaded onto a Criterion TGX Stain-Free Precast Gel. Imaging was performed with a ChemiDoc MP imaging system (Bio-Rad Laboratories, Hercules, California, U.S.).

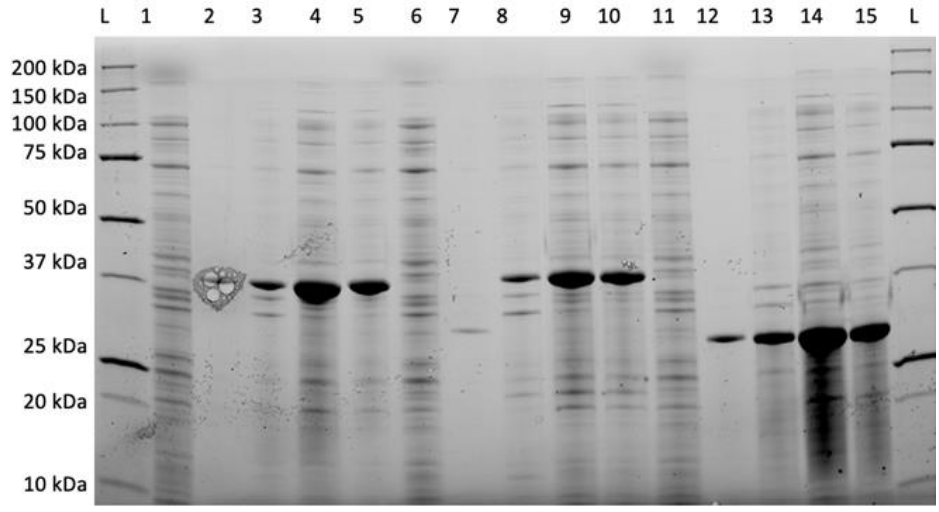

Figure S1. SDS-PAGE gel of RedAms hits. L: protein ladder. **1:** *Stro*RedAm before induction. **2:** *Stro*RedAm after IPTG induction. **3:** Cell lysate *Stro*RedAm. **4:** *Stro*RedAm 10x diluted CFE, **5:** *Stro*RedAm 20x diluted CFE. **6:** *Pau*RedAm before induction. **7:** *Pau*RedAm2 after IPTG induction. **8:** Cell lysate *Pau*RedAm. **9:** *Pau*RedAm 10x diluted CFE. **10:** *Pau*RedAm 20x diluted CFE. **11:** *Strep*RedAm before induction. **12:** *Strep*RedAm after IPTG induction. **13:** Cell lysate *Strep*RedAm. **14:** *Strep*RedAm 10x diluted CFE. **15:** *Strep*RedAm 20x diluted CFE.

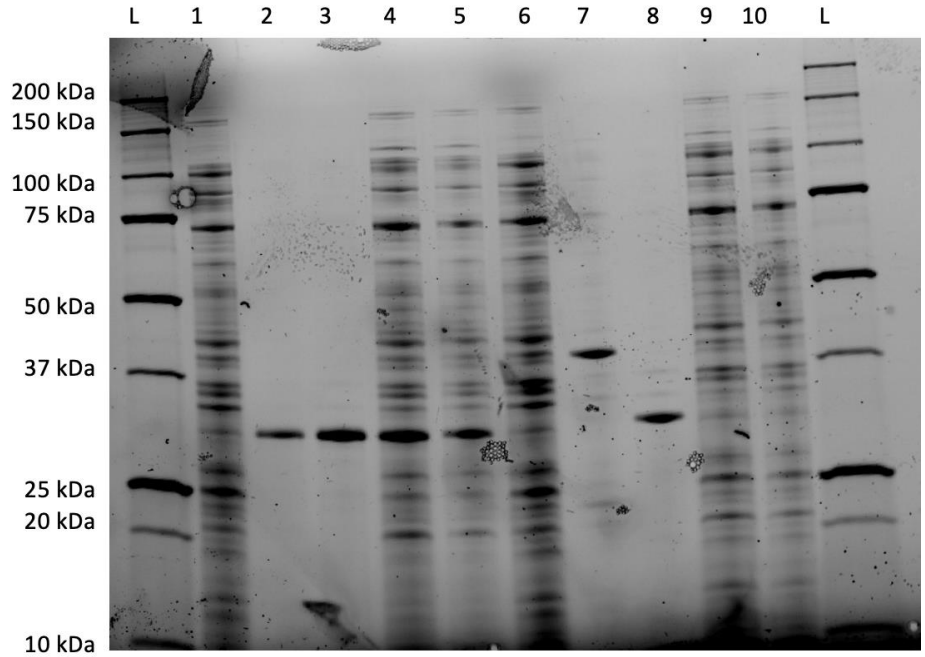

Figure S2. SDS-PAGE gel of RedAms hits. **L:** protein ladder. **1:** *Stro*RedAm2 before induction. **2:** *Stro*RedAm2 after IPTG induction. **3:** *Stro*RedAm2 cell lysate **4:** *Stro*RedAm2 10x diluted CFE. **5:** *Stro*RedAm2 20x diluted CFE. **6:** *Pau*RedAm2 IPTG induction. **7:** *Pau*RedAm after IPTG induction. **8:** Cell lysate *Pau*RedAm2. **9:** *Pau*RedAm2 10x diluted CFE. **10:** *Pau*RedAm2 20x diluted CFE.

Affinity chromatography of *Stro*RedAm, *Pau*RedAm and *Strep*RedAm

Two buffers were prepared: 50 mM Tris-HCl pH 8, 300 mM NaCl, 1 mM $MgCl_2$ with 30 mM imidazole for the binding buffer, and with 300 mM imidazole for the elution buffer. The buffers were filtered and degassed before use. The cell pellets were thawed and suspended in 5 mL/g_{wcw} binding buffer. After adding a spatula tip of deoxyribonuclease (DNase), $MgCl_2$, lysozyme from chicken egg white (Sigma Aldrich) and a pill of cOmplete™ Mini EDTA-free Protease Inhibitor (Merck), 3 g_{wcw} of cells were disrupted using a Constant Systems Continuous Flow Cell Disrupter CF1 (22 kpsi) and clarified by centrifugation (32,000 × *g*, 30 min, 4 °C). After filtering the CFE (0.2 µm), IMAC was performed with a 5 mL HisTrap™ FF crude column (GE Healthcare, Chicago, Illinois, U.S.) on a Bio-Rad NGC Chromatography system.

After equilibrating the column with binding buffer at 5 mL/min, the CFE was loaded on the column with a velocity of 3 mL/min. Then, the column was flushed with 10 column volumes (CVs) of binding buffer at 3 mL/min. after 10 CVs, or when the absorbance at 280 nm reached near zero, 75% of the elution buffer was pumped through the column, also at 3 mL/min. Elution fractions were collected, pooled, and kept on ice until desalted with a PD10 desalting column

(GE Healthcare). Enzyme concentration was determined by the Uptima bicinchoninic acid (BC) assay (Interchim, Montluçon, France).

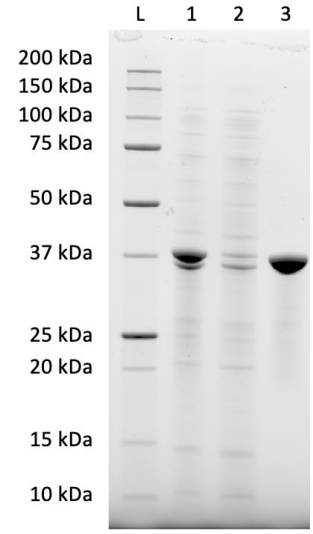

Figure S3. SDS-PAGE gel of *Stro*RedAm IMAC purification. **1:** CFE; **2:** flowthrough; **3:** *Stro*RedAm (35.2 kDa).

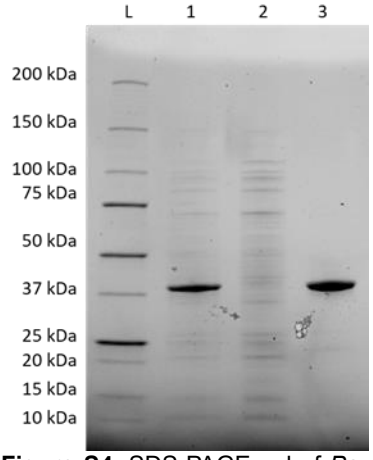

Figure S4. SDS-PAGE gel of *Pau*RedAm IMAC purification. **1:** CFE; **2:** flowthrough; **3:** *Pau*RedAm (34.3 kDa).

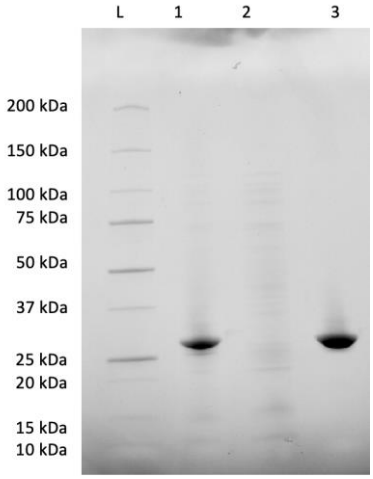

Figure S5. SDS-PAGE gel of *Strep*RedAm IMAC purification. **1:** CFE; **2:** flowthrough; **3:** *Strep*RedAm (30.6 kDa).

Carbonyl substrates, amine donors and products

Table S1. List of carbonyl substrates and amine donors used in this study.

Label	Carbonyl substrates	Label	Amine donors
1	cyclohexanone	a	ammonium chloride
2	hexanal	b	methylamine
3	hydrocinnamaldehyde	c	cyclopropylamine
4	benzaldehyde	d	propargylamine
5	ethyl levulinate	e	allylamine
6	1-indanone	f	benzylamine
7	acetophenone	g	*sec*-butylamine
8	phenylacetone		
9	β-tetralone		
10	2-methylcyclohexanone		
11	3-methylcyclohexanone		
(*R*)-11	(*R*)-3-methylcyclohexanone		
12	2-cyclohexen-1-one		

The ketone/aldehydes used for the experiments were prepared as 1 M stocks in dimethyl sulfoxide (DMSO). The amines were made as 1 M stocks in buffer, using HCl to adjust the pH to 7.

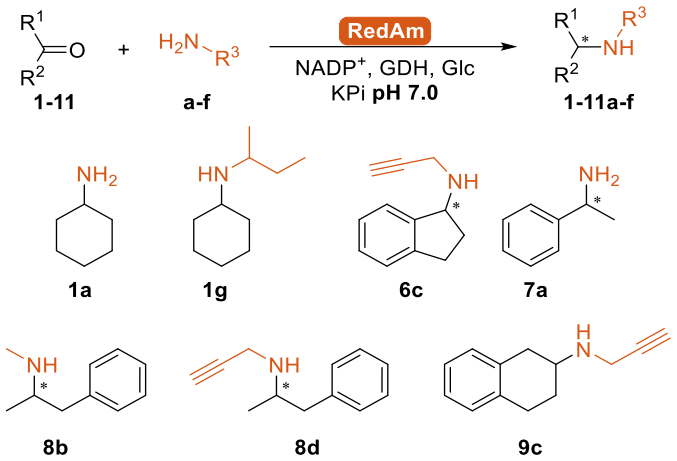

Figure S6. List of combinations tried in this work where no reductive amination was observed.

Amine product synthesis

The synthesis of cyclopropylcyclohexanamine (**1c**, 824-82-8), *N*-2-propyn-1-ylcyclohexanamine (**1d**, 18292-76-7), *N*-cyclopropylbenzenepropanamine (**3c**, 18381-62-9), *N*-2-propyn-1-ylbenzenepropanamine (**3d**, 56862-31-8) and *N*-allylbenzenepropanamine (**3e**, 528812-92-2 was performed as previously reported.[9]

In dry tetrahydrofuran (THF), 2 mmol of ketone/aldehyde, 2.2 mmol amine, 3 mmol sodium triacetoxyborohydride and 2 mmol glacial acetic acid were mixed and stirred under N_2 at room temperature overnight. The reaction was quenched with 10 mL of 10 M NaOH. The reaction mixture was mixed with EtOAc (10 mL), and the organic phase was separated. This step was repeated, the organic phases were combined and extracted with 1M HCl (3 x 10 mL). The aqueous phase was basified to pH 12 with a 5 M NaOH solution. The product was extracted into EtOAc (2 x 20 mL), dried with $MgSO_4$ and the solvent was removed under reduced pressure to afford the aforementioned amines.

The synthesis of 1-cyclopropyl-5-methyl-2-pyrrolidinone (**5c**, 1351473-78-3) and 5-methyl-1-(2-propyn-1-yl)-2-pyrrolidinone (**5d**, 18327-34-9) was performed based on literature.[9] In dry THF, 1 mmol of ketone, 2 mmol of amine, 2 mmol of acetic acid and 1.4 mmol of sodium triacetoxyborohydride were mixed and stirred under N_2 at room temperature overnight. The mixture was quenched with 1 M NaOH (5 mL) and extracted with EtOAc (3 x 5 mL). The organic layers were combined, dried over $MgSO_4$ and the solvent evaporated under reduced pressure to afford crude amine products. Yields of synthesized amines varied between 30 and 50 % isolated yield. The compounds were confirmed by NMR.

RedAm activity assays

For specific activity measurements, 4 mL UV grade polymethylmethacrylate (PMMA) plastic cuvettes were used to monitor the decrease of NADPH at a wavelength of 340 nm on a Cary 60 UV-Vis spectrophotometer. The extinction coefficient of NAD(P)H used was $\varepsilon_{340\ nm}$ = 6220 $M^{-1}cm^{-1}$.[37]

Carbonyl substrates were prepared as a 1 M stock solution in DMSO. Amines were prepared in 100 mM KP_i pH 7, titrated with HCl to adjust the pH to 7. NAD(P)H stock solutions were prepared in the mentioned buffer in a 10 mM concentration, confirmed by UV spectroscopy at 340 nm.

For buffers at different pHs the following salts were used: Tris-HCl pH 7.5-9 and KP_i pH 6-8. Activity assays at different temperatures were performed from 20-80 °C. Buffer pHs were thermodynamically corrected using Buffer Calculator© (Prof. Robert J. Beynon http://phbuffers.org/BuffferCalc/Buffer.htm, checked on 22/05/2024).

The model reaction was run by adding 10 mM hexanal, 100 mM allylamine, 0.2 mM NADPH, enzyme in 100 mM KP_i pH 7, 2 mL volume, measured at 30 °C. The amount of enzyme added to the sample mixture was based on a decrease in absorbance at 340 nm around 0.05-0.20 A/min.

pH profiles of *Stro*RedAm, *Pau*RedAm and *Strep*RedAm

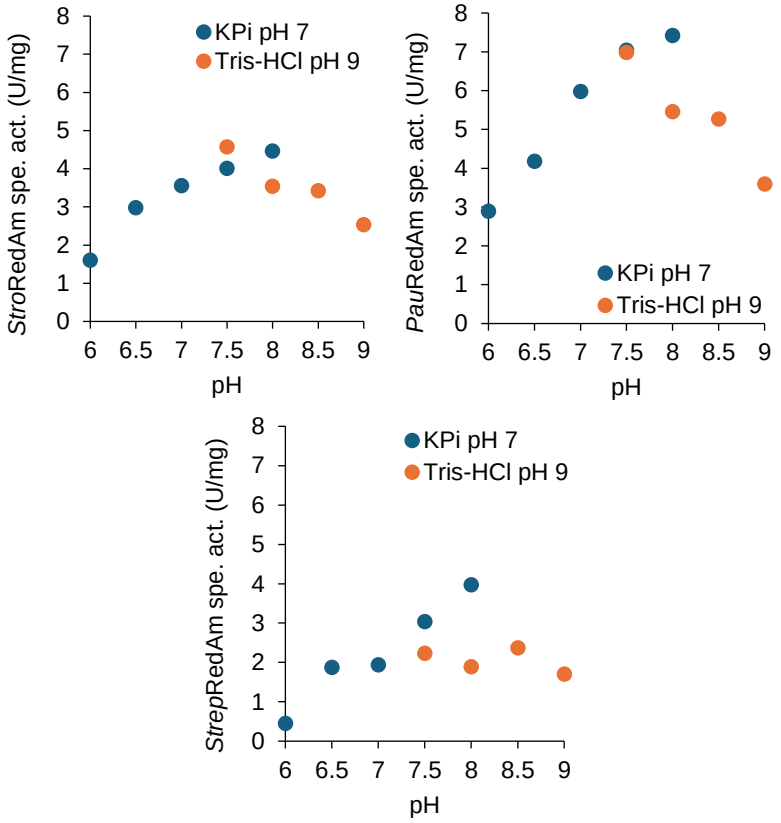

Figure S7. Activity of *Stro*RedAm (top left), *Pau*RedAm (top right) and *Strep*RedAm (bottom) according to pH. Conditions: 50 mM KP_i pH 7 or Tris-HCl pH 9, 10 mM hexanal, 100 mM allylamine, 0.2 mM NADPH and purified *Stro*RedAm, 2 mL volume, 30 °C. Average of duplicates.

Thermostability

The thermostability assay of the purified RedAms was carried out by incubating aliquots of the enzyme at 30 °C in the concentrations in which these were retrieved from the IMAC purification (**Figure S8**). The activity assay was performed as described as our model reaction.

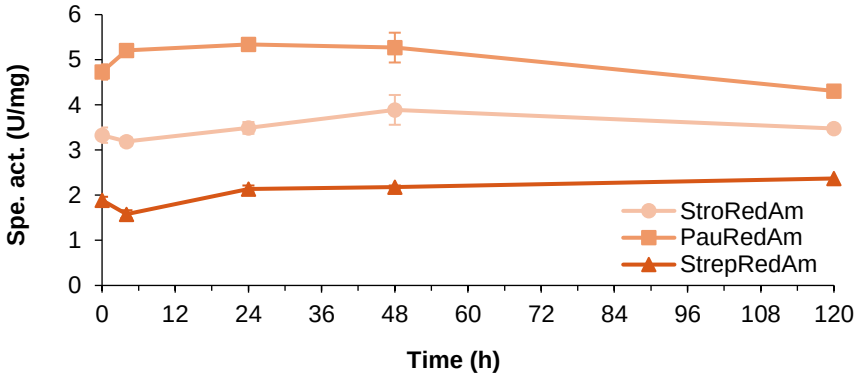

Figure S8. Specific activity of *Stro*RedAm, *Pau*RedAm and *Strep*RedAm stocks incubated at 30 °C over 120 h. Conditions: 100 mM KP_i pH 7, 100 mM allylamine **e**,10 mM hexanal **2**, 0.2 mM NADPH, purified *Stro*RedAm, *Pau*RedAm or *Strep*RedAm, 2 mL volume, 30 °C. Average of duplicates.

The thermostability assay measurements with pure RedAm were performed with the standard cuvette composition. Three samples with 0.5 mg/mL of pure *Stro*RedAm, *Pau*RedAm and *Strep*RedAm were stirred at 500 rpm and 30 and 40 °C. UV-VIS measurements were performed after 0, 4, 24, 48 and 120 h to determine the specific activity of the enzymes.

The stability assay measurements with RedAm in buffer were performed with model reaction mixture. Three samples were made with 10x diluted pure *Stro*RedAm, *Pau*RedAm and *Strep*RedAm, respectively, mixed at 500 rpm and 30 or 40 °C. Measurements were performed after 4, 24 and 48 h.

Steady-state kinetics of *Stro*RedAm, *Pau*RedAm and *Strep*RedAm with NAD(P)H

Michaelis-Menten curves were prepared for each RedAm using 0.05-0.4 mM NADH or NADPH combined with 10 mM hexanal and 100 mM allylamine in a 0.1 M KP_i buffer pH 7. RedAm 3 showed too low activity in presence of NADH to create a curve, hence only kinetics were determined with NADPH. Steady-state kinetics were analyzed using IGOR Pro 9 (WaveMetrics). Measurements were plotted onto the equation $f(S) = v_{max} \times (S/(K_M+S))$.

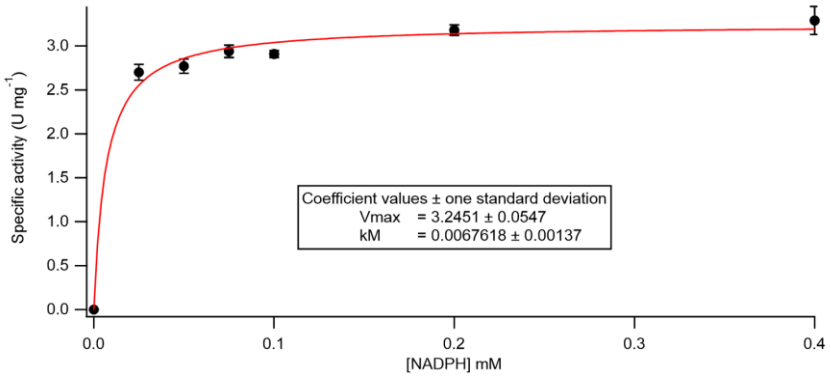

Figure S9. Steady-state kinetics for the reductive amination of hexanal and allylamine catalyzed by *Stro*RedAm with NADPH. Conditions: 100 mM KP_i pH 7, 0.025-0.5 mM NADPH, 10 mM hexanal, 100 mM allylamine, *Stro*RedAm, 30 °C. Average of duplicates.

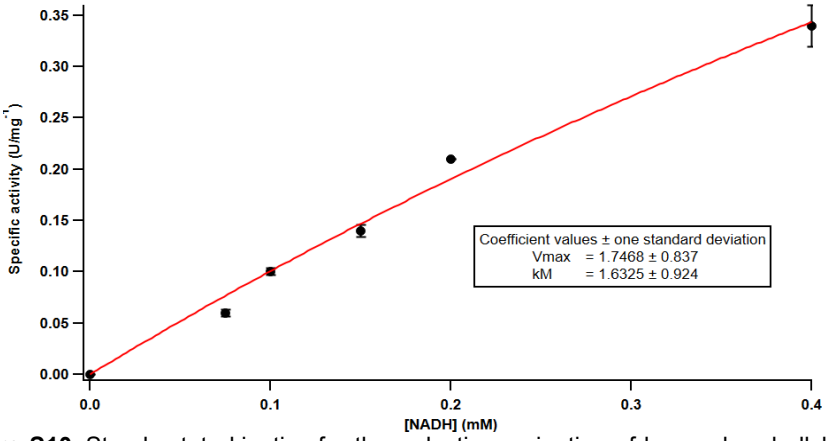

Figure S10. Steady-state kinetics for the reductive amination of hexanal and allylamine catalyzed by *Stro*RedAm with NADH. Conditions: 100 mM KP_i pH 7, 0.025-0.5 mM NADH, 10 mM hexanal, 100 mM allylamine, *Stro*RedAm, 30 °C. Average of duplicates. Pending further data points above 0.4 mM NADH.

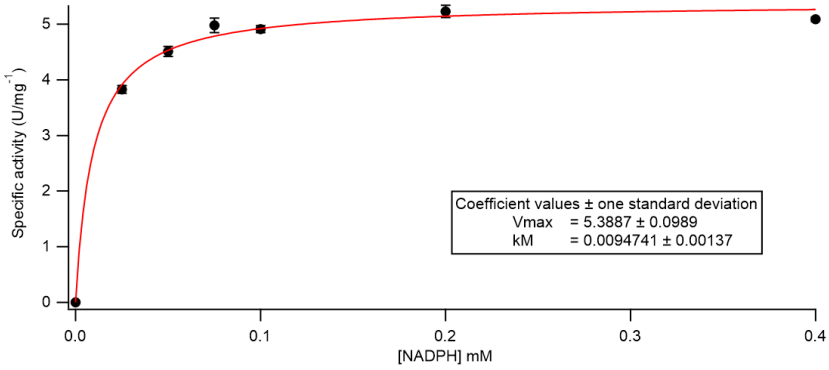

Figure S11. Steady-state kinetics for the reductive amination of hexanal and allylamine catalyzed by *Pau*RedAm with NADPH. Conditions: 100 mM KP_i pH 7, 0.025-0.5 mM NADPH, 10 mM hexanal, 100 mM allylamine, *Pau*RedAm, 30 °C. Average of duplicates.

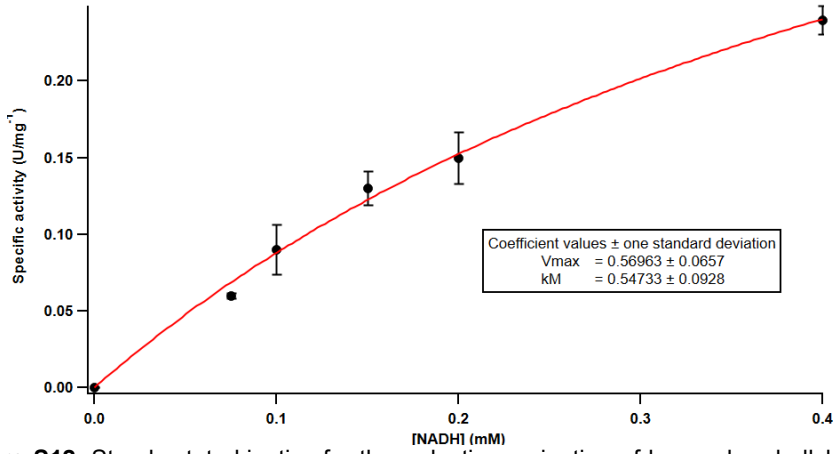

Figure S12. Steady-state kinetics for the reductive amination of hexanal and allylamine catalyzed by *Pau*RedAm with NADH. Conditions: 100 mM KP_i pH 7, 0.025-0.5 mM NADH, 10 mM hexanal, 100 mM allylamine, *Pau*RedAm, 30 °C. Average of duplicates. Pending further data points above 0.4 mM NADH.

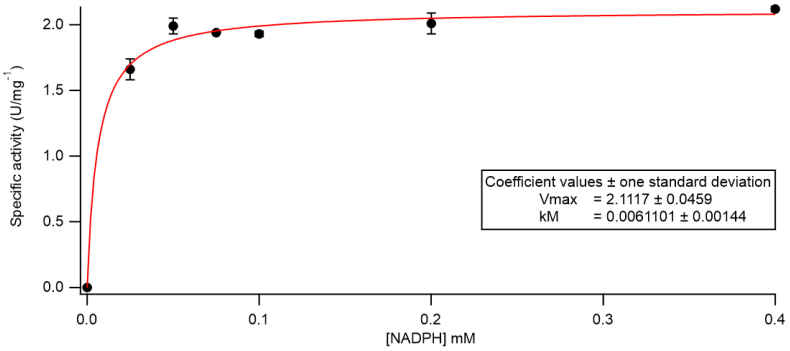

Figure S13. Steady-state kinetics for the reductive amination of hexanal and allylamine catalyzed by *Strep*RedAm with NADPH. Conditions: 100 mM KP_i pH 7, 0.025-0.5 mM NADPH, 10 mM hexanal, 100 mM allylamine, *Strep*RedAm, 30 °C. Average of duplicates.

GC analyses

GC columns and methods

The GC experiments are carried out on Shimadzu GC-2010 gas chromatographs containing an AOC-20i Auto injector and a flame ionization detector (FID). The used carrier gasses for the experiments are helium or nitrogen. The compounds were dissolved in ethyl acetate (EtOAc). The following different column types are used to separate the compounds in the GC reaction vials:

A: CP-Sil 8 CB (Agilent Technologies, Santa Clara, California, United States) (25 m × 0.25 mm × 1.20 µm), injection at 340 °C, split ratio 50, linear velocity 30 cm/sec, column flow 1.01 mL/min, nitrogen as carrier gas.

B: CP-Wax 52 CB (Agilent Technologies, Santa Clara, California, United States) (25 m × 0.53 mm × 2.0 µm), injection at 250 °C, split ratio 50, flow 4 mL/min, nitrogen as carrier gas.

C: Hydrodex β-TBDM (Macherey-Nagel, Düren, Germany), 50 m × 0.25 mm × 0.15 µm, heptakis-(2,3-di-O-methyl-6-O-t-butyldimethyl-silyl)-β-cyclodextrin, injection at 250 °C, split ratio 50, linear velocity 38 cm/s, column flow 2.23 mL/min, helium as carrier gas.

D: CP-Chirasil-DEX CB column (Agilent Technologies, Santa Clara, California, United States), 25 m x 0.32 mm x 0.25 µm injection at 250 °C, split ratio 150, linear velocity 30 cm/sec, flow 4.0 mL/min, helium as carrier gas.

Table S2. GC column and methods for substrate combinations.

		GC oven program				
GC column	**Method**	rate (°C/min),	temp. (°C),	hold (min)	**Compound**	**RT (min)**
A CP-Sil 8 CB	A1	- 5 25	80 100 345	3 4 1	methylamine **b** DMSO cyclohexylamine **1a** cyclohexanol (side product) cyclohexanone **1** *N*-methylcyclohexylamine **1b** dodecane	7.8 8.2 9.8 10.8 11.4 12.4 16.8
A	A2	- 5 10 25	80 100 200 345	3 4 2.2 1	DMSO cyclohexanol (side product) cyclohexanone **1** benzylamine **f** *N*-2-propyn-1-ylcyclohexanamine **1d** [a] *N*-allylcyclohexanamine **1e** *N*-cyclopropylcyclohexanamine **1c** [a] dodecane *N*-benzylcyclohexanamine **1f**	8.2 10.8 11.4 15.8 18.5 17.8 18.8 20.3 27.2
A	A3	- 5 20	100 250 345	3.25 1 0	DMSO benzaldehyde **11** benzyl alcohol dodecane *N*-benzylcyclopropanamine **11c** [b] *N*-benzylpropargylamine **11d** [b] dibenzylamine **11f**	5.7 9.5 11.6 16.7 18.5 18.5 32.4

A	A4	- 10 5 20	100 140 180 345	1.75 2 5 1	DMSO dodecane hydrocinnamaldehyde **3** *N*-allylbenzenepropanamine **3e** [a] *N*-2-propyn-1-ylbenzenepropanamine **3d** [a] *N*-cyclopropylbenzenepropanamine **3c** [a]	5.1 13.6 13.0 21.6 22.4 22.5
A	A5	- 5 10 25	80 100 180 345	3 4 2.2 1	DMSO cyclohexanol 2-cyclohexen-1-one **12** *N*-cyclopropylcyclohex-2-en-1-amine **12c**[a] *N*-(prop-2-yn-1-yl)cyclohex-2-en-1-amine **12d**[a] dodecane	8.2 10.6 12.9 18.8 19.0 20.3
B CP-Wax 52 CB	B1	- 5 20	80 150 250	3 1 1	hexanal **2** dodecane *N*-allylhexan-1-amine **2e** [a] DMSO	6.8 9.2 11.2 20.2
C Hydrodex β-TBDM	C1	- 5	100 220	2 1	DMSO ethyl levulinate **5** 1-cyclopropyl-5-methyl-2-pyrrolidinone **5c**[a] 5-methyl-1-(2-propyn-1-yl)-2-pyrrolidinone **5d**[a] dodecane	7.0 9.8 17.5-17.6 16.3, 16.6 11.5
C	C2	- 10 5 20	100 160 195 215	4 1 5 2	DMSO dodecane indanone **6** rasagiline **6d**[b]	7.7 10.8 16.1 18.9
C	C3	- 5 5 5 5 5 5 5 5 5 20 20 25	70 75 80 85 90 95 100 105 110 115 120 155 250	5 5 5 5 5 5 5 5 5 2 5 1 1	DMSO 3-methylcyclohexanone **11** 3-methylcyclohexanol tridecane 3-methyl-*N*-(prop-2-yn-1-yl)cyclohexan-1-amine **11d**[c] (3*R*)-methyl-*N*-(prop-2-yn-1-yl)cyclohexan-1-amine **(3*R*)-11d**[c] 3-methyl-2-cyclohexen-1-one	21.5 32.4, 33.1 43.4 57.9 51.5, 51.8, 52.4, 52.7 51.8, 52.4 50.6
D CP-Chirasil-DEX CB	D1	- 5 25	90 105 230	2 12.5 1	DMSO dodecane (2*R*)-methylcyclohexanone **(2*R*)-10** 2-methylcyclohexanol *N*-cyclopropyl-2-methylcyclohexan-1-amine **10c** [c] 2-methyl-N-(prop-2-yn-1-yl)cyclohexan-1-amine **10d**[c] 2-methyl-2-cyclohexen-1-one	5.8 13.4 7.8, 7.9 10.8, 10.9, 11.8, 11.9 13.8, 14.3, 14.6, 15.2

				16.7, 17.0, 17.7, 18.4 8.5
	D2	- 10 20 25 90 130 155 250 5 9.2 1	DMSO (3*R*)-methylcyclohexanone **(3*R*)-11** (3*S*)-methylcyclohexanone **(3*S*)-11** tridecane *N*-cyclopropyl-3-methylcyclohexan-1-amine **11c**[c] (3*R*)-*N*-cyclopropyl-3-methylcyclohexan-1-amine **(3*R*)-11c**[c] 3-methyl-2-cyclohexen-1-one 3-methylcyclohexanol	9.7 11.9 12.1 19.6 14.8, 15.2, 15.8, 16.1 15.8, 16.1 17.5 13.7, 13.8, 14.0

[a] synthesized product

[b] based on negative controls

[c] based on positive control with $NaBH_3CN$

Amine products from 2-methylcyclohexanone 10

*N-cyclopropyl-2-methylcyclohexan-1-amine **10c***

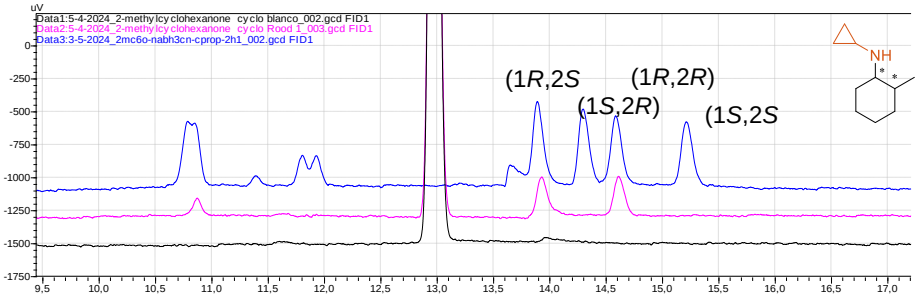

Figure S29. GC chromatograms of reaction mixture with $NaBH_3CN$ to chemically synthesize all four configurations of *N*-cyclopropyl-2-methylcyclohexan-1-amine **10c** (blue), aligned with a reaction mixture with *Stro*RedAm (pink) and a negative control without RedAm (black). CP-Chirasil DEX-CB method D1.

2-methyl-N-(prop-2-yn-1-yl)cyclohexan-1-amine ***10d***

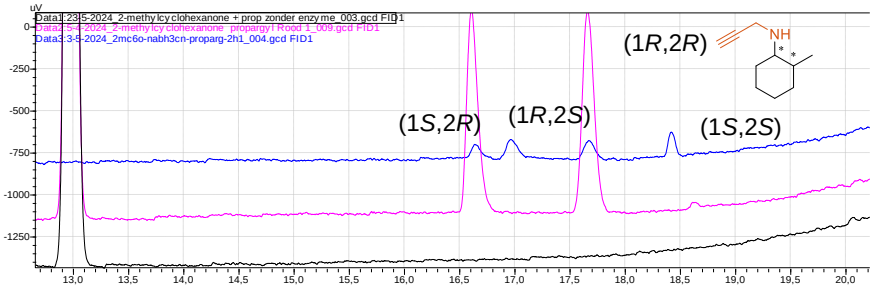

Figure S30. GC chromatogram of reaction mixture with *Stro*RedAm to synthesize 2-methyl-*N*-(prop-2-yn-1-yl)cyclohexan-1-amine **10d** (blue), aligned with a reaction mixture with *Stro*RedAm (pink) and a negative control without RedAm (black). CP-Chirasil DEX-CB method D1.

Amine products from 3-methylcyclohexanone 11 and (3*R*)-methylcyclohexanone (3*R*)-11

N-cyclopropyl-3-methylcyclohexan-1-amine ***11c***

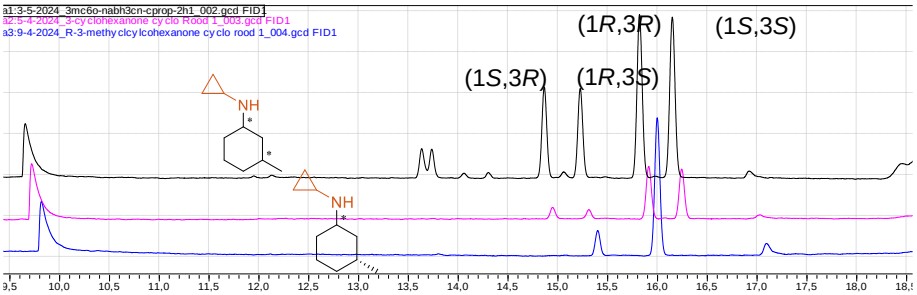

Figure S31. GC chromatogram of reaction mixture with $NaBH_3CN$ to chemically synthesize all four configurations of *N*-cyclopropyl-3-methylcyclohexan-1-amine **11c** (black), aligned with a reaction mixture with 3-methylcyclohexanone **11** and *Stro*RedAm (pink) and a reaction mixture with (*R*)-3-methylcyclohexanone **(*R*)-11** and *Stro*RedAm (blue). CP-Chirasil-DEX CB Method D2.

3-methyl-N-(prop-2-yn-1-yl)cyclohexan-1-amine ***11d***

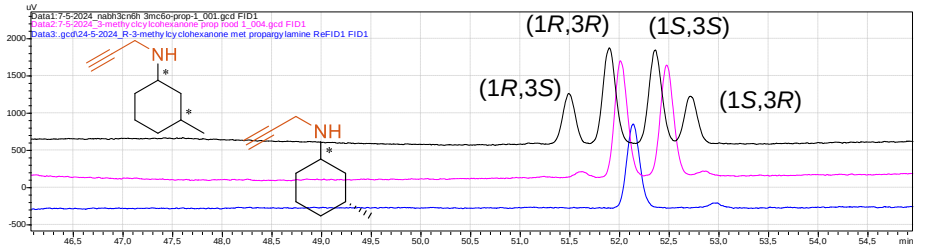

Figure S32. GC chromatogram of reaction mixture with $NaBH_3CN$ to chemically synthesize all four configurations of 3-methyl-*N*-(prop-2-yn-1-yl)cyclohexan-1-amine (**11d**) (black), aligned with chromatograms of a reaction mixture with 3-methylcyclohexanone **11** and *Stro*RedAm (pink) and a reaction mixture with (3*R*)-methylcyclohexanone (3*R*)-**11** and *Stro*RedAm (blue). Hydrodex β-TBDM method C3.

Amine products from 2-cyclohexen-1-one 12

N-cyclopropylcyclohex-2-en-1-amine ***12c***

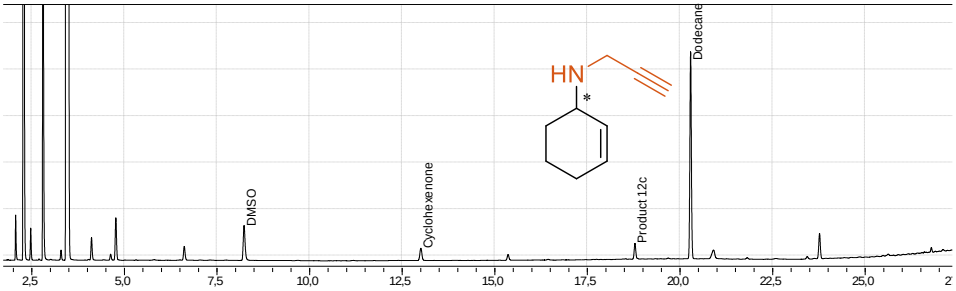

Figure S33. GC chromatogram of reaction mixture with *Pau*RedAm to synthesize *N*-cyclopropylcyclohex-2-en-1-amine **12c**. CP-Sil 8 CB method A5.

N-(prop-2-yn-1-yl)cyclohex-2-en-1-amine ***12d***

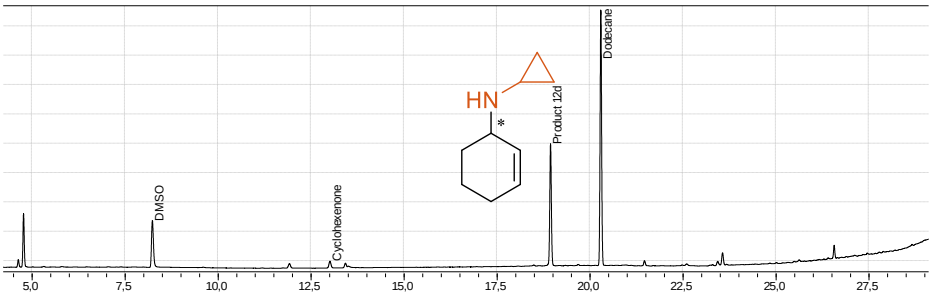

Figure S34. GC chromatogram of reaction mixture with *Stro*RedAm to synthesize *N*-(prop-2-yn-1-yl)cyclohex-2-en-1-amine **12d**. CP-Sil 8 CB method A5.

OYE-RedAm enzymatic cascades

2-methyl-2-cyclohexen-1-one

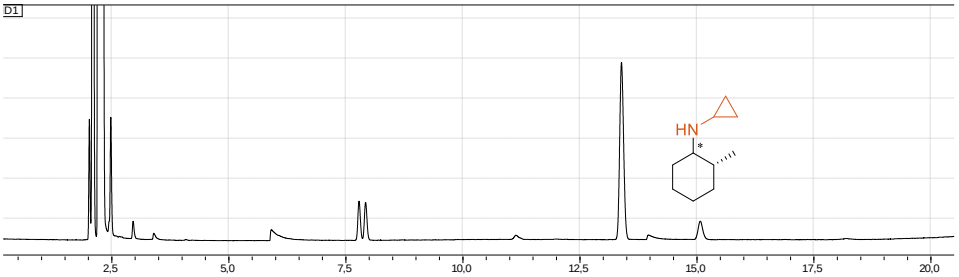

Figure S35. GC chromatogram of cascade reaction mixture containing 2-methyl-2-cyclohexen-1-one and cyclopropylamine with PETNR and *Pau*RedAm. CP-Chirasil-DEX CB Method D1.

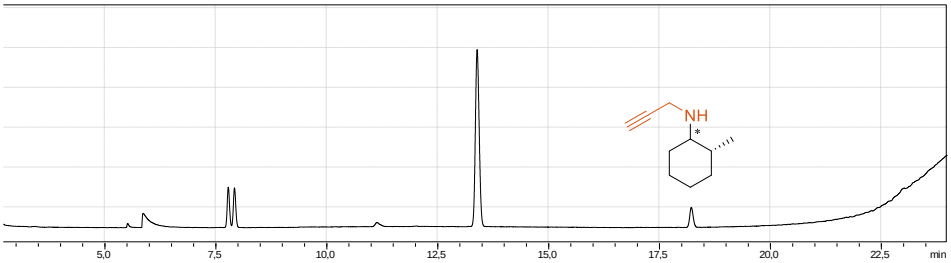

Figure S36. GC chromatogram of cascade reaction mixture containing 2-methyl-2-cyclohexen-1-one and propargylamine with PETNR and *Pau*RedAm. CP-Chirasil-DEX CB Method D1.

3-methyl-2-cyclohexen-1-one

GC chromatograms of the biocatalytic cascades with 3-methylcyclohexanone and propargylamine

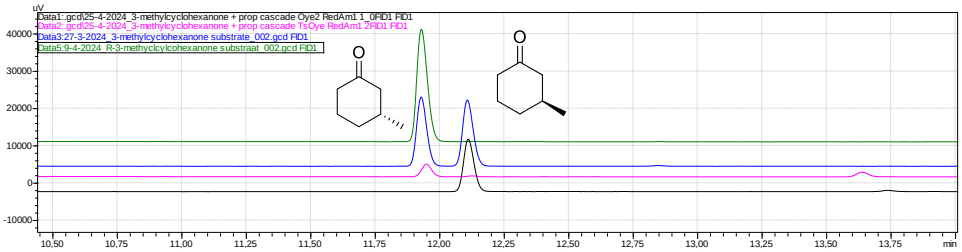

Figure S37. Overlay of (3*R*)-methylcyclohexanone (green), *rac*-3-methylcyclohexanone (blue), reaction intermediate catalyzed by the (*R*)-selective *Ts*OYE-C25D/I67T (pink) and the (*S*)-selective OYE2 (black). CP-Chirasil-DEX CB Method D2.

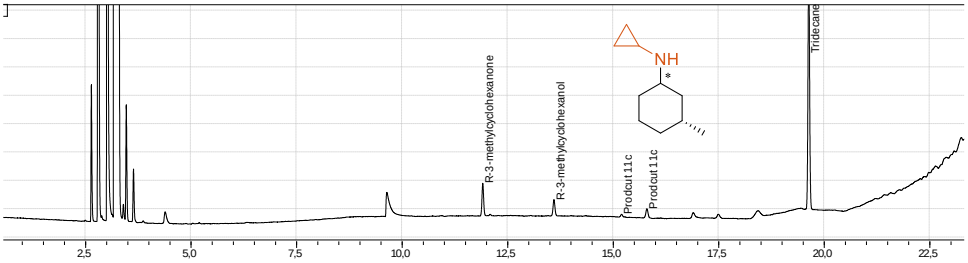

Figure S38. GC chromatogram of cascade reaction mixture containing 3-methyl-2-cyclohexen-1-one and cyclopropylamine with *Ts*OYE-C25D/I67T and *Stro*RedAm. CP-Chirasil-DEX CB Method D2.

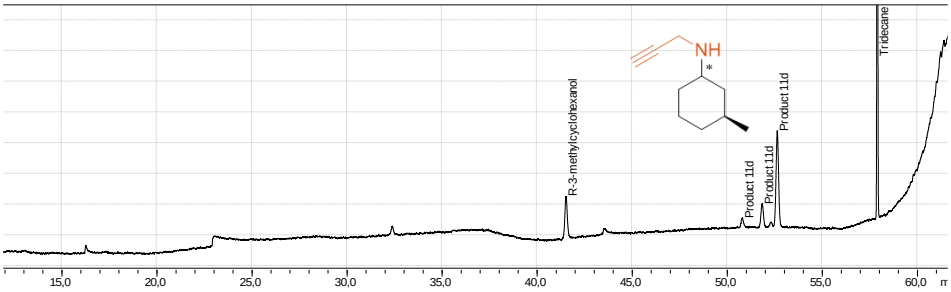

Figure S39. GC chromatogram of cascade reaction mixture containing 3-methyl-2-cyclohexen-1-one and propargylamine with OYE2 and *Pau*RedAm. Hydrodex β-TBDM method C3.

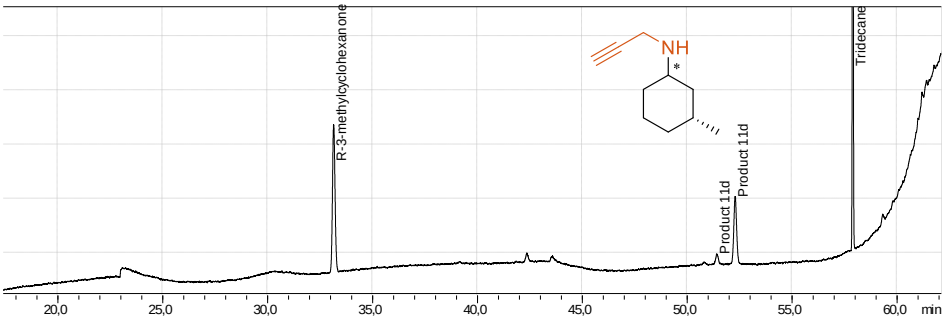

Figure S40. GC chromatogram of cascade reaction mixture containing 3-methyl-2-cyclohexen-1-one and propargylamine with *Ts*OYE-C25D/I67T and *Pau*RedAm. Hydrodex β-TBDM method C3.

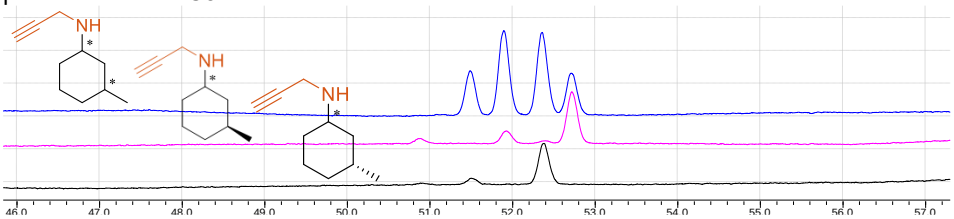

Figure S41. Overlay of synthesized product **11d** (blue), cascade reaction mixture with *Ts*OYE-C25D/I67T shown in **Figure S39** (pink) and the cascade reaction mixture with OYE2 shown in **Figure S40** (black).

GC chromatograms scale-up reactions

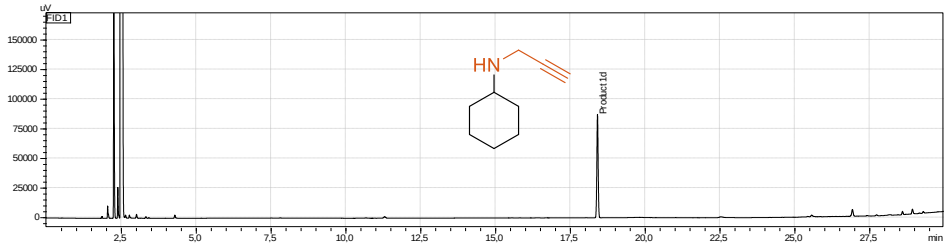

Figure S42. GC chromatogram of scale up reaction with cyclohexanone **1** and propargylamine **d** with *Pau*RedAm to produce *N*-2-propyn-1-ylcyclohexanamine **1d**. CP-Sil 8 CB method A2.

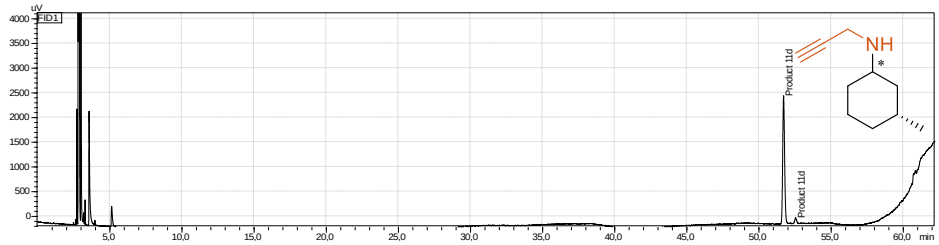

Figure S43. GC chromatogram of scale up reaction with (3*R*)-methylcyclohexanone (3*R*)-**11** and propargylamine **d** and *Stro*RedAm to produce (3*R*)-3-methyl-*N*-(prop-2-yn-1-yl)cyclohexan-1-amine (3*R*)-**11d**. Hydrodex β-TBDM method C3.

GC-MS columns and chromatograms

When the expected amine product was not commercially or synthetically available, extracted reaction samples were injected and analyzed on a GC-MS-QP2010 SE from Shimadzu.

Column E: CP-Sil-5 VF-1ms, 25 m × 0.25 mm × 0.4 µm, split ratio 50, injection temperature 340 °C, helium as carrier gas.

Table S3. GC-MS method and retention times of products which were commercially unavailable.

		GC oven program				
GC column	**Method**	rate (°C/min), temp. (°C), hold (min)			**Compound**	**Ret. time (min)**
E CP-Sil-5 VF-1ms	E1	-	80	3	DMSO	3.2
		5	100	4	*N*-cyclopropylcyclohex-2-en-1-amine **12c**	10.2
		10	200	2.2		10.3
		25	345	1	*N*-(prop-2-yn-1-yl)cyclohex-2-en-1-amine **12d**	13.7
					dodecane	

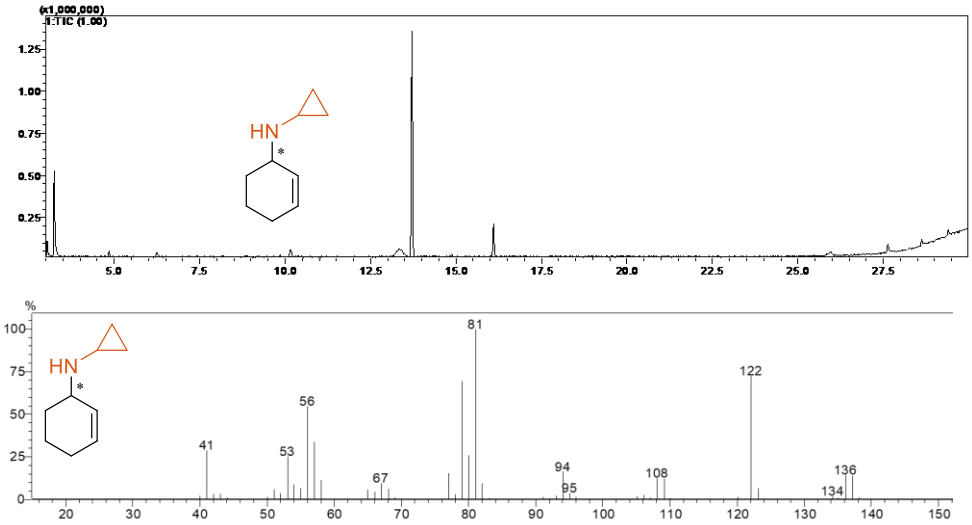

Figure S44. GC-MS chromatogram (top) and mass spectrum (bottom) of *N*-cyclopropylcyclohex-2-en-1-amine **12c** on CP-Sil-5 VF-1ms method E1. Molecular weight is equal to 137.2 g/mol.

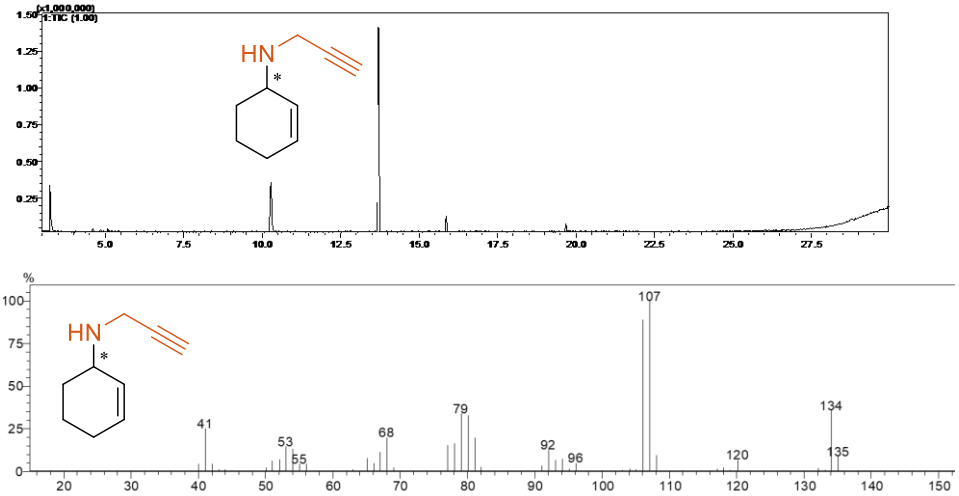

Figure S45. GC-MS chromatogram (top) and mass spectrum (bottom) of *N*-(prop-2-yn-1-yl)cyclohex-2-en-1-amine **12d** on CP-Sil-5 VF-1ms method E1. Molecular weight is equal to 135.1 g/mol.

RedAm scale-up reactions

Reductive amination of cyclohexanone and propargylamine by PauRedAm

In a 50 mL falcon tube were added 100 mM KP_i buffer pH 7, 50 mM cyclohexanone, 60 mM propargylamine, 150 mM glucose, 0.2 mM $NADP^+$, 12 U/mL *Bs*GDH, and 0.5 mg/mL *Pau*RedAm in a total volume of 14 mL. The reaction mixture was shaken at 350 rpm at 20 °C for 24 h. The workup was done as described by Mayol *et al.*,[38] After 24 h, the mixture was basified with 10 M

NaOH until the pH was 12. The product was extracted with 3 × 20 mL Et_2O. The organic layers were pooled, and the Et_2O was removed under reduced pressure until a small volume remained. A solution of 2 M HCl in Et_2O was added (2 mmol) to the liquid, and the precipitate was filtered and then washed with ice cold Et_2O. The residue was then dried under pressure to afford the corresponding product as amine hydrochloride salt (>99% conversion, 65 mg, isolated yield 53%).

NMR-spectra for *N*-2-propyn-1-ylcyclohexanamine **1d** were analyzed and is in accordance with literature[9]: ^{1}H NMR (400 MHz, $CDCl_3$) δ 9.86 (s, 2H), 3.84 (d, *J* = 2.6 Hz, 2H), 3.29 (tt, *J* = 11.3, 3.8 Hz, 1H), 2.54 (t, *J* = 2.6 Hz, 1H), 2.21 (m, 2H), 1.88 (m, 2H), 1.63 (m, 3H), 1.29 (m, 3H). ^{13}C NMR (101 MHz, $CDCl_3$) δ 77.7, 73.0, 55.3, 32.9, 28.9, 24.7, 24.4.

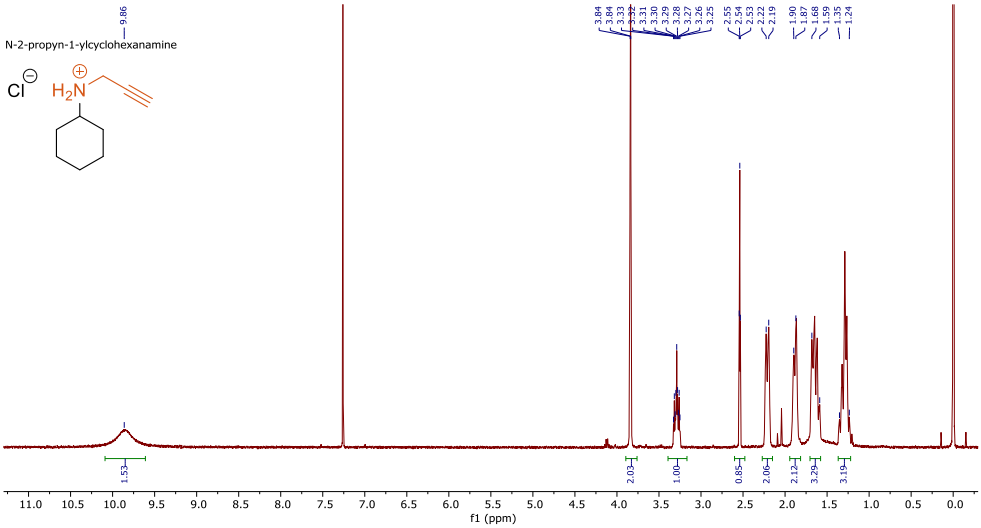

Figure S46. ^{1}H NMR spectrum of *N*-2-propyn-1-ylcyclohexanamine **1d** dissolved in $CDCl_3$.

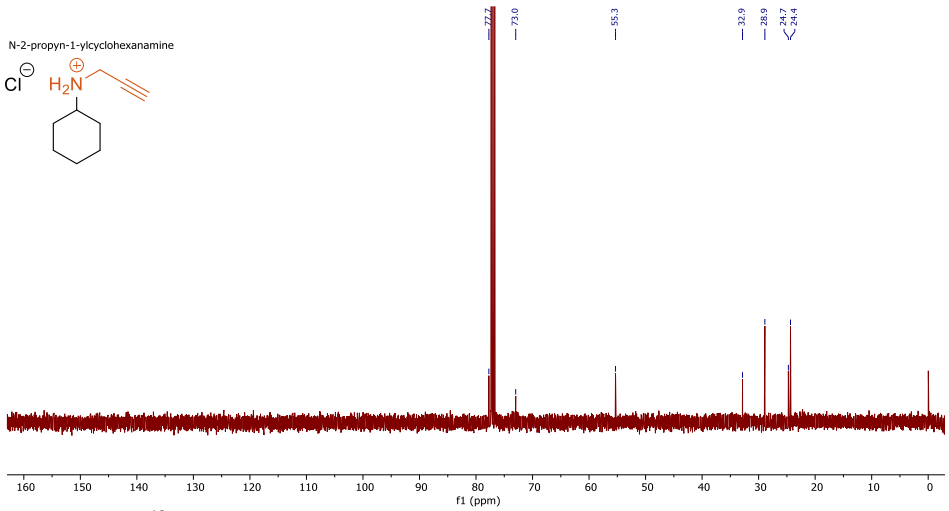

Figure S47. ^{13}C NMR spectrum of *N*-2-propyn-1-ylcyclohexanamine **1d** dissolved in $CDCl_3$.

Reductive amination of (3R)-methylcyclohexanone and propargylamine by StroRedAm

In a 50 mL falcon tube were added 100 mM KP_i buffer pH 7, 50 mM (*R*)-3-methylcyclohexanone, 100 mM propargylamine, 150 mM Glucose, 0.2 mM $NADP^+$, 12 U/mL *Bs*GDH, and 1.0 mg/mL RedAm 1 in a total volume of 14 mL. The reaction mixture was shaken at 350 rpm at 20 °C for 24 h. The workup was done as described by Mayol *et al.*[38] After 24 h, the mixture was basified with 10 M NaOH until the pH was 12. The product was extracted with 3 × 20 mL Et_2O. The organic layers were pooled, and the Et_2O was removed under reduced pressure until a small volume remained. A solution of 2 M HCl in Et_2O was added (2 mmol) to the liquid, and the precipitate was filtered and then washed with ice cold Et_2O. The residue was then dried under pressure to afford the corresponding product as amine hydrochloride salt (>99% conversion, *ee* >99%, *de* 93%, 9 mg, isolated yield 7%).

The isolated product (3*R*)-**11d** was dissolved in D_2O to a concentration of 10 mg/ml. Specific rotation was determined using a Perkin Elmer Model 343 S Polarimeter at 20 °C, at a wavelength of 589 nm. $[\alpha]_{589\,\mathrm{nm}}^{20\,^{\circ}\mathrm{C}} = +3.5°$.

NMR spectra for (3*R*)-3-methyl-*N*-(prop-2-yn-1-yl)cyclohexan-1-amine (3*R*)-**11d** were analyzed: ^{1}H NMR (400 MHz, $CDCl_3$) δ 9.90 (br s, 2H), 3.85 (s, 2H), 3.31 (m, 1H), 2.54 (s, 1H), 2.20 (m, 2H), 1.87 (m, 1H), 1.69-1.66 (m, 4H, H_2O?), 1.60-1.47 (m, 2H, H_2O?), 1.30 (m, 2H), 0.97 (m, 3H). ^{13}C NMR (101 MHz, $CDCl_3$) δ 77.8, 72.9, 55.3, 37.0, 33.4, 32.9, 31.5, 28.4, 24.1, 22.1.

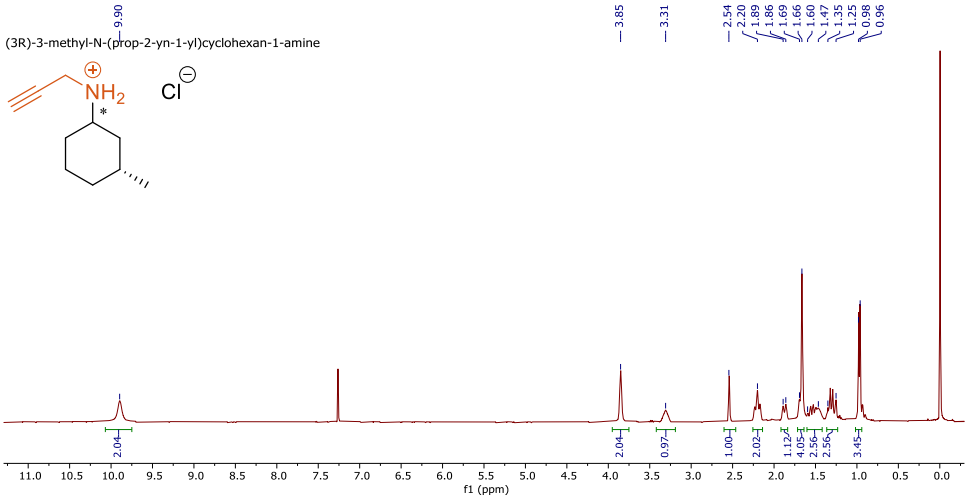

Figure S48. ^{1}H NMR spectrum of (3*R*)-3-methyl-*N*-(prop-2-yn-1-yl)cyclohexan-1-amine (*R*)-**11d** dissolved in $CDCl_3$.

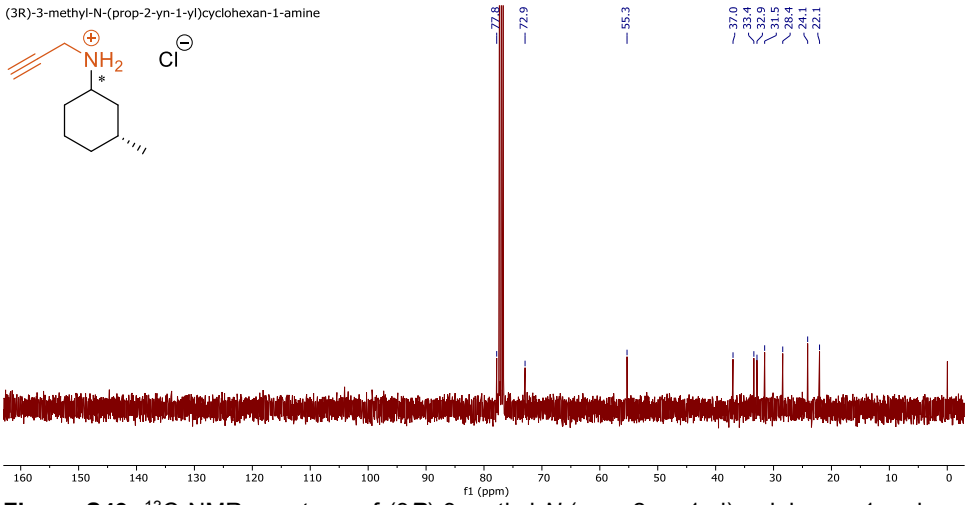

Figure S49. ^{13}C NMR spectrum of (3*R*)-3-methyl-*N*-(prop-2-yn-1-yl)cyclohexan-1-amine (3*R*)-**11d** dissolved in $CDCl_3$.

References

[1] D. Ghislieri, N. J. Turner, *Top. Catal.* **2014**, *57*, 284-300.
[2] M. D. Patil, G. Grogan, A. Bommarius, H. Yun, *ACS Catal.* **2018**, *8*, 10985-11015.
[3] J. Mangas-Sánchez, S. P. France, S. L. Montgomery, G. A. Aleku, H. Man, M. Sharma, J. I. Ramsden, G. Grogan, N. J. Turner, *Curr. Opin. Chem. Biol.* **2017**, *37*, 19-25.
[4] K. Mitsukura, M. Suzuki, K. Tada, T. Yoshida, T. Nagasawa, *Org. Biomol. Chem,* **2010**, *8*, 4533-4535.
[5] J. H. Schrittwieser, S. Velikogne, W. Kroutil, *Adv. Synth. Catal.* **2015**, *357*, 1655-1685.
[6] S. P. France, R. M. Howard, J. Steflik, N. J. Weise, J. Mangas-Sánchez, S. L. Montgomery, R. Crook, R. Kumar, N. J. Turner, *ChemCatChem* **2018**, *10*, 510-514.
[7] P. N. Scheller, M. Lenz, S. C. Hammer, B. Hauer, B. M. Nestl, *ChemCatChem* **2015**, *7*, 3239-3242.
[8] V. Saggiomo, U. Lüning, *Tetrahedron Lett.* **2009**, *50*, 4663-4665.
[9] G. A. Aleku, S. P. France, H. Man, J. Mangas-Sánchez, S. L. Montgomery, M. Sharma, F. Leipold, S. Hussain, G. Grogan, N. J. Turner, *Nat. Catal.* **2017**, *9*, 961-969.
[10] M. Sharma, J. Mangas-Sánchez, S. P. France, G. A. Aleku, S. L. Montgomery, J. I. Ramsden, N. J. Turner, G. Grogan, *ACS Catal.* **2018**, *8*, 11543-11541.
[11] F.-F. Chen, X.-F. He, X.-X. Zhu, Z. Zhang, X.-Y. Shen, Q. Chen, J.-H. Xu, N. J. Turner, G.-W. Zheng, *J. Am. Chem. Soc.* **2023**, *145*, 4015-4025.
[12] G. A. Aleku, G. R. Titchiner, G. W. Roberts, S. R. Derrington, J. R. Marshall, F. Hollfelder, N. J. Turner, D. Leys, *ACS Sustain. Chem. Eng.* **2022**, *10*, 6794-6806.
[13] K. Zhang, Y. He, J. Zhu, Q. Zhang, L. Tang, L. Cui, Y. Feng, *Front. Bioeng. Biotechnol.* **2021**, *9*, 798147.
[14] S. Fademrecht, P. N. Schell, B. M. Nestl, B. Hauer, J. Pleiss, *Proteins* **2016**, 600-610.
[15] M. Cárdenas-Fernandez, R. Roddan, E. M. Carter, H. C. Hailes, J. M. Ward, *ChemCatChem* **2023**, *15*, e202201126.
[16] A. K. Gilio, T. W. Thorpe, A. Heyam, M. R. Petchey, B. Pogrányi, S. P. France, R. M. Howard, M. J. Karmilowicz, R. Lewis, N. J. Turner, G. Grogan, *ACS Catal.* **2023**, *13*, 1669-1776.
[17] J. Steflik, A. Gilio, M. Burns, G. Grogan, R. Kumar, R. Lewis, C. Martinez, *ACS Catal.* **2023**, *13*, 10065-10075.
[18] R. Kumar, M. J. Karmilowicz, D. Burke, M. P. Burns, L. A. Clark, C. G. Connor, E. Cordi, N. M. Do, K. M. Doyle, S. Hoagland, C. A. Lewis, D. Mangan, C. A. Martinez, E. L. McInturff, K. Meldrum, R. Pearson, J. Steflik, A. Rane, J. Weaver, *Nat. Catal.* **2021**, *4*, 775-782.
[19] H. Li, Z. J. Luan, G. W. Zheng, J. H. Xu, *Adv. Synth. Catal.* **2015**, *357*, 1692-1696.
[20] J. Mangas-Sánchez, M. Sharma, S. C. Cosgrove, J. I. Ramsden, J. R. Marshall, T. W. Thorpe, R. B. Palmer, G. Grogan, N. J. Turner, *Chem. Sci.* **2020**, *11*, 5052-5057.
[21] A. K. Gilio, T. W. Thorpe, N. J. Turner, G. Grogan, *Chem. Sci.* **2022**, *13*, 4697-4713.
[22] M. Schober, C. MacDermaid, A. A. Ollis, S. Chang, D. Khan, J. Hosford, J. Latham, A. F. Ihnken, M. J. B. Brown, D. Fuerst, M. J. Sanganee, G. D. Roiban, *Nat. Catal.* **2019**, *2*, 909-915.
[23] J. Hon, S. Borko, J. Stourac, Z. Prokop, J. Zendulka, D. Bednar, T. Martinek, J. Damborsky, *Nucleic Acids Res.* **2020**, *48*, W104-W109.
[24] N. Borlinghaus, B. M. Nestl, *ChemCatChem* **2018**, *10*, 183-187.

[25] L. Josa-Culleré, A. S. K. Lahdenperä, A. Ribaucourt, G. T. Höfler, S. Gargiulo, Y.-Y. Liu, J.-H. Xu, J. Cassidy, F. Paradisi, D. J. Opperman, F. Hollmann, C. E. Paul, *Catalysts* **2019**, *9*, 207.
[26] C. E. Paul, I. W. C. E. Arends, F. Hollmann, *ACS Catal.* **2014**, *4*, 788-797.
[27] S. L. Montgomery, A. Pushpanath, R. S. Heath, J. R. Marshall, U. Klemstein, J. L. Galman, D. Woodlock, S. Bisagni, C. J. Taylor, J. Mangas-Sánchez, J. I. Ramsden, B. Dominguez, N. J. Turner, *Sci. Adv.* **2020**, *6*, eaay9320.
[28] T. W. Thorpe, J. R. Marshall, V. Harawa, R. E. Ruscoe, A. Cuetos, J. D. Finnigan, A. Angelastro, R. S. Heath, F. Parmeggiani, S. J. Charnock, R. M. Howard, R. Kumar, D. S. B. Daniels, G. Grogan, N. J. Turner, *Nature* **2022**, *604*, 86-91.
[29] V. Harawa, T. W. Thorpe, J. R. Marshall, J. J. Sangster, A. K. Gilio, L. Pirvu, R. S. Heath, A. Angelastro, J. D. Finnigan, S. J. Charnock, J. W. Nafie, G. Grogan, R. C. Whitehead, N. J. Turner, *J. Am. Chem. Soc.* **2022**, *144*, 21088-21095.
[30] E. P. J. Jongkind, A. Fossey-Jouenne, O. Mayol, A. Zaparucha, C. Vergne-Vaxelaire, C. E. Paul, *ChemCatChem* **2022**, *14*, e202101576.
[31] T. Knaus, M. L. Corrado, F. G. Mutti, *ACS Catal.* **2022**, *12*, 14459-14475.
[32] L. Skalden, C. Peters, L. Ratz, U. T. Bornscheuer, *Tetrahedron* **2016**, *72*, 7207-7211.
[33] C. E. French, S. Nicklin, N. C. Bruce, *J. Bacteriol.* **1996**, *178*, 6623-6627.
[34] N. Nett, S. Duewel, A. A. Richter, S. Hoebenreich, *ChemBioChem* **2017**, *18*, 685-691.
[35] A. Vorster, M. S. Smit, D. J. Opperman, *Org. Lett.* **2019**, *21*, 7024-7027.
[36] T. Knaus, F. G. Mutti, L. D. Humphreys, N. J. Turner, N. S. Scrutton, *Org, Biomol. Chem,* **2014**, *13*, 223-233.
[37] J. Ziegenhorn, M. Senn, T. Bucher, *Clin. Chem.* **1976**, *22*, 151-160.
[38] O. Mayol, K. Bastard, L. Beloti, A. Frese, J. P. Turkenburg, J.-L. Petit, A. Mariage, A. Debard, V. Pellouin, A. Perret, V. de Berardinis, A. Zaparucha, G. Grogan, C. Vergne-Vaxelaire, *Nat. Catal.* **2019**, *2*, 324-33

Chapter 7: Outlook

Biocatalysis is the chemistry involving enzymes to catalyze reactions towards valuable products. Enzymes are interesting catalysts because of their high selectivity and efficiency. Over the past decades, enzymes were investigated in synthesizing chiral amines, which are valuable building blocks for the pharmaceutical industry. Most of the recent applications employ oxidoreductases, which use electron transferring cofactors to catalyze redox reactions. Oxidoreductases such as RedAms were only recently discovered, yet already a lot of research has been done to bring them to industrial applications, which highlights their attractive synthetic properties. In general, oxidoreductases that catalyze reductive amination towards chiral amines, such as AmDHs, IREDs and RedAms, are known for their poor stability, and preference for NADP, which is economically unfavorable for potential industrial purposes. In this thesis we developed three different pathways using oxidoreductases to synthesize chiral amines (**Figure 1**):

- Using AmDHs, in a single step or in a multi-enzymatic cascade (Chapter 2 and 3)
- Engineering ADHs to induce AmDH/IRED activity (Chapter 4)
- Discovering bacterial RedAms via enzyme mining (Chapter 5 and 6)

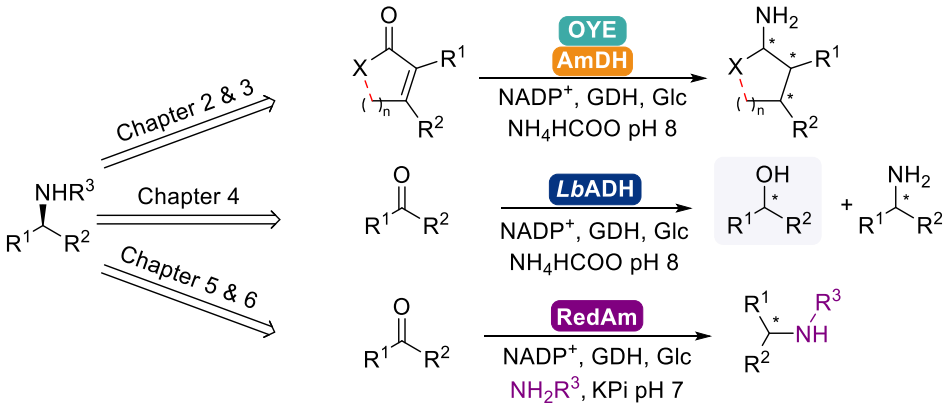

Figure 1. Overview of different biocatalytic approaches described in this dissertation to obtain chiral amines.

AmDHs and (ER-coupled) cascades

The multi-enzymatic cascade described in Chapter 2 demonstrates how chiral primary amines (up to 10 mM, >99% *ee*) were produced from this efficient cascade. Because OYEs yield products that are well-accepted substrates for AmDHs, these enzymes are nicely complementary to each other. By selecting diverse enzymes from the OYE and AmDH families, a variety of cyclic and aliphatic chiral amines were obtained in high enantio- and diastereopurity. Thanks

to the variety in OYE enantioselectivity, different configurations of amine products could be obtained by simply tuning the OYE.

In the last few years, many examples have emerged where OYEs were used in cascades to synthesize chiral amines.[1, 2] The OYE family has also expanded over time, and the new OYE classes potentially expand the diversity of the substrate scope by these enzymes.[3] In parallel, the AmDH family has expanded as well.[4, 5] As most AmDHs are (*R*)-selective, efforts have been made to switch AmDHs to become (*S*)-selective. Instead of altering the product through varying the type of OYE, switching the AmDH is a future possibility to produce even more complex primary amines.

Cascades are attractive reaction processes because no intermediates need to be isolated, less solvents are wasted and less purification steps are necessary, in addition to their tunability. For example, Monti and co-workers combined TAs with ERs to produce amines with high *ee* and *de*.[2] As we showed in Chapter 2, a multi-enzymatic cascade using only oxidoreductases creates a highly efficient process regarding the nicotinamide cofactor. Using a glucose dehydrogenase (GDH) or formate dehydrogenase (FDH), the cofactor is recycled after the consumption of glucose or formate, respectively. A process including FDH would be even more efficient, as the co-product CO_2 is released as a gas.[6] Alternatively, a hydrogenase coupled to a NAD(P)-reductase could be used instead, which uses hydrogen gas as electron donor.[7] By using one of these applications, the step towards biocatalytic processes on an industrial scale could be more sustainable.

The main challenge to overcome in cascades yielding chiral amines lies in the need for compromising reaction conditions for OYEs and AmDHs. For instance, alcohol by-product formation, as described in Chapter 2 and 3, is likely at pH 7 but was limited at pH 9. AmDHs display higher activity at pH 9 but OYEs are more active at near-neutral pH. In our screenings, we used 1 M of ammonium formate buffer which increases the AmDH activity but drastically decreases the OYE activity. However, due to the significantly lower activity of AmDHs than that of OYEs, the reductive amination step is most likely to be the rate limiting step, even in conditions favored by AmDHs. In the few cases where alkene reduction is the limiting step, a one-pot two-step cascade could be considered, where the amine donor and AmDH are added after all unsaturated substrate is reduced by the OYEs. Fine-tuning a cascade depends on which substrate-OYE-AmDH combination will be used, and being aware of these challenges will simplify where the cascade could be altered to improve yield.

*Lb*ADH engineering

Although we were unable to re-purpose an ADH into an AmDH, we gained more knowledge on the wildtype *Lb*ADH. Our work in Chapter 4 also shows how the reported characterized parameters such as activity and stability

have been inconsistent. We demonstrated how storage conditions of *Lb*ADH could impact the specific activity, ranging from 20 to almost 100 U/mg. Therefore, investigating the best reaction and storage conditions for *Lb*ADH will be worthwhile for the chemical building blocks industry.

The hypothesis to use this thermostable, highly active enzyme as the backbone seemed promising, but our approach to obtain reductive aminating mutants was unsuccessful. Mutating one of the amino acids from the catalytic tetrad was risky but seemed necessary to eliminate ketone reduction. For example, work from Lygidakis *et al.* demonstrated how an ene reductase could reduce alcohols after introducing a tyrosine in the active site. A glutamic acid was replaced, normally involved in stabilizing enol intermediates.[8] We replaced the tyrosine for glutamic acid in *Lb*ADH, and found that the *Lb*ADH-Y156E showed poor imine reduction. We tried using the energy minimization algorithm FuncLib on our rationally designed *Lb*ADH-Y156E and *Lb*ADH-S143E. Unfortunately, none of the FuncLib variants showed any imine reduction or reductive amination activity. Using computational algorithms such as FuncLib could only be successful after selecting more than only the three mutants from its output. High throughput screening of as many hits as possible from any computational tool is necessary for the best outcome. Based on our results, the described method in Chapter 4 is not recommended for enzyme re-purposing.

Despite this outcome, enzyme re-purposing was proven to be successful in several examples.[9] An important factor for successful engineering is to observe promiscuity already present in the targeted wildtype enzyme. For instance, Mutti and co-workers discovered ADH promiscuity in the LysEDH, an engineered amino acid dehydrogenase.[8] After further engineering of the LysEDH, the enzyme could catalyze both alcohol oxidation and reductive amination into the corresponding amine. Another example showed how certain short-chain dehydrogenases (SDRs) could reduce specific imines after protein engineering.[10, 11] Instead of targeting the catalytic residues, mutants were obtained by site-directed mutagenesis, leading to mutations of amino acids with more polar side chains in the active site. Because we observed no imine reduction or reductive amination promiscuity of *Lb*ADH-wt, it might be an unsuitable target for further engineering into an IRED or RedAm, unlike the recent successful example of an engineered GDH.[12]

Alcohol formation was observed as a by-product in AmDHs,[13, 14] IREDs and RedAms.[15] Because the reaction mechanism of the reduction of ketones and imines is so similar, ADH re-purposing into IREDs is likely to be further investigated in the future. However, the possible limitation of engineering SDRs into AmDHs or RedAms is the active site pocket size since the space for ammonia or more complex amine donors is limited. Realizing more complex synthesis might only be possible after engineering the active site pocket, allowing for this space. Obtaining successfully engineered ADHs would require intensive protein engineering, with the risk of having little to no reductive amination ability.

RedAm discovery

The search for reductive amination activity provided us with bacterial RedAms with unique properties. *Ryt*RedAm showed high affinity with both NADH and NADPH, with better kinetic parameters than engineered IREDs.[16] After crystallization, we gained insights about what amino acids are involved in this cofactor flexibility. This information could be applicable for other RedAms to obtain NADH acceptance. We also suggest to determine any future RedAm activity with both NADPH and NADH cofactors, since research on RedAms lacks research on NADH. *Ryt*RedAm is (*S*)-selective, which is an uncommon property for RedAms. Instead of using *Asp*RedAm, *Ryt*RedAm could fulfil as a new template for new potential RedAms to search for more (*S*)-selective enzymes. Other unique RedAms in this work are the *Stro*RedAm, *Pau*RedAm and *Strep*RedAm described in Chapter 6. These enzymes all displayed some NADH acceptance as well, although a preference for NADPH was clear. All three enzymes retained most enzyme activity at 30 °C, and at 40 °C for *Pau*RedAm. These enzymes demonstrate that interesting properties such as cofactor preference, selectivity and thermostability could be found in nature amongst bacterial IREDs/RedAms.

We also demonstrated different enzyme mining methods, with varying outcomes. Finding RedAms via sequence identity compared to the *Asp*RedAm was successful, as we found a few hits with reductive amination activity. However, because of the similarity with *Asp*RedAm, the activity was either similar to or worse than reported for the *Asp*RedAm. To contribute to the scope of amines produced by RedAms, a different approach is necessary. When we applied HMM, we found RedAms with more diverse properties for cofactor specificity, substrate scope, and thermostability. All hits were successfully expressed, purified, and characterized. These hits displayed different properties compared to the *Asp*RedAm, as this method focuses on structure similarity instead of sequence identity. The risk of using HMM is finding enzymes that are too unrelated. In addition, the distinction between IREDs and RedAms remains difficult to assess based on sequences and structures. Both of these mentioned approaches focused on only a few potential hits, whereas examples exist where a high-throughput screening (HTS) approach was performed.[17-19] It would also prevent selecting hits which turn out to express poorly in *E. coli* or precipitate after cell lysis. We concluded our approaches were successful, but HTS could also be considered, especially when a certain type of product formation is desired.

Our search methods did not focus on a certain product but on detectable activity. In our work from Chapter 5 and Chapter 6 we applied the activity assay described by Turner and co-workers,[20] comparing reductive amination of an aldehyde at neutral and basic pH. We tried to confirm reductive amination via an activity ratio (activity pH 7 : activity pH 9) and found enzymes more active at neutral than basic pH. The enzymes found in this work had a ratio below 1,

suggesting no dependence on imine formation in solution, which is more likely at pH 9. Although this method is subjective, the enzymes discovered in Chapters 5 and 6 with a low activity ratio proved to catalyze reductive amination for other substrate combinations as well. The IRED/RedAm database has expanded, but remains far from being exhaustive. If more enzymes are characterized that display reductive amination activity, we could learn more about what causes reductive amination in a RedAm and what is missing in IREDs, including knowledge on their NADPH- or NADH-cofactor dependence.

The characterization of RedAms described in Chapters 5 and 6 shows how these enzymes are not limited to the fungal kingdom. We found multiple hits with high similarity compared to the reductive aminases characterized from fungal organisms. Even though some of the hits we found from databases are annotated as IREDs, it could be worthwhile to screen reductive amination at neutral pH. Potentially, a pool of RedAms is present in bacteria, which could contain more RedAms with a different substrate scope.

Evaluation of methods

From the three described methods, the least successful one was the enzyme re-purposing approach. Engineering ADHs without reductive amination activity is currently still too challenging to be a future asset to the chiral amine synthesis industry. Although examples have shown re-purposing can be successful, and *Lb*ADH makes a great target for its activity and stability, it is uncertain to what extent this enzyme can catalyze amine formation. From the remaining two methods, the best method to synthesize chiral amines simply depends on the type of product desired. The multi-enzymatic cascade has a broad scope of primary amine products thanks to the wide a panel of OYEs and AmDHs to choose from. This method is robust, simple, and versatile thanks to the various positions to obtain a chiral center. Discovering bacterial RedAms potentially enables the production of secondary or tertiary amine products. Even though a high-throughput approach could be a better way to obtain RedAms with HMM, we successfully characterized bacterial RedAms we picked from the search output. As we described in Chapter 6, we hypothesized how our RedAms combined with OYEs could expand the amine scope even further. After understanding the RedAm and IRED difference, and characterizing more RedAms, we could use RedAms in this cascade as well.

Chiral amines by biocatalysis

Biocatalysis as a method for chemical synthesis is expected to continue growing in the future, including for chiral amine synthesis.[21-23] Over the past years, the panel of amine products made with oxidoreductases has expanded significantly, either with AmDHs, IREDs or RedAms. However, the number of amines synthesized on an industrial scale by these enzymes remains low,

wherein the general challenge lies in their poor stability. Examples from previous works contain multiple rounds of protein engineering, either to improve certain product acceptance or to improve thermostability. Based on our experience, a major factor of successful protein engineering is the targeted enzyme scaffold. *Ryt*RedAm described in Chapter 5 shows good activities, especially with the less costly NADH cofactor, but also displayed low stability. Therefore, studies to enhance thermostability would be an interesting follow-up. *Stro*RedAm, *Pau*RedAm and *Strep*RedAm show better thermostability, and might be good targets for engineering to accept different complex amine products. As for these examples, we can potentially use biocatalysis on an industrial scale after protein- and reaction engineering. With the computational tools we have at hand today, helpful for protein engineering, protein discovery or retrosynthesis, biocatalysis will become more accessible for designing reaction methods for complex products. Overall, the future of biocatalysis is exciting, and could become a more efficient and environmentally friendlier method to contribute to the chemical and pharmaceutical industries.

Conclusion

This work describes different pathways to synthesize chiral amines using oxidoreductases. We applied oxidoreductases in multi-enzymatic cascades, tried protein engineering and discovered enzymes with valuable properties. These approaches contributed to our understanding of these enzymes and the amines they produce, which will eventually aid in designing new enzymes and processes for chiral amine synthesis. In this way, biocatalysis could fulfill a leading role in producing pharmaceuticals and fine chemicals.

References

[1] T. Knaus, M. L. Corrado, F. G. Mutti, *ACS Catal.* **2022**, *12*, 14459-14475.

[2] D. Monti, M. C. Forchin, M. Crotti, F. Parmeggiani, F. G. Gatti, E. Brenna, S. Riva, *ChemCatChem* **2015**, *7*, 3106-3109.

[3] C. Peters, D. Frasson, M. Sievers, R. Buller, *ChemBioChem* **2019**, *20*, 1569-1577.

[4] E. Elisée, L. Ducrot, R. Méheust, K. Bastard, A. Fossey-Jouenne, G. Grogan, E. Pelletier, J.-L. Petit, M. Stam, V. de Berardinis, A. Zaparucha, D. Vallenet, C. Vergne-Vaxelaire, *Nat. Commun.* **2024**, *15*, 4933.

[5] V. Tseliou, M. F. Masman, T. Knaus, F. G. Mutti, *ChemCatChem* **2024**, *n/a*, e202400469.

[6] W. Hummel, H. Gröger, *J. Biotechnol.* **2014**, *191*, 22-31.

[7] L. Lauterbach, O. Lenz, K. A. Vincent, *FEBS J.* **2013**, *280*, 3058-3068.

[8] V. Tseliou, D. Schilder, M. F. Masman, T. Knaus, F. G. Mutti, *Chem. Eur. J.* **2021**, *27*, 3315-3325.

[9] R. B. Leveson-Gower, C. Mayer, G. Roelfes, *Nat. Rev. Chem.* **2019**, *3*, 687-705.

[10] S. Roth, P. Stockinger, J. Steff, S. Steimle, V. Sautner, K. Tittmann, J. Pleiss, M. Müller, *ChemBioChem* **2020**, *21*, 2615-2619.

[11] S. Roth, M. B. Kilgore, T. M. Kutchan, M. Müller, *ChemBioChem* **2018**, *19*, 1849-1852.

[12] X. Yi, F. Kleinbeck, C. Ching, L. Boghospor, S. Gomes, O. Alvizo, T. Allmendinger, J. Fell, N. Subramanian, M. Li, R. Garcia, J. Riggins, D. Entwistle, Y. Richter, D. Gschwend, L. Lauener, T. S. Peat, H. Lebhar, T. Schlama, T. Ruch, *ACS Catal.* **2024**, *14*, 7087-7096.

[13] A. Fossey-Jouenne, L. Ducrot, E. P. J. Jongkind, E. Elisée, A. Zaparucha, G. Grogan, C. E. Paul, C. Vergne-Vaxelaire, *Front. Catal.* **2023**, *3*, 1105948.

[14] E. P. J. Jongkind, A. Fossey-Jouenne, O. Mayol, A. Zaparucha, C. Vergne-Vaxelaire, C. E. Paul, *ChemCatChem* **2022**, *14*, e202101576.

[15] H. Y. Jia, Z. Y. Yang, Q. Chen, M. H. Zong, N. Li, *Front. Chem.* **2021**, *9*, 610091.

[16] N. Borlinghaus, B. M. Nestl, *ChemCatChem* **2018**, *10*, 183-187.

[17] S. P. France, R. M. Howard, J. Steflik, N. J. Weise, J. Mangas-Sánchez, S. L. Montgomery, R. Crook, R. Kumar, N. J. Turner, *ChemCatChem* **2018**, *10*, 510-514.

[18] M. Cárdenas-Fernandez, R. Roddan, E. M. Carter, H. C. Hailes, J. M. Ward, *ChemCatChem* **2023**, *15*, e202201126.

[19] J. R. Marshall, P. Yao, S. L. Montgomery, J. D. Finnigan, T. W. Thorpe, R. B. Palmer, J. Mangas-Sánchez, R. A. M. Duncan, R. S. Heath, K. M. Graham, D. J. Cook, S. J. Charnock, N. J. Turner, *Nat. Chem.* **2021**, *13*, 140-148.

[20] G. A. Aleku, S. P. France, H. Man, J. Mangas-Sánchez, S. L. Montgomery, M. Sharma, F. Leipold, S. Hussain, G. Grogan, N. J. Turner, *Nat. Catal.* **2017**, *9*, 961-969.

[21] S. P. France, R. D. Lewis, C. A. Martinez, *JACS Au* **2023**, *3*, 715-735.

[22] A. K. Gilio, T. W. Thorpe, N. J. Turner, G. Grogan, *Chem. Sci.* **2022**, *13*, 4697-4713.

[23] S. K. Wu, R. Snajdrova, J. C. Moore, K. Baldenius, U. T. Bornscheuer, *Angew. Chem. Int. Ed.* **2021**, *60*, 88-119.

Curriculum vitae

Name: Ewald Piet Jürgen Jongkind
Date of birth: 26 March 1997
Place of birth: Alphen aan den Rijn

Education

- BSc. Life Science and Technology, joint degree, Leiden University and TU Delft (08/2015-07/2018).
- *Cum laude* MSc. Life Science and Technology, TU Delft, (08/2018-07/2020).
- PhD-candidate in Biocatalysis, department of Biotechnology, TU Delft (09/2020-09/2024).

List of publications

- **E. P. J. Jongkind**, A. Fossey-Jouenne, O. Mayol, A. Zaparucha, C. Vergne-Vaxelaire, C. E. Paul, Synthesis of chiral amines via a bi-enzymatic cascade using an ene-reductase and amine dehydrogenase, *ChemCatChem* **2022**, *14*, e202101576
- X. Xu, H. Brasselet, **E. P. J. Jongkind**, M. Alcalde, C. E. Paul, F. Hollmann, A peroxygenase-alcohol dehydrogenase cascade reaction to transform ethylbenzene derivatives into enantioenriched phenylethanols, *ChemBioChem* **2022**, *23*, e202200017
- Y. Wu, C. E. Paul, T. Hilberath, **E. P. J. Jongkind**, W. Zhang, M. Alcalde, F. Hollmann, Peroxygenase-promoted enzymatic cascades for the valorisation of fatty acids, *ChemCatChem* **2023**, *15*, e202300411
- A. Fossey-Jouenne, L. Ducrot, **E. P. J. Jongkind**, E. Elisée, A. Zaparucha, G. Grogan, C. E. Paul, C. Vergne-Vaxelaire, Native amine dehydrogenases can catalyze the direct reduction of carbonyl compounds to alcohols in the absence of ammonia, *Frontiers in Catalysis* **2023**, *3*, 1105948
- **E. P. J. Jongkind**, J. Domenech, A. Govers, M. van den Broek, J.-M. Daran, G. Grogan, C. E. Paul, Discovery and synthetic applications of a NAD(P)H-dependent reductive aminase from *Rhodococcus erythropolis, ACS Catalysis* **2024***, 15,* 211-219.
- **E. P. J. Jongkind**, W. J. Kools, M. Pareek, S. C. L. Kamerlin, C. E. Paul, Mechanistic insights in *Lactobacillus brevis* alcohol dehydrogenase: stability and active site role of Ser143 and Tyr156, *in preparation.*

- **E. P. J. Jongkind**, M. H. de Jong, G. S. Nguyen, C. E. Paul, Discovery and synthetic applications of thermostable NAD(P)H-dependent reductive aminases, *in preparation.*

Acknowledgements

When I started my PhD in September 2020, the world looked much different from now. Due to the COVID-pandemic, my PhD-journey started from my desk at home. Thanks to my colleagues, we were able to proceed with our projects via online group meetings, discussions, and seminars. We managed the circumstances as well as possible, but I am thankful I am writing these acknowledgements whilst sitting in a fully occupied office.

First and foremost, I would like to thank my promoter and daily supervisor, Caroline Paul. You enabled a wonderful opportunity for me to become a PhD in this group. You also reached out to great collaborations abroad, which benefitted this thesis and my personal experience during my PhD. You were always helpful, kind and so passionate in this research field that it is contagious. I wish you all the best with inspiring many more students as much as you inspired me.

Thanks a lot to my promoter Ulf Hanefeld. You knew how to challenge me with my knowledge in organic chemistry and taught me how to explain my work better during our bi-weekly meetings. You made me a better and more critical researcher in the end. Thank you for all your advice and guidance during my time here in Delft.

I would like to thank the independent doctoral committee members, Willem van Berkel, Jean-Marc Daran, Rienk Eelkema, Francesco Mutti, Joerg Schrittwieser and Frank Hollmann for reviewing this dissertation.

Thank you to Frank Hollmann, Peter-Leon Hagedoorn, Kristina Djanashvili and Duncan McMillan, for your interest and questions or suggestions during our bi-weekly meetings and BOC seminar sessions. A big thanks as well to all the BOC technicians: Remco van Oosten, Marc Strampraad, Laura Koekkoek, Lloyd Mallée, Natalia Karakitsou, and Stephen Eustace. You were very approachable to help me out whenever I needed it. You made our labs such a wonderful place to work, I miss my fume hood in the lab already!

I strongly believe I worked in the ‘gezelligste’ office from this faculty, C2.260. This is mostly thanks to Remco. Whether it were your jokes, the (too) loud music you shared with us, or our discussions about Ajax and Oranje, it was a pleasure to share an office with you for so long. Thanks as well to the latest composition of this office: Angelique, Jacob, Lukas, Pablo and Tim, the ‘frequent visitors’ Hugo and Nicolas and all the students that sat here, you made this office a wonderful place to work at. Tim, another thanks to you for being my paranymph. I enjoyed your company in the office, and I am glad you are next to me during my defence.

The Biocatalysis group consists of many bright people, and I am thankful for our discussions and your help during my PhD. Thank you to Allison, Alice, Angelique, Aster, Chiara, Christian, Claudia, Hugo, Jacob, Nicolas, Pablo, Thijs,

Tim, Yinqi and Yutong. I had a wonderful time discussing work, but also our social moments. Whether these were sporting events, conferences, or trips abroad, it was great to spend it with you all.

Special thanks to Thomas Hilberath. Starting as a PhD I still had much to learn. Especially regarding work in the microbiology lab, protein purifications, discussions about our work or the future, you were always helpful. I also thank you for introducing me to the wonderful Altstadt in Düsseldorf, its Christmas market, and the (2nd) Bundesliga football stadiums. Hopefully, we can visit some game together again in the future!

The work described in this thesis could not have been possible without the input of four skilled Bachelor and Master students. Many thanks to Wouter Kools, Melis Teke, Arthur Govers and Mees de Jong for your efforts during your end projects. I appreciated your interest in these projects, your perseverance after inevitable challenges and the quality of your work. I hope you all look back at this time as fondly as I do, and that it made you even more enthusiastic about biocatalysis.

Thank you to Mieke van der Kooij and Irma Zomerdijk, for being the reliable and approachable secretaries whilst I was here. It has been a pleasure to see and talk to you and have the fruit basket with the whole group on Monday.

During my PhD, I shortly visited York, UK for crystallization studies. Thank you to Gideon Grogan for this opportunity to collaborate on this exciting work. A big thank you to Jack Domenech as well, for your great guidance around the labs in York during my stay. May you get as much protein and beautiful gels in the future as we made together in York!

Thanks to Marcel van den Broek for helping me with the database search for new reductive aminases, the crystallization could not have happened without you. Thank you to Giang-Son Nguyen for your mining efforts as well, we found some very interesting RedAms thanks to you. Another thanks to Carine Vergne-Vaxelaire for collaborating with us, it was great to work with you and the AmDHs.

Buiten mijn werkomgeving heb ik ook veel support gekregen. Daarom bedank ik mijn vriendengroep, Bart van Elswijk, Daan Broere, Daan Sikkes, Dirk Waagenaar, Mark Mijnsbergen en Stefan Tuin voor jullie gezelligheid en steun de afgelopen tijd. Het is bijzonder om zo lang na de middelbare school zo'n trouwe groep vrienden te hebben waarmee ik nog regelmatig afspreek.

Veel dank aan mijn moeder Diana en mijn vader Jürgen voor jullie onvoorwaardelijke steun. Jullie leerden mij om elk hoogtepunt tijdens mijn PhD te waarderen en te vieren, en vooruit te kijken als mijn dagen op het lab niet even succesvol waren. Ten slotte, veel dank aan mijn zus Demy voor je steun en onze gesprekken over hoe wij onze PhD hebben ervaren, wat nodig en grappig was. Ik ben trots dat jij je PhD in Leiden hebt afgerond en dat je naast me staat als mijn paranimf.